vol. 4, no. 2

February, 1958

THE SOVIET JOURNAL OF

ATOMIC ENERGY

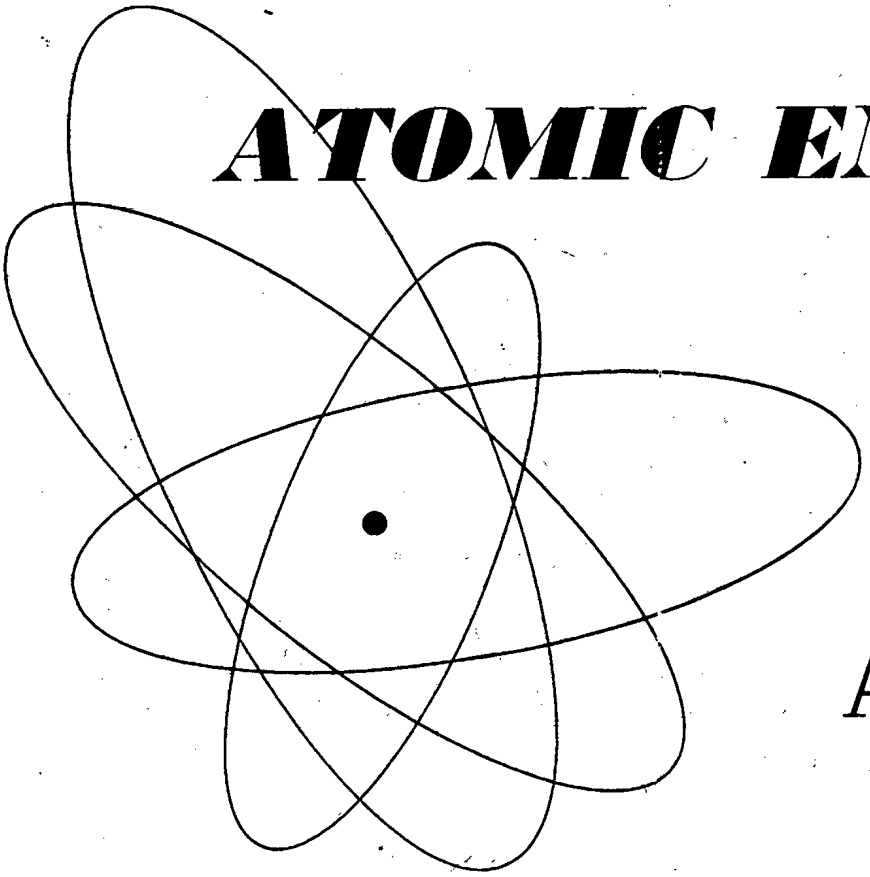

Атомная энергия

TRANSLATED FROM RUSSIAN

CONSULTANTS BUREAU, INC.

What are the Russians doing in my particular field? . . .

Is this information available in translation?

These pertinent questions which consistently confront technical librarians today, have pointed up the serious lack of a *standard source of reference* for translations of Soviet scientific information, and have led to the inauguration of a unique monthly service. . . .

Soviet Science and Technology

THIS HANDY MONTHLY GUIDE, available on an annual subscription basis, is specifically designed to furnish Western scientists with *English translations of the contents* of current Soviet journals being translated, cover to cover, on a *continuing basis* by Consultants Bureau, other firms and learned societies.

THROUGH SPECIAL ARRANGEMENT with the editors of these Soviet publications, expedited copies of the contents are made available, in translation, within two months after their release in Russia. Thus, each subscriber is constantly aware of the latest information available for translation in his specific field of scientific endeavor.

The format of SST is one which permits the reader instant access to all pertinent information:

a) *Estimated date of publication in English* (when information is available from publisher)

b) *Name and address of organization from which translation is available*

c) *Yearly subscription prices*

d) *Price of individual papers, or issues* (when sold separately)

e) *A special section devoted exclusively to editorial material on the most up-to-date translating techniques*

The worldwide acceptance of SST in its few short months of existence *(first issue published in May, 1958)*, has proved the urgent need for just such a service. And with the constant addition of *new* Russian journals-in-translation, each subscriber is assured of continuous, comprehensive and accurate information on the availability of the latest advances in SOVIET SCIENCE AND TECHNOLOGY.

ANNUAL SUBSCRIPTION

(includes 12 issues per year, which cover all calendar year issues of the original Russian journals)

1 copy	$25.00 per copy
10-100 copies	18.00 per copy
100-500 copies	15.00 per copy
500 copies and over	11.50 per copy

(500 copies includes, free of charge, your own special organizational cover)

AVAILABLE FOR A LIMITED TIME

One volume containing the contents for all 1957 issues of these journals, with the same information as in the 1958 SST. . . . $15.00

Write Consultants Bureau for free brochure on SST, and comprehensive catalogs of our current Russian translation-publishing program.

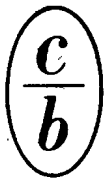

CONSULTANTS BUREAU, INC.
227 W. 17th St., NEW YORK 11, N.Y.

vol. 4, no. 2

February, 1958

THE SOVIET JOURNAL OF

ATOMIC ENERGY

ATOMNAIA ENERGIIA

A publication of the Academy of Sciences of the USSR

Annual Subscription $75.00
Single Issue 20.00

Year and issue of first translation:
volume 1, number 1 january 1956

TRANSLATED FROM RUSSIAN

CONSULTANTS BUREAU, INC.

Printed in the United States

HISTORICAL DEVELOPMENT OF THE CYCLOTRON

(SURVEY OF THE LITERATURE)

L. M. Nemenov

A short survey, based on the published literature, is given of the historical development of cyclotron devices. The basic parameters and main features of cyclotrons are given. The paper is illustrated by photographs taken from the literature.

Almost thirty years have passed since the first enunciation of the principle of the magnetic resonance accelerator – the cyclotron, a machine which has played an extremely important role in nuclear research. Because of its universal application, the cyclotron is, at present, one of the most widely used types of accelerators.

Using the published literature, we shall trace the evolution of the cyclotron during this time, a period in which the rapid development of nuclear physics imposed ever-increasing requirements on the cyclotron.

Using the cyclotron it is possible to accelerate ions of virtually all elements from hydrogen to neon and to study a large number of nuclear reactions which occur when charged particles interact with matter. The cyclotron is a source of fast, monochromatic neutrons and, with a sufficiently intense beam of charged particles, allows us to obtain a flux of partially polarized neutrons. By exploiting the discontinuous nature of the ion beam from a cyclotron it is possible to investigate neutron spectra, determining the fast-neutron energy by time-of-flight methods; using a so-called "pulsed beam" we can investigate the interaction of slow neutrons with matter. In certain cases the cyclotron is used as a source of hard γ-rays. Finally, it can be used to obtain a number of nuclides of high specific radioactivity.

The first paper on the principle of a cyclical resonance accelerator in which a high voltage is not used was that of Lawrence and Edlefsen [1] in 1930. In 1931, using a cyclotron with a pole diameter of 100 mm, Lawrence and M. Livingston were able to accelerate ions of molecular hydrogen to an energy of 80 kev. This primitive, laboratory-built device became the prototype of modern cyclical accelerators.

In that same year, Lawrence and M. Livingston, using an improved machine (Fig. 1), were successful in accelerating protons to an energy of 1.22 Mev. In this work it was noted that a change in the magnetic field of several tenths of a percent was sufficient to disturb the resonance condition. In their basic description the authors indicated the method used for correcting inhomogeneities (the introduction of pieces of iron between the pole pieces of the magnet and the roof of the accelerator chamber). The electric field of a condenser was used to deflect the beam of charged particles. The beam current at the terminal radius was 10^{-9} amp, but the authors discussed the possibility of obtaining currents of the order of 10^{-7} amp.

In 1932, using an improved machine, these same authors accelerated deuterons to 3.6 Mev. A current of 10^{-9} amp was detected with a measuring electrode (Faraday cylinder) which was set up beyond the deflection system. In 1933 ions of molecular hydrogen were accelerated to 4.8 Mev in this same accelerator. In this work an oscillator system consisting of two dees was used.

Using a chamber with a roof diameter of 690 mm, in 1934 the same workers accelerated ions of molecular hydrogen to 5 Mev (Fig. 2) while in 1935 a current of molecular hydrogen ions of 10^{-5} amp was obtained beyond the deflection system in this same apparatus.

In 1936 great progress was made. Lawrence and Cooksey [2] built a new chamber with a roof diameter of 700 mm and accelerated deuterons to 5 Mev; moreover, using a deflection system, for the first time it was possible to extract a beam of charged particles with a current strength of 5 μ amp from the chamber through a

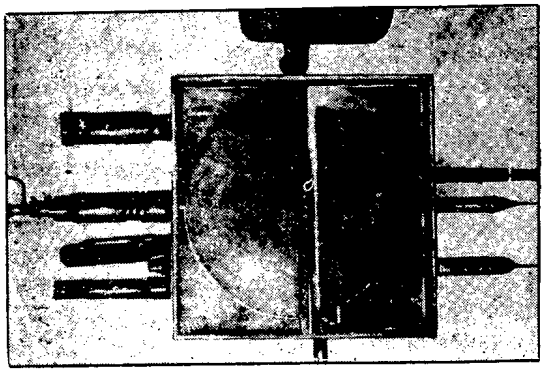

Fig. 1. Cyclotron with which protons were accelerated to an energy of 1.22 Mev. Upper photograph – general view; lower photograph – acceleration chamber with one dee.

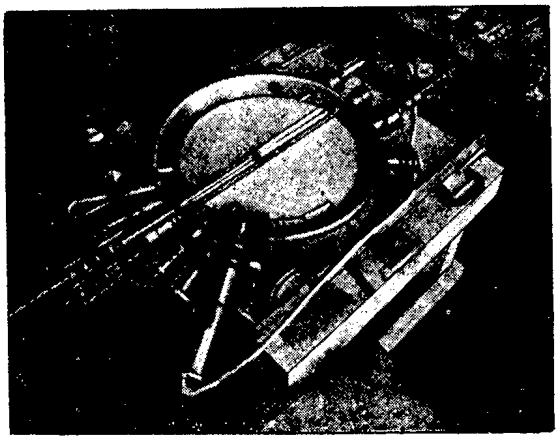

Fig. 2. Accelerator chamber with two dees with which ions of molecular hydrogen were accelerated to 5 Mev.

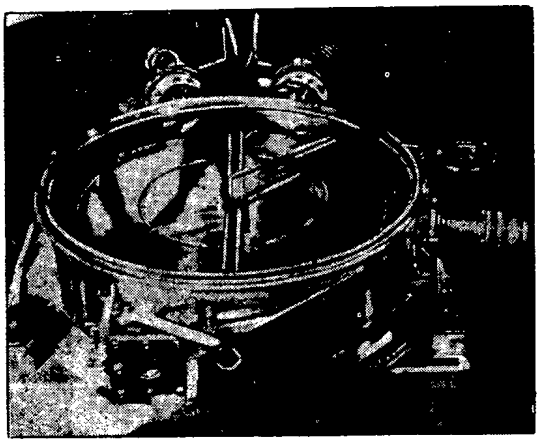

Fig. 3. Accelerator chamber in which deuterons were accelerated to an energy of 8 Mev and extracted.

thin platinum window. The radio-frequency generator, using a self-excited push-pull circuit, delivered radio-frequency power of the order of 25 kw. The potential difference between the dees was 50-100 kv. The magnetic field correction was realized by introducing iron discs between the pole pieces of the magnet and the ends of the accelerator chamber. For the first time attention was paid to the fact that the geometric center of the accelerator chamber does not coincide with the center of the particle orbit and it was shown that this effect can be avoided by additional corrections of the magnetic field. An electrode for measuring the beam current was located in the chamber beyond the deflection system. Provision was made for

mounting a target for exposure on this same device; the target was cooled by circulating water. In this cyclotron the first experiments with fast neutrons obtained by bombarding beryllium with deuterons were carried out. The authors also proposed that it was feasible to extract the beam in a tube under vacuum to a considerable distance from the cyclotron in order to reduce the background of radiation from the machine itself. In this same year Du Bridge and Barnes constructed a similar machine and accelerated protons to 6 Mev at a beam current of several microamperes.

Fig. 4. General view of the cyclotron in which vacuum coaxial resonance lines were first used.

In 1937 Lawrence and Cooksey [3] built a highly improved accelerator (Fig. 3). The dee circuit was water cooled. The chamber was provided with reliable vacuum valves. Means were provided for measuring the dee potentials. For the first time the deflection system was provided with a thin element of refractory metal in order to reduce the losses of charged particles from the beam which entered the condenser. Also, for the first time, use was made of a probe with a sliding seal developed by R. Wilson for measuring the current of accelerated particles at any radius (based on heating of water). It was also possible to fasten a target to this same probe. Vacuum ports placed beyond the deflection system made it possible to operate the apparatus and remove irradiated targets without disturbing the vacuum in the accelerator chamber. The beam was extracted to the outside through a thin metal foil fastened to a plate through which a large number of holes were drilled.

The authors obtained 8 Mev deuterons. The current at the terminal radius was 100 μ amp. The current in the extracted beam was several microamperes. The construction of this cyclotron represented an important achievement since it was the first machine to employ sophisticated engineering techniques.

In this same year, in Leningrad the first cyclotron in the USSR and Europe was built (magnet diameter of 1000 mm [4]); Alvarez and his co-workers made the first attempt to remove an exposed target from the cyclotron; Veksler and M. Leontovich, on the basis of work by Tuve and Lamar, constructed and tested the first capillary ion source for a cyclotron; Bethe published the first paper on the theory of the cyclotron.

1938 was an especially fruitful year in the development of accelerators.

Dunning and Anderson [5], using an idea proposed by Sloan, for the first time applied a quarter-wave coaxial resonant vacuum line for applying the radio-frequency voltage to the dees (Fig. 4). This improvement made it possible to eliminate the glass insulators which limited the magnitude of the voltage which could be applied to the dees.

Alvarez obtained an intermittent beam of thermal neutrons by modulating the beam of deuterons incident on a beryllium target. Wilson and Kamen carried out interesting experiments for verifying the theory of the cyclotron. Allen et al. accelerated deuterons to 9.7 Mev, obtaining a current of 1 μ amp in the extracted beam.

This year was also extremely fruitful in theoretical work. Here, we must mention the fundamental research carried out by Rose on the theory of the cyclotron [6], the work by Khurgin on the limiting particle energy in a cyclotron [7] and Wilson's work on electrostatic and magnetic beam focussing [8]. However, one of the most significant events of that year in the field of acceleration techniques was the appearance of a paper by Thomas who showed that charged particles can be accelerated to significantly higher energies in a cyclotron if an azimuthal asymmetry is introduced in the magnetic field. Actually, in this work Thomas touched upon the "strong focussing" principle. However, his proposal was not exploited since the creation of a magnetic field with the required configuration represented a problem of extreme difficulty. At that time even the problem of correcting the magnetic field in an ordinary cyclotron was one of no mean difficulty.

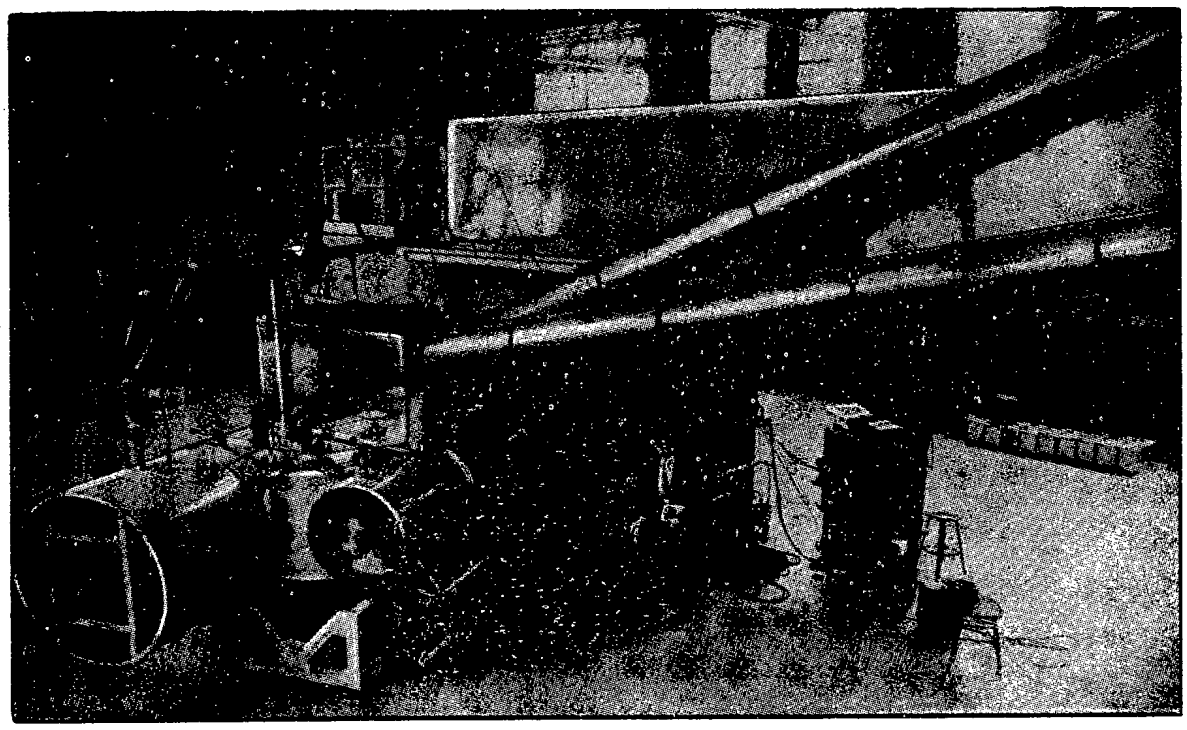

Fig. 5. General view of the Berkeley cyclotron with which deuterons were first accelerated to an energy of 22 Mev.

The design of a giant cyclotron with a pole-piece diameter of 4.7 m for accelerating deuterons to an energy of 100 Mev, proposed by Lawrence in the pre-war period, and the important discovery [10] made independently by Veksler (1944), and McMillan (1945) diverted the attention of physicists from the proposal made by Thomas for more than ten years.

In 1939 Lawrence, Alvarez and their colleagues put into operation the largest cyclotron in the world; this machine had a pole diameter of 1500 mm (Fig. 5) [11]. The weight of the magnet was 200 tons. The construction of the accelerator chamber was considerably different from that which had been used up to that time. Its basic advantage was the fact that the dees and the resonant lines could be removed from the chamber while the chamber remained between the poles of the magnet. Thus, this operation did not disturb the magnetic field corrections.

The resonant line of the cyclotron was rather complicated in construction. Special devices were used to permit adjustment of the position of the dees without disturbing the vacuum. At first the deflection system was set up inside the dees. In the early design a radiofrequency voltage was "induced" in the deflection system;

this had an effect on the intensity distribution in the extracted beam. The modified system was found to be free from this shortcoming.

In this apparatus McMillan, and Salisbury improved a capillary ion source developed by M. Livingston, Holloway and Becker. To improve the efficiency of ion extraction from the source a rib was added to the dees, thereby increasing the gradient of the radiofrequency field. This modification resulted in a seven-fold increase in the current of accelerated particle. The beam was extracted through a window cooled by a hydrogen jet which was developed by F. Curie.

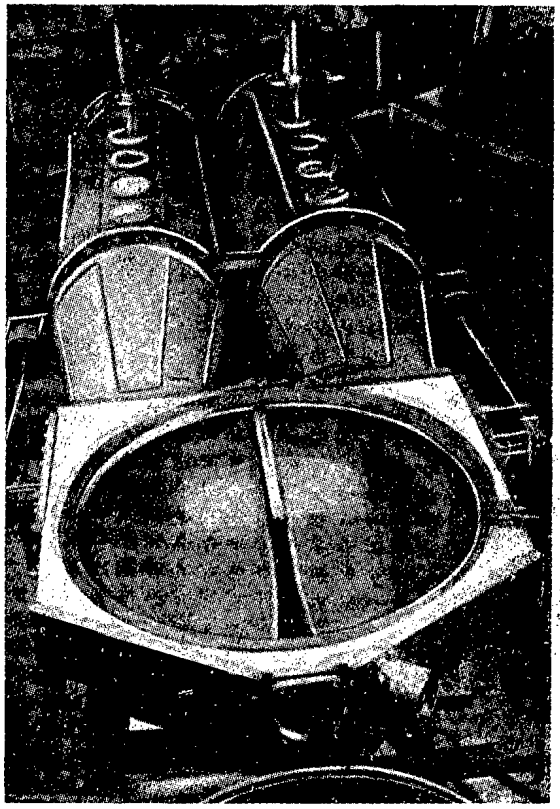

Fig. 6. Accelerator chamber with resonance lines and dees of the cyclotron at the Massachusetts Institute of Technology (the upper chamber cover is removed). Using this chamber deuterons with an energy of 15 Mev were obtained. Deuteron currents of up to 1 ma were achieved at the terminal radius.

The machine was evacuated by oil diffusion pumps with a capacity of 3000 liters/sec. The accelerator chamber was so large that it had to be mounted on a special flatcar. With this machine protons at 9 Mev were obtained on an internal target with a current of 25 μamp. Deuterons were accelerated to an energy of 16 Mev (the current on the internal target was 10 μamp, the current in the extracted beam was 1 μamp). Before the start of the war a deuteron energy of 22 Mev was obtained with this cyclotron; this was a record for the time.

In 1940, Alvarez accelerated C_{12}^{+6} ions to an energy of 50 Mev, carrying out experiments to investigate the interaction of multiply-charged ions with matter. The beam intensity at the terminal radius of the cyclotron was 500 ions/min.

In this same year Curtis was able to construct an ion source in which it was possible to replace the incandescent filament without disturbing the vacuum in the accelerator chamber. Wilson [12] published a paper in which consideration was given to problems of electric and magnetic focussing, ion production in the central part of the cyclotron and displacement of particle trajectories.

In 1942, Condit, using the $1\frac{1}{2}$ meter cyclotron at Berkeley, accelerated C_{12}^{+6} ions to 85 Mev and O_{16}^{+8} ions to 113 Mev. The interaction of multiply-charged ions with matter was studied in a Wilson chamber.

In 1944 M. Livingston [13] published data on a new machine which was one of the most advanced of its kind. He obtained outstanding results with a cyclotron having a magnet diameter of 1050 mm (magnet weight about 90 tons). In designing this machine Livingston made use of all the earlier theoretical results and experience acquired in operation of all existing machines. Livingston took particular pains in the correction of the magnetic field. The decrease in magnetic field at the extraction radius was 1.8%. The magnetic field corrections were applied by means of piles of discs which were placed in the gaps between the chamber covers and the pole pieces. A remotely controlled variable condenser was used to adjust the frequency of the resonant circuit. Movable shorting elements for the resonance lines were provided in the form of spring contacts. The intense beams of charged particles were detected by a rotating target which was constructed; with this rotating target it was possible to increase the thermal stability by distributing the heat load over a large surface.

Fig. 7. General view of the 1½ meter cyclotron at the Institute for Atomic Energy, Academy of Sciences, USSR. [The color plate has been graciously provided by the Soviet publishers of Atomnaia Energiia.]

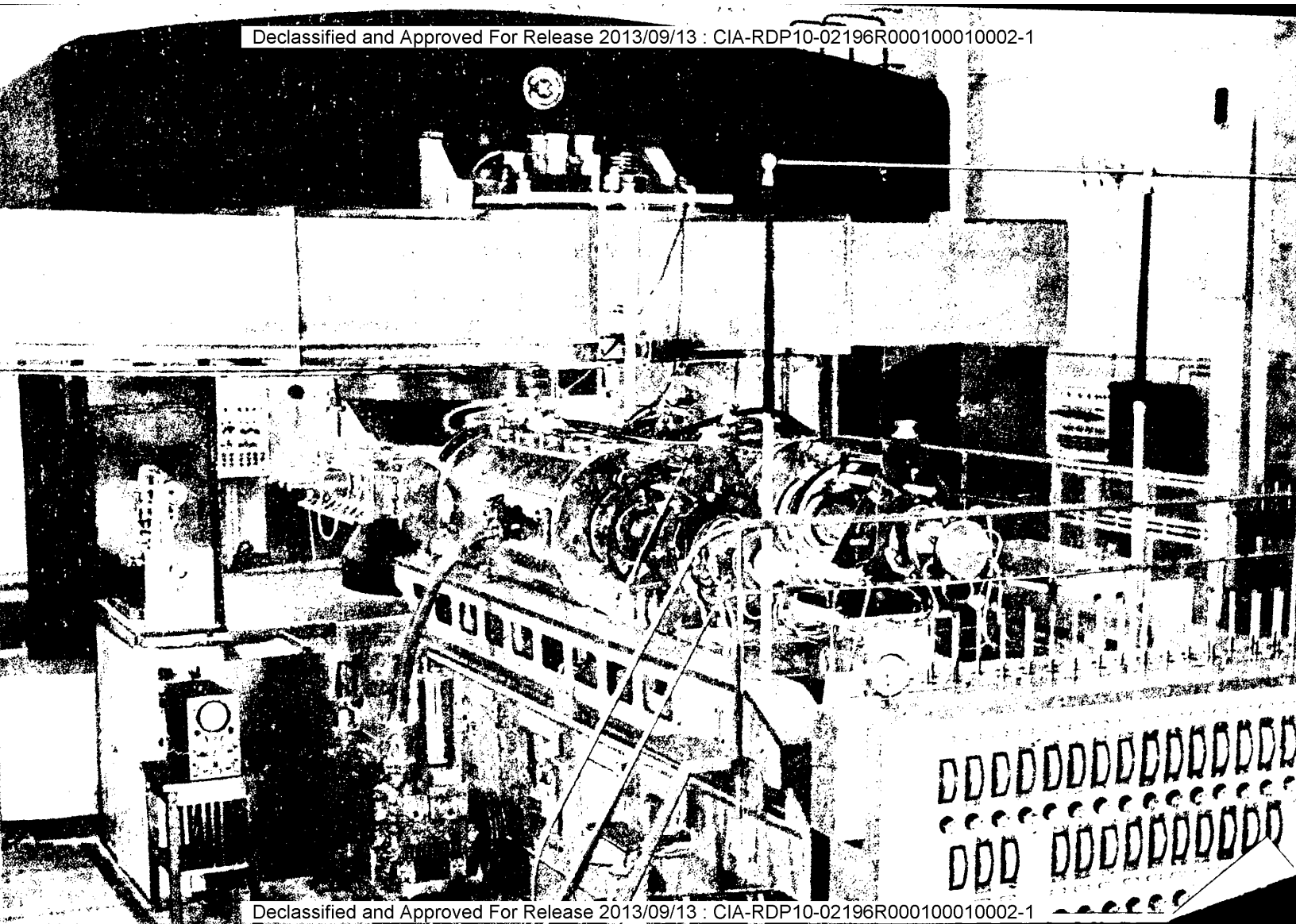

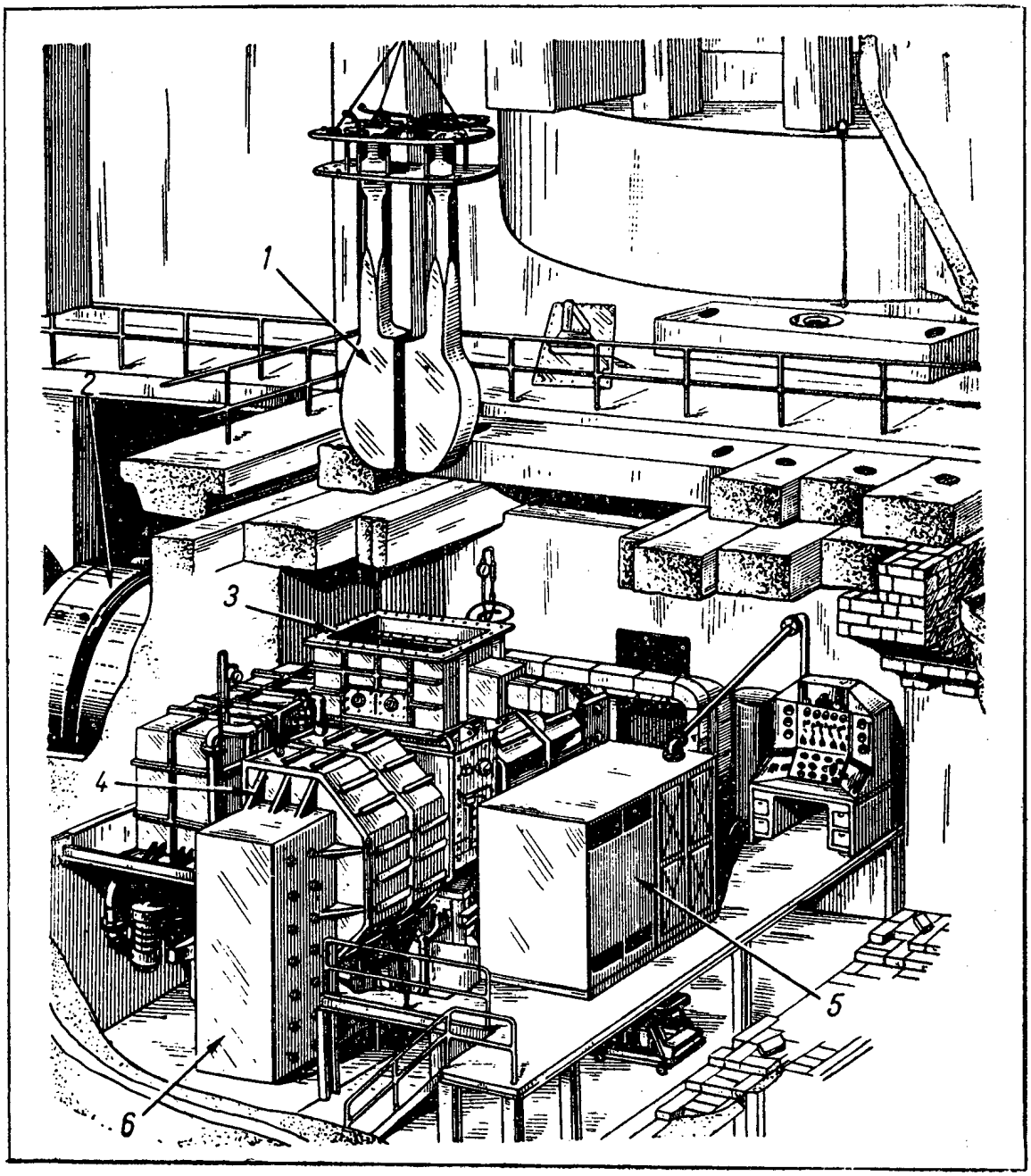

Fig. 8. Diagram of the Oak Ridge cyclotron with vertical acceleration chamber. 1) Dee system; 2) motor generator; 3) vacuum chamber; 4) magnet winding; 5) radiofrequency generator; 6) magnet yoke.

In addition, the Livingston design provided a number of features to facilitate all operations associated with adjustment, assembly, and disassembly of the various units of the cyclotron (Fig. 6). Most of the operations were carried out remotely from a central control panel. Livingston was one of the first to consider the problem of personnel protection against radiation and to take effective measures for radiation safety.

After adjustment of the cyclotron Livingston was able to obtain a record result: deuterons were accelerated to 15 Mev. The current at the terminal radius was about 1 ma and the current in the extracted beam was approximately 100 μamp. The potential difference between the dees under these conditions was 140 kv.

In this same year Kruger and his colleagues published a report on an interesting version of the cyclotron [14]. The deflection system made it possible to extract the beam of charged particles in a direction parallel to the slit between the dees. Under these conditions the magnet yoke does not hinder the extraction of the beam and the installation of an analyzing magnet. Setting up a potential difference of 150 kv between the dees, the authors accelerated deuterons to 10 Mev and obtained an extracted beam current of 100 μamp. In this apparatus the first attempt was made to obtain a monochromatic extracted beam of charged particles from a cyclotron. For this purpose use was made of an analyzing magnet which deflected the beam through an angle of 51°; collimating slits were set up in front of and in back of the magnet. The authors obtained a deuteron beam with an energy spread of 0.1 %.

In 1946 Tobias and Segre accelerated C_{12}^{+6} ions to an energy of 96 Mev at the Berkeley cyclotron. After several months York et al., using this same apparatus, accelerated ions of both carbon isotopes (C_{12}^{+6} to 135 Mev with a current of 10^5 ions/sec and C_{13}^{+6} to 146 Mev with a current of 10^3 ions/sec).

In 1947 the one-and-a-half meter cyclotron of the Institute for Atomic Energy, Academy of Sciences, USSR was started up [15] (Fig. 7). To reduce ion bunching, in 1950 a long ridge was added to the dees, thereby reducing the geometric dimensions of the electric-field region close to the source.

In this same cyclotron use was made, for the first time, of a deflection system with an inhomogeneous electric field which, in addition to deflecting the beam of charged particles, provided focussing in the horizontal direction. Later, calculations were carried out on deflection systems with electrodes of hyperbolic cross section. These calculations are used as a basis for the design of deflection systems for cyclotrons being built in the USSR. Use was also made of additional windings, connected in opposition, on the pole pieces of the magnet which, without disturbing the resonance conditions, made it possible to shift the median plane of the magnetic field upward or downward depending on the current in the windings. This system facilitates considerably the adjustment of the median plane of the magnetic field of the cyclotron.

In 1952, R. Livingston [16] published a description of the largest cyclotron in the world, built at Oak Ridge. With this machine a record proton energy was achieved – 24 Mev (the particle current at the terminal radius was 1 ma). The machine was built specially for work with internal targets.

Since this cyclotron was intended only for proton acceleration (low field intensity),in spite of the large pole-piece diameter (2100 mm) the magnet weighs only 250 tons. The magnet is C-shaped. In order to avoid collapse of the posts to which the dees are fastened, instead of using the usual (horizontal) configuration the accelerator chamber is placed between the poles of the magnet in a vertical position (Fig. 8).

The potential difference between the dees is 440 kv. In order to avoid electrical breakdown in the accelerator chamber at these high voltages, the dees are also connected to a fixed negative potential of 1000 volts. This is possible through the use of support rods insulated from the tank of the resonance line. To solve this problem Livingston departed from the use of two coaxial resonant lines, placing the supports for both dees in a common tank. To reduce the level of induced activity in this apparatus, for the first time use was made of graphite shielding on the inner surfaces of the dees which are suceptible to bombardment by the accelerated particles.

This cyclotron may well be considered the prototype of semi-industrial cyclotrons used for manufacture of radioisotopes.

In this same year a paper was published on the Birmingham cyclotron [17], the construction of which was started before the war under the leadership of Oliphant. In this cyclotron ions of molecular hydrogen and deuterons were accelerated to an energy of 25 Mev. The current at the terminal radius was 16 μamp. The

energy which was achieved represented a record for the one-and-a-half meter cyclotron. However, because of the difficulty of deflecting the beam, it was necessary to reduce the deuteron energy to 20 Mev. Under these conditions the particle current at the terminal radius was 350 μamp and in the deflected beam 70 μamp.

To eliminate the background of radiation from the cyclotron itself the beam of charged particles is extracted, by means of a supplementary magnet, through the main shielding into a special installation (at a distance of about three meters from the cyclotron). The current density at the target reached 1 μamp/ cm^2 with an energy spread of approximately 1% in the beam.

In 1952 Atterling and Lindstrom [18] reported on a cyclotron with a pole diameter of 2250 mm (Fig. 9). The construction of this cyclotron had been started in 1945. This machine was essentially the same as the machine at Oak Ridge but the accelerator chamber was in the horizontal position while the magnet (weight 430 tons) made it possible to obtain a larger induction in the space between the pole pieces. Deuterons have been accelerated to 25 Mev in this machine. The current at the terminal radius is 100 μamp. The cyclotron was designed for work with internal targets and was later used to accelerate multiply-charged ions.

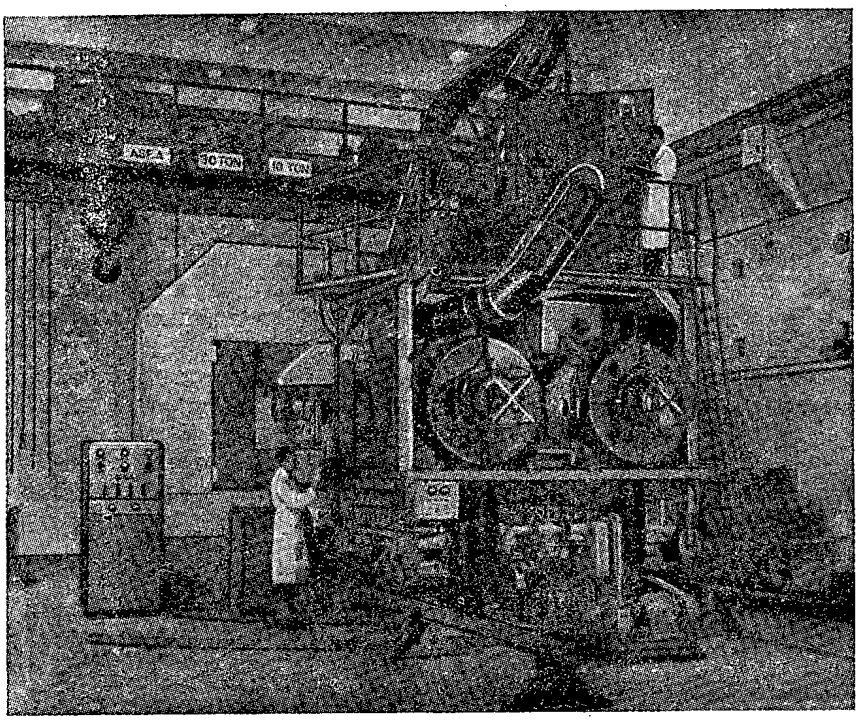

Fig. 9. Stockholm cyclotron with a pole piece diameter of 2250 mm.

In that same year, Bender et al. [19] published an original solution to the problem of extracting a beam of charged particles to a large distance from the cyclotron. The authors used two rotatable magnets. The first magnet was used to focus the particles and to analyze them by energy. This system made it possible to obtain an intermediate focus point at which it was possible to set up a movable diaphragm to collimate the beam. The energy spread in the proton beam (energy 8 Mev) was 0.1% while the particle current was 1 μamp. In the experimental chamber, in which the target was located, there was an additional magnet for energy analysis of products resulting from the reactions between protons and the target.

In 1953 Walker and Fremlin [20] reported on a new method for accelerating multiply charged ions based on the fact that in a cyclotron it is possible to accelerate simultaneously ions whose rotational frequencies are odd multiples. Thus, for example, it is possible to accelerate simultaneously sextuply charged and doubly charged

ions. In the course of acceleration, the doubly charged ions lose electrons as a result of "peeling" on the residual gas. The sextuply charged ions thus formed are then accelerated to the terminal radius. This method was used at the Birmingham cyclotron to accelerate C_{12}^{+6} ions to energies of the order of 120 Mev. A shortcoming of the method is the small current of accelerated particles which can be obtained and the large energy spread in the ions of the beam because of the large dimensions of the region in which the sextuply charged ions are formed.

In research on a number of problems in physics one requires a considerable reduction in the radiation background produced by the cyclotron itself at the location of the detection apparatus. This is achieved by locating the target and the detection apparatus in a special installation (experimental chamber) which is protected by shielding walls. Under these conditions the diverging beam extracted from the cyclotron chamber must be focussed on the target. At first this focussing was accomplished by means of a double focussing magnet, located in the neighborhood of the main magnet of the cyclotron. With the appearance of quadrupole magnetic lenses the problem of small aperture beam focussing for non-monochromatic beams was simplified considerably because of the flexibility of this type of system. At the same time, in working with quadrupole lenses, in neutron experiments it has become customary to use magnets which are set up in the cyclotron chamber; with these it is possible to bend the beam so that the irradiated target becomes "invisible," thereby removing a basic source of background radiation.

In 1954 R. Livingston reported data on a cyclotron (pole face diameter of 1580 mm) designed for obtaining intense beams of multiply-charged ions [21]. A slit ion source, developed by the author in 1949-1952, was employed. The resonance circuit was similar to that of the Oak Ridge cyclotron (Fig. 10). The capacity of the vacuum pumps was 12,000 liters/sec. This machine was designed as a model for a cyclotron with a pole diameter of 2500 mm in which it is proposed to accelerate multiply charged ions.

In the same year Schmidt et al. reported on a one-and-a-half meter cyclotron at the University of Washington [22]. The design of the machine was started in 1948 and in 1952 ions of molecular hydrogen were accelerated to 21 Mev at a current of 125 μamp at the terminal radius. The potential difference between the dees is 220-250 kv. Especially noteworthy are the planning of the cyclotron laboratory, the spacious experimental chamber for work with remote targets, and the excellent shielding against radiation.

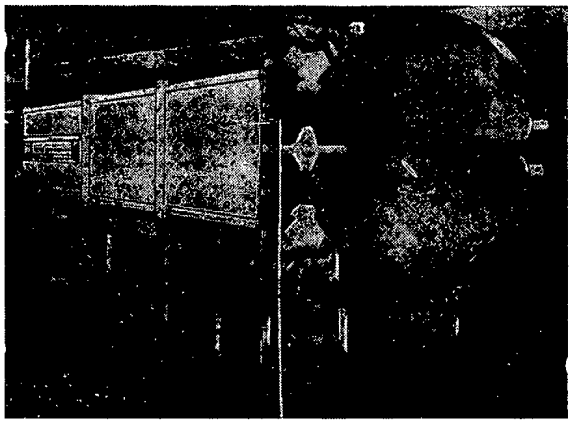

Fig. 10. Resonance circuit of the Oak Ridge cyclotron (diameter 1580 mm) built as a model of a larger cyclotron to be used for accelerating multiply-charged ions.

In 1955 Karo, Martin and Rose published information on the Melbourne variable-energy cyclotron with which protons can be accelerated to 2-12.5 Mev and deuterons to 4-6.3 Mev. To cover this wide frequency range the variable condenser is located at the point at which the dee is connected to the support rod of the resonance line. Reliable high frequency contact is provided by a hydraulic system. To improve the distribution of radio-frequency voltage along the accelerating slit, a scheme with one dee was chosen; the rod for the resonance line is at the center of this dee. Because the edges of the chamber cover are rounded it is possible to work without noticeable saturation effects at high fields. The radiofrequency potential with respect to ground is 100 kv. The weight of the magnet is 45 tons. As yet no data on the operation of the apparatus as a whole is available.

Thornton et al. [23] (University of California) have designed a cyclotron with a pole diameter of 2250 mm. The machine is designed to provide monoenergetic neutrons in the energy region from 2 to 30 Mev. With appropriate values of the magnetic field and adjustment of the frequency of the rf generator (which can be

carried out without disturbing the vacuum) the cyclotron can accelerate protons to energies ranging from 2.6 to 14 Mev, deuterons from 5.2 to 12.5 Mev, and tritons from 7.7 to 8.3 Mev. Another feature of this cyclotron is the special shape of the magnet pole pieces which reduces considerably the divergence of the deflected beam.

The correction of the magnetic field in this cyclotron is accomplished by means of special coils. The accelerator chamber has one dee (potential 170 kv). At the location of the second dee there is a system which deflects the beam of charged particles to a considerable distance from the terminal radius. The beam extracted from the cyclotron has an intermediate focal point which makes it possible (with some loss of intensity) to obtain a monochromatic beam of particles on a remote target which is located behind the shield, in a special experimental chamber.

Another interesting cyclotron is that at Los Alamos (pole diameter 105 cm) [23]. This machine was moved from Harvard University and reconstructed as a variable-energy cyclotron (proton energy 3.5-9 Mev, deuterons 7-17.5 Mev, and tritons 10.5-12 Mev).

This cyclotron makes use of a modification of an azimuthal variation in magnetic field as proposed by Thomas. 350° iron sectors are located inside the vacuum chamber (at the top and bottom). This apparatus provides "strong focussing" starting at the small acceleration radii and provides additional axial stability and tends to center the beam. In this way a certain reduction of the dee threshold voltage is obtained. One of the three sectors is located in front of the deflection system; this arrangement tends to increase the radial deflection of the ion beam. As reported by the authors, the weakening of the magnetic field in the azimuthal direction facilitates extraction of the beam and reduces considerably the voltage required for the deflection system. Iron wedges of appropriate shape reduce divergence of the extracted beam as it passes through the fringing field of the magnet. The final focussing of the beam is accomplished by means of quadrupole magnetic lenses. An additional analyzing magnet is used to steer the beam to the right or to the left. Two magnets, placed in front of the quadrupole lenses are used to obtain small displacements of the beam as a whole in the horizontal and vertical directions. Energy analysis is carried out by means of a system of slits located on both sides of the analyzing magnet. The magnetic field corrections for the cyclotron are realized by means of special coils which are located both in the vacuum chamber as well as in the space between the pole pieces of the magnet and the chamber covers. The focussed beam passes through the main field into the experimental chamber in which the target being investigated is installed. At the terminal radius of this cyclotron currents of the order of 2 ma are obtained for protons, deuterons, and tritons. The maximum current in the external beam is 100 μ amp.

A number of improvements have been incorporated into the one-and-one-half meter cyclotron at the Institute for Atomic Energy, Academy of Sciences, USSR between 1951 and 1956 [15].

To carry out experiments in which fast-neutron energies are determined by time-of-flight methods, stabilization systems have been installed for the dee potentials, frequency of the resonance system, and the voltage applied to the deflection system.

Azimuthal correction of the magnetic field is carried out by movable iron elements in the gap between the pole pieces and the cover by means of remote control from the control panel. In addition to accelerating protons, deuterons and α-particles, this cyclotron has been used to accelerate multiply charged ions of carbon, nitrogen and oxygen. An extremely effective source of multiply-charged ions [24] has been developed for use with this cyclotron.

To control the cyclotron during operation a number of special pickup units and probes, which are remotely controlled, have been developed. All the basic control operations for the machine are carried out at a central control console. The physics studies are carried out behind the main shielding wall in an experimental chamber; the beam of charged particles extracted from the cyclotron chamber comes to a focus at this point.

A new type of cyclotron machine (pole diameter 1200 mm) designed for university laboratories was developed in 1956 in the USSR. The deflection system used in this cyclotron which employs electrodes of hyperbolic cross section, makes it possible to extract virtually the entire deflected beam of charged particles to a distance of several meters, using small-aperture magnetic quadrupole lenses.

At the Geneva Conference in 1955, Lawrence reported on experiments carried out with electron models of a cyclotron with a magnetic field varying in the azimuthal direction.* The design of this

* This work was published in 1956 [25].

accelerator is based on the work by Thomas mentioned above.

Experiments carried out with a model using "clover-leaf" pole pieces offer convincing evidence of the possibility of constructing a fixed frequency cyclotron which will make it possible to accelerate charged particles to energies such as are obtained in presently available proton-synchrotrons but with much higher particle currents (the order of several milliamperes). The problem of deflection and extraction of the charged particle beam in a cyclotron of this type will be considerably easier, thus making it possible to achieve a particle extraction coefficient of 90% as compared with 5-7% in the proton-synchrotron.

In conclusion, we may expect that the cyclotron, used as an accelerator, will serve as one of the work horses of nuclear physics for a long time to come.

LITERATURE CITED

[1] E. O. Lawrence and N. E. Edlefsen, Science 72, 376 (1930).

[2] E. O. Lawrence and D. Cooksey, Phys. Rev. 50, 1131 (1936).

[3] E. O. Lawrence and D. Cooksey, Phys. Rev. 86, 411 (1937).

[4] V. N. Rukavishnikov, Phys. Rev. 52, 1077 (1937).

[5] J. R. Dunning and H. L. Anderson, Phys. Rev. 53, 334 (1938).

[6] M. E. Rose, Phys. Rev. 53, 675 (1938); 53, 715 (1938).

[7] Ia. L. Khurgin, Doklady Akad. Nauk SSSR 19, 5, 237 (1938).

[8] R. R. Wilson, Phys. Rev. 53, 213 (1938); 53, 408 (1938); 54, 240 (1938).

[9] L. N. Thomas, Phys. Rev. 54, 580 (1938); 54, 588 (1938).

[10] V. I. Veksler, Doklady Akad. Nauk SSSR 43, 363 (1944); 44, 393 (1944); E. M. Mc Millan, Phys. Rev. 68, 143 (1945).

[11] E. O. Lawrence et al., Phys. Rev. 56, 124 (1939).

[12] R. R. Wilson, J. Appl. Phys. 11, 12, 781 (1940).

[13] M. S. Livingston, J. Appl. Phys. 15, 2, 128 (1949).

[14] P. G. Kruger et al., Rev. Sci. Instr. 15, 333 (1944).

[15] L. M. Nemenov, S. P. Kalinin, L. F. Kondrashev, E. S. Mironov, A. A. Naumov, V. S. Panasiuk, N. D. Fedorov, N. N. Khaldin, and A. A. Chubakov, J. Atomic Energy (USSR) 2, 36 (1957).*

[16] R. S. Livingston, Nature 170, 4319, 221 (1952).

[17] Nature 169, 4299, 476 (1952).

[18] H. Atterling, and G. Lindström, Nature 169, 4298, 432 (1952).

[19] R. S. Bender et al., Rev. Sci. Instr. 23, 542 (1952).

[20] D. Walker and J. H. Fremlin, Nature 171, 189 (1953).

[21] R. S. Livingston, Nature 173, 54 (1954).

[22] F. H. Schmidt et al., Rev. Sci. Instr. 25, 499 (1954).

[23] R. L. Thornton et al., "Cyclotrons designed for precision fast neutron cross section measurements," (Report No. 584 presented by the U. S. Delegation to the International Conference on the Peaceful Uses of Atomic Energy, Geneva, 1955).

* See C. B. Translation.

[24] P. M. Morozov, B. N. Makov, and M. S. Ioffe, J. Atomic Energy (USSR) 2, 272 (1957).*

[25] B. H. Smith, and K. R. Mac Kenzie, Rev. Sci. Instr. 27, 485 (1956); L. Ruby, M. Heusinkveld et al., Rev. Sci. Instr. 27, 490 (1956); E. L. Kelly, R. V. Pyle et al., Rev. Sci. Instr. 27, 493 (1956).

Received May 21, 1957.

* See C. B. Translation.

ALLOWABLE FREQUENCY MULTIPLICATION RATIOS IN SYNCHROTRONS

E. M. Moroz and M. S. Rabinovich

The energy dependence of the amplitude of synchrotron oscillations due to radiation fluctuations is investigated. A simple stationary solution for the phase equation is obtained; this equation can be applied, with accuracy sufficient for practical purposes, to all large synchrotrons. It is shown that in accelerating electrons to energies to several millions of electron volts the value of the maximum allowable frequency multiplication is sharply limited and is determined by the limiting amplitude of the accelerating voltage. *

In the design of electron accelerators intended for high energies, the choice of the radiofrequency multiplication ratio is very important. In the present paper this problem is considered with regard to the deleterious effects of synchrotron oscillations produced by fluctuations in the electron radiation at high energies.

The linearized equation for the radial synchrotron oscillations is of the form

$$\ddot{y} + \rho\dot{y} + \Omega^2 y = g(t). \tag{1}$$

The frequency of the synchrotron oscillations Ω and the damping factor ρ are determined by the expressions

$$\Omega = \omega \sqrt{\frac{qKeV \sin \psi_s}{2\pi E_s}}, \tag{2}$$

$$\rho = \frac{3-4n}{1-n}\frac{P}{E_s} + \frac{E_s}{E_s}, \tag{3}$$

where ψ_s and E_s are the equilibrium phase and energy, ω is the electron rotation frequency, q is the radiofrequency multiplication ratio, n is the magnetic field index, P is the power associated with the electron radiation as averaged over 1 revolution (it is assumed that there is no radiation in the straight sections of the race track), i.e.,

$$P = \frac{2ce^2}{3R_s^2}\frac{\gamma^4}{1+\lambda}, \tag{4}$$

---

* Certain results of the present work are similar to the conclusions reached in [5] which appeared recently (note added in proof).

where

$$\gamma = \frac{E_s}{mc^2} = \frac{1}{\sqrt{1-\beta^2}}, \tag{5}$$

$$\lambda = \frac{Nl}{2\pi R_s} \tag{6}$$

(l is the length of a straight section, N is the number of sections, R_s is the equilibrium radius). Finally

$$K = \frac{1}{(1-n)(1+\lambda)}. \tag{7}$$

In all cases of practical interest the following inequality is satisfied:

$$\rho^2 \ll \Omega^2. \tag{8}$$

The problem is essentially that of finding a solution for Equation (1) in the case in which the external force g(t) is the effect of the radiation fluctuations. After finding the amplitude of the radial synchrotron oscillations A_y it is an easy matter to compute the amplitude of the phase oscillations A_ψ using the formula

$$\frac{A_y}{R_s} = \frac{A_\psi}{\beta^2 (1-n) qK} \frac{\Omega}{\omega} \tag{9}$$

or, taking account of (2) and (7),

$$A_\psi^2 = A_y^2 \frac{2\pi q (1-n)}{(1+\lambda) R_s^2} \frac{E_s}{eV \sin \psi_s}, \tag{10}$$

The expression for the mean square fluctuation amplitude $\langle A_\psi^2 \rangle$ given in [1] is rather complicated. However, it can be shown that in accelerators designed for high electron energies this solution is not significantly different from the simpler stationary solution

$$\langle A_\psi^2 \rangle = \frac{55\sqrt{3}\,\pi\hbar c q \gamma^3 F_1}{24 (1+\lambda)^2 (3-4n) R_s eV \sin \psi_s}, \tag{11}$$

where

$$F_1 = \left(1 + \alpha \frac{1-n}{3-4n} \frac{\dot{E}_s}{P}\right)^{-1}, \tag{12}$$

and α is of a factor of the order of unity.

The criterion for applying the solution in (11) is that the quantity $\langle A_\psi^2 \rangle$ change insignificantly during the course of the so-called damping time τ:

$$\frac{\tau V \sin \psi_s}{F_1 \gamma^3} \frac{d}{dt} \left(\frac{F_1 \gamma^3}{V \sin \psi_s}\right) \ll 1, \tag{13}$$

where

$$\tau = \frac{1}{\rho + \frac{\dot{\Omega}}{\Omega}}. \tag{14}$$

In addition the exact solution (10) which applies to the instant of time t must be approximated by the stationary Solution (11), i.e.,

$$\frac{\tau}{t} \ll 1. \tag{15}$$

After substituting the appropriate expressions in Equation (13) it is found that if (15) is satisfied, (13) is also satisfied. Thus, the expression in (15) is the single requirement which must be satisfied if simple formula given in (11) is to be applied. Estimates show that Equation (11) is satisfied for all large electron accelerators.

In deriving Equation (11) we have used the property of the oscillation equation that the amplitude of the stationary solution of Equation (1) coincides with the amplitude of the forced oscillations which satisfy the equation when damping is not taken into account:

$$\ddot{y}_1 + \Omega^2 y_1 = g_1(t); \quad g_1(t) = \begin{cases} 0 & \text{for } t < 0 \\ g(t) & \text{for } t > 0 \end{cases} \tag{1a}$$

at the instant of time t_1, where t_1 depends on the nature of the external force $g(t)$. In the case of resonant blow-up $g(t) = g_0 \cos \Omega t$ the coincidence of the solutions occurs at the instant $t_1 = 2\tau$, while in the case of blow-up due to a driving force with random impulses

$$g(t) = a\left[\sum_i \varepsilon_i \delta(t - t_i) - \int P\, dt\right] \tag{16}$$

the coincidence of the solutions of Equations (1) and (1a) occurs at the instant of time

$$t_1 = \tau. \tag{17}$$

Thus,

$$\langle A_y^2 \rangle = 2\langle y^2 \rangle = 2\tau \frac{d\langle y^2 \rangle}{dt}. \tag{18}$$

The equality on the left of Equation (18) is an obvious relation between the mean square deflection y and the mean square amplitude of the oscillation A_y.

Further, we can make use of the fact that in a weak-focussing accelerator the driving force $g(t)$ in the synchrotron oscillation equation coincides with the driving force in the betatron oscillation equation. Actually, in the emission of a photon by the accelerated electron $\hbar\omega_i = \epsilon_i$ the deviation of the instantaneous orbit from the equilibrium orbit is changed by an amount

$$\Delta y = \frac{R_s}{1-n} \frac{\varepsilon_i}{E_s},$$

it is precisely by this same quantity that the electron is deflected from its instantaneous orbit. Consequently, the quantity $\frac{d\langle y^2 \rangle}{dt}$, as computed from Equation (1a), should be the same for both synchrotron and betatron

oscillations. Hence we can make use of the solution for blow-up due to betatron oscillations

$$\frac{d\langle y^2\rangle}{dt} = \frac{55}{48\sqrt{3}} \frac{e^2\hbar}{m^2c^2} \frac{1}{(1-n)^2(1+\lambda)^2} \frac{\gamma^5}{R_s}, \tag{19}$$

obtained (without taking account of radiation damping) by Sokolov and Ternov [2] using a correction factor $\frac{1}{(1+\lambda)^2}$ which takes into account the fact that the electron radiation in the race track occurs only in the curved section of the trajectory. Substituting Equations (19), (18), and (14), into Equation (9) we obtain the equation being sought, Equation (11). In the absence of a rotational electric field

$$eV\cos\psi_s = \frac{2\pi(1+\lambda)}{c} R_s(P+\dot{E}_s) \tag{20}$$

and (11) assumes the form*

$$\langle A_\psi^2\rangle = \frac{55\sqrt{3}}{32} \frac{\hbar cq\,\mathrm{ctg}\,\psi_s}{e^2(1+\lambda)^2(3-4n)} \frac{F_1F_2}{\gamma}, \tag{21}$$

where

$$F_2 = \left(1+\frac{E_s}{P}\right)^{-1}. \tag{22}$$

Equation (21) differs from the expression obtained by Sands [3] in the presence of the factor F_1F_2 which although equal to unity at high energies plays an important role at energies of several hundreds of millions of electron volts and in essence determines the energy dependence of $\langle A_\psi^2\rangle$.

In the case $\cot\psi_S = \text{const}$, the curve $\langle A_\psi^2\rangle = F(\gamma)$ has a maximum which corresponds to the condition

$$P = 7\dot{E}_s \quad \left(\alpha\frac{1-n}{3-4n} \approx 1\right) \tag{23}$$

or

$$\gamma^4 = \frac{21}{2}\frac{mc}{e^2}(1+\lambda)R_s^2\dot{\gamma}. \tag{24}$$

In this case it turns out that $\frac{\tau}{t} = \frac{1}{8}$ and, consequently, at the maximum of the curve $F(\gamma)$ the stationary Solution (21) is a good approximation. At the maximum (23) the value of $\langle A_\psi^2\rangle$ is

$$\langle A_\psi^2\rangle_{\max} = \frac{385}{1024}\frac{3^{1/4}7^{1/4}}{2^{3/4}}\frac{\hbar c^{3/4}}{e^{3/2}m^{1/4}} \times \times \frac{q\,\mathrm{ctg}\,\psi_s}{(1+\lambda)^{5/4}(3-4n)R_s^{1/2}(\dot{\gamma})^{1/4}}. \tag{25}$$

The simple case being considered, $\cot\psi_S = \text{const}$, is not an optimum case. Furthermore, analysis of Equation (21) indicates that there is no real danger of particle loss due to the maximum in $\langle A_\psi^2\rangle$. By using a more rapid rate-of-rise for the accelerating voltage as compared with the V(t) function required for the condition

* 'tg' ≡ 'tan,' 'ctg ≡ 'cot' – Publisher.

cot ψ_s = const, it is easy to avoid the above-mentioned maximum. To obtain the highest allowable multiplication ratio it is necessary that the following inequality be satisfied during the entire acceleration cycle:

$$\langle A_\psi^2 \rangle < \langle A_\psi^2 \rangle_f, \tag{26}$$

where the index f denotes the end of acceleration. The relation in (26) is satisfied if the change of amplitude of the accelerating voltage satisfies the condition

$$V^2 \geqslant (V \sin \psi_s)_f^2 \left(\frac{\gamma_i}{\gamma_f} \right)^6 F_1^2 + \frac{4\pi^2 R_s^2 (1+\lambda)^2}{c^2} P^2 F_2^2 \tag{27}$$

In particular, if V = const the quantity $\langle A_\psi^2 \rangle$ increases monotonically during the acceleration process.

To keep a large part of the electrons to the end of acceleration it is necessary that the quantity $\langle A_\psi^2 \rangle^{1/2}$ be small as compared with the dimensions of the separator. An estimate of the allowable value of $\langle A_\psi^2 \rangle^{1/2}$ can be obtained from a solution of the Einstein-Fokker equation considering as lost all those particles which strike the edge of the separator. A similar problem has been considered by Blachman and Courant [4] in treating the scattering of particles on the residual gas in an accelerator chamber. In applying the solution obtained in that work to the present problem we arrive at an expression of the form

$$W = 2 \sum_{s=1}^{\infty} \frac{1}{\lambda_s J_1(\lambda_s)} \exp\left(-\frac{\lambda_s}{4} \frac{\langle A_\psi^2 \rangle}{d^2} \right), \tag{28}$$

where λ_s is the s-th root of the Bessel function $J_0(x)$; W is the probability that a particle does not go beyond the limits of a region, the limits of which are equal to the distance d from the equilibrium phase to the closest edge of the separator:

$$d \approx \psi_s \sqrt{2}. \tag{29}$$

In the majority of cases we need consider only one term in the summation in (28):

$$W = \frac{2}{\lambda_1 J_1(\lambda_1)} \exp\left(-\frac{\lambda_1^2}{4} \frac{A_\psi^2}{d^2} \right) = \\ = 1.6 \exp\left(-1.44 \frac{\langle A_\psi^2 \rangle}{d^2} \right). \tag{30}$$

In practice Equation (30) applies up to the point at which values W < 1. obtain. Under the condition that

$$\langle A_\psi^2 \rangle < 0.32 d^2, \tag{31}$$

with reasonable accuracy we may assume that W = 1. The relation given in (31) may be taken as a criterion for keeping the majority of accelerated particles. Substituting Equations (21) and (29) into Equation (31) and taking account of the fact that at the end of acceleration $(F_1 F_2)_f = 1$, we obtain a formula for the maximum allowable multiplication ratio of the radiofrequency:

$$q \leqslant 0.21 \frac{e^2}{\hbar c} (1+\lambda)^2 (3-4n) \gamma_f (\varphi_s^2 \operatorname{tg} \psi_s)_f. \tag{32}$$

It is apparent that the value of the allowable ratio depends on the position of the phase point ψ_s at the end of acceleration. The larger the accelerating voltage the larger the value of the multiplication ratio that

can be used without risk of particle loss. The relation between the accelerating voltage and the radiofrequency multiplication ratio becomes especially clear if we use the asymptotic expression

$$\frac{1}{\cos\varphi} = \frac{4}{\pi} + \frac{4}{\pi^2}\varphi^2 \operatorname{tg}\varphi, \tag{33}$$

which applies with good accuracy over the entire range of variation of the quantity being considered $1 < \frac{1}{\cos\varphi} < \infty$. Substituting Equation (33) in Equation (32) we find

$$\frac{1}{\cos\psi_s} \geqslant 1.27 + 0.13\frac{q}{(1+\lambda)^2(3-4n)E_{\text{Bev}}}. \tag{34}$$

It is difficult to satisfy the condition given in (34) in accelerators with high radiofrequency multiplication ratios and weak focussing; if this condition is not fulfilled it is possible that a rather large fraction of the particles will not be trapped in the acceleration cycle.

LITERATURE CITED

[1] A. A. Kolomenskii and A. N. Lebedev, Supplement No. 4, J. Atomic Energy (USSR) 1957, p. 31.*

[2] A. A. Sokolov and I. M. Ternov, Doklady Akad. Nauk SSSR 97, 823 (1954).

[3] M. Sands, Phys. Rev. 97, 470 (1955).

[4] N. M. Blachman and E. D. Courant, Phys. Rev. 74, 140 (1948).

[5] A. N. Dedenko, J. Tech. Phys. 27, 1624 (1957).

Received July 17, 1957.

* Original Russian pagination. See. C. B. Translation.

γ-RAY SPECTRA EXCITED IN INELASTIC SCATTERING OF FAST NEUTRONS ON MANGANESE, ALUMINUM, IRON, COPPER, TIN, AND ANTIMONY*

I. F. Barchuk, M. V. Pasechnik, and Iu. A. Tsybul'ko

The study of inelastic scattering of fast neutrons is an important problem of both theoretical and practical interest. From the theoretical point of view the importance of this work lies in the possibility of obtaining data concerning levels in stable nuclei. The practical value arises in connection with the important role played by inelastic scattering of neutrons in fast-neutron reactors as well as the fact that the extension of reactor theory to fast-neutron reactors requires data on the spectra of inelastically scattered neutrons [1, 2]. In this connection the necessity for developing a neutron spectrometer for fast neutrons and γ-spectroscopy for inelastic neutron scattering is obvious. In the last 5-7 years a great deal of work has been devoted to this problem.

The present work reports on measurements of γ-ray spectra excited in inelastic scattering of 2.8 Mev neutrons by manganese, aluminum, iron, copper, tin and antimony. The measurements were carried out with a scintillation spectrometer consisting of an NaI(Tl) crystal, a FEU-1B photomultiplier and a 50-channel pulse-height analyzer with a magnetic-drum memory. The spectrometer resolution was 6.5-7% for γ-rays from Co^{60}. γ-Rays of the following energies (Mev) were found: in manganese 0.97, 1.41, 1.92, 2.3; in aluminum 0.84, 1.00, 1.80, 2.16; in iron 0.84, 1.25, 1.46, 1.70; in copper 0.63, 0.78, 0.96, 1.12, 1.38, 1.46, 1.72, 2.03; in tin 0.84, 1.16, 1.50, 1.80, 2.16; in antimony 1.04, 1.50, 1.84, 2.16.

The present paper is devoted to a description of experiments in which studies were made of the γ-spectra excited in inelastic scattering of 2.8 Mev neutrons on manganese, aluminum, iron, copper, tin and antimony.

The measurements of the γ-spectra excited in inelastic neutron scattering were performed with the apparatus shown in Fig. 1. The neutrons were obtained by means of the D(d, n)He^3 reaction using a low-voltage accelerator operating at voltages of 140-150 kv. The deuteron beam, with a current strength of 100-110 μ amp, bombarded an aluminum hemisphere 40 mm in diameter with walls 0.3 mm in thickness. The hemisphere was the end of the target part of the accelerator vacuum system. As a result of deuteron occlusion in the aluminum a deuterium target was obtained. The intensity of the neutron source was 200-300 μ curies radon beryllium equivalent. The target part of the apparatus was fabricated from a thin-walled duraluminum tube 50 mm in diameter and 190 cm long. Thus the target was at a distance of 2-3 meters from all massive elements of the accelerator and walls, ceiling, and floor of the installation. With this arrangement in the target part of the apparatus the neutron source emitted a negligibly small amount of γ-radiation as compared with the other targets.

---

* Abbreviated version of a paper appearing in the "Ukrainian Journal of Physics."

The scintillation spectrometer consisted of an NaI(Tl) crystal 60 mm in diameter and 50 mm high and a FE U-1B photomultiplier. The photomultiplier and crystal were located inside a thin-walled cylindrical container of sheet iron as protection against light.

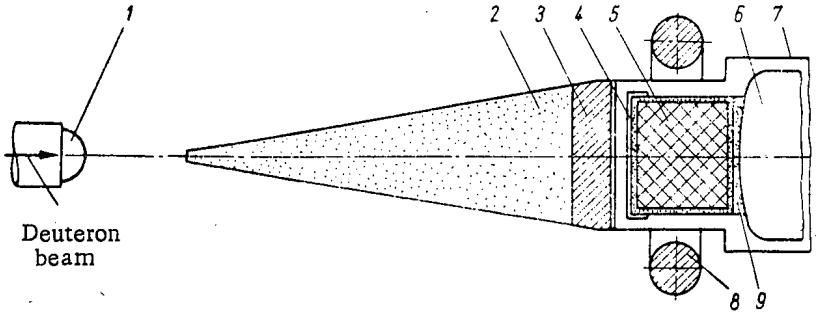

Fig. 1. Diagram of the experiment. 1) Target; 2) paraffin plus boron; 3) lead; 4) manganese oxide; 5) NaI(Tl) crystal; 6) FEU-1B photomultiplier; 7) case; 8) toroidal scatterer; 9) glass.

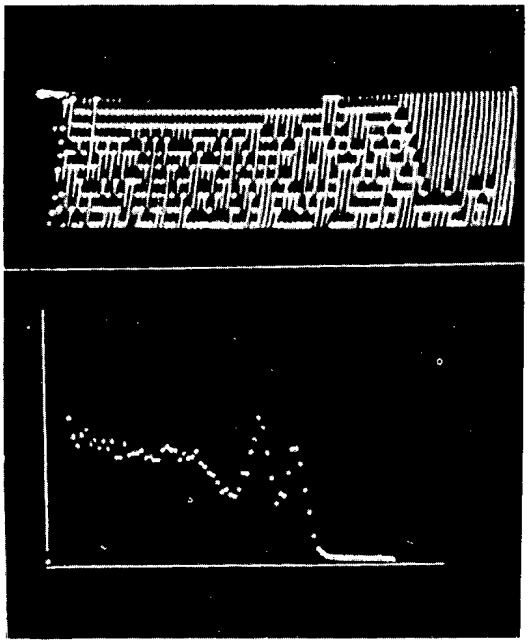

Fig. 2. γ-Ray pulse spectrum emitted by a Co^{60} sample. Upper photograph – pulse spectrum in a binary system; lower photograph – pulse spectrum in a linear system.

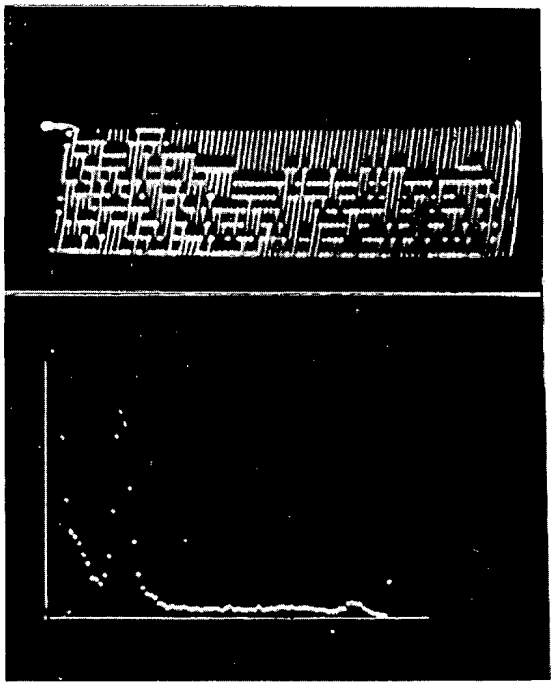

Fig. 3. γ-Ray pulse spectrum emitted by a Sb^{124} sample. Upper photograph – pulse spectrum in a binary system; lower photograph – pulse spectrum in a linear system.

The pulses from the photomultiplier were fed to a preamplifier, amplifier and the multi-channel pulse height analyzer. The pulse analyzer, with a magnetic-drum memory [3], made it possible to use 50 or 80 channels with a capacity of 2^{17} or 2^{11} pulses per channel, respectively. The pulse spectrum was observed in binary and linear systems by means of two cathode-ray tubes. The time resolution of the analyzer was 1.5μ sec; the departure from linearity of the amplitude characteristic was less than 1% for a pulse height of 50 volts. The amplifier of the spectrometer was linear to better than 0.25% for a pulse height of 80 volts. To obtain the best resolution and linearity for γ-ray energies up to 3 Mev, the optimum operating conditions for the FEU-1B were determined experimentally [4]. All units of the spectrometer were fed by electronically stabilized power supplies. A detailed description of the circuit and adjustment of the spectrometer will be given in a separate paper.

In Figs. 2 and 3 are shown photographs of the pulse spectra obtained with the spectrometer crystal irradiated by γ-rays from Co^{60} (γ-ray energy of 1.17 and 1.33 Mev) and Sb^{124} (γ-ray energy of 0.60 and 1.68 Mev [5]) with 80 channels in operation and a discriminator threshold applied to fifteen channels. In the upper parts of these figures are shown photographs of the pulse spectra in the binary system; the bottom part shows the spectra in the linear system. As is apparent from Fig. 2 the energy resolution of the spectrometer is approximately 6.5-7% for γ-rays from Co^{60}. To shield the spectrometer crystal from the direct neutron beam and γ-rays from the target use was made of a truncated cone, the upper part of which was made from paraffin (95 %) with a mixture of amorphous boron (5%); the lower part was made from lead. The paraffin cone was 25 cm high and 12 to 80 mm in cross section diameter while the lead was 5 cm high and 80 to 90 mm in cross-section diameter. The addition of boron to the paraffin reduced considerably the background of γ-rays produced by radiative capture of neutrons in the paraffin.

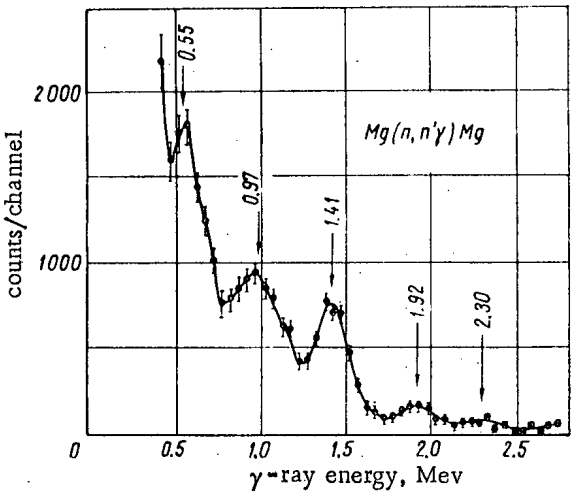

Fig. 4. γ-Ray pulse spectrum produced in inelastic scattering of 2.8 Mev neutrons on manganese.

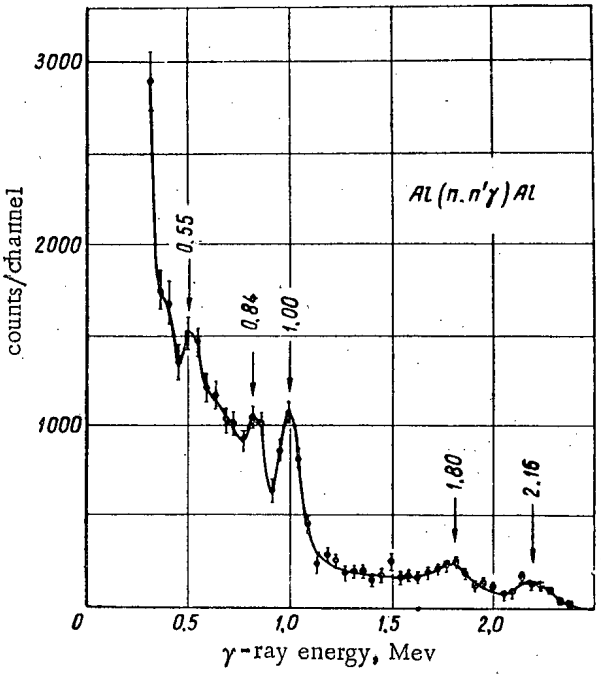

Fig. 5. γ-Ray pulse spectrum produced in inelastic scattering of 2.8 Mev neutrons on aluminum.

The scatterer was a toroid made from the element being investigated, 130 mm in diameter and with a cross-section diameter of 20-30 mm (the thicker scatterers were those of the light element).

The spectrometer, shield cone and scatterer were attached to the ceiling and walls of the installation by steel rods which were coaxial with the deuteron beam so that the distance from the target to the center of the crystal was 40 cm. Using this experimental geometry the neutrons and γ-rays which reached the center of the crystal from the scatterer were scattered at an angle of 100°.

The neutron flux was monitored by means of an aluminum AS-1 β-counter to which was attached a silver cylinder 10 mm in diameter, 50 mm high and with a wall thickness of 0.3 mm. The counter and this cylinder were placed inside a cylinder of paraffin 30 cm in diameter and 30 cm high along its axis. Readings were made for electrons with short half lives (24.2 seconds and 2.3 minutes) produced in the silver upon neutron absorption. The operation of the monitor was checked by comparison with readings of an "all-wave" boron counter. The comparison indicated that the ratio of counts for these two counters was within the limits of the statistical errors. The monitor was placed at a distance of 1.5 meters from the accelerator target at an angle of 150° with respect to the deuteron beam.

Two measurements were made to obtain the γ-ray spectrum – with the scatterer and without the scatterer, using the same total number of counts in the monitor. The pulse spectrum produced by γ-rays incident on the spectrometer crystal from the scatterer was obtained by subtracting the number of pulses in each channel of the analyzer obtained in these measurements. It should be noted, however, that a definite contribution to the results is due to pulses produced by γ-rays arising as a result of inelastic scattering and radiative capture of neutrons in the NaI(Tl) crystal. These neutrons reach the crystal from the scatterer.

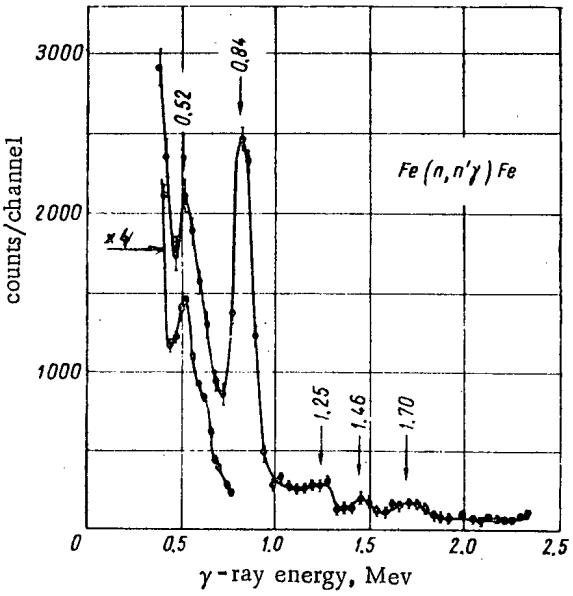

Fig. 6. γ-Ray pulse spectrum produced in inelastic scattering of 2.8 Mev neutrons on iron.

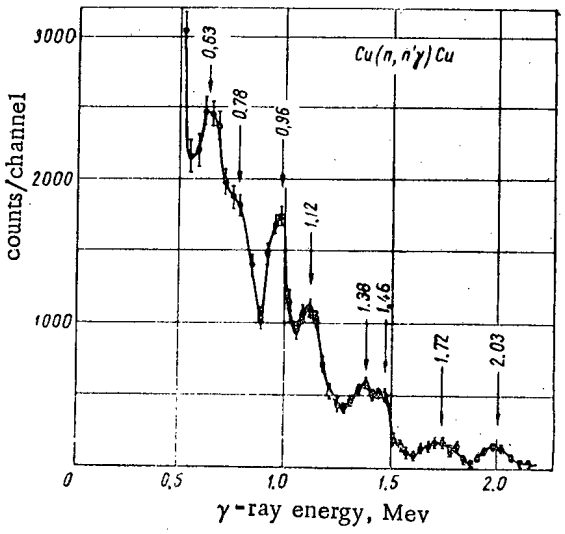

Fig. 7. γ-Ray pulse spectrum produced in inelastic scattering of 2.8 Mev neutrons on copper.

An investigation was made of the pulse-height distribution for the background of γ-rays and neutrons produced when the apparatus was operated without the scatterer. The necessity for such a study arises as a result of the fact that this distribution is not smooth; it has a complicated structure with peaks. Drift in the spectrometer amplifier and the appearance of new background peaks during the experiment can introduce considerable errors in the spectra when the background is subtracted. In the present experiments a control on amplifier drift in the spectrometer was realized by taking pulse spectra for γ-rays from Sb^{124} and Co^{60} after each exposure. In the calculations only those data were taken in which no drift effects were noted. It was shown that the shape of the pulse spectrum due to the background when the apparatus was operated without a scatterer was constant within the limits of the statistical errors.

The increase during the experiment of the long period of the component background of γ-rays produced as a result of neutron absorption by the surrounding elements and the crystal had no noticeable effect on the pulse spectrum. This was verified by subtracting two background pulse spectra measured before and after operation of the neutron generator.

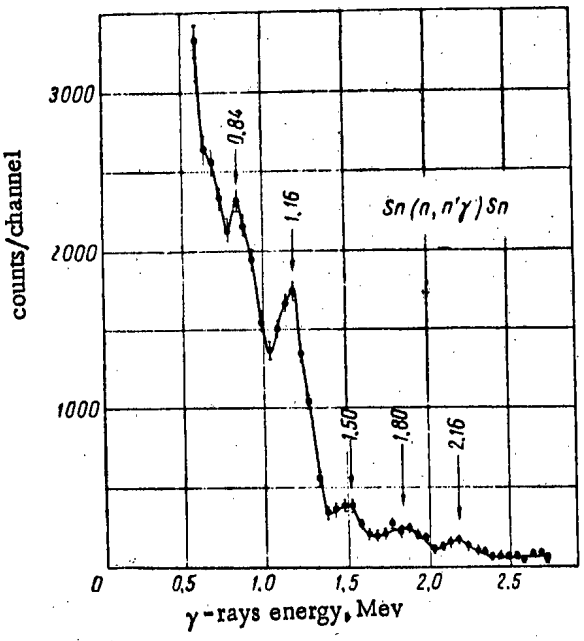

Fig. 8. γ-Ray pulse spectrum produced in inelastic scattering of 2.8 Mev neutrons on tin.

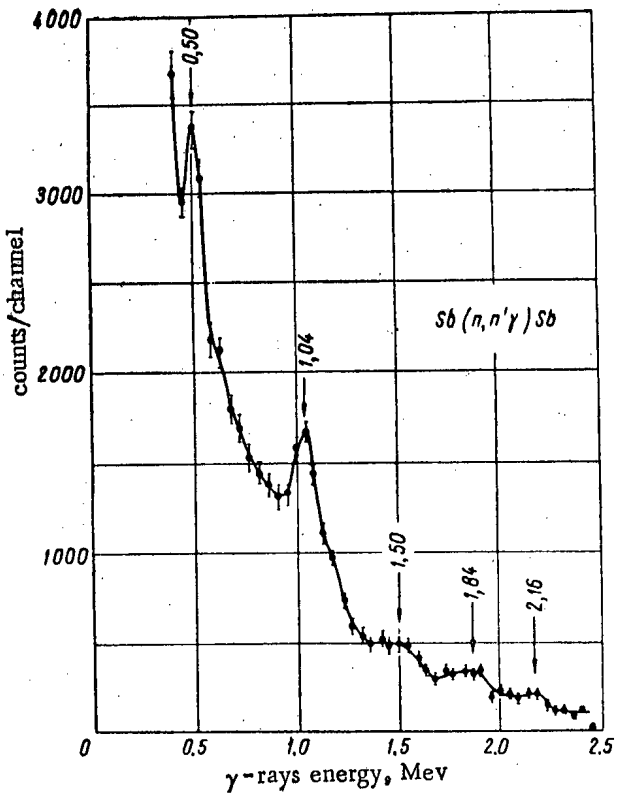

Fig. 9. γ-Ray pulse spectrum produced in inelastic scattering of 2.8 Mev neutrons on antimony.

TABLE 1

Gamma Rays Excited in Inelastic Scattering of 2.8 Mev Neutrons.

Element	γ-Ray energy, Mev	Relative intensity of γ-line
Manganese	0.97±0.05 1.41±0.02 1.92±0.04 2.3	0.3 1.0 0.2
Aluminum	0.84±0.02 1.00±0.02 1.80±0.05 2.16±0.03	0.6 1.0 0.8 0.7
Iron	0.84±0.02 1.25±0.04 1.46±0.04 1.70±0.04	1.0 0.1 0.1 0.1
Copper	0.63±0.04 0.78±0.08 0.96±0.02 1.12±0.04 1.38±0.04 1.46±0.04 1.72±0.04 2.03±0.04	0.3 0.6 1.0 0.9 0.6 0.5 0.4 0.4
Tin	0.84±0.02 1.16±0.02 1.50±0.04 1.80±0.04 2.16±0.04	0.6 1.0 0.3 0.4 0.3
Antimony	1.04±0.02 1.50±0.04 1.84±0.04 2.16±0.04	1.0 0.4 0.4 0.2

In Figs. 4-9 are shown spectra of γ-rays produced in the exposure of the scatterer to 2.8 Mev neutrons measured with fifty channels of the analyzer in operation. In all cases in which the spectrometer covers the low energies a clearly defined peak is noted at a γ-ray energy of 0.5 Mev. This is due to γ-rays excited by scattered neutrons in the NaI(Tl) crystal. It follows from [6-8] that in inelastic scattering of neutrons by sodium and iodine an intense γ-line with

an energy of approximately 0.5 Mev is excited. Gamma lines at other energies, excited by neutrons in the crystal, have small intensities and had no noticeable effect on the spectra being studied.

The γ-ray energies for all elements measured in the present work are shown in the second column of the table. In the third column are given the relative intensities of the γ-lines with respect to the most intense line for each element individually. The intensities of the lines are determined in very approximate fashion because of the difficulties encountered in resolving the complicated spectrum into the elementary spectra. In carrying out this resolution use was made of the line shapes obtained by exposing the crystal of the spectrometer to γ-rays of known energy from radioactive isotopes. In determining the intensities of the γ-lines using the data of [9] corrections were introduced to take account of the dependence of the photo-effect in the NaI(Tl) crystal on γ-ray energy. In view of the fact that the crystal was of rather large dimensions the peak intensities show contributions due to the Compton effect and the effects of pair-production in the crystal. However no corrections were introduced to take account of the energy dependence of these effects. From a qualitative evaluation of these effects it may be concluded that the relative γ-line intensities shown in the table are somewhat low for γ-rays with energies below 2 Mev and somewhat high for higher energy γ-rays.

The authors wish to take this opportunity to thank L. M. Beliaev and G. F. Dobrzhanskii of the Institute of Crystallography, Academy of Sciences, USSR for making the NaI(Tl) crystal and for kindly allowing us to use it in carrying out the present work.

LITERATURE CITED

[1] G. Gurvits et al., Proceedings of the International Conference on the Peaceful Uses of Atomic Energy, Geneva, 1955 (Academy of Sciences Press, USSR Moscow, 1957) Vol. IV, p. 387.

[2] D. Okrent, R. Avery, and H. Hummel, Proceedings of the International Conference on the Peaceful Uses of Atomic Energy, Geneva, 1955,(U. N., 1956,) Vol. 5, p. 347.

[3] R. G. Ofengenden, Dissertation, Institute of Physics, Academy of Sciences, Ukrainian SSR, Kiev (1956).

[4] I. F. Barchuk, E. A. Galkin, M. V. Pasechnik, and N. N. Pucherov, Izv. Akad. Nauk SSSR, Ser. Fiz. 19, 352 (1955).

[5] B. S. Dzhelepov and L. K. Peker, Decay Schemes for Radioactive Isotopes, Academy of Sciences Press, USSR (1957).

[6] U. E. Scherrer, B. A. Allison, and W. R. Faust, Phys. Rev. 96, 386 (1954).

[7] J. L. Morgan, Phys. Rev. 103, 1031 (1956).

[8] E. A. Wolf, Phil. Mag. 1, 102 (1956).

[9] G. Birks, Scintillation Counters, IL (1955).

Received August 22, 1957.

TRANSMISSION OF SCATTERED γ-RADIATION IN WATER

V. I. Kukhtevich, Iu. A. Kazanskii,
Sh. S. Nikolaishvili, and S. G. Tsypin

Measurements have been made of the attenuation of doses of scattered γ-photons from Au^{198}, Co^{60}, and Na^{24} sources as a function of the distance between the source and the detector for various collimation angles, thereby eliminating the possibility of primary γ-radiation from entering the detector. The measurements were carried out at distances ranging from 3 to 4 and 8 to 12 mean-free-paths for the γ-photons. The collimation angles were varied from 30 to 80°. The experimental data which were obtained are compared with the results of calculations based on an assumption which allows the problem to be reduced to the calculation of a triple integral rather than the direct solution of the kinetic equation. Satisfactory agreement is found between the experimental and theoretical results.

In analyzing the transmission of scattered radiation in low-Z materials (air, water, concrete, earth, etc.) the distance between the source and the detector may conveniently be divided into three regions. In the first region, which is less than one mean-free-path in length, the γ-photons experience a single scattering. The second region is a transition region in which multiple scattering of γ-photons becomes more important than single scattering; this region extends from 1 to 3-4 mean-free-paths for the γ-photons. Finally, the third region, which is greater than 3-4 mean-free-paths for the γ-photons, is characterized by an overwhelming predominance of multiple scattering of γ-photons as compared with single scattering.

The transmission of scattered γ-radiation in media of low-Z has been considered in the first and second regions in [1-3]. In [1] a study was made of the transmission of γ-radiation from Au^{198}, Co^{60}, and Na^{24} sources. The measurements were carried out in water with source-detector distances of one mean-free-path of the γ-photon (first region). In [2] an investigation was made of the attenuation of scattered radiation from a Co^{60} source in air. The detector was covered by lead cones with various opening angles (from 10 to 180°). The distance between the source and the detector was varied from 0.7 to 2.5 mean-free-paths of the γ-photons (first and second regions). In [3] a determination was made of the attenuation of scattered γ-photons from a unidirectional Co^{60} source in water at distances of 1 to 3-4 mean-free-paths of the γ-photons (second region).

In the present paper we present the results of an investigation of the transmission of γ-photons in water in the "asymptotic" region (third region). The measurements were made in water using doses of scattered γ-radiation from sources with energies of 0.4-2.8 Mev using collimated γ-sources.

EXPERIMENTAL METHODS

The measurements of γ-radiation scattering in water were carried out in an iron tank 6 m in diameter and 4 m high (Fig. 1). The γ-radiation sources were placed in an opening in a lead container fastened to the I-beams by means of a suspension arrangement. The container was located at a distance of 2 m from the bottom of the tank and the side wall. The upper aperture of the container was covered with a lead plug. The γ-photon collimation angle was changed by varying the vertical position of the γ-source along the axis of the hole.

The water level in the tank was maintained at the height sufficient to guarantee "infinite" geometry under the experimental conditions. The thickness of the container walls was 40 cm, corresponding to an attenuation of more than 10^7 for the primary flux of γ-photons for the most penetrating γ-rays from a Na^{24} source (E = 2.76 Mev) and in the worst case the background due to the primary radiation was less than 1% of the scattered radiation.

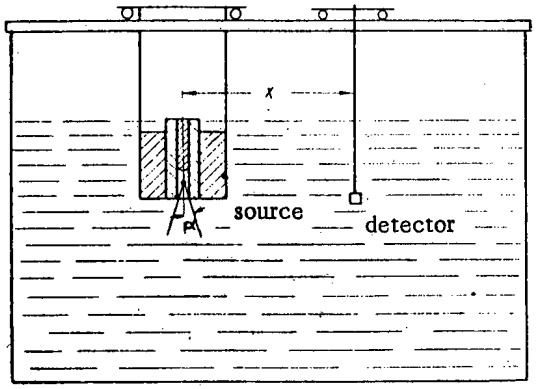

Fig. 1. Diagram of the experimental arrangement. α: collimation angle.

The detector was a counter with a sensitive volume of approximately 4 cm^3. The use of the γ-counter was conditioned by the fact that the intensity of the scattered γ-photons in water is not very large while the slopes of the attenuation curves in water, measured by a γ-counter and a small ionization chamber, agree in the energy region 0.4-2.8 Mev (from the data of preliminary experiments).

The detector was placed in a water-tight container of plexiglas in the same horizontal plane as the lower base of the source container. The distance from the detector to the axis of the collimator was measured with an accuracy of ± 0.1 cm. The Au^{198} source (basic energy E_0 = 0.411 Mev) was a slab of dimensions 1 × 1 × 0.05 cm^3, enclosed in an aluminum jacket of wall thickness 0.01 cm. The initial activity of the source was 15 curies.

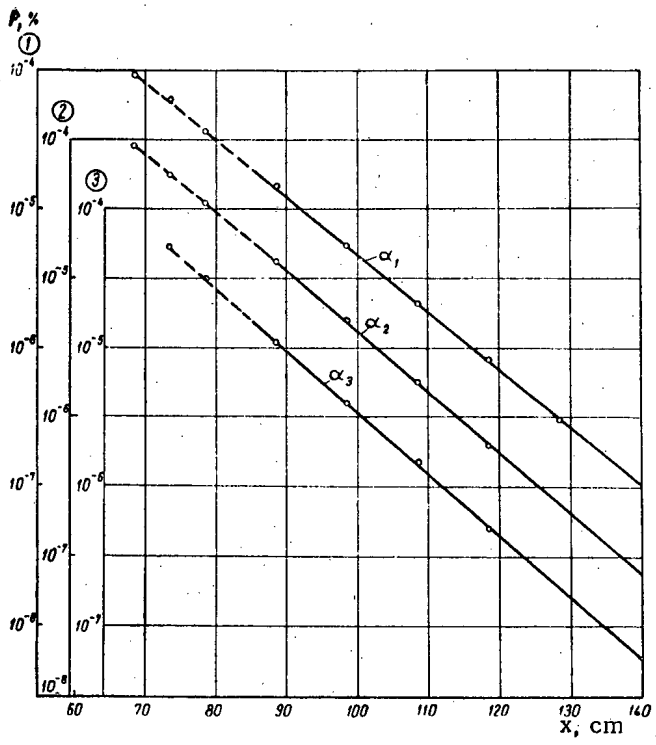

Fig. 2. The dose percent P as a function of the distance x from an Au^{198} source (α_1 = 79°, α_2 = 52.5°, α_3 = 32°).

The Co^{60} source (energy E_0 = 1.17 Mev and E_0 = 1.33 Mev) was in the form of a cylinder 1 cm high and 1 cm in diameter which was also enclosed in an aluminum shell of wall thickness 0.02 cm. The activity of this source during the time of the measurements was 3.5 curies. The Na^{24} source (energies E_0 = 1.38 Mev and E_0 = 2.76 Mev) was a sphere of nickel of wall thickness 0.01 cm and radius 1.35 cm filled with NaF. At the beginning of the measurements the activity of this source was 2 curies.

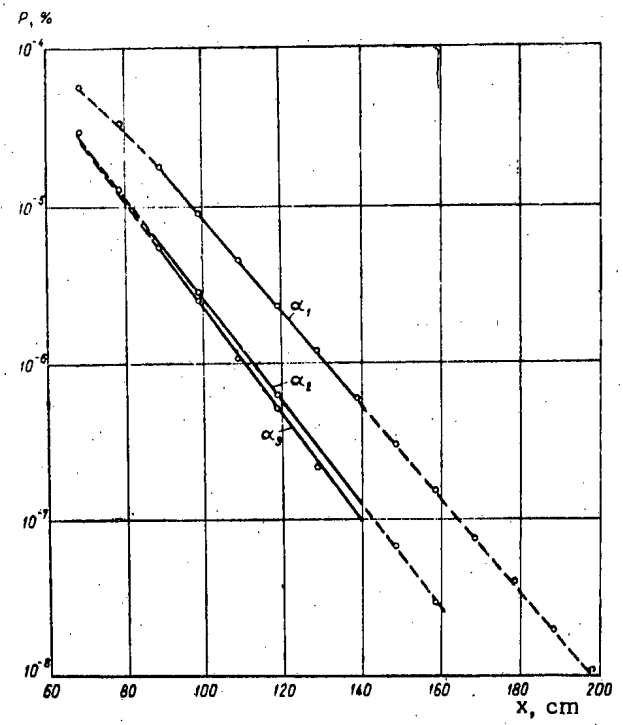

Fig. 3. The dose percent P as a function of the distance x, from a Co^{60} source ($\alpha_1 = 82°$, $\alpha_2 = 59°$, $\alpha_3 = 47°$).

Results of the Measurements

The results of the measurements are shown in Figs. 2-4, giving the dose percentage P (radiation scattered and transmitted through the water) as a function of the distance x between the detector and the axis of the container at various collimation angles α. The dose percentage P is defined as the percent ratio of the radiation dose recorded by the detector to the radiation dose which leaves the collimator aperture, in accordance with the expression

$$P(x,\ E_0,\ \alpha) = \frac{I(x,\ E_s,\ \alpha)}{F(E_0)\,\Omega K(E_0,\ E_s)}\,100, \qquad (1)$$

where $I(x, E_s, \alpha)$ is the intensity of the scattered γ-photons with mean energy E_s, as measured by a detector located in the water at a distance x for a collimation angle α; $F(E_0) = 4\pi R^2 I_0(E_0, R)$ is the intensity of the γ-radiation of the source; here $I_0(E_0, R)$ is the intensity of the γ-radiation of the primary energy E_0 measured by a detector in air at a distance R from the source (to eliminate effects due to scattered radiation the measurements of the quantity $I_0(E_0, R)$ was carried out at a height of 4 m above the earth); $K(E_0, E_s)$ is a factor for converting the number of counts in the γ-counter into dose units [4].

The mean energy of the scattered γ-photons E_s was computed from the slope of the attenuation curve for the γ-radiation, taking multiple scattering into account [5]; Ω is the solid angle at which the γ-radiation emerges from the lead collimator; the calculation of Ω was carried out taking into account the transmission of the γ-photons through the edge of the lead collimator.

It should be noted that in the dose percent measured with the Na^{24} source (Fig. 4) the main contribution is due to 2.76 Mev γ-photons. A calculation indicates that in this case the contribution in dose percent, due to 1.38 Mev γ-photons, even at the closest distance ($x \approx 70$ cm) is less than 5-10% (see also [3]).

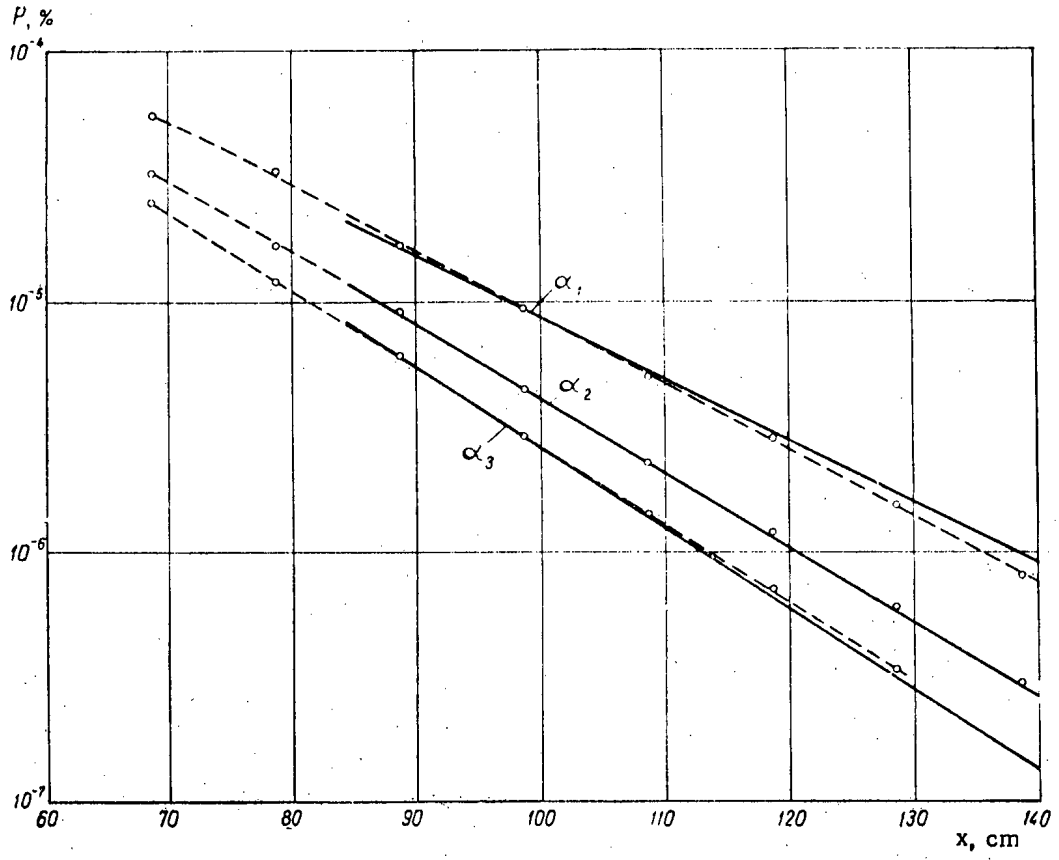

Fig. 4. The dose percent P as a function of the distance x from an Na^{24} source ($\alpha_1 = 80°$, $\alpha_2 = 62°$, $\alpha_3 = 46°$).

The contribution in the dose percent for γ-photons from Au^{198} with energies of 0.68 and 1.09 Mev is less than 5-8% of the 0.411 Mev γ-photons at the greatest distance between the source and detector.

The mean-square error in the measurements for all γ-sources was less than 5%.

Calculation*

The calculation of the dose of γ-radiation scattered in the water using the above-described arrangement of source and detector was carried out under the following assumptions:

1. It is assumed that the γ-radiation source is an isotropic, monochromatic point source.

2. The γ-radiation source is inside a cylinder made of a material which absorbs completely all radiation incident upon it. The source of scattered radiation is the "radiating" cone (Fig. 5), the opening angle of which is determined by the position of the source along the axis of the cylinder.

---

* The numerical calculations were carried out by T. I. Stavinskii and V. A. Mosolov.

3. The medium is assumed to be infinite and the cylinder does not disturb the homogeneity of the medium.

Denoting by $N_0(x, E)$ the spectral distribution of the scattered γ-photons at the point D, we define the dose $I(x)$ at the point D by the following integral:

$$I(x) = \int_0^{E_0} N_0(x, E)\,\mu_a(E)\,E\,dE, \tag{2}$$

where E_0 is the energy of the incident γ-photon and $\mu_a(E)$ is the absorption coefficient for the γ-photon energy in air.

Thus the calculation of $I(x)$ means essentially finding the spectral distribution $N_0(x, E)$ of the scattered radiation at the point D.

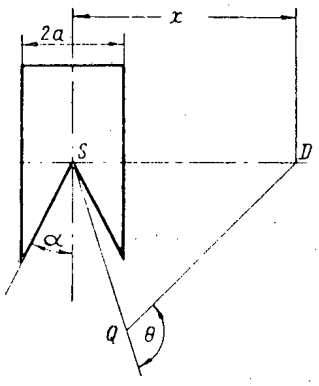

Fig. 5. Geometry for calculating the dose of scattered γ-radiation in water.
a) Radius of the aperture in a container; s) source; α) collimation angle; D) detector; Θ) scattering angle; Q) point volume element of the "radiating" cone.

Finding the function $N_0(x, E)$ is a mathematical problem of great difficulty. In order to solve this problem an assumption was made which allowed us to use the results of the solution of a simpler problem: it is assumed that the element of volume of the "radiating" cone at point Q is an isotropic point source of monochromatic radiation. The total number of γ-photons emitted by the source is equal to the total number of primary γ-photons scattered at the elementary volume being considered, where the energy of the scattered γ-photons is

$$E = \frac{E_0}{1 + K_0(1 - \cos\Theta)}, \qquad (K_0 = E_0/m_0c^2), \tag{3}$$

where Θ is the angle between $\overrightarrow{SQ}$ and $\overrightarrow{QD}$ (Fig. 5).

Granting this assumption the function $I(x)$ can be given by the integral

$$I(x) = \frac{FE_0\mu_s(E_0)}{32\pi^2 x} \int_{\Theta_1}^{\Theta_2} d\Theta \frac{\mu_a(E)}{1 + K_0(1 - \cos\Theta)} \times$$

$$\times \int_{-\varphi^*}^{+\varphi^*} d\varphi \int_{x_1}^{x_2} dx B\left(E, \mu x \frac{\sin\frac{\Theta + x}{2}}{\sin\Theta}\right) \times$$

$$\times \exp\left[-\frac{x}{\sin\Theta}\left(\mu_0 \sin\frac{\Theta - x}{2} + \mu \sin\frac{\Theta + x}{2}\right)\right], \tag{4}$$

where F is the total number of γ-photons emitted by the source S with energy E_0; $B(E, \mu x)$ is the dose accumulation factor for an isotropic point source of γ-photons with energy E at the distance x from the source; $\mu_s(E_0)$ is the scattering coefficient for γ-photons with energies E_0; $\mu = \mu(E)$, $\mu_0 = \mu(E_0)$ are the attenuation factors for γ-photons with energies E and E_0, respectively.

The limits of integration in Equation (4) for values of $\underline{x}$ large as compared with the dimensions of the collimator are obtained from the following relations: *

$$\left.\begin{aligned} &\begin{cases} x_1 = \pi - \Theta \quad 2\alpha_1,\ \alpha_1 = \operatorname{arc\,tg} \sqrt{\frac{\cos^2\varphi}{\cos^2\alpha} - 1}, \\ x_2 = \Theta, \end{cases} \\ &\operatorname{tg}\varphi^* = \sqrt{\operatorname{tg}^2\alpha - \operatorname{ctg}^2\Theta}, \\ &\Theta_1 = \frac{\pi}{2} - \alpha,\ \ \Theta_2 = \frac{\pi}{2} + \alpha, \end{aligned}\right\} \tag{5}$$

where α is the opening angle of the "radiating" cone.

The relations given in (5) are correct to an accuracy up to quantities of order $\frac{a}{x}$ ($\underline{a}$ is the radius of the collimator).

We now assume that $\underline{x}$ varies over some limited energy region. Then the function $B(E, \mu x)$ can be given by the approximate expression

$$B(E, \mu x) \approx B_0(E)\, e^{\varkappa \mu x}, \tag{6}$$

where $\varkappa$ is a parameter which depends on the energy E and the values of $\underline{x}$ being considered.

Further, we take

$$\mu_{\text{eff}} = (1 - \varkappa)\,\mu; \tag{7}$$

after a suitable transformation, in place of Equation (4), we obtain

$$\begin{aligned} I(x) = \frac{FE_0\mu_a(E_0)}{8\pi^2 x} \int_0^{2\alpha} d\xi\, \frac{\mu_a(E)B_0(E)}{1 + K_0(1 - \cos\Theta)} \times \\ \times \int_0^{\operatorname{arc\,tg}\sqrt{\operatorname{tg}^2\alpha - \operatorname{ctg}^2\Theta}} d\varphi \times \\ \times \int_0^{\xi + \alpha_1 - \alpha} \exp\left[-x \left(\frac{\mu_0 - \mu_{\text{eff}}\cos\Theta}{\sin\Theta} \times \right.\right. \\ \left.\left. \times \sin z + \mu_{\text{eff}} \cos z \right)\right] dz, \end{aligned} \tag{8}$$

where $\xi = \Theta + \alpha - \frac{\pi}{2}$, while E is determined in accordance with Equation (3).

A direct computation of the integral in (8) is difficult. In order to obtain an approximate value for this integral, at the outset, we may note that the inner double integral, multiplied by $\frac{\mu_a(E)B_0(E)}{1 + k_0(1 - \cos\Theta)}$, is a function of $\underline{x}$ which reaches a maximum at a certain value $\xi = \xi_0$. The larger $\underline{x}$ the smaller is ξ_0 and the sharper the maximum. Hence, in computing the inner double integral we may limit ourselves to values of ξ in the region of zero.

* 'tg' ≡ 'tan,' 'ctg' ≡ 'cot' – Publisher.

On the basis of these remarks we may replace the quantities $\sin z$ and $\cos z$ respectively by $\underline{z}$ and 1 under the integral sign. Then, neglecting the difference between α_1 and α and carrying out the double integration over $\underline{z}$ and φ, we obtain

$$I(x) = \frac{FE_0\mu_s(E_0)\mu_a(E_0)}{8\pi^2 x} \times \times \int_0^{2\alpha} f(\xi)\, e^{-\text{eff}\ (\xi)\, x}\, d\xi, \tag{9}$$

where

$$f(\xi) = \frac{\left[\frac{\mu_a(E)}{\mu_a(E_0)}\right] B_0(E)}{1+K_0(1-\cos\Theta)} \times \times \frac{1-\exp\left(-x\xi\frac{\mu_0-\mu_{\text{eff}}\cos\Theta}{\sin\Theta}\right)}{x\frac{\mu_0-\mu_{\text{eff}}\cdot\cos\Theta}{\sin\Theta}} \times \times \operatorname{arc\,tg}\sqrt{\operatorname{tg}^2\alpha - \operatorname{ctg}^2\Theta},$$

and by μ_{eff} we are to understand $\mu_{\text{eff}}[E(\xi)]$. We rewrite Equation (9):

$$I(x) = \frac{FE_0\mu_s(E_0)\mu_a(E_0)}{8\pi^2 x} \int_0^{2\alpha} e^{-\lambda(\xi)\, x}\, d\xi, \tag{10}$$

where

$$\lambda(\xi) = \mu_{\text{eff}}(\xi) - \frac{1}{x}\ln f(\xi).$$

Now, to find an approximate value for the integral in (10) we make use of the method of "steepest descent" [6]:

$$I(x) = \frac{FE_0\mu_s(E_0)\mu_a(E_0)}{4\pi\sqrt{2\pi}} \cdot \frac{f(\bar{\xi})}{\sqrt{\lambda''(\bar{\xi})}} \cdot \frac{e^{-\mu_{\text{eff}}(\bar{\xi})\, x}}{x\sqrt{x}}, \tag{11}$$

where the values of the functions $f(\xi)$, $\lambda''(\xi)$ and $\mu_{\text{eff}}(\xi)$ are to be taken at the point $\xi = \bar{\xi}$, where $\bar{\xi}$ is the root of the equation

$$\lambda'(\xi) = 0. \tag{11'}$$

Finally, relating the dose $I(x)$ to the dose of primary radiation which emerges from the collimator, we obtain the following expression for the dose percent:

$$P(x, E_0, \alpha) = 100 \cdot \frac{\mu_s(E_0)}{2\pi\sqrt{2\pi}} \times \times \frac{[f(\bar{\xi})/\sqrt{\lambda''(\bar{\xi})}]}{E_2\left[\frac{\mu_0 a}{\operatorname{tg}\alpha} - \cos\alpha\, E_\alpha\left(\frac{\mu_0 a}{\sin\alpha}\right)\right]} \times \frac{e^{-\mu_{\text{eff}}(\bar{\xi})\cdot x}}{x\sqrt{x}}, \tag{12}$$

where

$$E_2(y) = \int_1^\infty e^{-\mu s} \frac{ds}{s^2}.$$

SUMMARY

In Figs. 2-4, in addition to the experimental curves for the dose percent of scattered radiation, we show calculated curves computed from Equation (12). The values of the functions $\mu(E)$, $\mu_a(E)$, and $B(E, \mu x)$ were taken from [5].

The computed values are normalized to the experimental values at the point x = 98.5 cm. The absolute values of the computed curves differ from the experimentally obtained values by less than a factor of 2.

It should be noted that since the effective attenuation coefficients of the dose percent obtained from the experimental data are in agreement with the calculated data the discrepancy indicated remains essentially constant regardless of the source-detector distance.

These discrepancies are explained by error in the measurement of the distance at which the computed dose is determined. This error is about 5-10 centimeters.

It is interesting to note that in the source-detector distance region being investigated (third region) the change of dose percent with distance may be given by the relation $[e^{-\mu_{eff} x} / x\sqrt{x}]$, whereas the intensity of singly scattered γ-photons falls off with distance in accordance with relation $[e^{-\mu_{eff} x}/x]$.

In conclusion the authors wish to express their gratitude to Dr. Phys.-Math. Sciences A. K. Krasin for setting up the problem and for illuminating discussions on the results of the measurements, to Dr. Phys.-Math. Sciences G. I. Marchuk for a number of remarks concerned with the calculation and also to V. A. Tolstikov for participating in the present series of experiments.

LITERATURE CITED

[1] M. A. VanDilla, and G. J. Hine, Nucleonics 10, 1, 54 (1952).

[2] B. W. Soole, Proc. Roy. Soc. 230, 343 (1955).

[3] T. Rockwell, Shielding of Nuclear Reactors, IL (1958).

[4] W. K. Sinclair, Nucleonics 7, 6, 21 (1950).

[5] U. Fano, Nucleonics 11, 8, 8 (1953); 9, 55 (1953).

[6] M. A. Lavrent'ev and B. V. Shabat, Methods of the Theory of Functions of a Complex Variable, (State Tech. Press, Moscow-Leningrad, 1951).

Received March 16, 1957.

ESTIMATE OF DOSE IN THE INHALATION OF RADON

L.S. Ruzer

The inhalation of radon takes place both in industry and in natural conditions (by far the major part of the natural radiation dose is due to radon). The question of computing the dose due to inhalation of radon is therefore of practical interest.

This paper gives an analytical expression for $A_\gamma(t)$ – the γ-ray activity of RaC in the inhalation of radon – and demonstrates a method of computing the mean coefficient of retention of short-lived products of radon decay. The link between $A_\gamma(t)$ and the value of the integral absorbed dose due to Rn, RaA, RaC' is established; formulas are given for computing the dose due to long-lived products of radon decay.

INTRODUCTION

The biological action of radon and its short-lived decay products on the respiratory organs is due mainly to the α-emitters Rn, RaA and RaC', since the total α-particle energy of these elements is considerably greater than the β- and γ-ray energies of RaB and RaC, and also because of the greater biological effectiveness of α-rays as compared with β- and γ-rays.

The quantity of short-lived products of radon decay deposited in the respiratory system may be estimated from the γ-emission of RaB and, mainly, RaC. In the present article the link is found between the integral absorbed dose due to the α-emitters mentioned and the γ-activity of products deposited in the respiratory system, mainly RaC.

Basic Premises

1. The short-lived daughter products of radon decay are always present in the air. The ratio of their quantity to the "equilibrium" we will call the degree of equilibrium η_A (for RaA), η_B (for RaB) and η_C (for RaC).

2. If the biological object is in a space of sufficiently large volume, the radon concentration in the respiratory system will be equal to the concentration in an "emanatorium"* (q curies/liter) and the respiration volume per minute will be

$$v_l = v \cdot n \text{ liter/min},$$

where v is the volume of one inhalation, and n is the number of inhalations per minute.

3. After each inhalation a definite part of RaA (δ_A), RaB (δ_B) and RaC (δ_C) is retained; the rate of entry of each of the elements will be $3.7 \cdot 10^{10} \cdot 60 \cdot \frac{qv_l \cdot \eta}{\lambda}$ atoms/min, and the rate of accumulation in the respiratory system will be

$$Q = a \frac{qv_l \eta \delta}{\lambda} \text{ atoms/min} \qquad (1)$$

*The term "emanatorium" is used arbitrarily and denotes merely a space containing radon.

where λ is the decay constant (in min^{-1}) for RaA, RaB, RaC, respectively; $a = 222 \cdot 10^{10}$ dis/min per 1 curie of active matter.

4. According to the existing data [1] for the half-periods of elimination of short-lived radon products from the lungs, complete decay takes place before excretion in appreciable quantities begins.

Analytical Expression for the γ-Ray Activity of RaC

To find an analytical expression for the γ-ray activity of RaC as a function of time $A_\gamma(t)$ we will assume that this activity is due to RaC retained in the respiratory system and also to RaC formed from RaA, RaB and Rn.

An expression for the number of RaC atoms present at a given moment, allowing for decay (N_C^I), and for the number of RaC atoms obtained from RaB (N_C^{II}), from RaA (N_C^{III}) and from Rn (N_C^{IV}) can be obtained by using the solution of the equation for a chain of radioactive transformations of $\underline{i}$ links, where only the primary radioactive substance is present initially:

$$(N_2^0 = N_3^0 = \ldots = N_i^0 = 0)\ *.$$

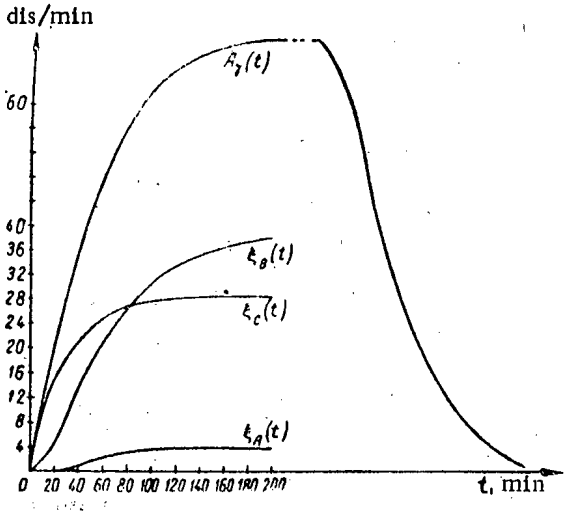

Fig 1. Functions $\xi_A(t)$, $\xi_B(t)$ and $\xi_C(t)$ (min), representing the contributions of RaA, RaB and RaC to $A_\gamma(t)$.

In this case the solution has the form [2]:

$$N_i = c_1 \cdot e^{-\lambda_1 t} + c_2 \cdot e^{-\lambda_2 t} + \ldots + c_i \cdot e^{-\lambda_i t}, \quad (2)$$

$$\left.\begin{aligned} c_1 &= N_1^0 \cdot \lambda_1 \frac{\lambda_2 \cdot \lambda_3 \ldots \lambda_{i-1}}{(\lambda_2-\lambda_1)(\lambda_3-\lambda_1)\ldots(\lambda_i-\lambda_1)} \\ &\ldots\ldots\ldots\ldots\ldots\ldots \\ c_i &= N_1^0 \cdot \lambda_1 \frac{\lambda_2 \lambda_3 \ldots \lambda_{i-1}}{(\lambda_1-\lambda_i)(\lambda_2-\lambda_i)\ldots(\lambda_{i-1}-\lambda_i)}. \end{aligned}\right\} \quad (3)$$

Formulas (2) and (3) are applicable also when the element with index 2 accumulates at some constant rate Q, as happens in the case considered.

Then

$$A_i = \lambda_i \cdot N_i = Q\left[1 - \frac{\lambda_2 \cdot \lambda_4 \ldots \lambda_i \cdot e^{-\lambda_2 t}}{(\lambda_3-\lambda_2)\ldots(\lambda_i-\lambda_2)} - \right.$$

$$\left. - \frac{\lambda_2 \cdot \lambda_4 \ldots \lambda_i e^{-\lambda_3 t}}{(\lambda_2-\lambda_3)\ldots(\lambda_i-\lambda_3)} - \ldots \quad \ldots - \frac{\lambda_2 \cdot \lambda_3 \ldots \lambda_{i-1} e^{-\lambda_i t}}{(\lambda_2-\lambda_i)\ldots(\lambda_{i-1}-\lambda_i)}\right]. \quad (4)$$

Substituting in turn in Expression (4) the values Q_A, Q_B and Q_C from (1), we obtain

$$A_C^I = a\frac{q v_t \cdot \eta_C \cdot \delta_C}{\lambda_C}\left(1 - e^{-\lambda_C t}\right), \quad (5)$$

$$A_C^{II} = a\frac{q v_t \delta_B \cdot \eta_B}{\lambda_B}\left(1 + \frac{\lambda_C \cdot e^{-\lambda_B t} - \lambda_B \cdot e^{-\lambda_C t}}{\lambda_B - \lambda_C}\right), \quad (6)$$

$$A_C^{III} = a\frac{q v_t \delta_A \eta_A}{\lambda_A}\left[1 - \frac{\lambda_B \cdot \lambda_C \cdot e^{-\lambda_A t}}{(\lambda_B-\lambda_A)(\lambda_C-\lambda_A)} - \right.$$

$$\left. - \frac{\lambda_A \cdot \lambda_C \cdot e^{-\lambda_B t}}{(\lambda_A-\lambda_B)(\lambda_C-\lambda_B)} - \frac{\lambda_A \cdot \lambda_B \cdot e^{-\lambda_C t}}{(\lambda_A-\lambda_C)(\lambda_B-\lambda_C)}\right], \quad (7)$$

$$A_C^{IV} = aqV\left[1 - \frac{\lambda_B \cdot \lambda_C \cdot e^{-\lambda_A t}}{(\lambda_B-\lambda_A)(\lambda_C-\lambda_A)} - \right.$$

$$\left. - \frac{\lambda_A \cdot \lambda_C \cdot e^{-\lambda_B t}}{(\lambda_A-\lambda_B)(\lambda_C-\lambda_B)} - \frac{\lambda_A \lambda_B \cdot e^{-\lambda_C t}}{(\lambda_A-\lambda_C)(\lambda_B-\lambda_C)}\right], \quad (8)$$

*N_2^0, N_3^0, . . . , N_i^0 are the number of atoms of elements with indices 2, 3, . . . , $\underline{i}$, respectively, at the initial moment.

where V is the mean volume of respiratory paths. Assuming in the future that $\delta_A = \delta_B = \delta_C = \delta$ and neglecting the contribution of radon itself we obtain an expression for the total activity A_γ by summation:

$$A_\gamma = aqv_l\delta[\eta_A \cdot \xi_A(t) + \eta_B\xi_B(t) + \eta_C\xi_C(t)]. \tag{9}$$

Functions $\xi_A(t)$, $\xi_B(t)$ and $\xi_C(t)$, the graphs of which are given on Figure 1, characterize the contributions to A_γ of RaA, RaB and RaC, respectively. Here we also give the summed curve

$$a_\gamma(t) = \xi_A(t) + \xi_B(t) + \xi_C(t)$$

A_γ may be obtained experimentally by comparison with sources of radon or by using a dummy; η_A, η_B and η_C are determined by the usual methods [3, 4].* Expression (9) makes it possible to determine the mean retention coefficient δ. In particular, with t > 200 min,

$$\delta = \frac{A_\gamma}{aqv_l\left(\frac{\eta_A}{\lambda_A} + \frac{\eta_B}{\lambda_B} + \frac{\eta_C}{\lambda_C}\right)}. \tag{10}$$

The rising branch of curve $a_\gamma(t)$ is in good agreement with experimental results obtained on white rats [5], the descending portion corresponds to the natural decay of the accumulated daughter products of radon and also agrees well with the experimental results of the same work. The form of this curve characterizes the change in the γ-ray activity in time for any object breathing radon when $\eta_A = \eta_B = \eta_C$.**

Formula for Computing the Integral Absorbed Dose

The integral absorbed dose for the respiratory paths is

$$D_1 = D_1' + D_1'' = D_{Rn} + D_A + D_{C'} + D_1'', \tag{12}$$

where D'_1 and D''_1 are fractions of dose during stay in the emanatorium and after removal from it;

$$D_1 = D_1' + E_{Rn}\int_0^t A_{Rn}(t)\,dt + E_A\int_0^t A_A(t)\,dt + E_{C'}\int_0^t A_{C'}(t)\,dt, \tag{13}$$

where E is the α-particle energy of Rn, RaA and RaC'. Applying to this case the Solution (4) and assuming that $\lambda_{C'} \gg \lambda_A, \lambda_B, \lambda_C$, neglecting Rn decay, we obtain

$$D_1' = aqv_l\delta[\eta_A\varphi_A(t) + \eta_B\varphi_B(t) + \eta_C\varphi_C(t)] \tag{14}$$

---

*In the USSR we have now produced an electrofilter EF-2 (see J. Atomic Energy (USSR) 3, 10, 356 (1957) [C. B. translation page 1217] which may be used for this purpose. (Note added in proof.)

**For a tentative estimate of the mean degree of equilibrium η a comparatively simple method, proposed by G.E. Gur'e and the author, may be employed.

Usually, for determining radon concentration in an emanatorium a sample is taken into a previously evacuated ionization chamber (for instance, the "emanation" chamber of the SG-1M electrometer assembly) and the value of the ionization current is measured. The nature of the current increase and its value at t = 0 are connected with the mean degree of equilibrium.

We denote: J_0 – ionization current due to radon at t = 0; J_1 – current due to decay products at t = 0; $J_2 = J_0 + J_1$ – sum of currents at t = 0 and J – maximum value of ionization current. Taking $J_0 = 0.460J$ [6] we obtain

$$\eta = \frac{J_1}{J - J_0} = \frac{J_2 - J_0}{J - J_0} = \frac{J_2 - 0.460J}{0.540J} = 1.85\left(\frac{J_2}{J} - 0.460\right). \tag{11}$$

Figure 2 shows functions $\varphi_A(t)$, $\varphi_B(t)$ and $\varphi_C(t)$ which indicate the contributions of RaA, RaB and RaC to D'_1, and also $d'_1(t) = \varphi_A(t) + \varphi_B(t) + \varphi_C(t)$.

For $t > 200$ min

$$d'_1(t) = (0.93t - 45.0) \cdot 10^{-3} \text{ erg} \cdot \text{min}^2 \tag{15}$$

Comparing (14) with (9) we have

$$D'_1 = A_\gamma \frac{\eta_A \varphi_A(t) + \eta_B \varphi_B(t) + \eta_C \varphi_C(t)}{\eta_A \xi_A(t) + \eta_B \xi_B(t) + \eta_C \xi_C(t)}. \tag{16}$$

Expression (4) may be used to determine the number of atoms of RaA, RaB and RaC existing at time t (time of leaving the emanatorium) in the respiratory system (η_A, η_B, and η_C).

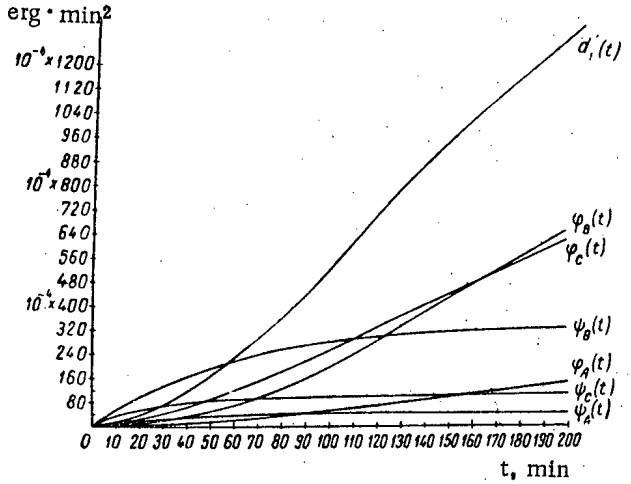

Fig. 2. Dose functions $\varphi_A(t)$, $\varphi_B(t)$, $\varphi_C(t)$ and $\psi_A(t)$, $\psi_B(t)$ and $\psi_C(t)$ (erg · min²).

Then the integral absorbed dose after leaving the emanatorium, D''_1, is

$$D''_1 = n_A E_A + (n_A + n_B + n_C) E_C = aqv_l\delta [\eta_A \psi_A(t) + \eta_B \psi_B(t) + \eta_C \psi_C(t)], \tag{17}$$

where $\psi_A(t)$, $\psi_B(t)$ and $\psi_C(t)$ are the dose characteristics due to RaA, RaB and RaC after leaving the emanatorium.

Finally

$$D_1 = aqv_l\delta \{\eta_A [\varphi_A(t) + \psi_A(t)] + \eta_B [\varphi_B(t) + \psi_B(t)] + \eta_C [\varphi_C(t) + \psi_C(t)]\} \text{ erg}, \tag{18}$$

or

$$D_1 = A_\gamma \frac{\eta_A [\varphi_A(t) + \psi_A(t)] + \eta_B [\varphi_B(t) + \psi_B(t)] + \eta_C [\varphi_C(t) + \psi_C(t)]}{\eta_A \xi_A(t) + \eta_B \xi_B(t) + \eta_C \xi_C(t)} \text{ erg} \tag{19}$$

(A_γ is the number of disintegrations per minute).

For the case $\eta_A = \eta_B = \eta_C$

$$D_1 = A_\gamma \frac{d'_1(t) + d''_1(t)}{a_\gamma(t)}, \tag{20}$$

where $d''_1(t) = \psi_1(t) + \psi_2(t) + \psi_3(t)$.

Expressions (18) and (19) make it possible to compute the integral absorbed dose for any object either from known q, v_t, η and δ, or from A_γ determined by a counter [6]. Here the dose may be calculated both for the whole respiratory system and for its separate parts. It is possible, as was done in [5], to estimate the dose from the area bounded by curve $A_\gamma(t)$ and the x-axis, but this requires recording the whole curve — a very laborious operation. The values obtained by both methods practically coincide. From (20) the dose for a man was computed, taking $t = 6$ hours, $q = 10^{-11}$ curie/liter, $v_t = 16.4$ liter/min, $\eta = 1$, $\delta \approx 0.5$ and the weight of the respiratory organs ~0.8 kg. It was found to be ~0.0007 rad on the average for the whole respiratory system although in separate parts it may be considerably higher.

It was shown [5, 8, 3] that the action of short-lived products of radon decay, deposited in the respiratory system, on the breathing organs considerably exceeds that of the action of radon itself and the products accumulated during the retention of radon in the organism. It is not out of the question, however, that continuous inhalation of radon in conditions of a very low degree of equilibrium may result in a relatively higher dose value due to radon itself, and in this case the action may not be localized in the breathing organs.

The dose due to radon is computed from the area bounded by the curve of radon content of the organism as a function of time [5].

The short-lived decay products, deposited in the lungs and also formed from the radon, are transformed into RaD which initiates a group of long-lived elements. The accumulation of RaD, RaE and RaF (Po^{210}) in different organs gives rise to local irradiation mainly from the β-emitter RaE and the α-emitter RaF. The integral dose absorption due to these long-lived elements may be estimated by taking account of the data on their elimination [9] from the following relations:

$$D_E = kE_E\lambda_D N_D\left(\frac{1-e^{-\lambda_D t}}{\lambda_D} - \frac{1-e^{-\lambda_E t}}{\lambda_E}\right), \tag{21}$$

$$D_F = kE_F\lambda_D\lambda_F N_D\left\{(\lambda_E-\lambda_F)\frac{1-e^{-\lambda_D t}}{\lambda_D} - (\lambda_F-\lambda_D)\frac{1-e^{-\lambda_E t}}{\lambda_E} + \lambda_E\frac{1-e^{-\lambda_F t}}{\lambda_F}\right\}, \tag{22}$$

where N_D is the number of RaD atoms present in the organism after the decay of radon and its short-lived products; k is the absorption coefficient of RaD for the particular organ; t is the time after leaving emanatorium.

It should be emphasized once more that in the inhalation of radon, generally speaking, there occurs the simultaneous entry into the organism of several radioactive elements: isotopes of polonium RaA (Po^{218}), RaC' (Po^{214}) and RaF (Po^{210}) which are α-emitters; of bismuth RaC (Bi^{214}), RaE (Bi^{210}) and of lead RaB (Pb^{214}), RaD (Pb^{210}) (β- and γ-emitters).

All these isotopes (except RaF) contribute to the irradiation of the organism by their own decay, as well as by the decay of the following elements of the series obtained from them. It is not excluded here that long-lived elements, by accumulating in different organs, and by their irregular distribution in them (in lungs, bones, etc.), may with relatively low activities produce over a number of years considerable local doses.

A clarification of the details of the distribution of long-lived decay products along with a consideration of the role of the group of short-lived elements and radon itself must be of great importance for evaluating the possible remote consequences connected with the inhalation of radon.

LITERATURE CITED

[1] B. Hultquist, Kungl. Svenska vetenskapsakademiens Handlingar 6, 3 (1956).

[2] G. Friedlander and J. Kennedy, in the book: Introduction to Radiochemistry [Russian translation] (IL, 1952), p. 119.

[3] J.H. Harley, Nucleonics 11, 7, 12 (1953).

[4] E.C. Tsivoglou, H.E. Ayer and D.A. Holladay, Nucleonics 11, 9, 40 (1953).

[5] E.S. Shchepot'eva, F.L. Leites and L.S. Ruzer, Report of the Radiological Laboratory of the Central Institute of Health Resort Studies* (1956).

[6] An.N. Nesmeianov, V.I. Baranov, et al., in the book: Practical Manual of Radiochemistry* (Goskhimizdat, Moscow, 1956), p. 389.

[7] E.C. Anderson, Nucleonics 14, 1, 26 (1956).

[8] S.H. Cohn, J.K. Gong and R.K. Skow, Arch. Industr. Hygiene and Occupat. Med. 7, 508 (1953).

[9] Recommendations of the International Commission on Radiological Protection, Brit. J. Radiol. Supplement No. 6 (1955).

Received January 15, 1957

*In Russian.

INVESTIGATION OF INTENSE PULSED DISCHARGES IN GASES BY MEANS OF HIGH-SPEED PHOTOGRAPHY*

N. A. Borzunov, D. V. Orlinskii, and S. M. Osovets

A qualitative description is given of the basic processes which occur in the initial stages of intense discharges; this description is based on a comparison of voltage and current oscillograms with photographs of intense pulsed discharges in deuterium and certain inert gases. The experimental data are found to be in basic agreement with the work of M. A. Leontovich and S. M. Osovets on the "inertia" theory of plasma compression.

In the present paper we report the results of an investigation of intense electric discharges in gases (deuterium, neon, argon, krypton, and xenon) carried out by means of high-speed photography. The results presented here pertain to discharges with current strength of greater than 10^5 amp at gas pressures ranging from 0.01 to 1 mm Hg. The basic effects characteristic of discharges of this type have already been described in [1-4].

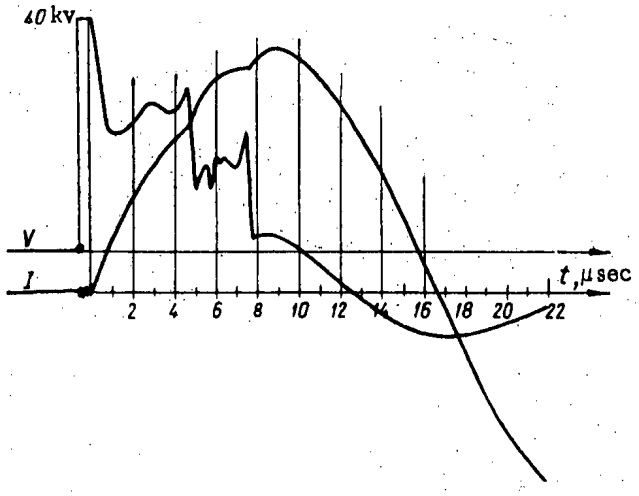

Fig. 1. Oscillogram showing the current and voltage in a deuterium discharge (p_0 = 0.2 mm Hg).

In Fig. 1 is shown a typical oscilloscope pattern for discharge current and electrode voltage obtained with an initial deuterium pressure of 0.2 mm Hg. The current I(t) in the initial stage of the discharge exhibits several discontinuities. Each of these breaks corresponds to a sharp reduction in the voltage between

* This work was carried out in 1953.

the electrodes. In what follows the discontinuities in the current curve will be called "breaks" while the time between the initiation of a discharge and a break will be called the "break time."

In [1] it was shown that the break time and the current at the instant the break occurs are functions of the initial gas pressure and the voltage applied to the electrodes. In [4] these properties were explained in terms of the motion of the gas from the periphery to the center under the effect of the electromagnetic forces. It was shown that the basic force responsible for the compression of the gas is the inertia force. Visual observation of the discharge, i.e., photographs at various instants of time allows a qualitative verification of this interpretation. In addition, pictures showing the behavior of the discharge in the course of time are of interest in themselves.

The discharge was produced in a glass cylindrical chamber with an internal diameter of 18.5 cm and a distance of 97 cm between the electrodes. The current source was a condenser bank with a total capacity of 35 μf which was charged to 40 kv. The discharge current was measured by beams of a pickup coil with $\omega L \gg R$, thus making it possible to measure the magnitude of the current rather than its derivative, as would be the case if $\omega L < R$. The signal from this coil was applied to the deflection plates of an OK-17 oscilloscope. The maximum current in the first half-cycle under these conditions was approximately 220 kiloamps.

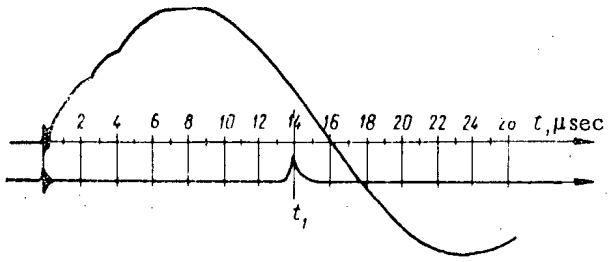

Fig. 2, a. Oscillogram of the current and phasing pulse in a deuterium discharge for $p_0 = 0.03$ mm Hg.

The discharge was photographed with a high-speed camera (SFR) operated in the "time-magnification" mode. This device provides exposure rates up to two million frames per second. To determine the phase of the discharge pertaining to a given frame, the following method was used. An FEU-19 photomultiplier was located directly behind the exposed plate. The cathode of the multiplier was covered by a diaphragm in such a way that light could reach it only through one of the lenses of the housing in the device. The signal at the output of the photomultiplier was fed to a cathode follower and amplifier and then applied to a second pair of plates in the oscilloscope (Fig. 2, a). The frame whose exposure corresponds to the instant at which light strikes the photomultiplier, is denoted by t_1. The neighboring frame (in position, not time) is not exposed (Fig. 2, b). Thus, on the photograph of the discharge we can ascertain the frame which corresponds to the pulse on the oscilloscope. Knowing the rate of rotation of the mirror and the time scale of the oscilloscope picture, it is possible to determine the phase of the development of the discharge corresponding to a given frame. The accuracy of this method of phasing depends on the rate of rotation of the mirror. With n = = 60,000 rpm, i.e., the velocities with which all photographs in this paper were taken, the error in the determination of the phase is less than ± 0.25 μ sec.

In Figs. 3-6 are shown photographs of discharges in deuterium, neon, argon, and krypton obtained with various values of the initial gas pressure. In Figs. 7 and 8 are shown photographs of discharges in deuterium and xenon, taken with the same SFR device but operated in the "continuous-sweep" mode. In this case there is a slit located between the first and second objectives at the plane of the intermediate image. The width of the slit is chosen so that only part of the cylinder (discharge chamber) of height 1-2 mm is projected on the rotating mirror. As the mirror rotates the image is displaced along the film in the direction of the cylinder axis. Thus, on the film it is possible to obtain a picture of the time behavior of a small part of the discharge (with n = 60,000 rpm the rate of displacement of the image along the film is $3 \cdot 10^5$ cm/sec).

The development of the discharge may be pictured qualitatively as follows. At the initial stage the luminous radiation from the gas is observed only near the walls since in this time period the current flows near the periphery of the discharge chamber because of the skin effect. Then the plasma column starts to contract. The rate of contraction is larger, the smaller the mass of the gas. Curves showing the change in the luminous radius of the plasma column as a function of time in a deuterium discharge are shown in Fig. 9. During the time of contraction the inductance of the column increases; for this reason the discharge-current curve exhibits a marked departure from sinusoidal shape (see Figs. 1 and 2). During this period the electrode voltage increases. The decay of the luminous radiation (consequently the current at the periphery) is an indication that the pressure at the chamber walls is reduced. This means that not only ionized particles but also neutral gas are swept toward the center of the chamber. The measurements described in [3] and [5] indicate that in the initial stage of the discharge the degree of ionization is small. The entrapment of the neutral gas occurs as a result of charge exchange with ions. When an ion collides with a neutral particle the ion is neutralized and continues to move in the same direction, maintaining its momentum, whereas the neutral particle is ionized. The new ion enters into the general motion of the plasma and, along with other charged particles, moves toward the axis of the discharge chamber. The effective cross section for charge exchange is much greater than the cross section for other possible collision processes (neglecting elastic scattering which, in itself, does not play an important role in the process being considered). Thus, the main mass of neutral particles is swept toward the center of the system. At the end of the contraction process accumulation of neutral particles at the walls of the chamber may start; the momentum of these particles in charge exchange is directed toward the periphery.

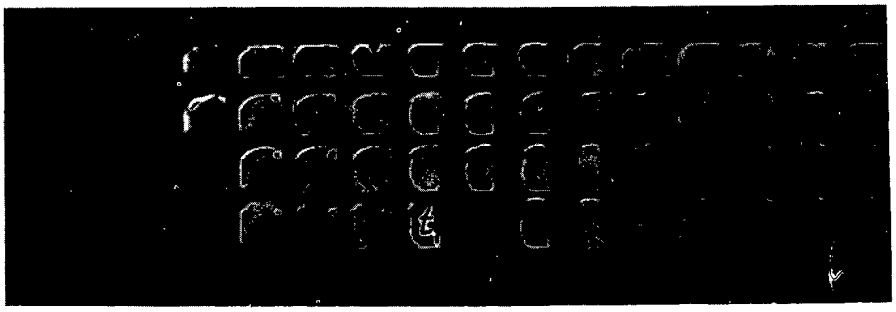

Fig. 2, b . Photograph of the discharge the oscillogram of which is shown in Fig. 2, a.

As is apparent from the photographs which have been presented, the plasma column contracts to a fine (radius $a \approx 1$ cm) pinch. The minimum value of the luminescent radius of the pinch is virtually independent of the type of gas and initial pressure. Starting at the instant of time which corresponds to the first break in the current curve, the gas at the chamber walls once again becomes luminescent. It is apparent that the test gas moves to the walls and a plasma shell is formed. This effect is especially obvious in the photographs of discharges in neon, argon, and krypton (see also Curve 1 in Figs. 10 and 11). Subsequently, this newly formed plasma shell moves toward the discharge axis. In this case, if the mass of the gas in the discharge chamber is large enough, the first compression occurs at the end of the first half cycle, when the electrode voltage is small and the process is not repeated. (See Curve 2, Figs. 10 and 11).

At the end of the first contraction of the plasma column short-wave instabilities arise. After the compression, when the pinch has already started to expand, the instability becomes stronger. On the photographs can be seen the small unordered vibrations about the pinch axis which increase from frame to frame.

The pinch continues to expand up to the point at which it starts to be compressed along with the second plasma shell moving in from the periphery. If the pressure is low [for example, in the xenon discharge, at a pressure of 0.005 mm Hg (see Fig. 8)] at the instant the second break occurs, i.e., at the time of the second contraction, the gas at the walls of the chamber again becomes luminous. If, however, the discharge occurs in a heavy gas at high pressures, then even up to the instant at which the second contraction starts the discharge current is so small that the electromagnetic forces remain extremely weak in the second contraction.

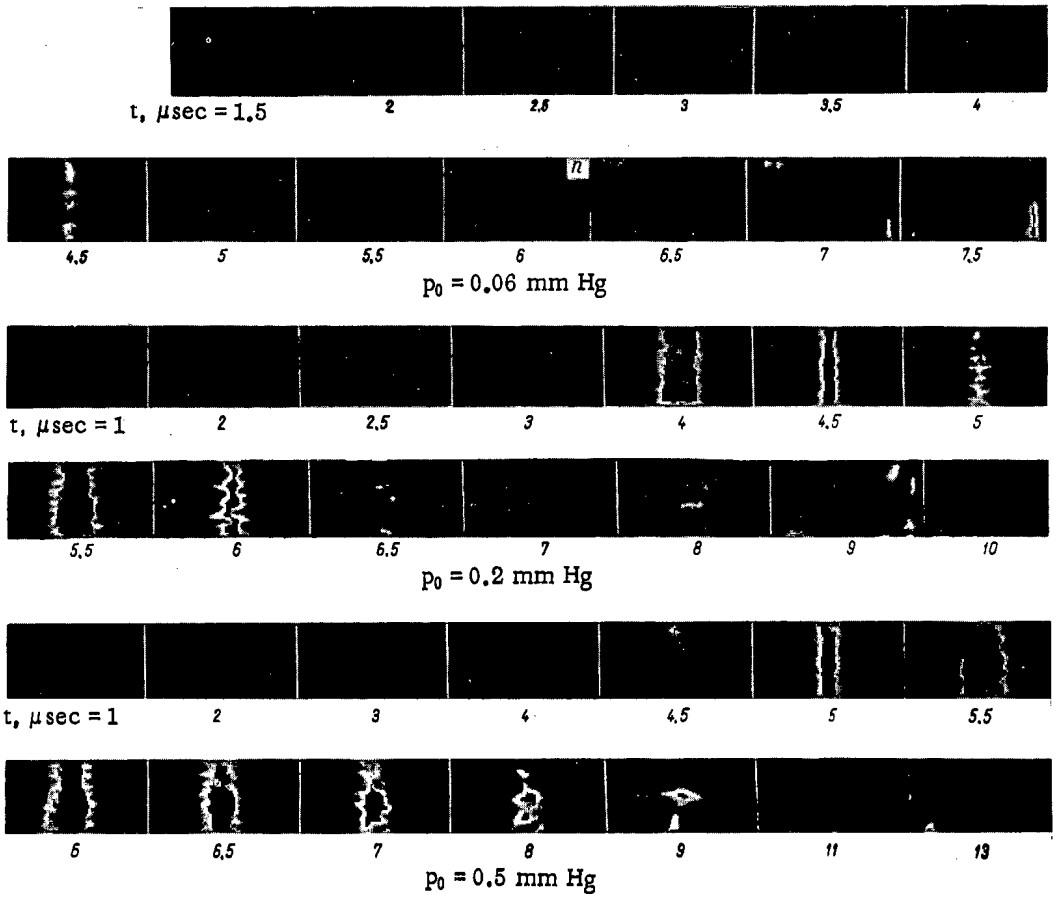

Fig. 3. Photographs of deuterium discharges with various initial pressures p_0.

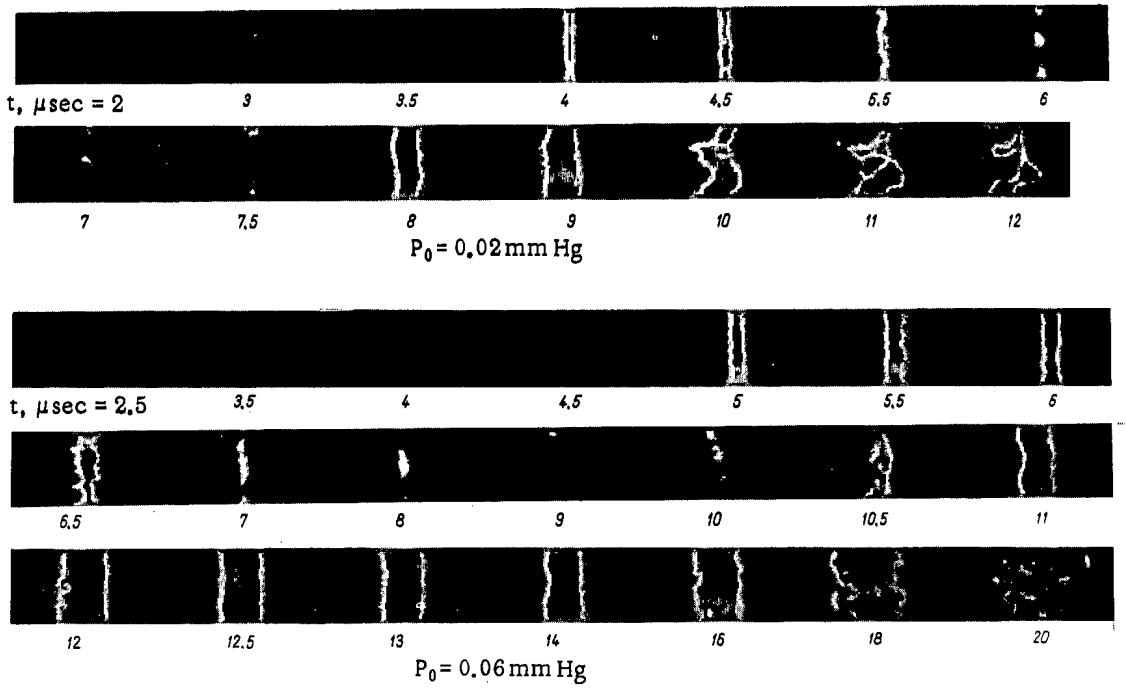

Fig. 4. Photographs of neon discharges for various initial pressures p_0.

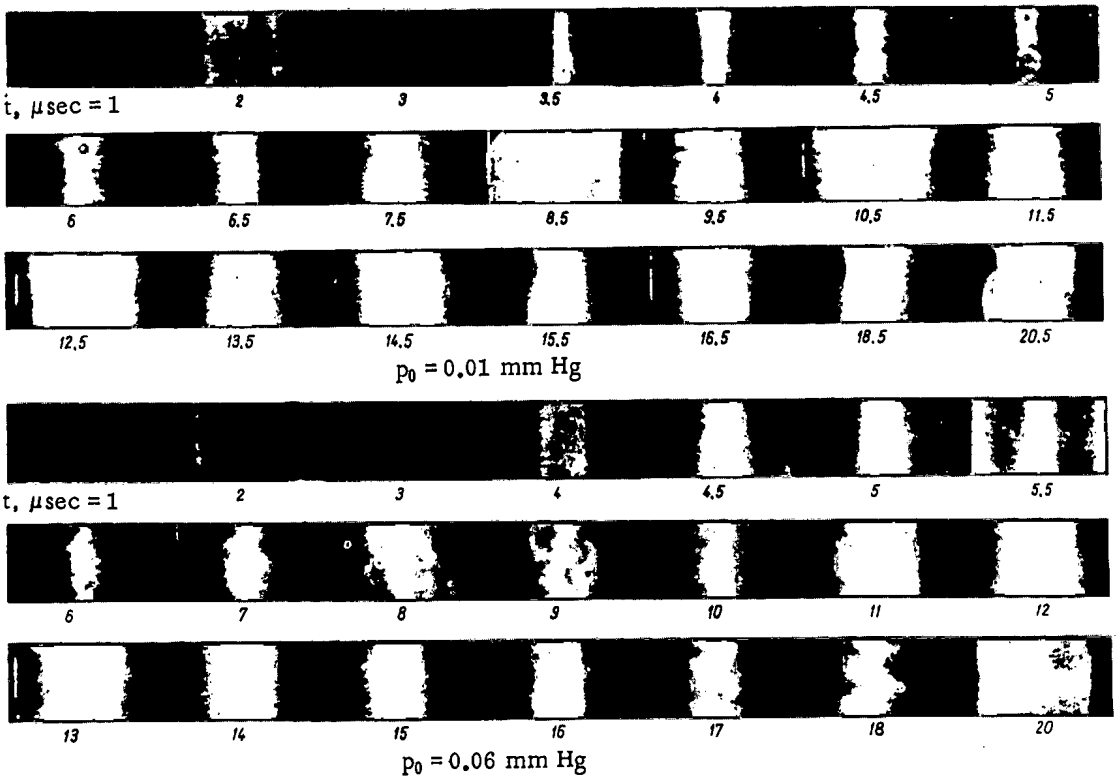

Fig. 5. Photographs of argon discharges with various initial pressures p_0.

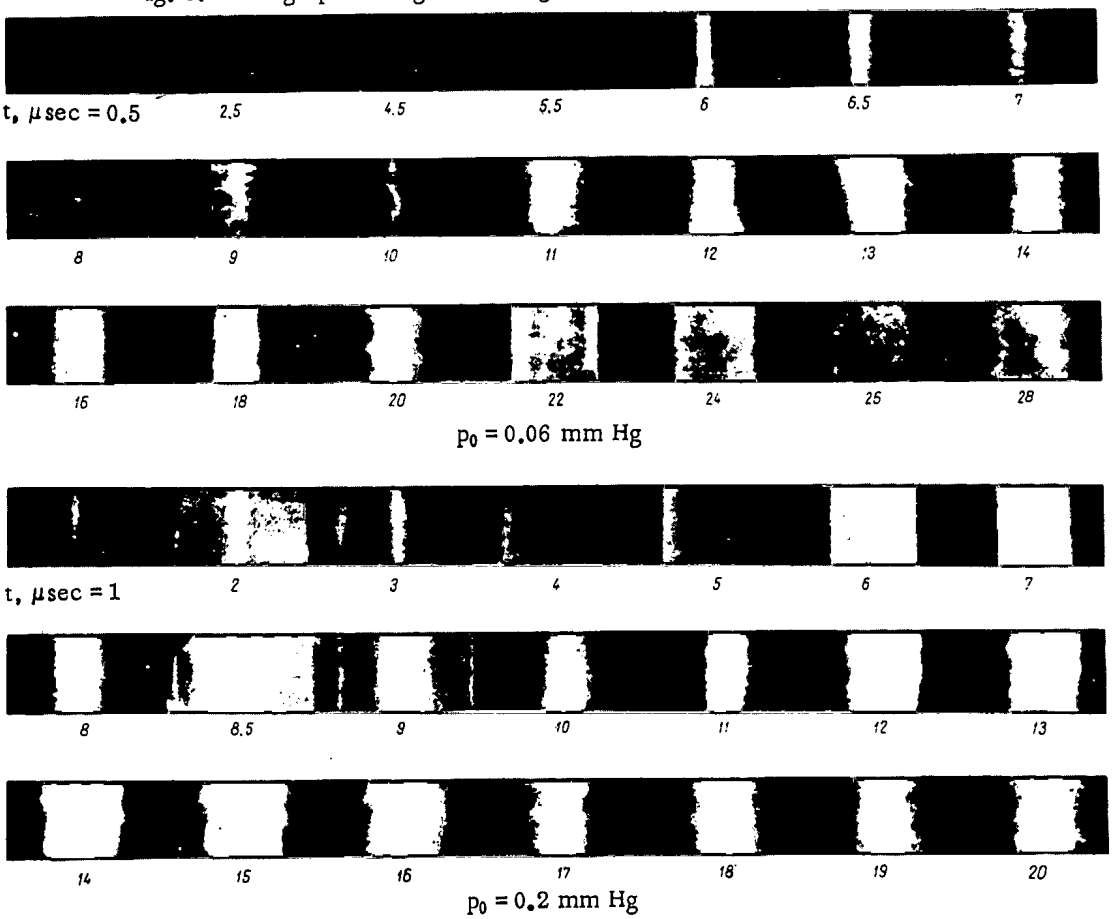

Fig. 6. Photographs of krypton discharges for various initial pressures p_0.

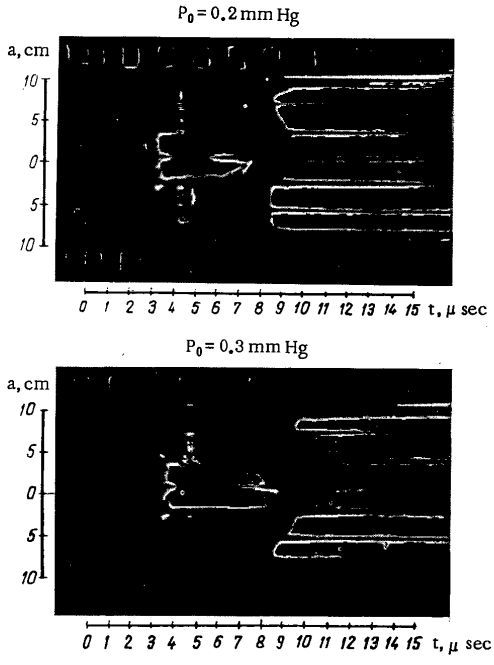

Fig. 7. Photographs of the discharge in deuterium obtained by means of the SFR operated in the continuous-sweep mode.

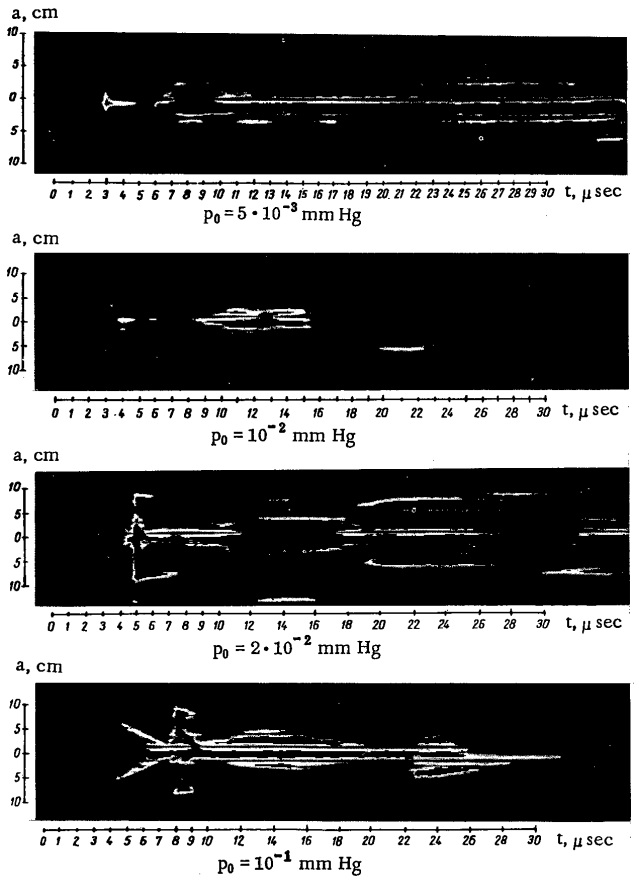

Fig. 8. Photographs of xenon discharge obtained with the SFR operated in the continuous-sweep mode.

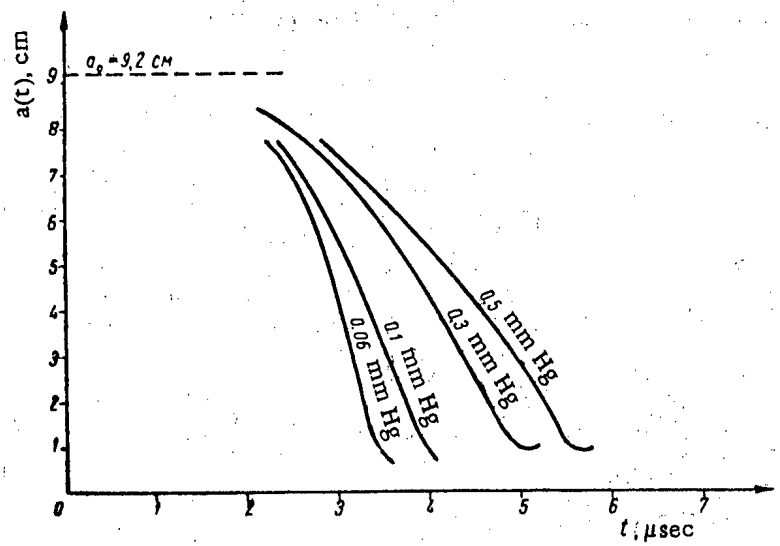

Fig. 9. Curve showing a(t) for a discharge in deuterium.

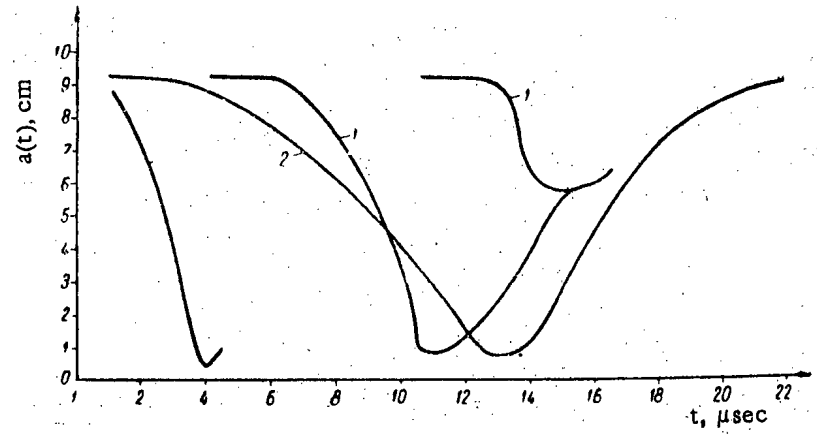

Fig. 10. Curves showing a(t) for a discharge in argon.
1) Curve obtained with p_0 = 0.02 mm Hg; 2) curve obtained with p_0 = 1.0 mm Hg.

In a deuterium discharge, when the second break occurs in the first quarter cycle of the current period the intensity of the radiation in the visible part of the spectrum is insufficient for a third peripheral process. In this case, after several small oscillations of the plasma column about the chamber axis (see Fig. 7) the luminescent radiation essentially vanishes and after approximately 1 μ sec appears again but at the periphery. Since the visible radiation of the gas occurs as a result of the excitation of neutral atoms in interaction with the other particles, the reduction of this radiation may be produced either by a reduction in the intensity of the interaction of particles or by a reduction in the number of neutral atoms in the region in which the current flows. A measurement of the current density distribution in the discharge chamber [1] indicates that in the time during which the amount of visible radiation is reduced the current density near the chamber axis continues to increase. Hence, the intensity of the interaction should also increase. Thus, the reduction in the radiated light can be explained only if it is assumed that in the region in which the current flows there are virtually no neutral atoms and, consequently, that the gas is almost completely ionized. In this case the ratio of the total number of ions to the total number of deuterium particles in the discharge chamber may become insignificant since the neutral atoms move from the region of maximum current density to the periphery as a

result of charge exchange. The radiation at the periphery appears as a result of the interaction of the plasma with the chamber walls after the plasma column breaks up. In this case atoms of silicon and oxygen enter the discharge region [3]; these atoms emit strongly in the visible part of the spectrum.

Neutron and hard x-ray radiation [2] are observed before the pinch breaks up. In the photograph of the deuterium discharge with an initial pressure of 0.06 mm Hg (see Fig. 3) the frame corresponding to the neutron pulse is denoted by the letter n.

In the case in which the discharge takes place in a heavy gas (argon, krypton, or xenon) the pinch does not break up. The pinch expands slowly up to a point at which it does not fill the entire volume of the chamber.

The fact that with high initial pressures of heavy gas in the discharge chamber the contraction in the column occurs at the end of the first half period of the current variation, i.e., the fact that the plasma still continues to contract when the current is already reduced, is a direct indication of the importance of inertia effects in the plasma contraction process [4].

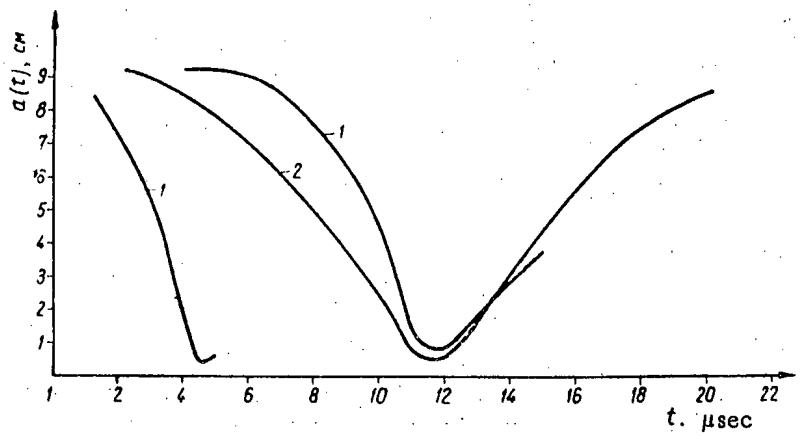

Fig. 11. Curve of a(t) for a discharge in xenon. 1) Curve obtained with $p_0 = 0.01$ mm Hg; 2) curve obtained with $p_0 = 0.3$ mm Hg.

It should be noted that the present interpretation of the behavior of the discharge is basically in agreement with recent measurements of the current density distribution over the cross section of the discharge chamber [1]. In spite of the fact that these measurements were carried out under somewhat different conditions, it is still reasonable to believe that the data obtained by means of high-speed photography and those obtained by measurements of the distribution of the electromagnetic field are in essential agreement although it is obvious that a more complete picture of the process is obtained in the latter case.

LITERATURE CITED

[1] L. A. Artsimovich, A. M. Andrianov, O. A. Bazilevskii, Iu. G. Prokhorov, and N. V. Filippov, J. Atomic Energy (USSR) 1, 76 (1956).*

[2] S. Iu. Luk'ianov and I. M. Podgornyi, J. Atomic Energy (USSR) 1, 97 (1956).*

[3] S. Iu. Luk'ianov and V. I. Sinitsyn, J. Atomic Energy (USSR) 1, 88 (1956).*

[4] M. A. Leontovich and S. M. Osovets, J. Atomic Energy (USSR) 1, 81 (1956).*

[5] N. A. Borzunov, V. I. Kogan, and D. V. Orlinskii, J. Atomic Energy (USSR) 4, 180 (1958).*

Received September 11, 1957.

* Original Russian pagination. See C. B. Translation.

THE EFFECT OF RADIATION ON THE VALENCE STATE OF PLUTONIUM IN NITRIC ACID SOLUTIONS

N. I. Popov, V. I. Medvedovskii, and N. A. Bakh

We investigated the effect of x-radiation on the valence state of plutonium in nitric acid solutions from 0.3 to 2.0 M and also in 0.3 M nitric acid solutions containing varying concentrations of $UO_2(NO_3)_2$ and $K_2Cr_2O_7$. The effect of radiation on nitric acid solutions, not containing $UO_2(NO_3)_2$, causes only oxidation of plutonium and the oxidation yield decreases with an increase in the concentration of NO_3^- ions and acidity of the solution. We put forward the hypothesis that the oxidation is effected by OH radicals. Under certain conditions the reduction of plutonium was observed in the presence of $UO_2(NO_3)_2$. Apparently, it is not effected by atomic hydrogen but by UO_2^+ ions. Potassium dichromate causes an acceleration in radiation oxidation of plutonium but under the given conditions it does not retard its reduction.

The effect of radiation on the valence state of plutonium in solution is hardly mentioned in the literature. The few reports on this problem refer to the effect of the α-radiation of plutonium itself and are observations of a casual nature [1, 2].

We systematically investigated changes in the valence state of plutonium in nitric acid solutions when treated with external radiation.

Besides pure nitric acid solutions, we investigated solutions containing also uranyl nitrate and potassium dichromate, which have the capacity of increasing the reduction or the oxidation of plutonium during irradiation.

Experimental Procedure

Radiation. As the radiation source we used a sealed x-ray tube, operating at 50 kv and 200 ma with the beam directed vertically upward. A cylindrical glass cell with a thin membrane was used in the work [3]. All investigations were carried out with constant mixing of the solution in an atmosphere of nitrogen. The temperature of the solution being irradiated was controlled by a thermocouple and in separate experiments it fluctuated from 20 to 25° C. The apparatus was shut off for short periods when samples were taken for analysis.

Dosimetry. The dose strength in the solutions was determined by the ferrous sulfate dosimetric method, considering 15.6 Fe^{++} ions oxidized per 100 ev of absorbed energy [4]. We took into consideration the relation of the soft x-radiation absorption to the thickness of the solution being irradiated and the difference in the energy absorption of the dosimetric solution and that of the systems being investigated. The dose strength in our experiments was from $5 \cdot 10^{16}$ to $9 \cdot 10^{16}$ ev/cm^3 · sec.

Analysis. In solution plutonium may have four valence states: Pu^{+3}, Pu^{+4}, PuO_2^+, and PuO_2^{++}. We did not aim at the identification of all the valence states of plutonium but limited ourselves to separating them into two forms: oxidized and reduced, considering the sum of $PuO_2^+ + PuO_2^{++}$ as the oxidized form and the sum of $Pu^{+3} + Pu^{+4}$ as the reduced form.

The two forms were separated by isolating Pu^{+3} and Pu^{+4} by precipitating the double sulfate of potassium and lanthanum from a solution saturated with potassium sulfate [5]. The amount of plutonium in the precipitate and in the solution was determined by the α-activity.

Reagents. All the salts used were specially purified to remove foreign materials and, before the experiment, recrystallized three times from doubly distilled water.

The working solutions of plutonium were prepared from a starting solution containing a mixture of oxidized and reduced plutonium with a total concentration of 2 g/liter of plutonium in 0.5 N HNO_3. The oxidized plutonium solutions were prepared by heating the starting solution on a boiling water bath. The reduced plutonium was prepared by passing hydrogen through the starting solution in the presence of platinized platinum. This method had been used previously only for the reduction of Pu^{+4} in hydrochloric acid solutions [6].

Results

We examine below the oxidation and reduction processes of plutonium in solutions containing nitric acid, sodium nitrate, uranyl nitrate and potassium dichromate in various concentrations and combinations.

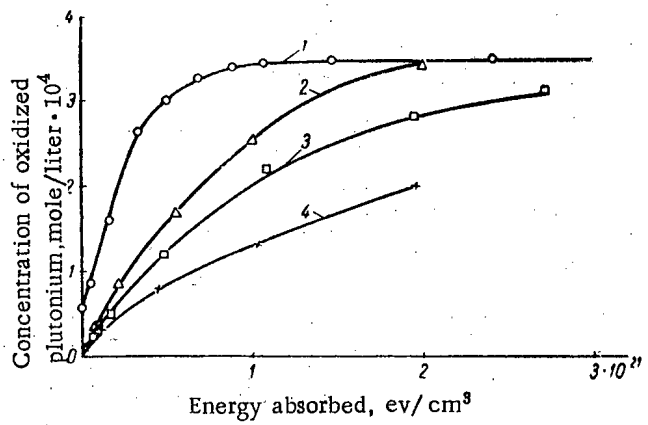

Fig. 1. Plutonium oxidation under the effect of x-radiation. The total plutonium concentration was $3.4 \cdot 10^{-4}$ mole/liter. 1) 0.3 N HNO_3; 2) 0.35 M $NaNO_3$ in 0.3 N HNO_3; 3) 0.88 M $NaNO_3$ in 0.3 N HNO_3; 4) 1.76 M $NaNO_3$ in 0.3 N HNO_3.

Solutions of HNO_3 and $NaNO_3$. When nitric acid solutions of reduced plutonium were treated with x-radiation, the latter was oxidized. The character and the rate of the process depended both on the NO_3^- ion concentration and on the acidity. Figure 1 gives plutonium oxidation curves in solutions of 0.3 N HNO_3 containing varying concentrations of $NaNO_3$. The curves show that the rate of increase in the concentration of oxidized plutonium in all the solutions investigated decreased with the absorption of energy. The initial oxidation yield decreased with an increase in the $NaNO_3$ concentration. Plutonium behaved similiarly when solutions of it in pure nitric acid were subjected to x-radiation, the only difference being that nitric acid depressed the oxidation yield of plutonium more efficiently than sodium nitrate.

Figure 2 gives the values of the oxidation yields of plutonium, determined from the tangent of the initial parts of the corresponding curves.

In solutions with equal NO_3^- ion contents but with different H^+ ion concentrations the initial oxidation yield of plutonium is lower, the greater the acidity of the solution. This conclusion was confirmed by results from direct experiments with solutions of variable H^+ ion concentrations and constant NO_3^- ion concentration (Fig. 3).

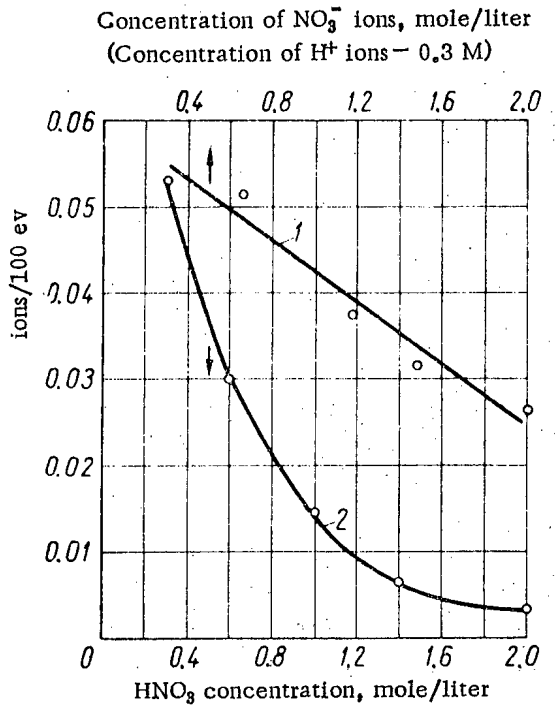

Fig. 2. The relation of the oxidation yield of plutonium 1) to $NaNO_3$ concentration; 2) to HNO_3 concentration.

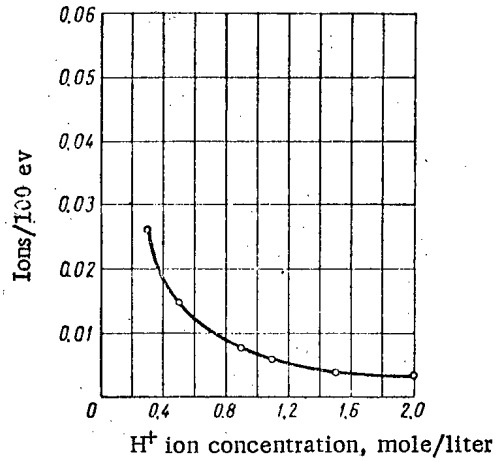

Fig. 3. The relation of the oxidation yield of plutonium to acidity. NO_3^- ion concentration – 2.0 M.

Solutions of $UO_2(NO_3)_2$ in 0.3N HNO_3. The behavior of plutonium in nitric acid solutions containing $UO_2(NO_3)_2$ was very closely related to the concentration of the latter.

In solutions with $UO_2(NO_3)_2$ concentrations not greater than 0.3 M the plutonium was oxidized due to the radiation. The initial oxidation yield fell from 0.052 ions/100 ev for pure acid to 0 in a 0.3 M solution of $UO_2(NO_3)_2$, in which the ratio of the oxidized and reduced forms of plutonium remained unchanged during the irradiation process. We observed plutonium reduction at $UO_2(NO_3)_2$ concentrations higher than 0.3 M. The reduction yield increased with an increase in the $UO_2(NO_3)_2$ concentration from 0 to 0.17 ion/100 ev at 0.88 M $UO_2(NO_3)_2$.

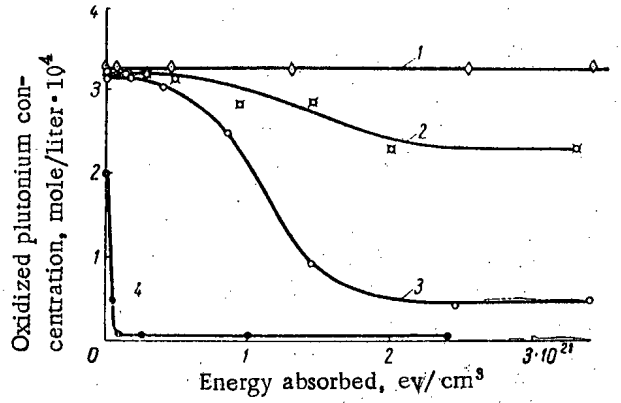

Fig. 4. The effect of x-radiation on the valence state of plutonium in 0.3 N HNO_3 solutions containing $UO_2(NO_3)_2$ in concentrations of: 1) 0.3 M; 2) 0.45 M; 3) 0.6 M; 4) 0.88 M.

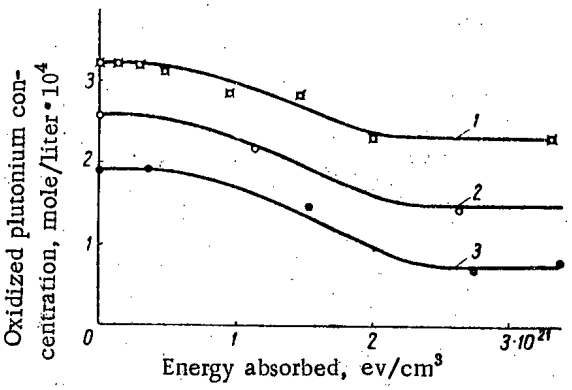

Fig. 5. The effect of radiation on the valence state of plutonium in solutions of 0.3 N HNO_3 and 0.45 M $UO_2(NO_3)_2$ at various initial concentrations of oxidized plutonium. 1) $3.3 \cdot 10^{-4}$ M; 2) $2.6 \cdot 10^{-4}$ M; 3) $1.8 \cdot 10^{-4}$ M.

The plutonium reduction curves are given in Fig. 4. The initial solutions contained plutonium wholly in the oxidized form.

The curves for solutions of intermediate $UO_2(NO_3)_2$ concentrations were of a complicated character. At concentrations of 0.45 and 0.6 M, reduction of plutonium was observed only after the absorption of a definite energy dose and did not proceed to the end but to a definite stationary state. The reduction of plutonium began earlier and proceeded in higher yield the higher the $UO_2(NO_3)_2$ concentration. In a solution of 0.45 M $UO_2(NO_3)_2$ plutonium was reduced at approximately $5 \cdot 10^{20}$ ev/cm^3, and the reduction yield, calculated from the tangent at the inflection point of the curve, equals approximately 0.002 ion/100 ev, and at a 0.6 M concentration the reduction began after the absorption of approximately $2 \cdot 10^{20}$ ev/cm^3 and proceeded with a yield of 0.02 ion/100 ev.

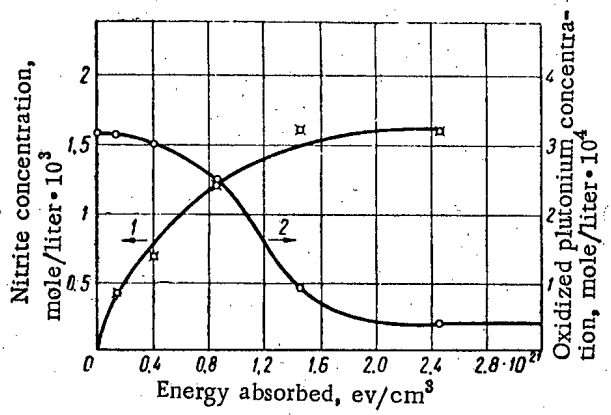

Fig. 6. The relation of the concentration of nitrite formed (1) and oxidized plutonium (2) to the radiation dose in a 0.3 N HNO_3 and 0.6 M $UO_2(NO_3)_2$ solution. The total plutonium concentration was $3.2 \cdot 10^{-4}$ mole/liter.

The degree of plutonium reduction increased with an increase in the $UO_2(NO_3)_2$ concentration. However, the ratio of oxidized and reduced forms in the stationary state could be different even at the same $UO_2(NO_3)_2$ concentration, if the starting concentrations of the oxidized form were different. This may be seen from Fig. 5, using as an example solutions with a 0.45 M content of $UO_2(NO_3)_2$. In the initial solution all the plutonium was in the oxidized form.

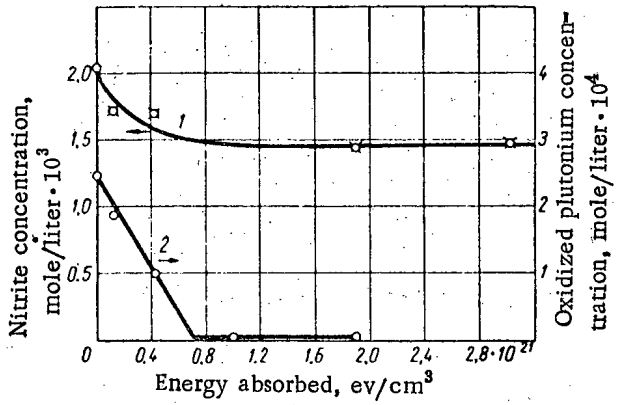

Fig. 7. The relation of nitrite (1) and oxidized plutonium (2) concentrations to radiation dose in a solution of 0.3 N HNO_3, 0.6 M $UO_2(NO_3)_2$ and $2.1 \cdot 10^{-3}$ M $NaNO_3$. The total plutonium concentration was $2.5 \cdot 10^{-4}$ mole/liter.

Besides determining the valence forms of plutonium, the irradiated solutions were analyzed for nitrite content, which was formed due to the radiation. It was interesting to compare the nitrite accumulation with the behavior of the plutonium in the same solutions. Figure 6 gives the corresponding curves for a solution containing 0.6 M $UO_2(NO_3)_2$. Noticeable reduction of oxidized plutonium started only after the accumulation of a certain nitrite concentration in the solution (approximately $5 \cdot 10^{-4}$ mole/liter) and proceeded only to a constant value for the nitrite concentration.

The relation between plutonium reduction and the change in nitrite concentration under the effect of radiation was observed also in the case when, before irradiation, nitrite was introduced into the solution at a concentration higher than its stationary value in this system (Fig. 7).

Solutions of $UO_2(NO_3)_2$ and $K_2Cr_2O_7$ in 0.3 N HNO_3. As is known, potassium dichromate is capable of oxidizing reduced plutonium to a hexavalent state. This nonradiation effect was taken into account when calculating the initial yield of the radiation oxidation of plutonium.

On introducing $K_2Cr_2O_7$ into the solutions investigated above, in all cases plutonium oxidation and potassium dichromate reduction was observed from the beginning of the irradiation. However, if oxidation occurred without potassium dichromate, its yield rose.

When the $UO_2(NO_3)_2$ concentration was not greater than 0.3 M, the plutonium, oxidized at the start of the irradiation, remained in an oxidized state up to a dose of $4.2 \cdot 10^{21}$ ev/cm^3. The reduction of plutonium was observed in solutions with higher uranyl nitrate concentrations and energy absorptions greater than a dose of $1.2 \cdot 10^{21}$ ev/cm^3.

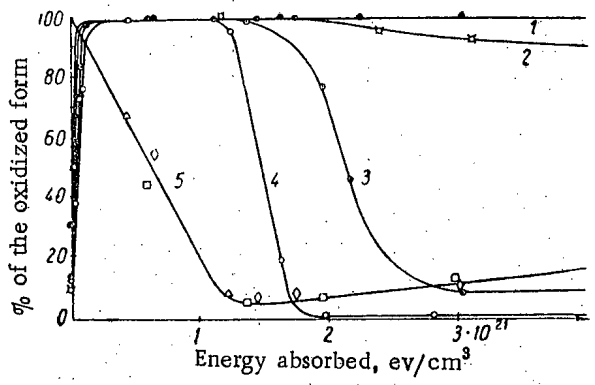

Fig. 8. The effect of radiation on the valence state of plutonium in solutions of 0.3 N HNO_3 and 0.1 N $K_2Cr_2O_7$, containing $UO_2(NO_3)_2$. 1) 0.3 M; 2) 0.45 M; 3) 0.6 M; 4) 0.88 M; 5) disappearance curve for $K_2Cr_2O_7$: ○) 0.3 M $UO_2(NO_3)_2$; △) 0.6 M; □) 0.88 M.

The reduction curves (Fig. 8) are very similar to the curves obtained without potassium dichromate. A dose equal to $1.2 \cdot 10^{21}$ ev/cm^3 corresponded to almost complete disappearance of hexavalent chromium (Curve 5), whose concentration was determined polarographically with a 1 N KOH background. The reduction yield for hexavalent chromium did not depend on the uranyl nitrate concentration. It is interesting to note that under the effect of radiation the hexavalent chromium concentration passed through a minimum after which it increased slowly.

On increasing the HNO_3 concentration from 0.3 to 1.5 N, after the absorption of a certain amount of energy, we observed the reduction of oxidized plutonium; however, as Curves 1 and 2 in Fig. 9 show, it began long before the complete disappearance of potassium dichromate. A similar phenomenon was observed on simultaneously increasing the $K_2Cr_2O_7$ concentration to 0.3 N and only the initial plutonium reduction was displaced.

Solutions with high HNO_3 and $K_2Cr_2O_7$ concentrations were irradiated by an electron beam with 0.8 Mev energy at a dose strength of approximately $5 \cdot 10^{17}$ ev/cm^3 · sec. The oxidized plutonium concentration was determined in these experiments by extraction with ethyl ether in the presence of ammonium nitrate.

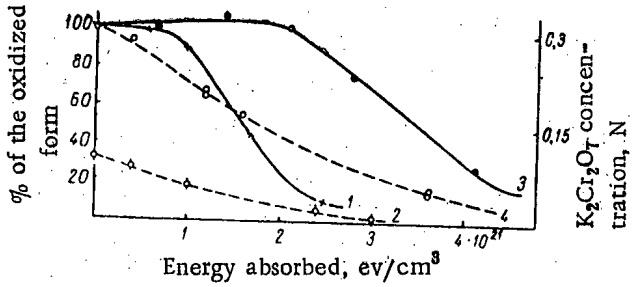

Fig. 9. The effect of radiation on the valence state of plutonium. 1) 1.5 N HNO_3, 0.1 N $K_2Cr_2O_7$ and 0.8 M $UO_2(NO_3)_2$; 3) 1.5 N HNO_3, 0.3 N $K_2Cr_2O_7$ and 0.8 M $UO_2(NO_3)_2$; reduction of $K_2Cr_2O_7$: 2) in solution 1; 4) in solution 3.

DISCUSSION

Some conclusions may be drawn from the results examined on the mechanism of the effect of x-radiation on the valence state of plutonium in nitric acid solutions. The direct effect of radiation on plutonium ions and the effect of its own α-radiation may be disregarded at low plutonium contents. All changes in the valence state of plutonium should be considered as the result of a reaction of plutonium ions with the radiolysis products of the medium, which were formed under the effect of external radiation.

Of the series of oxidation-reduction conversions of plutonium ions from Pu^{+3} to PuO_2^{++}, occurring due to radiation, the conversions Pu^{+3} - Pu^{+4} and PuO_2^+ - PuO_2^{++} proceed most readily, as they only consist of the transfer of one electron. In contrast to this, the conversion at the Pu^{+4}-PuO_2^+ stage or the reverse is more difficult as it requires the breaking or formation of the chemical bond of the oxygen-plutonium ion; the conversion can occur only under the effect of strong oxidants or reducing agents.

In the radiolysis of aqueous solutions of HNO_3 and $NaNO_3$, in which oxidation of plutonium ions was observed, in the absence of oxygen, various products were formed: H, OH, H_2, H_2O_2, HNO_2 and nitrogen oxides. Molecular hydrogen does not react with plutonium in the absence of platinum. Hydrogen peroxide and nitrous acid, as is known, are incapable of oxidizing tetravalent plutonium to the hexavalent state, as they reduce the latter and this reduction proceeds with disproportionation [7, 8], which takes place very slowly (days). These reactions cannot be used to explain the processes occurring under the effect of x-radiation for short periods of time (of the order of tenths of a minute). For the same reason the stable nitrogen oxides: NO, NO_2 and N_2O_4, formed in the solutions, are not taken into consideration.

Plutonium oxidation under the effect of radiation may be explained by a reaction involving OH radicals, by the scheme

$$Pu^{+4} + OH + H_2O \rightarrow PuO_2^+ + 3H^+, \qquad (1)$$

as it is known that the OH radical is a strong oxidant in an acidic medium. Its normal potential for reduction to H_2O equals 2.8 v [9]. It is also possible that oxidation also occurs with the participation of unstable higher nitrogen oxides.

The radiation-chemical oxidation yield of plutonium was very low. The highest yield, obtained in 0.3 N HNO_3, was equal to approximately 0.05 ion/100 ev. The decrease in the initial yield with an increase in the NO_3^- ion concentration was, apparently, due to the capacity of reduced plutonium to form complexes with the nitrate ion [10-12]. The low reactivity of such a complex was confirmed with nonradiation experiments. It is known, for example, that the thermal oxidation of plutonium with nitric acid was considerably slowed down at high nitric acid or uranyl nitrate concentrations [13]. We observed a similar phenomenon in the nonradiation oxidation of plutonium with potassium dichromate. In this reaction the oxidation was retarded much more strongly by nitric acid than by nitrate salts at equal NO_3^- ion concentrations. The results of the radiation-chemical oxidation of plutonium are also related to this phenomenon. It was suppressed more effectively by nitric acid than by sodium nitrate.

The absence of reduction in these solutions could be explained by a possible reaction with atomic hydrogen

$$PuO_2^+ + H + 3H^+ \rightarrow Pu^{+4} + 2H_2O \qquad (2)$$

being fully suppressed by the reaction

$$NO_3^- + H \rightarrow NO_2 + OH^- \qquad (3)$$

with the existing ratio of plutonium ion and NO_3^- concentrations. As the experimental data given show, plutonium reduction in nitric acid solutions becomes possible if the solution contains $UO_2(NO_3)_2$.

Miller et al. [14] established that under the effect of ionizing radiation, pentavalent uranium formed in solutions of uranyl salts. The normal oxidation-reduction potential of the UO_2^{++}/UO_2^+ pair is equal to 0.05 v [15], i.e., close to that of hydrogen. On this basis the following scheme for plutonium reduction under the effect of UO_2^+ ions may be proposed:

$$PuO_2^+ + UO_2^+ + 4H^+ \rightarrow Pu^{+4} + UO_2^{++} + 2H_2O. \qquad (4)$$

Due to the commensurable concentration of uranyl and nitrate ions the H radicals were distributed between them. With this, the reduction rate of the NO_3^- ion by the UO_2^+ ion was considerably less than its reduction by atomic hydrogen and as a result UO_2^+ accumulated to a concentration that was sufficient for plutonium reduction.

The changes observed in the valence state of plutonium in solutions containing $UO_2(NO_3)_2$ may be explained by the simultaneous occurrence, from the very beginning of irradiation, of two opposed processes – oxidation and reduction–with oxidation predominating up to 0.3 M $UO_2(NO_3)_2$ and reduction predominating after 0.6 M. At the start of irradiation the oxidation and reduction rates were equal in the range of $UO_2(NO_3)_2$ concentrations from 0.3 to 0.6 M. The start of plutonium reduction only after the absorption of a definite energy dose showed that it was possible only after certain radiation-chemical reactions in the system. Direct experiments, whose results are given graphically in Figs. 6 and 7, showed that plutonium reduction in suitable solutions was due to the presence of sufficient nitrous acid in them, formed due to radiation or introduced into the starting solution. However, its role in this process remains unclear. It is possible that it slows down plutonium oxidation as it is an acceptor of OH radicals.

Turning to solutions containing $K_2Cr_2O_7$, we may note that plutonium oxidation was observed in them at any $UO_2(NO_3)_2$ concentrations at the start of irradiation. The increase in yield due to $K_2Cr_2O_7$ may be caused by the oxidation of pentavalent uranium that was formed by $Cr_2O_7^{--}$ ions. After the reduction of all the potassium dichromate in solutions of 0.3 M HNO_3 and 0.1 N $K_2Cr_2O_7$ with varying $UO_2(NO_3)_2$ concentrations, the character of the changes in the valence state of plutonium was, in general, the same as in solutions not containing $K_2Cr_2O_7$.

Plutonium reduction in the presence of $K_2Cr_2O_7$, observed in solutions with 1.5 N HNO_3, apparently should be attributed to increased complex formation by the reduced plutonium at this acidity. This hypothesis requires additional experimental data for substantiation.

LITERATURE CITED

[1] M. Kasha and G. E. Sheline, The Transuranium Elements, (McGraw-Hill Co., New York, 1949) 1, p. 180.

[2] M. Kasha, ibid., p. 295.

[3] V. I. Medvedovskii, N. A. Bakh, and E. V. Zhuravskaia, Collection of Works on Radiational Chemistry (Acad. Sci. USSR Press, 1955) p. 71.

[4] J. Weiss, W. Bernstein, and B. Kuper, J. Chem. Phys. 22, 1593 (1954).

[5] B. V. Kurchatov, V. I. Grebenshchikova, N. B. Cherniavskaya, and G. N. Iakovlev, Investigations in the Fields of Geology, Chemistry, and Metallurgy (Reports of the Soviet Delegation to the International Conference on the Peaceful Uses of Atomic Energy) (Acad. Sci. USSR Press, 1955) p. 219.

[6] R. E. Connick and W. H. McVey, The Transuranium Elements (McGraw-Hill Co., New York, 1949) 1, p. 142.

[7] R. E. Connick, ibid., p. 280.

[8] G. Seaborg and J. Katz, Actinides, (Foreign Lit. Press, 1955) p. 231 (Russian translation).

[9] V. Latimer, The Oxidation States of Elements and Their Potentials in Aqueous Solutions (Foreign Lit. Press, 1954) p. 51 (Russian translation).

[10] J. C. Hindman and D. P. Ames, The Transuranium Elements, (McGraw-Hill Co., New York, 1949) 1, p. 348.

[11] J. C. Hindman, ibid., p. 348.

[12] C. E. McLane, J. S. Dixon, and J. C. Hindman, ibid., p. 388.

[13] K. A. Kraus, ibid., p. 264.

[14] N. B. Miller, Ts. I. Zalkind, and V. I. Veselovskii, The Effect of Ionizing Radiation on Inorganic and Organic Systems, Coll. of Articles (Acad. Sci. USSR Press, 1958) p. 93.

[15] H. G. Heal and G. N. Thomas, Trans. Farad. Soc. 45, 11 (1949).

Received April 23, 1957.

STUDY OF THE ZIRCONIUM APEX OF THE Zr – Ta – Nb PHASE DIAGRAM

V. S. Emel'ianov, Iu. G. Godin, and A. I. Evstiukhin

Metallographical examination, thermal analysis and electrical resistance measurements have been applied to a study of the zirconium apex, up to 82% zirconium and a temperature of 1200° C, of the ternary system Zr–Ta–Nb, with limited solubility of tantalum and niobium in α- zirconium (γ phase), limited solubility and complete solubility of niobium in β-zirconium, with eutectoid decomposition of the β solid solution and three-phase eutectoid equilibrium $\beta \rightleftharpoons \alpha + \gamma$ between α- and β-zirconium. In the investigated portion of the Zr–Ta–Nb phase diagram, the following phase regions were found: a) two one-phase regions α and β; b) three two-phase regions $\alpha + \beta$, $\beta + \gamma$ and $\alpha + \gamma$; c) one three-phase region $\alpha + \beta + \gamma$; the β region contracts as the temperature falls below 1200° C.

The solubility of tantalum and niobium in α-zirconium in the system Zr–Ta–Nb is about 0.5%. On passing from Zr–Ta to Zr–Nb, the $\alpha + \beta$ and $\beta + \gamma$ regions are displaced toward lower temperatures and high niobium concentrations; the boundaries of the $\alpha + \gamma$ and $\alpha + \beta + \gamma$ regions are lowered from 790° for Zr–Ta to 612° C for Zr–Nb. Passing between the $\alpha + \beta$ and $\beta + \gamma$ regions is a binary eutectoid line which, from Zr–Ta to Zr–Nb is displaced toward lower temperatures and higher niobium concentrations. The solubility of niobium in α zirconium in the Zr–Nb system is about 0.5% by weight. Eutectoid decomposition in the Zr–Ta system shifts the maximum of the martensitic-like transformation to the left and results in an increase in the stability of the β phase at room temperature in quenched alloys.

The literature contains no information on the ternary system Zr–Ta–Nb. The constitutional diagrams for the Zr–Ta and Zr–Nb phases comprised in this system have already been studied [1-3]. In the investigations [2] and [3] of the Zr–Nb system, however, there are discrepancies in the temperature of the eutectoid decomposition (615-560° C), the position of the eutectoid point (17.5-12 % niobium) and the temperature of the minimum on the solidus curve. It is also known [4] that the eutectoid temperature in this system is 800° C, and that the solubility of niobium in α zirconium at 750° C is less than 5%. As regards the binary system Ta–Nb, this system is represented by a continuous series of solid solutions [5].

We have studied the zirconium apex of the ternary diagram bounded by the curves corresponding to 82% zirconium and the temperature 1200° C and have also investigated the solid state transformation in the Zr–Nb system. The metallographical and thermal and x-ray analysis methods described in the previous paper [1] were used in the investigation.

In constructing the zirconium apex of the phase diagram of the system Zr–Ta–Nb, five polythermal cross sections were taken through the point of the apex with the ratio $\frac{\%\,Nb}{\%\,Ta}$ = 0.2, 0.5, 1.0, 2.0, and 5.0. The serial numbers of these cross sections are 1, 2, etc. Alloys containing 0.5, 1.0, 2.0, 3.0, 4.0, 7.0, 10.0, 12.0, 14.0, 16.0, and 18.0% by weight of tantalum and niobium were prepared for each polythermal cross section.

In preparing the alloys, rods of zirconium iodide of the following composition (% by weight) were used: hafnium 1.1, nitrogen $2 \cdot 10^{-3}$, iron $3 \cdot 10^{-3}$, silicon $1.5 \cdot 10^{-2}$, calcium $5 \cdot 10^{-3}$, carbon $9 \cdot 10^{-3}$, chlorine $2.6 \cdot 10^{-3}$, tungsten $3 \cdot 10^{-3}$, molybdenum $1.4 \cdot 10^{-3}$, manganese $1.5 \cdot 10^{-4}$, oxygen $5 \cdot 10^{-3}$, hydrogen $3 \cdot 10^{-3}$.

Tantalum and niobium were used in the form of thin ribbon. The tantalum contained the following impurities (% by weight): niobium 0.5, titanium 0.06, tungsten 0.02, iron < 0.05, molybdenum 0.03, silicon < 0.1; the niobium contained: tantalum 0.5, titanium 0.2, iron 0.08, silicon 0.08.

No chemical analysis was made of the specimens, due to the difficulty in separating tantalum and niobium. As a check on the composition, the alloys as cast were weighed on an industrial balance. Usually, the difference in weight before and after melting amounted to hundredths of a gram. The heat-treatment conditions of the alloys are shown in the following table:

Heat-Treatment Conditions of the Alloys

Annealing temp., °C	Annealing period, hours	Annealing temp., °C	Annealing period, hours
1200	60	730	450
1000	80	700	560
900	190	670	600
820	260	645	600
790	360	625	600
765	370	600	600

The temperature records were made at heating and cooling rates of 6-8 degree/min. The results of the thermal analysis of the polythermal cross sections Nos. 1, 3, and 5 are represented in Figs. 1, 3, and 5 by thin dot-and-dash lines. They show that the temperature of the $\alpha-\beta$ transformation decreases with increase in tantalum and niobium content of each polythermal cross section. The boundaries of the three-phase region ($\alpha + \beta + \gamma$), as well as the boundaries of the two-phase region ($\alpha + \beta$) fall from the first to the fifth polythermal cross section.

According to the data of the thermal analysis, the solubility of tantalum and niobium is: for the first cross section 4%, for the third 5%, for the fifth 6%. The temperatures at which maximum solubility of tantalum and niobium in zirconium is observed decrease from 750° C in the first cross section to 675° C in the fifth.

Metallographical Examination

A study of the structure of the cast alloys showed that solid solutions of tantalum and niobium were present in the system investigated. Alloys containing small amounts of tantalum and niobium had a martensitic-like structure of the transformed β phase. X-ray phase analysis established that in alloys of high tantalum and niobium content, the β phase is stabilized by quenching, and is partly transformed into a needle-like phase. In the structure of all these alloys, needle-like precipitations of α phase were observed against the light background of β-phase.

Figures 1 to 5 show the polythermal cross sections based on the results of metallographical examination of the quenched alloys. Study of the microstructure of the alloys quenched after annealing at 1200 and 1000° C showed that at these temperatures, throughout the entire region examined, there is a continuous range of solid solutions based on β-zirconium and having different structures. Alloys containing slight additions of tantalum and niobium have a characteristic martensitic-like structure (Fig. 6). As the content of tantalum and niobium is increased, the martensitic-like structure of the transformed β phase passes into the needle structure of the α phase on a background of fixed β phase (Fig. 7). It is observed that the higher the ratio of niobium content to that of tantalum in a given polythermal cross section, the lower is the content of tantalum and niobium at which fixing of the β phase by quenching commences, i.e., the addition of niobium to alloys of the Zr–Ta system increases the stability of the β phase at room temperature.

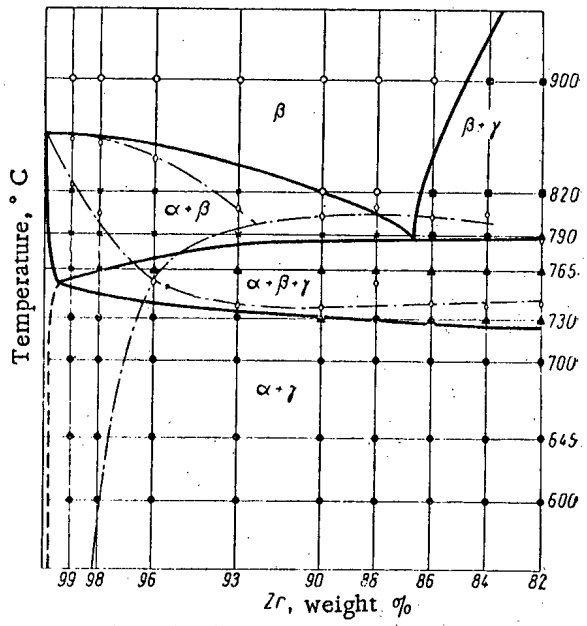

Fig. 1. Polythermal cross section No. 1 of the system Zr–Ta–Nb, with constant ratio of percentage content of niobium to tantalum equal to 0.2. ——————— results of thermal analysis; ○ β phase; ■ β + γ phases; × α + β phases; ▲ α + β + γ phases; ● α + γ phases.

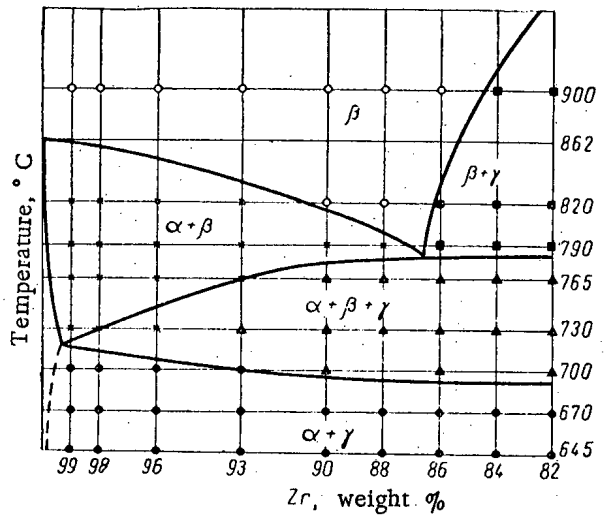

Fig. 2. Polythermal cross section No. 2 of the system Zr–Ta–Nb with constant ratio of the percentage content of niobium to tantalum equal to 0.5. ○ β phase; ■ β + γ phases; × α + β phases; ▲ α + β + γ phases; ● α + γ phases.

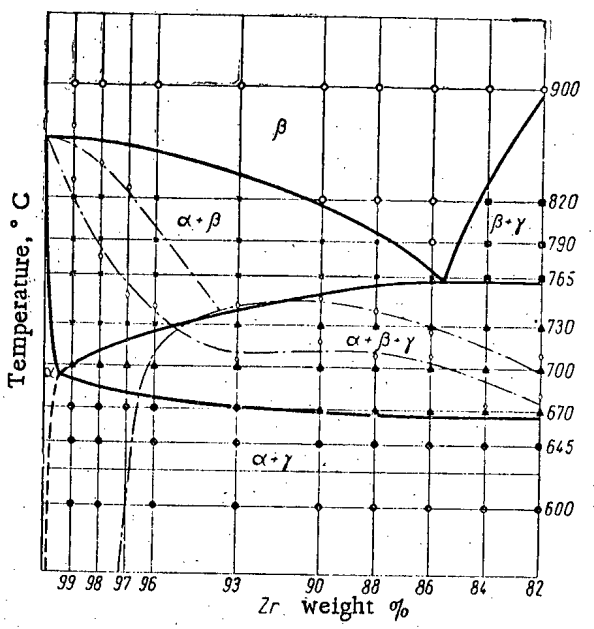

Fig. 3. Polythermal cross section No. 3 of the system Zr–Ta–Nb with constant ratio of the percentage content of niobium to tantalum equal to 0.1. ——————— results of thermal analysis; ○ β phase; ■ β + γ phases; × α + β phases; ▲ α + β + γ phases; ● α + γ phases.

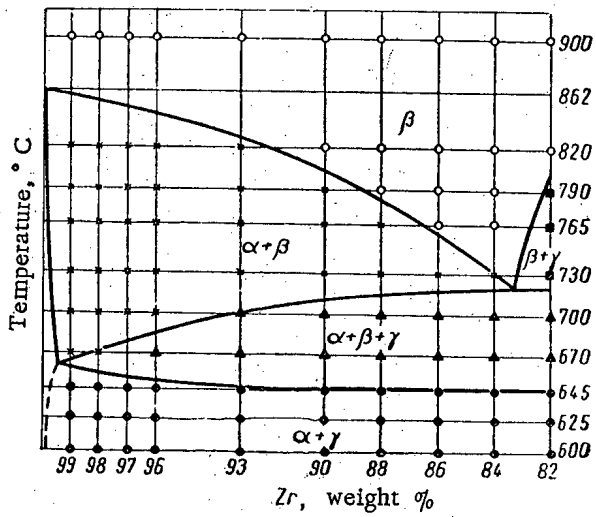

Fig. 4. Polythermal cross section No. 4 of the system Zr– Ta–Nb with constant ratio of the percentage content of niobium to tantalum equal to 2.0. ○ β phase; ■ β + γ phases; × α + β phases; ▲ α + β + γ phases; ● α + γ phases.

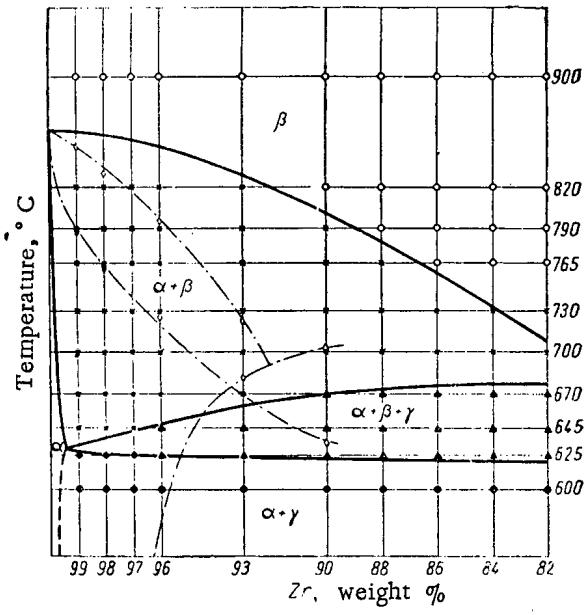

Fig. 5. Polythermal cross section No. 5 of the system Zr–Ta–Nb with constant ratio of the percentage content of niobium to tantalum equal to 5.0.

– – – – – – results of thermal analysis; ○ β phase; ■ β + γ phases; × α + β phases; ▲ α + β + γ phases; ● α + γ phases.

On quenching from 900° C in alloys of the first and second polythermal cross sections, there is precipitation of the γ-phase, a solid solution of α-zirconium in a solid solution of tantalum and niobium. The existence of the γ-phase was confirmed by x-ray phase analysis: lines of this phase appeared on the diffraction pattern of the alloy of the first polythermal cross section, containing 18% tantalum and niobium, quenched from 900° C. On lowering the quenching temperature, the precipitation of γ phase was also revealed in alloys of the third (Fig. 8) and fourth polythermal cross sections. In alloys of the fifth polythermal cross section, separations of the γ-phase were not observed on quenching from a temperature above the α + β + γ region. The results of the metallographical examination of the quenched alloys showed that the boundary between the β phase and β + γ phase, with increase in the ratio $\frac{\%\text{Nb}}{\%\text{Ta}}$ in the alloys, is shifted toward a lower zirconium content (see Figs. 2-6) and the temperature of the commencement of the separation of the γ-phase from the β solid solution is lowered.

The two-phase region α + β was found in all polythermal cross sections at temperatures below 862° C. The typical structure of the two-phase α + β region is shown in Fig. 9. The upper boundary of this region is shifted, from the first cross section to the fifth, toward a lower concentration of zirconium and an increase in the %Nb / %Ta ratio in the alloys, and in the fifth cross section passes beyond the limit of the investigated region.

Fig. 6. Microstructure of the alloy from the first polythermal cross section containing 7% tantalum and niobium. Martensitic-like structure of the transformed β phase. Quenched from 1000° C. (× 200).

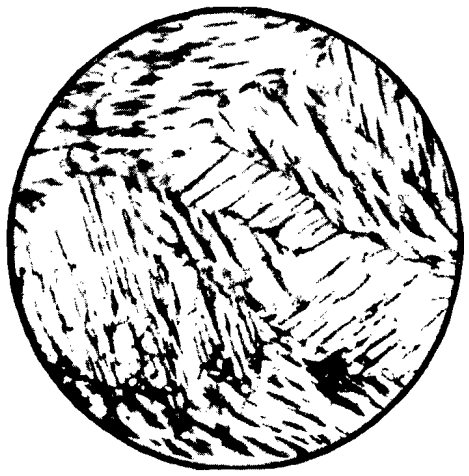

Fig. 7. Microstructure of the alloy from the fifth polythermal cross section containing 16% tantalum and niobium. Needle structure of the α phase on a background of fixed β phase. Quenched from 1200° C. (× 200).

By extrapolating the upper boundaries of the $\alpha + \beta$ and $\beta + \gamma$ regions to intersection, we obtained points on the four polythermal cross sections which, when connected, form a line of eutectoid transformation. With increase in the $\frac{\%\ Nb}{\%\ Ta}$ ratio of the alloys, this line is shifted toward higher niobium concentrations and lower temperatures. In the fifth polythermal cross section, the point situated on the binary eutectoid line is outside the region of concentrations investigated.

According to the data of this metallographical examination, the maximum solubility of tantalum and niobium in α- zirconium is about 0.5% by weight.

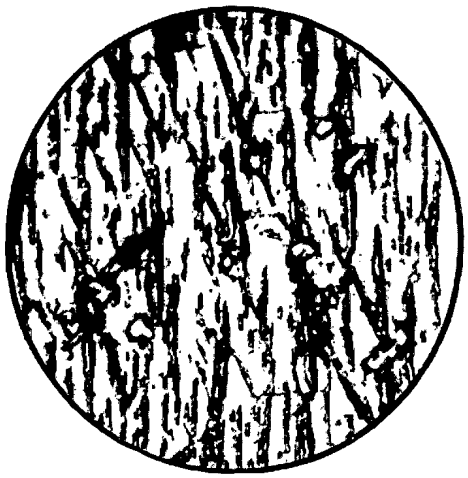

Fig. 8. Microstructure of the alloy from the third polythermal cross section containing 18% tantalum and niobium. Separations of the γ phase visible on a background of fixed β phase and needle α- phase. Quenched from 800° C. (× 500).

Fig. 9. Microstructure of the alloy from the fourth polythermal cross section containing 10% tantalum and niobium. Two-phase $\alpha + \beta$ structure. Quenched from 730° C. (× 500).

An x-ray study of the solubility of tantalum and niobium in zirconium using an IKROS back-reflection camera failed to reveal any appreciable variation in the lattice constants of α-zirconium for alloys of all five polythermal cross sections containing 0.5 and 1.0 % by weight of niobium and tantalum. This is also evidence of the insignificant solubility of tantalum and niobium in α-zirconium.

The temperature of the commencement of the eutectoid decomposition of the β solid solution was determined from the appearance of dark, finely dispersed precipitates of eutectoid in the structure of the alloys. The x-ray diffraction patterns of such alloys, even for low tantalum and niobium contents, showed lines of the γ phase, the intensity of which increases with decrease in the quenching temperature.

The temperature of complete decomposition of the β solid solution was determined from the disappearance of elongated separations of α or β phase from the structure of the quenched alloys. Figure 10 shows the structure of the alloy of the second polythermal cross section containing 7% tantalum and niobium, quenched from 700° C, the coagulated precipitations of γ phase being visible on the background of α phase.

Since the data obtained in our study of the ternary system Zr–Ta–Nb, with regard to solubility in the α phase and the position of the binary eutectoid line, were not in agreement with the data of [2] and [3] concerning the Zr–Nb system, we made an additional study of the latter.

Alloys were prepared containing 0.3, 0.7, 1.0, 1.5, 2.5, 4.0, 10.0, 12.5, 14.0, 16.0, 18.0, and 20% by weight of niobium. After homogenizing at 1200° C for 40 hours, the alloys were annealed at 600 and 625° C, followed by quenching in water.

All the alloys quenched from 625° C had a two-phase structure $\alpha + \beta$, except the alloy containing 0.3% niobium. Extrapolation of the binary eutectoid line in the ternary system to intersection with the binary system Zr–Nb showed that the eutectoid point of the Zr–Nb system is at about 24% niobium.

Fig. 10. Microstructure of alloy from the second polythermal cross section containing 7% tantalum and niobium. $\alpha + \beta$. Quenched from 700° C. (× 1000).

Fig. 11. Microstructure of alloy containing 20% niobium. Two-phase $\alpha + \gamma$ structure. Quenched from 600° C. (× 500).

Fig. 12. Microstructure of alloy containing 0.3% niobium. One-phase α solid solution. Quenched from 625° C. (× 500).

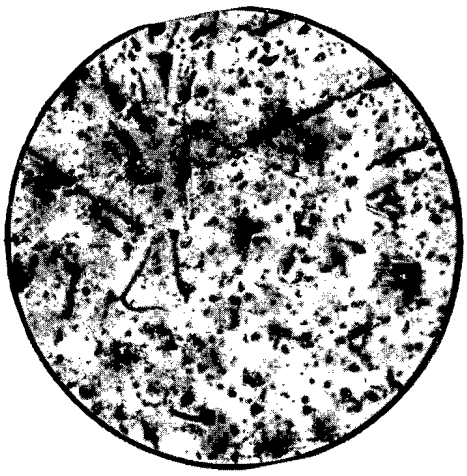

Fig. 13. Microstructure of alloy containing 0.7% niobium. Precipitations of β phase visible on background of α phase. Quenched from 625° C. (× 500).

All the alloys quenched from 600° C, with the exception of the alloy containing 0.3 % niobium, had a two-phase $\alpha + \gamma$ structure. Figure 11 shows the structure of the alloy containing 20% niobium quenched from 600° C. The $\alpha + \gamma$ eutectoid is visible on the background of α phase. The temperature of eutectoid decomposition accordingly lies between 600 and 625° C. We assumed it to be equal to 612 ± 13° C, which is in good agreement with the values of [2].

Examination of the microstructure of alloys with 0.3 and 0.7% niobium, quenched from 625° C, showed that the alloy with 0.3 % niobium consists of one-phase α solid solution (Fig. 12), and the alloy with 0.7 % niobium consists of α solid solution and transformed β-phase (Fig. 13). It was therefore assumed that the solubility of niobium in α-zirconium is about 0.5%, which is in good agreement with the solubility of tantalum and niobium in α zirconium as determined for the ternary system.

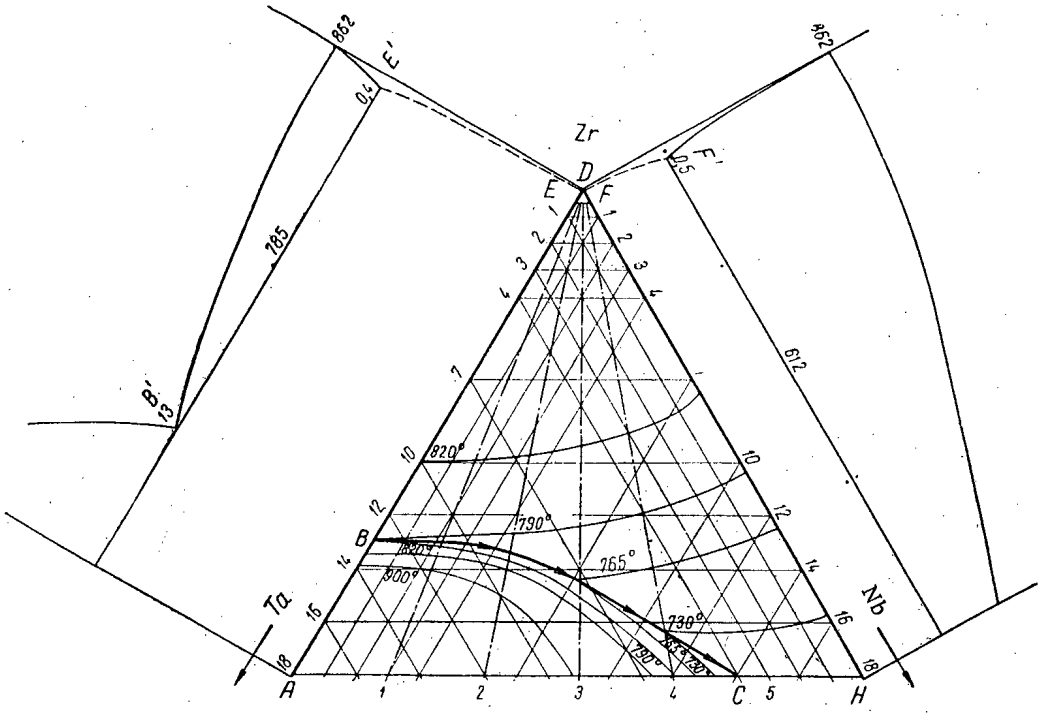

Fig. 14. Projection of parts of the ternary phase diagram Zr–Ta–Nb on the concentration plane of the triangle.

It will be seen from Figs. 1, 3, and 5, that the data of the metallographical analysis of the ternary system Zr–Ta–Nb differ considerably from the results of the thermal analysis. There are also considerable discrepancies between published results of thermal and dilatometer analyses and on the measurement of the electrical resistance on heating of alloys of the Zr–Nb system, and the results of our metallographical studies of this system (Fig. 14). These discrepancies are evidently due to the different degrees of approximation of the alloys to the equilibrium condition according to the methods of investigation employed. It is evident that metallographical examination of the alloys quenched after deformation and lengthy annealing (which assists in bringing them to the equilibrium condition) produces more reliable information regarding the phase diagrams. The methods of thermal and dilatometer analyses and the method of measuring the electrical resistance, where heating and cooling of the alloys proceed at a relatively high rate, in the present case evidently fix the nonequilibrium phase transitions.

The results of the metallographical analysis were used in constructing a number of isothermal cross sections of the investigated region (Fig. 15) of the phase diagram of the system Zr–Ta–Nb.

The isothermal cross section at 900° C has two regions: a one-phase region of β-solid solution and a two-phase region β + γ.

The isothermal section at 820° C, in addition to the foregoing regions, has two new regions: the two-phase α + β and the one-phase α region. In this section, the β region has become narrower and the β + γ region has widened.

In the isothermal section at 720° C, the three-phase region α + β + γ appears; the β and β + γ regions are narrower and the α and α + β regions are wider.

The isothermal section at 730° C has six phase regions; the dimensions of the α region are practically unchanged; the α + β + γ region has widened considerably; the α + β, β and β + γ regions have become narrower and the α + γ region has appeared.

In the isothermal sections for the temperatures 700 and 645° C, two regions are absent: the two-phase β + γ region and the one-phase β region.

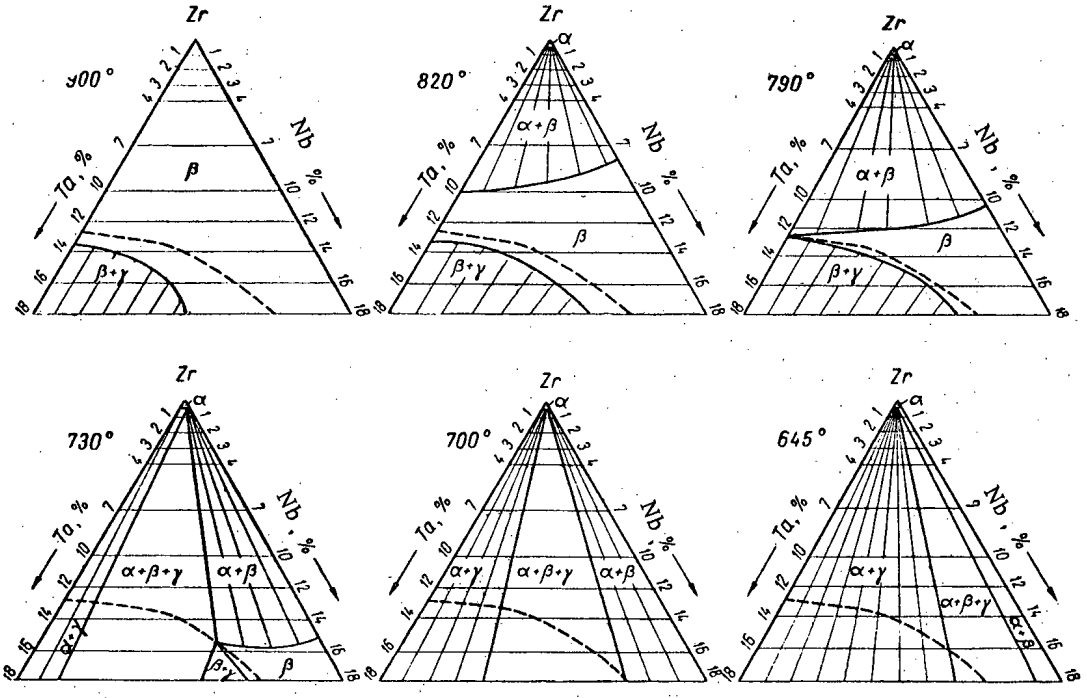

Fig. 15. Isothermal sections of the system Zr–Ta–Nb.

The region constructed for the zirconium apex of the ternary system Zr–Ta–Nb has limited solubility of tantalum and niobium in α–zirconium, limited solubility of these elements in β-zirconium with eutectoid decomposition of the β solid solution and three-phase eutectoid equilibrium $\beta \rightleftarrows \alpha + \gamma$ between α and β zirconium. Figure 14 shows the projections of these regions on the concentration plane of the triangle.

The three-phase eutectoid equilibrium $\beta \rightleftarrows \alpha + \gamma$ corresponds to the monovariant lines BC and EF descending from the nonvariant points B' and E' of the Zr–Ta system to the corresponding nonvariant points C' and F' of the Zr–Nb system below them.

The two-phase equilibrium $\beta \rightleftharpoons \alpha$ corresponds to the surfaces DBCH and DEF of the transformation of β-zirconium to α-zirconium; the two-phase equilibrium $\beta \rightleftharpoons \gamma$ to the solubility surface ABC. The three-phase solid of the eutectoid equilibrium $\beta \rightleftharpoons \alpha + \gamma$ is formed by the three ruled surfaces BCHFE, ABC, and AEFH. In projection, the latter surface merges with the higher surfaces.

Measurement of the Hardness and Electrical Resistance of Cast and Quenched Alloys

With the object of obtaining additional information on the system Zr–Ta–Nb, the hardness and electrical resistance of cast and quenched alloys were measured. The hardness was measured on a Rockwell instrument according to the Rc_{60} scale. The results obtained were converted into standard Brinell hardness values H_B. Figure 16 shows curves of hardness values plotted against composition for alloys cast and quenched from the temperatures 1200, 820, 765, 700, and 600°C for all five polythermal cross sections. Examination of these curves shows that the addition of tantalum and niobium to zirconium considerably increases its hardness. In the third, fourth and fifth cross sections, the hardness curves show a well-pronounced maximum, due to the martensitic-like transformation of the cubic β phase into the hexagonal α phase on quenching. This maximum is observed for these cross sections in alloys, quenched from a temperature above the boundary of the $\alpha + \gamma$ region. In the second section, the maximum is just beginning to show and in the first section it is absent altogether. The existence of a maximum on the hardness curves of binary alloys (quenched from 1200°C) of the system Zr–Ta [1], corresponding to the alloy containing about 28% by weight of tantalum, shows, however, that such a maximum ought also to be present on the hardness curves of the first polythermal cross section, but beyond the limits of the concentration region investigated.

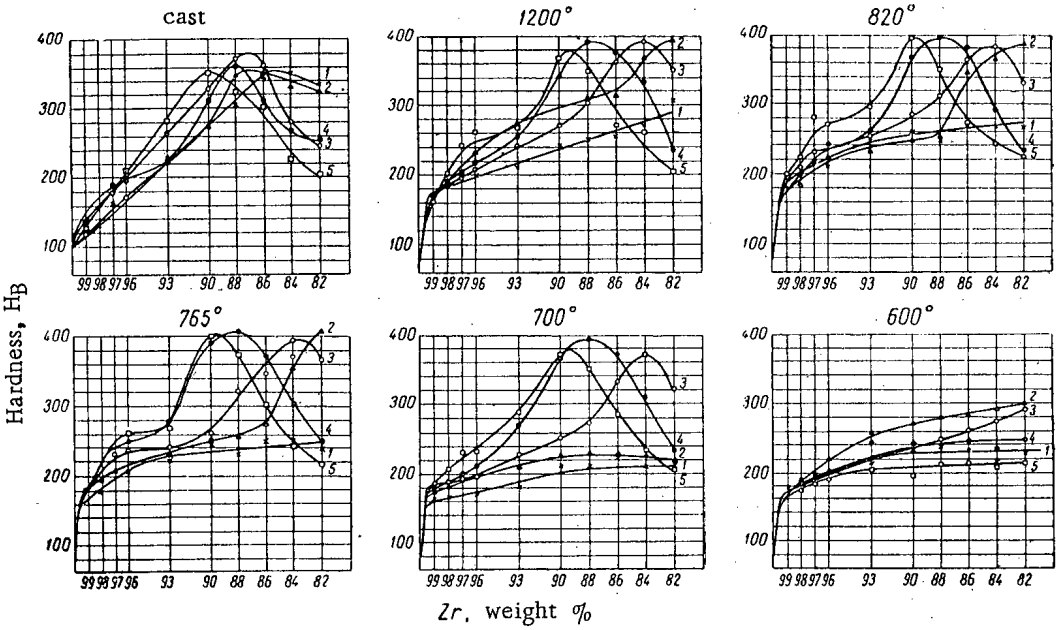

Fig. 16. Hardness curves of alloys of the system Zr–Ta–Nb cast and quenched from different temperatures for five polythermal cross sections (1-5) with constant ratio of the percentage content of niobium to tantalum.

The position of the maxima on the hardness curves of alloys, quenched from temperatures above the boundaries of the two-phase region $\alpha + \gamma$, makes it impossible to determine by the hardness method the phase boundaries situated in the investigated concentration region.

The position of the maxima on the hardness curves of the alloys corresponds to the different total contents of tantalum and niobium in all five polythermal cross sections and shifts toward alloys of high zirconium content when the ratio of the content of niobium to tantalum for the given cross section is increased. This indicates that an increase in the addition of niobium to binary alloys of the system Zr–Ta results in a narrowing of the range of martensitic-like transformation and, consequently, in an increase in the stabilization of the β phase, by quenching, at room temperature. There are no maxima on the hardness curves of alloys quenched from the two-phase region $\alpha + \gamma$.

The dependence of hardness upon the composition of alloys quenched from the two-phase region $\alpha + \gamma$ (600° C) shows that the solubility of tantalum and niobium in α-zirconium is not high, which is in agreement with the results of the metallographical examination.

The dependence of hardness upon composition of alloys of the system Zr–Nb quenched from 600° C is similar to the curve of Fig. 16. It shows that the solubility of niobium in α-zirconium is low, being about 0.5 % niobium, which is in good agreement with the results of metallographical examination.

The curves of electrical resistance versus composition for alloys of the first, third and fifth polythermal cross sections, quenched from the $\alpha + \gamma$ region, are similar in character to the corresponding hardness curves.

LITERATURE CITED

[1] V. S. Emel'ianov, Iu. G. Godin, and A. N. Evstiukhin, J. Atomic Energy (USSR) 2, 1, 42 (1957).*

[2] B. A. Rodgers and D. F. Atkins, J. Metals 9, 1034 (1955).

[3] Iu. F. Bychkov, A. N. Rozanov, and D. M. Skorov, J. Atomic Energy (USSR) 2, 2, 146 (1957).*

[4] R. F. Domogala and D. J. M. McPherson, J. Metals, 5, 619 (1956).

[5] S. A. Pogodin, K. P. Belova, N. F. Blagov, L. M. Venediktov, E. A. Kamenskaia, and M. B. Reifman, Jubilee Collection of the Work of the State Rare Metals Scientific Research Institute (In Press).

Received April 10, 1957.

* See C. B. Translation.

PROBLEM OF THE IODINE METHOD OF PURIFICATION OF ZIRCONIUM

K.D. Sinel'nikov, F.I. Busol and G.I. Stepanova

A method is proposed for the determination of the equilibrium constants k and k' for the reactions $Zr + 2I_2 - ZrI_4 = 0$ and $2I - I_2 = 0$, which is based on the measurement of the amount of iodine or zirconium liberated in the decomposition of zirconium tetraiodide on a heated surface in the process of establishing equilibrium. The decomposition of the tetraiodide was carried out at 900-1600°C on a tungsten filament. The temperature distribution between filament and vessel walls was neglected.

The dependence of the sum of atomic and molecular iodine pressures $p_I + p_{I_2}$ on zirconium tetraiodide pressure p_{ZrI_4} was determined at 1430°C, and on temperature for $p_{ZrI_4} \approx 50$ mm Hg. The values of $kk'^2 \approx 35$ (mm Hg)^3 at 1430°C and $k \approx 0.07$ mm Hg at 400°C, found from the results, differ substantially from known thermodynamic data, but give good agreement between the authors' formula [1] and experimental results on the iodide process of zirconium purification.

INTRODUCTION

Reference [1] proposed a theory for the iodide process of zirconium purification, which was based on the supposition that in the region of a filament on which pure zirconium is being deposited and in the region of the original metal, there is equilibrium between the reactions

$$Zr + 2I_2 - ZrI_4 = 0, \quad (1)$$

$$2I - I_2 = 0. \quad (2)$$

This supposition is valid for the pressure range in which the mean free path length of the molecules is much less than the dimensions of the reaction vessel. Since the temperature of the filament is higher than the temperature of the original metal, the equilibrium concentration of ZrI_4 close to the filament is less than its equilibrium concentration close to the unpurified zirconium. The resulting diffusion flow ensures the transport of zirconium to the filament. The dependence of the flow of zirconium upon the equilibrium constants of Reactions (1) and (2) and upon the ZrI_4 pressure in the region of the original metal, this pressure being usually known, is determined in [1]. The relationships obtained in particular provide an explanation for the existence of maximum flow with variation in pressure of zirconium tetraiodide and the displacement of the maximum towards higher pressures when the filament temperature is increased. When, however, the constants k and k' calculated from thermodynamic data [2] are used, the results obtained in [1] do not agree quantitatively with experiment.

Since the satisfactory qualitative explanation of many aspects of the process described cannot be accidental, we assumed that the thermodynamic data [2], obtained for zirconium chlorides by an indirect method, were erroneous, and we carried out direct measurements of the constants in which we were interested.*

It should be pointed out that very little is known about the equilibrium constant of Reaction (1), although attempts have been made to measure this magnitude at high temperatures [3-5]. The constant k' has been determined in a wide temperature range.

*Doubt as to the accuracy of the thermodynamic data [2] has also been expressed previously [3].

Measurement of the Constants

Principle of the method. For determining the equilibrium constants of Reaction (1)

$$k = p_{I_2}^2/p_{ZrI_4} \tag{3}$$

and Reaction (2)

$$k' = p_I^2/p_{I_2} \tag{4}$$

it is necessary to measure the partial pressures of zirconium tetraiodide p_{ZrI_4}, atomic iodine p_I and molecular iodine p_{I_2} at the given temperature. We measured the pressure of the tetraiodide p_{ZrI_4} and the sum of the pressures of atomic and molecular iodine $p_I + p_{I_2}$ connected by the relationship

$$p_I + p_{I_2} = (kk'^2)^{1/4} p_{ZrI_4}^{1/4} + k^{1/2} p_{ZrI_4}^{1/2}. \tag{5}$$

Knowing the relationship between $p_I + p_{I_2}$ and p_{ZrI_4}, the values of the constants can be found.

The following method was used for making the measurements. A fairly large amount of zirconium tetraiodide is introduced into the usual zirconium purification apparatus. The pressure of the ZrI_4 vapor in the apparatus is determined by the temperature of the coldest part. Some of the tetraiodide introduced is dissociated with the separation of zirconium and iodine. The dissociation of the tetraiodide will obviously continue until the pressure of the liberated iodine attains equilibrium value, determined by the highest temperature in the apparatus. (The iodine vapor should not of course be saturated.) In the present case, the electrically heated tungsten filament had the highest temperature.

In the dissociation of ZrI_4 close to the filament, both molecular and atomic iodine are liberated, the relation between their partial pressures being determined by the value of the constant k' at the temperature of the equilibrium region, which extends for at least several mean free path lengths.* The concentration of atomic iodine rapidly falls as the distance from the filament increases. Since the region of effective dissociation of iodine is small compared with the volume of the vessel, the number of iodine atoms N_I in the vessel is small compared with the number of iodine molecules N_{I_2}. With this approximation N_{I_2} is determined from the amount m of zirconium separated on the filament or the amount of liberated iodine m' by means of the relationships

$$N_{I_2} = \frac{2m}{A} N_0; \qquad N_{I_2} = \frac{m'}{\mu} N_0, \tag{6}$$

where A and μ are, respectively, the atomic weight of zirconium and the molecular weight of iodine; N_0 is Avogadro's constant. The pressure of molecular iodine in the vessel and consequently the sum of the pressures of atomic and molecular iodine close to the filament is then determined by the approximate equation

$$p_I + p_{I_2} \approx \frac{N_{I_2} RT}{N_0 V}, \tag{7}$$

where R is the gas constant, T the mean temperature in the vessel and V the total volume of the vessel.

Experimental method and results. The apparatus is shown diagrammatically in Figure 1. The glass vessel 12 was evacuated and outgassed for two hours at ~500°C and a vacuum of $\sim 10^{-5}$ mm Hg, after which the apparatus was sealed off at 2 and the ampoule containing 1 g of tetraiodide was broken. The entire apparatus, with the exception of the lower half of bulb 6, was heated to 400°C. The temperature of the lower half of bulb 6, determining the pressure of zirconium tetraiodide in the apparatus, was regulated by means of a bath filled with molten tin. After the given pressure p_{ZrI_4} had been established in the apparatus, the heating current for the filament 13

*It should be pointed out that the temperature is much less than the filament temperature, due to the fact that when thin filaments are heated in rarefied gases, there is a temperature drop between filament and gas. Thus, according to Langmuir [6], for nitrogen and hydrogen at pressures of 1-10 mm Hg and a filament temperature ~1500°C, the temperature drop amounts to several hundred degrees over a mean free path length.

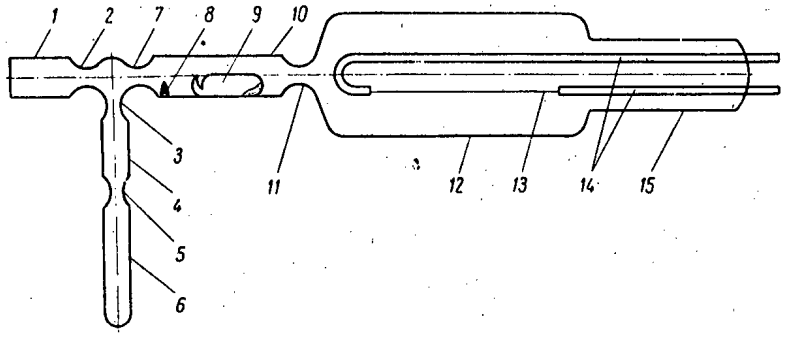

Fig. 1. Diagram of apparatus: 1) connecting piece; 2,3,5,7,11) pinches; 4,6) bulbs; 8) striker; 9) ampoule containing ZrI_4; 10) tube; 12) vessel; 13) tungsten filament; 14) molybdenum electrodes; 15) end of apparatus.

was switched on. In the first series of experiments, the filament was a tungsten wire 0.08 mm in diameter, in the second series the diameter of the wire was 1.2 mm. The filament temperature was measured by means of an optical pyrometer.

The course of the dissociation of ZrI_4 could be observed by the variation of current in the filament, which was appreciable when thin filaments were used. At first, the current increased somewhat (by 0.2-0.5 amp) depending upon p_{ZrI_4}, but the increase in current soon ceased (after three to five minutes). This meant that the deposition of zirconium on the filament had ceased and consequently the partial pressure of the iodide had reached equilibrium value.

Some time after switching on the filament heating current (~20 min) the tin bath was quickly removed and bulb 6 was immersed in liquid nitrogen. The result was that the vapors of iodine and tetraiodide froze practically instantaneously.

In the first series of experiments, the equilibrium pressure of iodine was determined from the amount m of zirconium deposited on the filament and found by weighing the filament before and after the experiment. The filament temperature was maintained at 1430°C. The pressure p_{ZrI_4} was varied within the limits 0.2-50 mm Hg. The results of the measurements are given in Table 1.

TABLE 1

Temperature of bulb 6, °C	Pressure of tetraiodide vapor p_{ZrI_4}, mm Hg	Weight of zirconium m, mg	Volume V, cm^3	Sum of pressures $p_I + p_{I_2}$, mm Hg
235	0.2	1	555	1.7
263	1.0	1.8	528	3.1
310	10	3.6	525	6.3
340	34	8.3	577	13.2
350	50	3.9	528	6.8

In the second series of experiments, the equilibrium pressure of the iodine was determined by weighing the liberated iodine. For this purpose, after freezing the iodine and tetraiodide vapors in bulb 6, the latter was sealed off at 3, the iodine was sublimed from 6 to 4 and the latter sealed off at 5. The amount of liberated iodine was found by weighing 4 with and without iodine and introducing a correction for the weight of air contained in bulb 4.

The first group of the second series of experiments repeated the experiments of the first series and was carried out for the purpose of comparing the two sets of experiments and also for obtaining more exact information of the dependence of $p_I + p_{I_2}$ upon p_{ZrI_4}. (The first series of experiments showed considerable scatter, evidently

due to insufficiently accurate temperature measurement in this case.) The filament temperature was 1430°C. The pressure of zirconium tetraiodide was measured within the limits 1-50 mm Hg. Table 2 shows the results of this group of measurements.

TABLE 2

Temperature of bulb 6, °C	Pressure of tetraiodide vapor, mm Hg	Weight of iodine m, mg	Volume V, cm^3	Sum of pressures $p_I + p_{I_2}$, mm Hg
263	1	12.1	640	3.1
281	2.5	13.7	656	3.5
295	5	16.3	660	4.1
311	10	17.2	655	4.3
328	20	18.7	655	4.7
339	35	17.4	647	4.4
350	50	18.9	640	4.9

In the second group of the second series of measurements, the pressure of the tetraiodide vapor was kept constant (~50 mm Hg) and the temperature of the filament was varied from 1570 to 960°C. The results of these measurements are given in Table 3.

TABLE 3*

Filament temperature, °C	Weight of iodine m', mg	Volume V, cm^3	Sum of pressures $p_I + p_{I_2}$, mm Hg
1570	48	545	14.5
1510	30	565	8.8
1510	35	565	10.2
1450	24	562	7.1
1390	29	590	8.1
1330	19	530	5.0
1330	21	600	5.8
1270	21	540	6.4
1270	23	620	6.2
1210	15	560	4.4
1150	15	560	4.4
1150	12.5	565	3.7
1080	13	560	3.8
1030	16	567	4.7
960	9	565	2.6
400	7	560	2.1
400	6.8	555	1.7

*The last two measurements were made without switching on the filament heating current.

Comparison of the data of Tables 1 and 2 shows that for corresponding vapor pressures of ZrI_4, the values of the iodine pressure agree sufficiently well. This means that the liberation of iodine is in fact due to dissociation of the tetraiodide on the filament and not to any other reactions.

The slow variation in the value of $p_I + p_{I_2}$ with variation in the vapor pressure of ZrI_4 suggests that the principal term in the measured sum for a filament temperature of 1430°C is the pressure of atomic iodine, which is proportional to the fourth root of p_{ZrI_4} ($p_I = (kk'^2)^{1/4} p^{1/4}_{ZrI_4}$). This is confirmed by the graph (Figure 2) where the values of $p_I + p_{I_2}$ (from Tables 1 and 2) have been plotted on the ordinate axis and $p^{1/4}_{ZrI_4}$ on the abscissa axis.

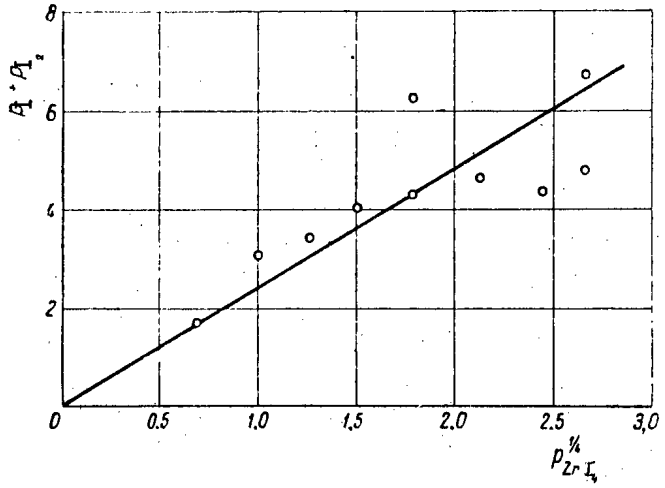

Fig. 2. Dependence of the total iodine pressure $P_I + P_{I_2}$ on $(P_{ZrI_4})^{1/4}$. $T_{filament} = 1430°$ C.

The experimental points lie satisfactorily on a straight line, the tangent of the angle of slope of which gives $kk'^2 \approx 35$ (mm Hg)^3. According to the thermodynamic data [2] at 1400°C, $kk'^2 \approx 0.4$ (mm Hg)^3. If we consider, however, that in our experiments k' corresponds to a much lower temperature, the discrepancy between the value of kk'^2 found and that calculated is still greater.

Examination of the data of Table 3 draws attention to the fact that the equilibrium pressure of iodine varies appreciably only in the range of 1570-1200°C. On further reduction in the temperature, the rate of change of $p_I + p_{I_2}$ diminishes and becomes particularly small in the range 1000-400°C. At the same time, it is important that even at 400°C, the pressure of the liberated iodine is quite considerable. Since the dissociation of iodine is negligible at this temperature the predominant term in the sum $p_I + p_{I_2}$ is the pressure of molecular iodine, equal to

$$p_{I_2} = k^{1/2} p_{ZrI_4}^{1/2}.$$

From this we obtain the value of interest to us for the equilibrium constant of Reaction (1) at 400°C, i.e., $k \approx$ ≈ 0.07 mm Hg, differing by many orders from the value determined in accordance with the formula

$$\ln k = -\frac{\Delta F}{RT}, \tag{8}$$

where ΔF is the change in free energy in the dissociation of tetraiodide calculated from the data of [2].

The causes of such a large discrepancy are obscure. It may be thought, however, that the value of ΔF used is high, due to the high value for the heat of formation of zirconium cited in [2] ($\Delta H_{298} = -160$ kcal/mole and $\Delta F = -73T - \Delta H_{298} = 111$ kcal/mole at 400°C). This is supported, for example, by the data of [4] and [7], in which the dependence of the degree of dissociation of the molecules of ZrI_4 on the temperature of the support was obtained in the range 1100-1500°C. Evaluation of the results of [4] and [7] gives a value of $E \approx 20$ kcal/mole for the bond energy of a mole of tetraiodide, approximately equal to the heat of formation of the tetraiodide.

We shall now show that the values obtained by us for the constants ensure fairly good agreement of the formulas in [1] with experimental data on the iodide process of zirconium purification. We shall use for this purpose the experimental dependence of the rate of deposit of zirconium upon the pressure of the tetraiodide vapor*

*The curve shown in Figure 3 was obtained in an investigation of the factors affecting the rate of deposition of zirconium. The experiments were made in glass vessels of ~1 liter capacity, having a special branch, the temperature of which was regulated by the vapor pressure of ZrI_4. The starting material was 20 g of zirconium chips. The temperature of filament and starting material was kept constant at 1450 and 400°C. 0.5-1 g of iodine was introduced into the vessel. The zirconium was deposited on a tungsten filament 800 mm long and 0.08 mm in diameter.

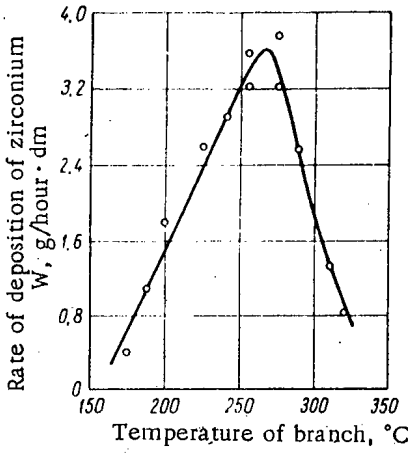

Fig. 3. Dependence of rate of deposition of zirconium upon temperature of branch-piece (pressure of zirconium tetraiodide vapor). $T_{filament} = 1450°C$.

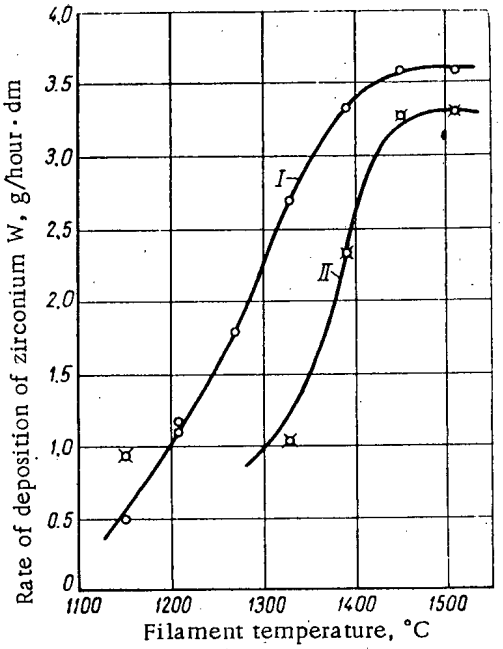

Fig. 4. Dependence of rate of zirconium deposition upon filament temperature: I) $p_{ZrI_4} = 0.9$ mm Hg; II) $p_{ZrI_4} = 0.2$ mm Hg.

(Figure 3) and Formula (20) from [1], which is correct for intermediate pressures*:

$$W = B\left(1 - \frac{k_1^{1/2}}{p_{ZrI_4}^{1/2}} - \frac{p_{ZrI_4}^{3}}{k_2 k_2'^{2}}\right), \qquad (9)$$

where k_1 and k_2 are the values of the constant $\underline{k}$ at 400 and 1450°C, respectively; k'_2 is the value of the constant k' at 1450°C. After substituting in (9) the values $W_1 = 3.24$, $W_2 = 3.63$ and $W_3 = 3.20$ g/hour · dm for pressures of tetraiodide vapor of 0.5, 1.12 and 2.14 mm Hg, respectively, we obtain a system of three equations with three unknowns. Solution of this system gives $k_1 \approx 0.072$ mm Hg, $k_2 k_2'^{2} \approx 54$ (mm Hg)^3, $B \approx 5$ g/hour · dm. It is not difficult to see that the values of k_1 and $k_2 k_2'^{2}$ agree with the measured values.

The limit values of the rate of deposition at high filament temperatures, expressed by the formula

$$W_{limit} = \frac{B}{1 + \frac{k_1^{1/2}}{p_{ZrI_4}^{1/2}}}. \qquad (10)$$

are likewise in good agreement with the measured value of the constant k_1. Figure 4 shows the experimental curves for the dependence of rate of zirconium deposition upon filament temperature at pressures p_{ZrI_4} 0.9 and 0.2 mm Hg.** It will be seen from the curves that above 1450°C, the rate of deposition reaches a limit value, W_{limit} being 3.60 and 3.30 g/hour · dm, respectively. By substituting B = 5 g/hour · · dm in Formula (10) we get $W_{limit} = 3.95$ and $W_{limit} = 3.14$ g/hour · dm.

It should be pointed out that such an important factor as the true temperature distribution between filament and vessel wall was not taken into account in this investigation. At the same time, a knowledge of this distribution is absolutely necessary, since the value of constant k' depends materially upon the temperature distribution in the vicinity of the filament. Furthermore, the value of constant $\underline{k}$ is determined, in all probability, by the surface temperature of the filament. Nevertheless, the values obtained for the constants are of definite interest, since the temperature distribution in the vicinity of the filament is practically the same as in the iodide method of zirconium purification. Thus, the measured values of the constants do actually define the behavior of the purification process. Furthermore, the determination of the constant $\underline{k}$ at 400°C is free from the above-mentioned deficiency.

LITERATURE CITED

[1] G.I. Stepanova and F.I. Busol, J. Atomic Energy (USSR) 3, 10, 344 (1957)***

*Transition from the value of flow to rate of deposition merely involves introduction of the constant B instead of A.

**The curves of Figure 4 were obtained in the same conditions as the curve of Figure 3.

***Original Russian pagination. See C.B. translation.

[2] L.L. Quill, The Chemistry and Metallurgy of Miscellaneous Materials (McGraw Hill Book Co., Inc., 1950).

[3] Lustmann and Kerze, The Metallurgy of Zirconium (McGraw Hill Book Co., Inc., 1955), p. 135.

[4] J.H. Doring and K. Moliere, Z. Elektrochem. 56, 403 (1956).

[5] V.S. Emel'ianov, P.D. Bystrov and A.I. Evtiukhin, J. Atomic Energy (USSR) 1, 1, 43 (1956).*

[6] I. Langmuir, J. Amer. Chem. Soc. 37, 417 (1915).

[7] R.B. Holden and B. Kopelman, J. Electrochem. Soc. 100, 120 (1953).

Received April 11, 1957

*Original Russian pagination. See C.B. translation.

LETTERS TO THE EDITOR

HIGH-VOLTAGE SOURCES FOR ONE-SHOT HIGH-CURRENT ACCELERATORS

B. S. Novikovskii

The particle currents available from electrostatic generators are limited, in the best cases, to the order of several tens of microamperes; on the other hand, at the present time there are problems whose solution requires particle currents of the order of several milliamperes and even tens of milliamperes at energies of 2-3 Mev. The construction of an electrostatic generator with currents of this type is not feasible. For this reason attention is once again merited by one-shot accelerators which use voltage-multipliers.

The usual voltage multiplier (Fig. 1) is not convenient since the output voltage has a high ripple component and the internal resistance is high; these factors limit the application of the circuit as a high-voltage source for high-current, one-shot accelerators.

There are three basic formulas for making circuit calculations: these give the output-voltage ripple δU, the voltage drop ΔU, and the optimum number of voltage-multiplying stages n_{opt}:

$$\delta U = \frac{i}{fC} \cdot \frac{n(n+1)}{2},$$

$$\Delta U = \frac{i}{fC}\left(\frac{2}{3}n^3 + \frac{1}{2}n^2 - \frac{1}{6}n\right),$$

$$n_{opt} = \sqrt{\frac{U_{max} fC}{i}},$$

where i is the load current, f is the frequency of the supply voltage, C is the capacity for one stage, U_{max} is the maximum voltage at the input to the circuit and n is the number of stages.

These formulas indicate that the construction of a high-voltage accelerator to obtain protons with energies of the order of 2 Mev and currents of 5-10 ma is an extremely difficult technical problem when ordinary voltage multiplying circuits are used. In a great deal of experimental research, especially for work with thin targets, the energy of the accelerated particles from the accelerator must be extremely precise, generally to within an accuracy of 0.1-0.05 %. Attempts have been made to construct a high-current accelerator which satisfies the requirements given above.

At the end of 1955 a paper by Heilpern appeared* in which a proposal was made for a symmetric voltage-multiplying circuit (Fig. 2) having better characteristics than the usual circuit (Fig. 1). As compared with the ordinary circuit, the symmetric circuit requires twice the number of rectifiers, plus an additional condenser column. Unfortunately, in this paper, as in other papers on the cascade generator, no analysis is given of the operation of the circuit nor are basic calculation formulas presented (except the formula for δU), thus making the analysis of the feasibility of this proposed method very difficult.

The author has made an analysis of the operation of the symmetric circuit, deriving the basic formulas and checking them in practice. From this work it has been found that the symmetric circuit has an unquestioned advantage as compared with the ordinary voltage-multiplying circuit. It was found that in the symmetric circuit the basic formulas for δU, ΔU, and n_{opt} are the following:

---

* W. Heilpern, Helv. phys. acta 28, 485 (1955).

$$\delta U = \frac{i}{fC}\,\frac{n}{2},$$

$$\Delta U = \frac{i}{fC}\left(\frac{1}{6}n^3 + \frac{1}{4}n^2 + \frac{1}{12}n\right),$$

$$n_{opt} = 2\sqrt{\frac{U_{max}\,fC}{i}}.$$

Thus, the ripple voltage in a circuit of this kind is (n + 1) times smaller, the voltage drop is four times smaller and the optimum number of cascades is twice as large as in the usual multiplying circuit.

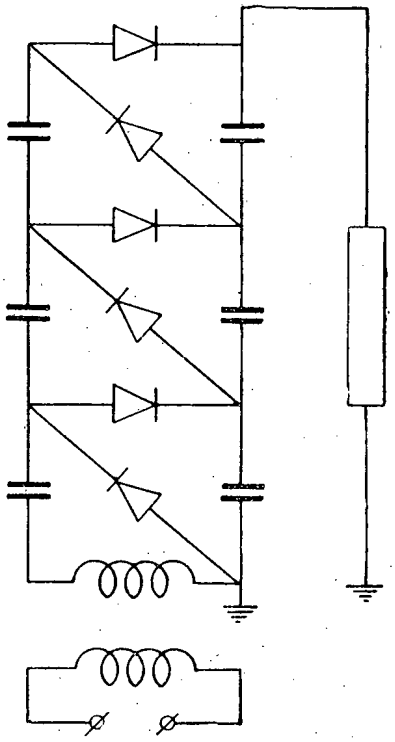

Fig. 1. Ordinary voltage-multiplying circuit.

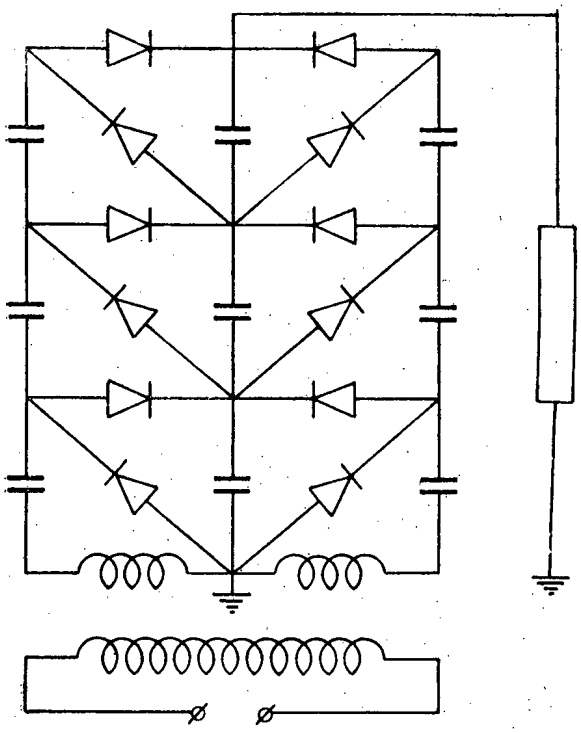

Fig. 2. Symmetric voltage-multiplying circuit.

To clarify this point we consider a cascade generator made up of an ordinary circuit and a symmetric circuit. We assume that i = 5 ma, f = 10 kc, C = 0.1 μf, U_{max} = 50 kv, and n = 25. Under unloaded conditions both generators produce the same voltage (without taking account of the voltage drop due to parasitic capacities) $U_{XX} = 2U_{max} \cdot n$ = 2500 kv. Under load, however, the behavior of these two generators is completely different.

The results of a comparison are shown in the table; it is apparent that as far as voltage excursions are concerned the symmetric circuit is as good as an electrostatic generator at load currents which can not be achieved in the latter.

In the future it may be feasible to use three-phase (Fig. 3) and multi-phase voltage multiplying circuits, especially in those cases in which still higher currents are required. A three-phase circuit requires four condenser columns but an ordinary voltage multiplier made from these condensers (actually two ordinary circuits in parallel) is considerably worse than the three-phase circuit both with regard to voltage drop and ripple.

To verify these considerations a voltage multiplier circuit was constructed which could be easily converted from ordinary operation to symmetric operation and three-phase operation. The capacity of a stage was 1 μf; the rectifiers were Type AVS−7−3p selenium banks; the number of stages was varied from 2 to 10; the frequency of the supply voltage was 50 cps.

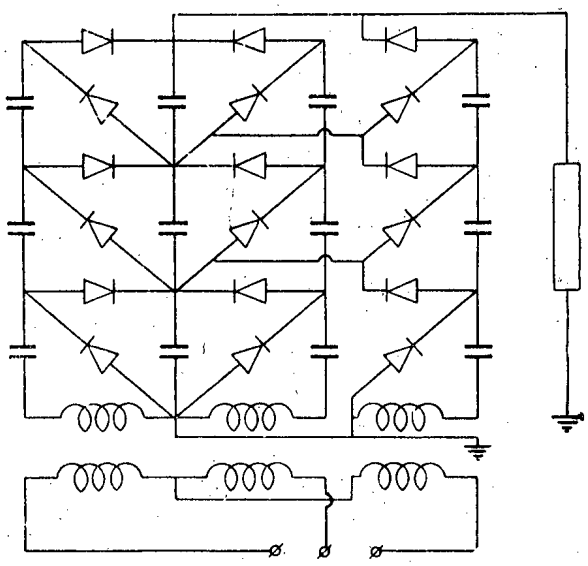

Fig. 3. Three-phase voltage-multiplying circuit.

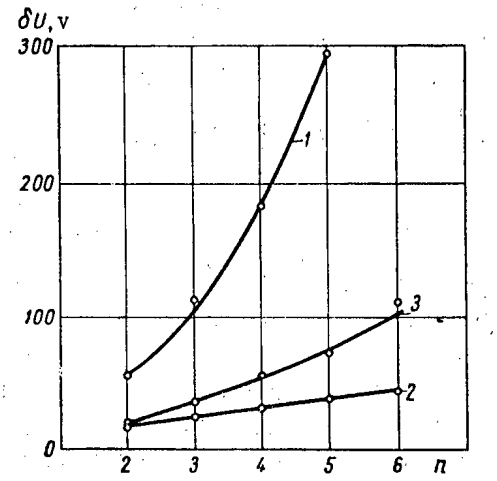

Fig. 4. The ripple in the output voltage δU has a function of the number of stages n for a load current i = 1 ma. 1) Ordinary circuit; 2) symmetric circuit; 3) three-phase circuit.

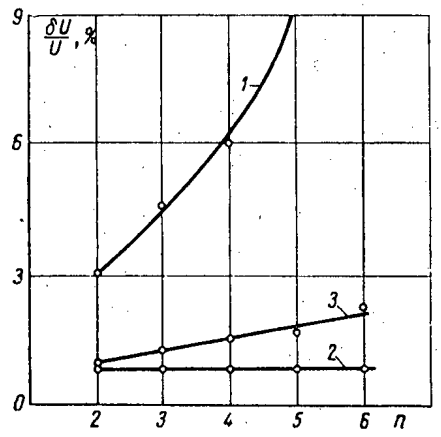

Fig. 5. The quantity $\frac{\delta U}{U}$ as a function of the number of stages n for a load current i = 1 ma. 1) Ordinary circuit; 2) symmetric circuit; 3) three-phase circuit.

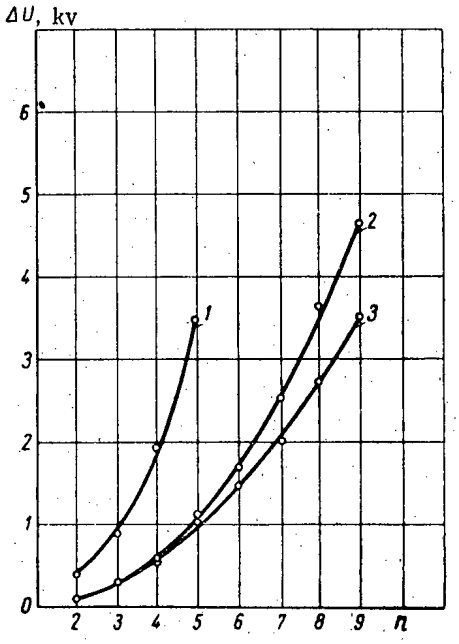

Fig. 6. The output voltage drop ΔU as a function of the number of stages n for a load current i = = 2 ma. 1) Ordinary circuit; 2) symmetric circuit; 3) three-phase circuit.

TABLE 1

Comparison of the Ordinary and Symmetric Circuits.

	Ordinary circuit	Symmetric circuit
δU, kv	16.25	0.625
ΔU, kv	~520	~130
$U_{gen} = U_{XX} - \Delta U$, kv	1980	2370
δU, %	0.82	0.03

The experiments indicated that the ripple voltage in the symmetric circuit was reduced by more than a factor of (n + 1) as compared with the ordinary voltage multiplying circuit. The three-phase circuit was characterized by a ripple voltage higher than that of the symmetric circuit but considerably smaller than the ordinary circuit (Fig. 4). It is of interest to note that in the symmetric circuit the ratio $\frac{\delta U}{U}$ is a fixed quantity for any number of stages (Fig. 5). The voltage drop in the symmetric circuit is down by a factor somewhat less than 4 as compared with the ordinary circuit (Fig. 6). This is probably explained by the fact that the selenium column operates at a reduced voltage. The three-phase circuit is characterized by the smallest voltage drop. The advantage of this circuit is particularly pronounced when the number of stages is increased. The optimum number of stages is found to be in agreement with the formula which was obtained; in the symmetric circuit the number is larger than the ordinary circuit by a factor of 2 while in the three-phase circuit it is approximately a factor of 2.5 larger (Fig. 7).

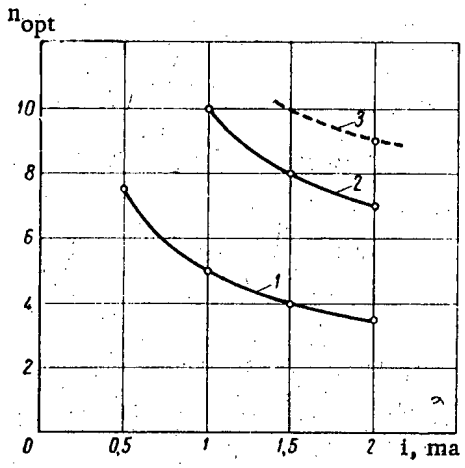

Fig. 7. The optimum number of stages n_{opt} as a function of load current i. 1) Ordinary circuit; 2) symmetric circuit; 3) three-phase circuit (in the form shown).

Thus, the ordinary voltage multiplier circuit cannot compete with the symmetric or three-phase circuits in any respect. In machines in which the basic requirement is voltage stability, the symmetric circuit appears to be most advantageous. In machines in which the highest possible current and voltage are required, the three-phase voltage multiplier circuit is to be preferred.

Received June 27, 1957.

ELECTRON TEMPERATURE AND DEGREE OF IONIZATION IN THE INITIAL STAGES OF AN INTENSE PULSED DISCHARGE[1]

V.I. Kogan

In the present paper we present certain approximation formulas for the electron temperature and the degree of ionization in the initial stages of an intense pulsed discharge in hydrogen [1], based on the assumption that the electronic ionization mechanism is the predominant one.

1. In the case being considered, in which the discharge occurs in the course of several microseconds at low pressure (approximately 0.05-2 mm Hg), the hydrogen cannot achieve thermal dynamic equilibrium nor, in general, any stationary state. Hence, the relation between the electron temperature and the degree of ionization cannot be written in terms of the Saha thermodynamic formula alone, but also requires formulas based on an equilibrium of independent inverse processes (for example, ionization by electron impact and pair recombination). We proceed directly from the simplified equations for balance between ionized and excited atoms,[2] assuming the chief mechanism for excitation and ionization to be electron impact:

$$\dot{n} = \langle v\sigma_i \rangle n n_0 \equiv \Psi n n_0, \tag{1}$$

$$\dot{n}^* = \langle v\sigma_e \rangle n n_0 - \frac{1}{\tau} n^*. \tag{2}$$

Here n_0, n^* and $\underline{n}$ are the number of unexcited atoms, the number of excited atoms, and the number of electrons (ions) in 1 cm^3, respectively; $\underline{v}$ is the velocity of the electron; σ_i and σ_e are the cross sections for atomic ionization and excitation by the electron; τ is the mean radiation lifetime for the excited atom; the angular brackets indicate averages taken over the electron velocity distribution. In these equations we neglect recombination and removal of electrons from the volume as well as slow processes. Estimates show that these assumptions are justified for the densities and times being considered.

It has been shown experimentally [2] that the intensity of the radiation (proportional to the number of photons n^*/τ) increases up to a time t_1 equal to $\sim 10^{-6}$ sec. Consequently, $\dot{n}^* \sim n^*/t_1$. Since τ is approximately 10^{-8} sec and is much smaller than t_1, $n^*/\tau \gg \dot{n}^*$. Simplifying Equation (2) and using Equation (1) we have

$$\frac{\dot{n}}{(n^*/\tau)} \approx \frac{\langle v\sigma_i \rangle}{\langle v\sigma_e \rangle}. \tag{3}$$

Thus, the rate of ionization ($\dot{n}$) is approximately proportional to the number of photons (n^*/τ) emitted per second. This result is used as a basis for the remainder of the analysis.

2. Since the atom has many levels and a corresponding number of transitions from excited and emissive levels, whereas in the experiments [2] the lines of the Balmer series were observed, Equations (1-3) should be written for each transition $1s \rightarrow nl \rightarrow n'l'$, where $n' = 2$; $n = 3, 4, 5, \ldots$ The literature contains data on cross sections for ionization and excitation of hydrogen atoms by electrons [3, 4], computed in Born approximation, as well as the intensities of the Balmer lines [5]. Using these data we can compute the number of ioniza-

[1] This work was completed in 1954.

[2] The hydrogen may be assumed to be almost completely dissociated since no molecular bands are observed in the luminous radiation from the discharge.

tion events ζ, which occur for one "average" (cf. below) Balmer quantum as a function of electron energy ϵ. The results of the calculations are given in Table 1.

TABLE 1

The Number of Ionization Events ζ for One "Average" Balmer Photon as a Function of Electron Energy

ϵ, ev	13.5	20	30	50	100	200	300	∞
ζ	0	3.0	5.5	8.2	10.0	10.8	10.4	5.55

The computed ratio between the number of Balmer photons H_α, H_β, $H_{\bar\gamma}$ ($H_{\bar\gamma}$ denotes the summation over the line H_γ in all higher lines of the Balmer series) which are found for the same number of ionization events, depends weakly on energy and may be represented roughly by the ratio $\nu_\alpha : \nu_\beta : \nu_{\bar\gamma} \approx 3:1:1$. This proportionality justifies the introduction of an "average" energy for the Balmer photon used in computing ζ:

$$\bar\varepsilon_\delta = (\varepsilon_\alpha \nu_\alpha + \varepsilon_\beta \nu_\beta + \bar\varepsilon_{\bar\gamma} \nu_{\bar\gamma})(\nu_\alpha + \nu_\beta + \nu_{\bar\gamma})^{-1} \approx 2{,}25\,\text{ev} \approx 1{,}2\varepsilon_\alpha.$$

From the last relations it follows that under the conditions of excitation and emission being considered (absence of thermodynamic equilibrium) the intensity of the H_α line amounts to about half the total intensity of the Balmer series.

3. Using a method similar to that employed in Section 2 we can compute the following quantities, averaged over a Maxwellian distribution of electron velocities at a temperature T_e: 1) the ionization intensity $\Psi = \langle v\sigma_i \rangle$; 2) the total intensity of the Balmer lines J_B (erg · cm^{-3} · sec^{-1}); 3) the number of ionization events ζ which occur for a Balmer photon. The results are shown in Table 2.

TABLE 2

The Intensity of Ionization Ψ, the Total Intensity of the Balmer Lines J_B/nn_0 and the Number of Ionization Events ζ Associated with One Balmer Photon as a Function of Electron Temperature T_e

T_e (ev)	0	3	5	10	15	20	30	50	100	200	300	∞
$\Psi\left(10^{-8}\frac{\text{cm}^3}{\text{sec}}\right)$	0	0.05	0.25	1.3	2.4	3.1	4.2	5.1	5.5	5.0	4.3	—
$J_B/nn_0\left(10^{-20}\frac{\text{erg}\cdot\text{cm}^3}{\text{sec}}\right)$	0	0.06	0.25	0.84	1.26	1.47	1.70	1.85	1.88	1.73	1.68	—
ζ	0	2.2	3.7	5.7	6.9	7.7	8.8	10.0	10.5	10.4	9.4	5.55

The asymptotic expression for $\Psi(T_e)$ as $T_e \to \infty$ can be written analytically:

$$\Psi \equiv \langle v\sigma_i \rangle \approx 0.92 \cdot 10^{-7}\, T_{ev}^{-1/2} \ln(3.5 T_{ev})\ \text{cm}^3/\text{sec} \qquad (4)$$

Using the functional dependence of $\sigma_i(\epsilon)$ close to threshold [4], we can find an approximate formula for the other limiting case $T_e \ll W_i$ ($W_i = 13.5$ ev is the ionization energy):

$$\Psi \approx \sigma_0 \sqrt{\frac{2T_{erg}}{m}}\left(1+\frac{2T_e}{W_i}\right)\exp\left(-\frac{W_i}{T_e}\right)\text{cm}^3/\text{sec}, \qquad (5)$$

where $\sigma_0 \approx 4 \cdot 10^{-17}$ cm^2 and m is the mass of the electron.

We may note that our use of the theoretical values for σ_i and σ_e, computed in Born approximation, does not reduce significantly the reliability of the calculations even with T_e equal to several electron volts; this result does not necessarily apply to the higher temperatures.

4. The calculations carried out in Sections 2 and 3, based on the introduction of the function $\zeta(T_e)$, represent an average of Equation (3) over excitation and emission processes relating to the Balmer series. The "average" equation corresponding to Equation (3) is of the form

$$\dot{n} = n_{ph}\zeta(T_e), \tag{6}$$

where n_{ph} is the number of Balmer photons emitted in one second per 1 cm^3 of volume. Assuming that T_e and n_0 are fixed over the cross section of the discharge and that n_0 also remains constant in time,* integrating Equations (1, 6) over this cross section we have

$$\dot{N} = Nn_0\Psi(T_e), \tag{7}$$

$$\dot{N} = N_{ph}\zeta(T_e), \tag{8}$$

where $N(t)$ and $N_{ph}(t)$ are the number of electrons and photons emitted in one second per centimeter of discharge length. N_{ph} is measured experimentally while the functions Ψ and ζ are found above, so that (7) and (8) are essentially a system of two equations for the functions $N(t)$ and $T_e(t)$.

We solve this system under the assumption that $T_e \ll W_i$ and that T_e does not change essentially in the time interval of interest. If these conditions are satisfied we can use Equation (5) and also assume, in the first approximation, that $\Psi \approx$ const and $\zeta \approx$ const; the equation can then be integrated directly. Eliminating N and then Ψ (5), we obtain the following equation for T_e:

$$T_e = W_i \left\{ \ln \frac{\sigma_0 \sqrt{\frac{2T_e}{m}} \left(1 + \frac{2T_e}{W_i}\right) n_0 t}{\ln\left[\frac{1}{N(0)}\zeta(T_e)\int_0^t N_{ph}dt + 1\right]} \right\}^{-1}. \tag{9}$$

Solving this equation for given values of n_0 and t, we are convinced of the validity of the assumptions used in deriving it (the fact that the logarithms are insensitive to changes in the arguments is an important factor in this respect). It turns out that the function $T_e(t)$ has a plateau in the interval Δt, which is equal to several microseconds in the region of the "break" in the current curve. The value of T_e at the plateau depends on the initial pressure and is equal to approximately 4 ev with $p_0 = 0.1$ mm Hg and approximately 2.5 ev for $p_0 = 2$ mm Hg [2]. Thus, an analysis of photometric measurements (as well as for the current measurements cf. Section 5) indicates a "saturation" effect for the electron temperature in the region of discharge parameters being considered: virtually all the energy obtained by the electrons is dissipated in ionization and excitation.** Knowing $T_e(t)$, in accordance with Equation (8) we can find the number of ions in one centimeter length of the discharge: $N(t) = N(0) + \int_0^t \zeta N_{ph}dt \approx \int_0^t \zeta N_{ph}dt$, and then the degree of ionization (averaged over the cross section of the discharge column).

5. In addition to Equations (7) and (8) we can use a third equation which contains a new unknown – the effective "value" of the electron $\tilde{\epsilon}$:

$$\dot{N} = \frac{Q_J}{\tilde{\varepsilon}} \approx \frac{m}{e^2\tau_1}\frac{I^2}{N\tilde{\epsilon}}, \tag{10}$$

*In [2] consideration is given to the case in which n_0 is not constant.

**A situation of this kind was pointed out earlier by C.I. Braginskii and A.B. Migdal.

where Q_J is the Joule heat generated in one second per centimeter length of discharge*; I(t) is the total current; τ_1 is the mean free time for an electron in hydrogen. The quantity $\tilde{\epsilon}$ depends on the time, but at sufficiently large values of E/p, may be considered constant. By virtue of this fact we can estimate T_e without knowing $\tilde{\epsilon}$, using the measurements of the current I. Actually with $\tilde{\epsilon} = \text{const}$, Equation (10) can be integrated directly and yields $N^2\tilde{\epsilon}$. On the other hand, $N^2\tilde{\epsilon}$ can be expressed by eliminating N from (7) and (10). Equating both expressions and using Equation (5) we have

$$T_e = W_i \left\{ \ln \left[\sigma_0 \sqrt{\frac{2T_e}{m}} \left(1 + \frac{2T_e}{W_i} \right) \frac{2n_0 \int_0^t I^2 dt}{I^2} \right] \right\}^{-1}. \tag{11}$$

This equation is consistent with Equation (9) and is easily solved by successive approximations for given values of I(t) and n_0. If the current increases in linear fashion ($I = \dot{I}t$) Equation (11) assumes the form

$$T_e = W_i \left\{ \ln \left[1.1 \cdot 10^3 T_e^{1/2} \left(1 + \frac{2T_e}{W_i} \right) pt \right] \right\}^{-1}, \tag{12}$$

where T, p and t are expressed in electron volts, millimeters of mercury and seconds, respectively. The slow drop in T_e with time, which is found in Equation (12)** may be understood qualitatively from the assumptions which have been made. Actually, with $\tilde{\epsilon} = \text{const}$ and $\dot{I} = \text{const}$, $N \backsim I^{3/2}$ so that the total conductivity, which is proportional to N, increases faster than the current; in accordance with Ohm's law the electric field in the discharge falls off along with the mean energy accumulated by the electrons, i.e., the quantity T_e. The values of T_e obtained from Equations (11) or (12) are close to the values from Equation (9); this fact partially substantiates the assertion that $\tilde{\epsilon}$ is roughly constant for the conditions being considered. Substituting in Equation (10) the values of N(t) found earlier [2], and $\tau_1 (\text{sec}) = 1.7 \cdot 10^{-10} p_{\text{mm}}^{-1}$ [6] we find $\tilde{\epsilon} \sim 100$ ev, in accordance with the results of [6].

We wish to express our gratitude to L.A. Artsimovich and M.A. Leontovich for valuable discussions and to D.V. Orlinskii for help in the numerical calculations.

LITERATURE CITED

[1] L. A. Artsimovich, A.M. Andrianov, O.A. Bazilevskaia, Iu.G. Prokhorov and N.V. Filippov, J. Atomic Energy (USSR) 1, 3, 76 (1956).***

[2] N.A. Borzunov, V.I. Kogan and D.V. Orlinskii, J. Atomic Energy (USSR) 4, 180 (1958).***

[3] Mott and Massey, Theory of Atomic Collisions**** (State Tech. Press, 1951).

[4] H.S.W. Massey and E.H.S. Burhop, Electronic and Ionic Impact Phenomena (Oxford, Clarendon Press, 1952) Ch. III.

[5] H. Bethe, Quantum Mechanics of Simple Systems**** (State Tech. Press, 1935).

[6] L. Varnerin and S. Brown, Phys. Rev. 79, 946 (1950).

Received November 11, 1957

*For times close to the "break" time an important role in the electron energy balance is played by the exchange of energy with the heated neutral gas: $Q_{ne} = \frac{3m}{M} \frac{N}{\tau_1} (T_n - T_e)$.

**This result is somewhat different from that obtained in Section 4 ($T_e \approx \text{const}$ for a certain time interval t).

***Original Russian pagination. See C.B. translation.

****In Russian.

ESTIMATE OF THE ELECTRON TEMPERATURE AND DEGREE OF IONIZATION IN THE INITIAL STAGES OF AN INTENSE PULSED DISCHARGE*

N. A. Borzunov, V. I. Kogan, and D. V. Orlinskii

In the present paper we present the results of an investigation of the radiation of an intense pulsed discharge in hydrogen [1] in the visible part of the spectrum and also interpret the results on the assumption that the electron mechanism is the primary ionization factor.

1. The discharge was formed in a cylindrical glass chamber with an internal diameter of 18.5 cm and a distance of 97 cm between the electrodes. The current source was a condenser bank with a total capacity of 35 μf. In all the experiments the current was measured by means of a Rogovskii loop and had a maximum value of approximately 250 kiloamps in the first half cycle.

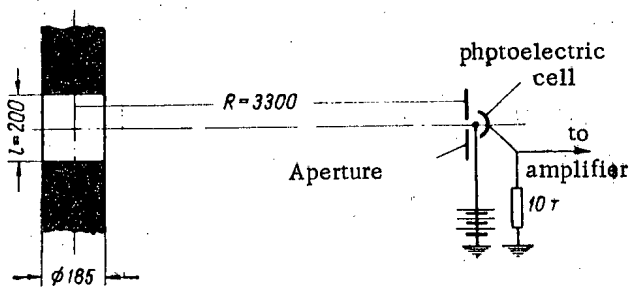

Fig. 1. Diagram of the experiment.

The radiation from the discharge was detected with a vacuum cesium-oxide photoelectric cell having an integrated intensity of 40 μamp/lumen (Fig. 1). The signal from the photoelectric cell was fed to an amplifier through a coaxial cable and then to the plates of a two-beam oscilloscope (OK-17). The radiation could reach the photoelectric cell only from a limited section along the length of the chamber (l = 20 cm). The remaining parts were covered by an opaque screen. In Fig. 2 is shown a typical oscillogram of the discharge current I and the photocurrent I_{ph}, taken with an initial hydrogen pressure of 0.1 mm Hg.

The curves showing the variation of photocurrent were taken at initial hydrogen pressures ranging from 0.1 to 2.0 mm Hg. In Fig. 3 are shown curves obtained with initial pressures p_0 = 0.3, 0.5, 1.0, and 2.0 mm Hg. On this same figure, for comparison, is shown a curve of the time variation of the luminous radius of the contracting plasma column obtained with p_0 = 1 mm Hg [2]. From these curves it is apparent that up to the time

* This work was carried out in 1954.

at which the current starts to move away from the walls of the chamber, i.e., up to the start of contraction, the photocurrent increases rather slowly. Then the photocurrent increases rapidly, and passes through a maximum at the instant corresponding to the maximum contraction of the plasma column. The breakup which follows the contraction is accompanied by a reduction in the radiation. As a result of a breakup the column of gas interacts with the walls of the chamber and produces intense evaporation of materials from the walls. A large number of silicon and oxygen atoms enter the discharge; these atoms have very strong lines in the visible part of the spectrum. Hence, the amount of radiated light increases. For relatively large values of p_0 (1-2 mm Hg) this increase is not observed because of the relatively small number of "contaminating" atoms as compared with the number of hydrogen atoms.

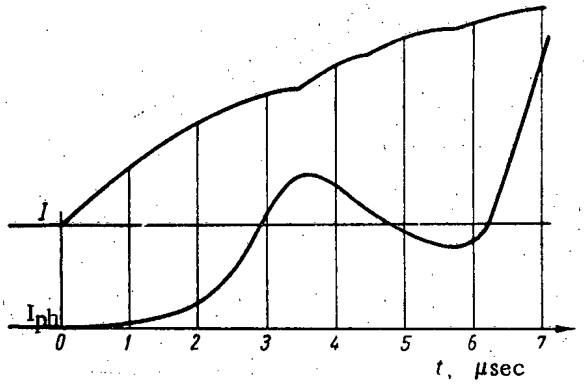

Fig. 2. Oscillogram of the current and photocurrent.

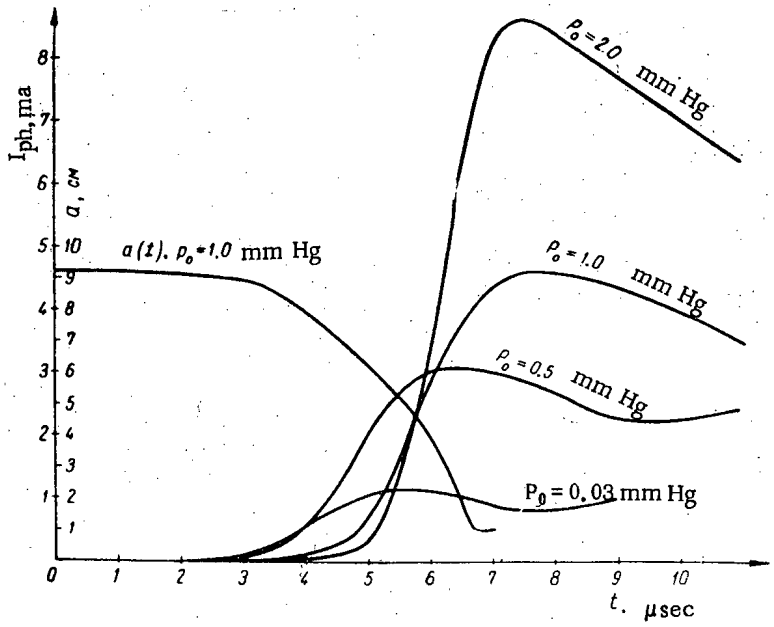

Fig. 3. Curves for $I_{ph}(t)$ with various initial hydrogen pressures.

The curves for $I_{ph}(t)$ give the dependence of the rate of photon emission as a function of time. The total number of radiated protons up to time t can be obtained by integrating these curves over time from 0 to t. It is assumed that: 1) the contaminants in the discharge are not present up to the breakup of the column, which leads to partial evaporation of materials from the wall; 2) the photoelectric cell is so far removed from the radiating volume that the light source may be considered a point source; 3) within the limits of the visible part of the spectrum the quantum yield of the photocathode is independent of wavelength and equal to $^3/_4$ of the maximum yield (in the present case, 1/200 of an electron per quantum); 4) in the time which is of interest to us the deionization is relatively small. Then the number of "average" photons of the Balmer series associated with one centimeter of the height of the cylinder at the time t will be

$$\int_0^t N_{ph}\,dt = \left(\frac{4R}{d}\right)^2 \frac{10^{-12}}{ekhq} \int_0^t I_{ph}(t)\,dt, \quad (1) \tag{1}$$

where d is the diameter of the aperture, $e = 1.6 \cdot 10^{-19}$ coul, $k = 5 \cdot 10^{-3}$ is the mean photon sensitivity of the photocathode, $q = 0.75$ is a factor which takes into account the absorption and scattering of light by the walls of the chamber. The photo current, I_{ph}, is expressed in microamperes and the time t in microseconds. The results of the calculations are shown in Table 1.

TABLE 1

Number of "Average" Balmer Photons $\int_0^t N_{ph}dt$

p_0 mm Hg \ t, μsec	1	2	3	4	5	6	7	8	9	10
0.1	$2.7 \cdot 10^{14}$	$1.6 \cdot 10^{15}$	$6.4 \cdot 10^{15}$	$1.4 \cdot 10^{16}$	$2.0 \cdot 10^{16}$	—	—	—	—	—
0.15	$2.7 \cdot 10^{14}$	$1.7 \cdot 10^{15}$	$1.0 \cdot 10^{16}$	$4.5 \cdot 10^{16}$	$7.9 \cdot 10^{16}$	—	—	—	—	—
0.3	—	$2.5 \cdot 10^{15}$	$5.0 \cdot 10^{15}$	$5.0 \cdot 10^{16}$	$1.7 \cdot 10^{17}$	$3.4 \cdot 10^{17}$	$4.9 \cdot 10^{17}$	—	—	—
0.5	—	$1.0 \cdot 10^{15}$	$6.0 \cdot 10^{15}$	$4.0 \cdot 10^{16}$	$2.3 \cdot 10^{17}$	$6.2 \cdot 10^{17}$	$1.2 \cdot 10^{18}$	$1.5 \cdot 10^{18}$	$1.9 \cdot 10^{18}$	—
1.0	—	—	$6.7 \cdot 10^{15}$	$1.5 \cdot 10^{16}$	$6.0 \cdot 10^{16}$	$3.1 \cdot 10^{17}$	$8.5 \cdot 10^{17}$	$1.5 \cdot 10^{18}$	$2.2 \cdot 10^{18}$	$2.8 \cdot 10^{18}$
2.0	—	—	$6.7 \cdot 10^{15}$	$1.5 \cdot 10^{16}$	$4.0 \cdot 10^{16}$	$3.2 \cdot 10^{17}$	$1.3 \cdot 10^{18}$	$2.5 \cdot 10^{18}$	$3.7 \cdot 10^{18}$	$4.8 \cdot 10^{18}$

2. An analysis of the experimental data was carried out using the following equation for the electron temperature T_e [3]:

$$T_e = W_i \left\{ \ln \frac{\sigma_0 \sqrt{\frac{2T_e}{m}} \left(1 + \frac{2T_e}{W_i}\right) n_0 t}{\ln\left[1 + \frac{\zeta(T_e)}{N(0)} \int_0^t N_{ph}\,dt\right]} \right\}^{-1}, \tag{2}$$

where $W_i = 13.5$ ev is the ionization energy of the hydrogen atom, n_0 is the number of atoms in 1 cm^3; $\sigma_0 \approx 4 \cdot 10^{-17}$ cm^2; $N(0)$ is the initial number of ions in 1 cm of length of the discharge chamber, $\underline{m}$ is the mass of the electron, $\zeta(T_e)$ is the number of ionization events associated with one "average" Balmer photon. The function $\zeta(T_e)$ is plotted graphically in accordance with [3].

TABLE 2
Electron Temperature T_e, ev.

p_0 mm Hg \ t, μsec	1	2	3	4	5	6	6.6	7.0	7.5
0.1	3.6	3.9	4.1	4.1	—	—	—	—	—
0.3	—	—	3.0	3.3	3.3	3.3	—	—	—
0.5	—	—	2.6	2.9	3.0	3.0	—	3.0	—
2.0	—	—	—	1.8	2.0	2.2	2.3	—	2.3

Equation (2) was solved by successive approximations for a number of values of p_0, i.e., n_0 and times $\underline{t}$.* The results are shown in Table 2.

These results tend to corroborate the assumption that the quantity T_e is a weak function of time ("saturation" of T_e) used in deriving Equation (2). Knowing $T_e(t)$ we can find the number of ions in 1 cm length of discharge from the expression

$$N(t) = N(0) + \int_0^t \zeta N_{ph} dt. \qquad (3)$$

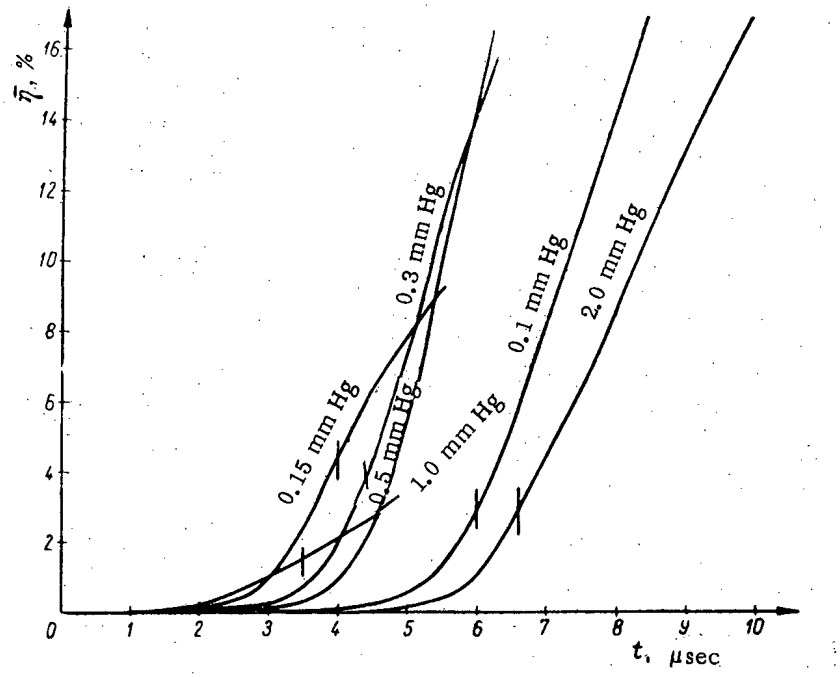

Fig. 4. Curves for $\overline{\eta(t)}$ for various initial hydrogen pressures.

* For values of $\underline{t}$ which are not too small the results are insensitive to the choice of $N(0)$; we take $N(0)$ as equal to approximately 0.001 of the total number of atoms.

For all important values of t, $N(0)$ is negligibly small. The intensity of ionization, averaged over the cross section of the discharge, is $\overline{\eta(t)} = \frac{N(t)}{N_0}$, where N_0 is the total number of atoms in 1 cm of the discharge. The results of the calculation of $\overline{\eta(t)}$ are given as curves in Fig. 4. The vertical lines on the curves denote the time of the first break [2] corresponding to each initial pressure.

Thus, an analysis of the measurements of the intensity of the radiation from a discharge in the visible portion of the spectrum lead to the following conclusions:

1) for a given initial pressure T_e changes slowly over a rather wide time interval in the region of the break on the current curve;

2) as the initial pressure is increased T_e falls off slowly from approximately 4 ev at $p_0 = 0.1$ mm Hg to approximately 2.5 ev at $p_0 = 2.0$ mm Hg;

3) the degree of ionization of the gas, averaged over the cross section of the discharge at the instant of the break t_b is several percent.

In deriving Equation (2) it has been assumed that $n_0 = \text{const}$. The change (increase) in n_0 in time can be roughly taken into account on the basis of the assumption of complete entrainment of the neutral particles in the radial contraction of the discharge, taking $n_0(t)a^2(t) = n_0(0)a^2(0)$, where $a(t)$ is the luminous radius of the discharge column [2]. However this refinement does not effect the conclusions.

The authors are indebted to L. A. Artsimovich, S. Iu. Luk'ianov, and S. M. Osovets for discussion of the results and valuable remarks.

LITERATURE CITED

[1] L. A. Artsimovich, A. M. Andrianov, O. A. Bazilevskaia, Iu. G. Prokhorov, and N. V. Filippov, J. Atomic Energy 1, 76 (1953).

[2] N. A. Borzunov, D. V. Orlinskii, and S. M. Osovets, J. Atomic Energy (USSR) 4, 149 (1958).*

[3] V. I. Kogan, J. Atomic Energy (USSR) 4, 178 (1958).*

Received November 11, 1957.

* Original Russian pagination. See C. B. Translation.

NOTES ON THE THEORY OF PROBES

N. P. Generalov

The electric probe is widely used to measure potentials, densities, and temperatures in a plasma. As is well known, the probe creates a perturbation in the plasma: in the layer which surrounds the probe there is an electric field which separates the charges.

In existing theories various assumptions are made as to the distribution of electric field and the boundary layer and the dimensions of the layer are estimated on the basis of these assumptions.

The diffusion approximation equation was used to investigate the plasma in the present work; the use of this approximation is valid at sufficiently high densities. Under these conditions it is possible to find the variation of electric field in the boundary layer.

In the diffusion approximation the plasma equations assume the form:

$$
\begin{aligned}
J_\alpha^+ &= -D_{\alpha\beta}^+ \frac{\partial n^+}{\partial x_\beta} + b_{\alpha\beta}^+ n^+ E_\beta, \\
J_\alpha^- &= -D_{\alpha\beta}^- \frac{\partial n^-}{\partial x_\beta} - b_{\alpha\beta}^- n^- E_\beta, \\
\frac{\partial n^+}{\partial t} &+ \frac{\partial J_\alpha^+}{\partial x_\alpha} = q^+, \\
\frac{\partial n^-}{\partial t} &+ \frac{\partial J_\alpha^-}{\partial x_\alpha} = q^-, \\
\frac{\partial^2 \varphi}{\partial x_\alpha^2} &= -4\pi e\,(n^+ - n^-), \\
E_\alpha &= -\frac{\partial \varphi}{\partial x_\alpha}, \\
\alpha, \beta &= 1, 2, 3,
\end{aligned}
\tag{1}
$$

where $J_\alpha^\pm$ is the density of the ion current and electron current, $n^\pm$ is the density, $D_{\alpha\beta}^\pm$ is the diffusion coefficient, $b_{\alpha\beta}^\pm$ is the mobility coefficient for ions and electrons and φ is the potential associated with the electric field.

There are two boundary conditions associated with these equations:

$$\left.\begin{aligned}(\alpha^{\pm} n^{\pm} - J_{\nu}^{\pm})|_S = 0,\\ \alpha^{\pm} = \frac{1-p^{\pm}}{1+p^{\pm}} \frac{v^{\pm}}{2},\end{aligned}\right\} \tag{2}$$

these indicate that a certain fraction $p^{\pm}$ of the particle flux, incident on the boundary surface S with normal ν are reflected from this surface ($p=1$ corresponds to total reflection and $p=0$ corresponds to total absorption of the incident flux), $v^{\pm}$ are the thermal velocity components, q^{+} and q^{-} are the strengths of the sources.

Applying the potential distribution at the boundary we obtain one additional boundary condition:

$$\varphi|_S = \varphi_S. \tag{3}$$

The initial conditions for this system are as follows:

$$n^{\pm}(x_\alpha, t)|_{t=0} = n^{\pm}(x_\alpha). \tag{4}$$

The diffusion and mobility coefficients of the plasma components are related by the well-known Einstein relation

$$b_{\alpha\beta}^{\pm} = \frac{e}{\theta^{\pm}} D_{\alpha\beta}^{\pm}, \tag{5}$$

where e is the charge and $\theta^{\pm}$ is the temperature.

In the plane, one-dimensional, stationary case, in the absence of sources, from Equation (1), we find

$$\left.\begin{aligned}k^- n^+ + k^+ n^- = \frac{k^+ k^-}{8\pi e} E^2 - (k^- i^+ + k^+ i^-)\, x + C,\\ n^+ - n^- = \frac{1}{4\pi e} \frac{dE}{dx},\\ \frac{d^2E}{dx^2} = \frac{k^+ k^-}{2} E^3 + (k^+ - k^-)\, E \frac{dE}{dx} +\\ + 4\pi e\, [C - (k^- i^+ + k^+ i^-)\, x]\, E - 4\pi e\, (i^+ - i^-),\end{aligned}\right\} \tag{6}$$

where

$$i^{\pm} = \frac{J^{\pm}}{D^{\pm}}, \qquad k^{\pm} = \frac{b^{\pm}}{D^{\pm}} = \frac{e}{\theta^{\pm}}.$$

The last equation is similar to the Penlev equation and, in particular, with $k^+ = k^-$ reduces to an equation of this type.

Making a substitution of variables

$$\left.\begin{aligned}\frac{4\pi e\, [C - (k^- i^+ + k^+ i^-)\, x]}{[4\pi e\, (k^- i^+ + k^+ i^-)]^{2/3}} = z,\\ E = \frac{2}{\sqrt{k^+ k^-}} [4\pi e\, (k^- i^+ + k^+ i^-)]^{1/3} W,\end{aligned}\right\} \tag{7}$$

$$A=-\frac{2}{\sqrt{k^+k^-}}(k^+-k^-);\quad B=-\frac{\sqrt{k^+k^-}}{2}\frac{i^+-i^-}{k^-i^++k^+i^-}$$

we arrive at an equation which contains two dimensionless parameters:

$$\frac{d^2W}{dz^2}=AW\frac{dW}{dz}+2W^3+zW+B. \tag{8}$$

In the vicinity of the singularity points the solutions are of the form

$$\left.\begin{aligned} W_1&=\frac{a_1}{z-C_1}-\frac{1}{6}\frac{C_1}{a_1}(z-C_1)+\\ &\quad+\frac{a_1+B}{2-Aa_1-6a_1^2}(z-C_1)^2+\dots\\ W_2&=\frac{a_2}{z-C_1}-\frac{1}{6}\frac{C_1}{a_2}(z-C_1)+\\ &\quad+\frac{a_2+B}{2-Aa_2-6a_2^2}(z-C_1)^2+\dots \end{aligned}\right\} \tag{9}$$

$$a_1=\sqrt{\frac{k^-}{k^+}};\quad a_2=-\sqrt{\frac{k^+}{k^-}}.$$

At higher values of z the solution W (z) either oscillates (z < 0) or assumes an asymptotic form (z > 0):

$$W=-\frac{B}{z}, \tag{10}$$

which in the original variable yields:

$$E=-\frac{i^+-i^-}{k^-i^++k^+i^-}\frac{1}{x}+\dots \tag{11}$$

Thus, the field E penetrates deep into the plasma for current flows J^+ and J^- which are nonzero.

In the absence of current flow, from Equation (1) it is easy to obtain the following expression for the potential of the electric field: *

$$\Delta\tilde{\varphi}(\vec{x})-\lambda^2\,\mathrm{sh}\,\tilde{\varphi}(\vec{x})=0,$$

where

$$\lambda^2=\frac{8\pi e^2n_0}{kT};\quad \tilde{\varphi}=\frac{e\varphi}{kT}. \tag{12}$$

At weak fields we arrive at the usual result, which stems from the equation

$$\Delta\varphi-\lambda^2\varphi=0. \tag{13}$$

* 'sh' ≡ 'sinh' – Publisher.

In particular, the field penetrates into the plasma only to a distance equal to several Debye radii.

Similarly, it can be shown that in the one-dimensional cylindrical case

$$k^-n^+ + k^+n^- = \frac{k^+k^-}{8\pi e}\left(E^2 + 2\int \frac{E^2}{x}dx\right) + I + C,$$

$$n^+ - n^- = \frac{1}{4\pi e}\left(\frac{dE}{dx} + \frac{E}{x}\right),$$

$$\frac{d^2E}{dx^2} = (k^+ - k^-)E\frac{dE}{dx} - \frac{1}{x}\frac{dE}{dx} + \frac{k^+k^-}{2}E^3 + (k^+ - k^-)\frac{E^2}{x} +$$

$$+ k^+k^-E\int \frac{E^2}{x}dx + 4\pi e\left(C + \frac{1}{4\pi e x^2} + I\right)E - 4\pi e(i^+ - i^-), \qquad (14)$$

where

$$I = -(k^-i^+ + k^+i^-)\,x \ln x.$$

At high values of $\underline{x}$ we obtain the following asymptotic expression:

$$E = -\frac{i^+ - i^-}{k^-i^+ + k^+i^-}\cdot\frac{1}{x \ln x}. \qquad (15)$$

Finally, in the one-dimensional spherical case we arrive at the equation

$$k^-n^+ + k^+n^- = \frac{k^+k^-}{8\pi e}\left(E^2 + 4\int \frac{E^2}{x}\,dx\right) + I + C;$$

$$n^+ - n^- = \frac{1}{4\pi e}\left(\frac{dE}{dx} + \frac{2E}{x}\right);$$

$$\frac{d^2E}{dx^2} = (k^+ - k^-)E\frac{dE}{dx} - \frac{2}{x}\frac{dE}{dx} +$$

$$+ \frac{k^+k^-}{2}E^3 + 2(k^+ - k^-)\frac{E^2}{x} + 2k^+k^-E\int \frac{E^2}{x}dx +$$

$$+ 4\pi e\left(C + \frac{1}{2\pi e x^2} + I\right)E - 4\pi e(i^+ - i^-),$$

$$i^+ = \frac{j^+}{x^2}; \quad j^+ = \text{const}, \qquad (16)$$

$$i^- = \frac{j^-}{x^2}; \quad j^- = \text{const},$$

where $I = (k^-i^+ + k^+i^-)x$.

At high values of $\underline{x}$ we obtain the asymptotic expression

$$E = \frac{j^+ - j^-}{C}\frac{1}{x^2}. \qquad (17)$$

Here, the constant C can be determined from the first relation given in (16) with $x \to \infty$:

$$C = (k^+ + k^-)\,n_0,$$

where n_0 is the density of the quasi-neutral plasma at large distances from the probe. Thus, in the absence of currents, the solution of the plasma equations in the diffusion approximation yields the usual result: the field decays at a distance of the order of several Debye radii.

In the case in which the currents J^+ and J^- to the probe are different from zero, the situation is markedly different. Near the probe surface (where the one-dimensional plane equation can be used) the field falls off as $1/x$. As the separation is increased to a distance which becomes much greater than the diameter of the probe, the field starts to fall off at a faster rate: $1/x \ln x$. At distances much greater than the dimensions of the probe the field falls off as the inverse square of the distance.

In conclusion we wish to thank E. P. Tambovtsev, Iu. A. Popov, and V. I. Pistunovich for discussion of the results.

Received September 5, 1957.

MEASUREMENTS OF ν_{eff} AND $\sigma_f + \sigma_c$ FOR FAST NEUTRONS IN U^{235} AND Pu^{239}

V.N. Andreev

The variation with energy of the quantity $\nu_{eff} = \nu \frac{\sigma_f}{\sigma_f + \sigma_c}$ for fast neutrons has been studied in [1]. In a number of papers the following quantities have been studied as a function of energy:

$$\sigma_f + \sigma_c\ [2];\ \alpha = \frac{\sigma_c}{\sigma_f}\ [3],\ [4];\ \nu\ [5]\text{—}[9];\ \sigma_f\ [10].$$

In the present note are described measurements of ν_{eff} and $\sigma_f + \sigma_c$ for U^{235} and Pu^{239} for photoneutrons with the following energies: 24 kev (Sb—Be source), 240 kev ($Na-D_2O$ source), and 880 kev (Na—Be source). The measurements of ν_{eff} and $\sigma_f + \sigma_c$ were carried out using a spherical geometry such that elastic neutron scattering could be neglected in the first approximation.

The neutron absorption in the spheres was determined with a U^{235} fission chamber set up at the center of the sphere or removed entirely; the secondary fission neutrons at the center of the sphere were recorded with a U^{238} chamber and these effects were subtracted from the results obtained with the U^{235} chamber. The accuracy of the measurements was 0.2-0.4%.

The spheres of metallic U^{235} (90% enriched) and Pu^{239} had an internal diameter of 5 cm and walls 1 cm thick. The multiplication and elastic scattering of fission neutrons in the spheres were measured experimentally by alternately exposing to thermal neutrons the operating spheres and thin spherical shells of the same material, at the center of which were located fission chambers with U^{235}, U^{238} and Pu^{239}.

The neutron multiplication in the spheres, measured with the U^{235} and Pu^{239} detectors, was found to be essentially the same (difference less than 1%). This indicates that the U^{235} detector was not very sensitive to inelastic scattering of fission neutrons.

In the photoneutron experiments the fission-neutron sources are distributed over the entire volume of the sphere whereas in the thermal neutron exposure these sources are located mainly at the surface; hence, the experimental values were converted from a surface source to a distributed source. Account was also taken of multiplication and inelastic scattering of the fission neutrons in the shells.

The relative calibrations for the fission chambers with U^{235} and U^{238} in the spectrum of U^{235} and Pu^{239} fission was carried out at the center of thin shells of U^{235} and Pu^{239}, placed in a thermal neutron flux. By using this procedure it was possible to exclude the effect of the difference in the U^{235} and Pu^{239} fission spectra [11, 12] in the determination of ν_{eff} and $\sigma_f + \sigma_c$.

To determine ν_{eff} one also requires a relative calibration of the U^{235} chamber for photoneutrons and fission neutrons. For this purpose the relative intensities of the neutron sources were measured with an accuracy of 2% in a water tank with a spherical volume 10 cm in diameter. At neutron energies of 24 and 880 kev the calibration indicated good agreement between the U^{235} fission cross section and that published in the Hughes atlas [10]; at neutron energy of 240 kev the cross section was found to be about 15% higher than the published value.

In analyzing the results, account was taken of the neutrons scattered from the walls of the apparatus, the finite distances between the neutron sources and the detectors, the uncertainties in the dimensions of the sources and detectors, the U^{238} and U^{235} content and a number of less important factors. An important consideration in

the spherical geometry is the change of neutron effect (with respect to the "all wave" detector located inside the sphere) in processes in which these are neutron energy changes (for example, photoneutron capture and fission neutron emission in inelastic scattering).

The appropriate calculations were carried out on the basis of the Peierls kinetic equation for a hollow sphere. A similar method, in conjunction with a successive-collision analysis, was used to compute the multiplication in the spheres, the effect of inelastic scattering, etc. In all cases the transport values of the cross section were used [13]. The results are shown in the table.

TABLE

E_n kev	ν_{eff}		$\sigma_f+\sigma_c$, barns	
	U^{235}	Pu^{239}	U^{235}	Pu^{239}
24	1.94±0.05	2.17±0.07	3.70±0.09	2.56±0.09
240	1.98±0.08	2.82±0.12	2.05±0.09	1.89±0.11
880	2.22±0.12	3.00±0.19	1.58±0.09	1.79±0.13

These results are based on the assumption that either there is no inelastic photoneutron scattering in the spheres or that the sensitivity of the U^{235} detector to inelastic scattering of neutrons in the sphere remains fixed. Actually, neither assumption is completely justified; however, estimates carried out on the basis of the available information on inelastic scattering in U^{235} [14] indicate that in the U^{235} case the quantity ν_{eff} cannot change by more than 5% while in the Pu^{239} case the variation is still smaller.

In conclusion the authors wish to thank A.I. Leipunskii, Member of the Academy of Sciences, Ukrainian SSR, and O.D. Kazachkovskii for their interest in this work and a number of illuminating remarks.

LITERATURE CITED

[1] P.E. Spivak, B.G. Erozolimskii, G.A. Dorofeev, V.N. Lavrenchik, I.E. Kutikov and Iu.P. Dobrynin, J. Atomic Energy (USSR) 1, 21 (1956).*

[2] R.L. Maclin, H.W. Schmitt and J.R. Gibbons, Phys. Rev. 102, 797 (1956).

[3] V.R. Kenney, et al., Proceedings of the International Conference on Peaceful Use of Atomic Energy, Geneva, 1955, Vol. IV** (Academy of Sciences Press, USSR, 1957), p. 370.

[4] M.G. Inghram, et al., Proceedings of the International Conference on Peaceful Use of Atomic Energy, Geneva, 1955, Vol. IV** (Academy of Sciences Press, USSR, 1957), p. 130.

[5] R.B. Leachman, Determination of Fission Quantities of Importance to Reactors (Report No. 592 presented by the U.S. Delegation to the International Conference on the Peaceful Use of Atomic Energy, Geneva, 1955).

[6] V.I. Kalashnikova, V.P. Zakharova, A.V. Krasnushkin, V.I. Lebedev and M.I. Pevzner, Conference of Academy of Sciences, USSR on the Peaceful Use of Atomic Energy (Division of Physico-Mathematical Sciences)** (Izv. Akad. Nauk SSSR, 1955), p. 161.

[7] V.I. Kalashnikova, V.I. Lebedev and P.E. Spivak, J. Atomic Energy (USSR) 2, 18 (1957).*

[8] J.M. Auclair, H.H. Landon and M. Jacob, Physica 22, 1187 (1956).

[9] G.N. Smirenkin, I.I. Bondarenko, L.S. Kutsaeva, Kh.D. Mishchenko, L.I. Prokhorova and B.P. Shemetenko, J. Atomic Energy (USSR) 4, 188 (1958).*

[10] Neutron Cross Sections (Appendix to the Atlas by D. Hughes), 1957.

*Original Russian pagination. See C.B. translation.

**In Russian.

[11] V.P. Kovalev, V.N. Andreev, M.M. Nikolaev and A.G. Guseinov, J. Exptl.-Theoret. Phys. (USSR) 33, 1069 (1957).*

[12] J.A. Grundl and J.R. Neuer, Bull. of Am. Phys. Soc., ser. II 1, 2, 95 (1956).

[13] R.C. Allen, R.B. Walton, R.B. Percins, R.A. Olson and R.F. Taschek, Phys. Rev. 104, 731 (1956).

[14] J.R. Beyster, M. Walt and E.W. Salmi, Phys. Rev. 104, 1319 (1956).

Received August 28, 1957

* See English translation.

THE NUMBER OF PROMPT NEUTRONS IN THE FISSION OF U^{235}, U^{238}, Th^{232} AND Np^{237} BY FAST NEUTRONS

B.D. Kuz'minov, L.S. Kutsaeva and I.I. Bondarenko

Measurements were made of the mean number of prompt neutrons $\nu(E)$ produced in the fission of U^{235}, U^{238}, Th^{232} and Np^{237} by fast neutrons with a spectrum close to that of fission neutrons.

A fission chamber containing the isotope under investigation was placed in the path of a beam of fast neutrons emerging from the active zone of a BR-2 reactor [1]. For registration of secondary neutrons we used proportional counters, filled with BF_3 enriched with isotope B^{10}, placed outside the neutron beam in a cylindrical block of paraffin.* An electronic device registered the chamber and counter pulses and the coincidence pulses.

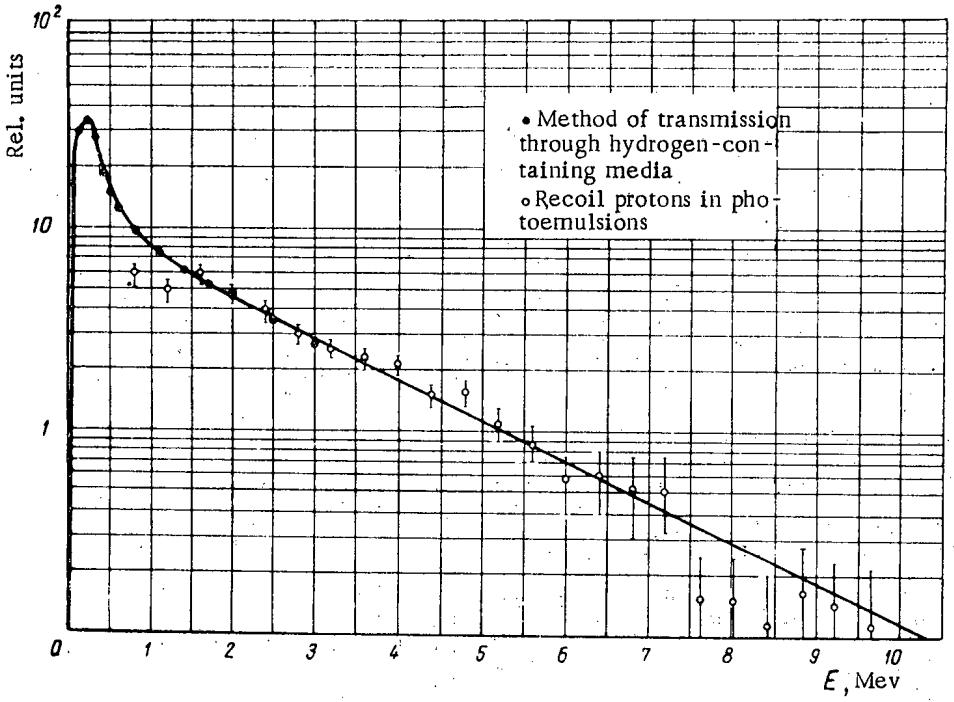

Spectrum of fast neutrons in the beam from the active zone of the BR-2 reactor.

The number of secondary neutrons born in the fission of the isotope under investigation is proportional to the ratio of the number of coincident pulses (after exclusion of chance coincident pulses) to the number of pulses from the chamber.

The resolving time of the coincidence circuit was approximately $2 \cdot 10^{-4}$ sec. For the measurements we used two geometrically identical chambers, one of which contained uranium enriched to 90% U^{235} and the other –

*This method has been described in [2-4].

TABLE

Results of Measuring the Number of Prompt Neutrons

Isotope undergoing fission	Mean energy of neutrons inducing fission, Mev	Secondary neutron detector	$\frac{\nu(E)}{\nu_T^{U^{235}}}$	$\nu(E)$
U^{235}	1.20	Fission chamber containing natural uranium	1.05±0.01	2.59±0.05
U^{238}	3.1	Ditto	1.17±0.02	2.9 ±0.1
U^{238}	3.1	Fission chamber containing U^{235} (enrichment 75%)	1.15±0.04	2.84±0.15
U^{238}	3.1	BF_3 counters in paraffin block	1.16±0.02	2.87±0.10
Th^{232}	3.5	Ditto	0.95±0.02	2.35±0.07
Np^{237}	2.5	Ditto	1.10±0.04	2.72±0.15

one of the elements being studied (U^{238}, Th^{232}, Np^{237}). The chamber containing U^{235} served for calibration.

$\nu(E)$ for U^{238} was also measured by another method, in which the secondary neutrons were registered by fission chambers containing uranium enriched to 75% U^{235} and natural uranium. These chambers consisted of coaxial cylindrical electrodes containing a large amount of fissionable material (5 g natural uranium and 1 g U^{235}) and were placed outside the neutron beam. The resolving time of the coincidence circuit in these measurements was about 10^{-7} sec, and the background of chance coincidences did not exceed 20%. From measurements with a threshold detector we were able to conclude that the spectra of secondary neutrons of U^{235} and U^{238} do not differ substantially.

From additional measurements conducted in a beam of thermal neutrons (the thermal column of the BR-2 reactor was used) we obtained the ratio $\nu(E)/\nu_T = 1.05\pm0.01$ for U^{235}. The measurements were carried out under the same geometrical conditions as for fast neutrons. By comparing the counting rates of chambers containing natural uranium and U^{235} (enrichment 90%) placed in a beam of thermal and fast neutrons we obtained the ratio of the fission cross sections of U^{235} and U^{238} for fast neutrons equal to 9.4±0.1. This result was used in the calculations to correct for the isotopic composition of the uranium.

In elaborating the results we took into account the angular anisotropy of fragments [5, 6] and secondary neutrons. Here the angular distribution of secondary neutrons relative to the fragments for all isotopes was assumed to be the same as for U^{235} fission by thermal neutrons [7].

The total corrections for isotopic composition and angular anisotropy for the investigated elements did not exceed 3%. The results of measurements with the corrections taken into account are given in the table.

The mean energy of the neutrons was computed by averaging from the known behavior of the fission cross section relative to the energy and from the measured spectrum of neutrons in the beam (figure). In the evaluations $\nu_T^{U^{235}}$ was taken equal to 2.47±0.03.

From measurements of ν for U^{238} where the secondary neutrons were registered by a chamber containing U^{235} (enrichment 75%) and by counters filled with BF_3, we deduced the mean value of $\nu^{U^{238}} = 2.86\pm0.10$.

The authors express their deep gratitude to O.D. Kazachkovskii and G.N. Smirenkin for valuable advice and participation in this work.

The authors are very grateful to Active Member of the Academy of Sciences Ukrainian SSR, A.I. Leipunskii, for valuable advice and constant interest in the work.

LITERATURE CITED

[1] A.I. Leipunskii, D.I. Blokhintsev, et al., J. Atomic Energy (USSR) 2, 497 (1957).*

[2] V.I. Kalashnikova, V.I. Lebedev, L.A. Mikaelian and M.I. Pevzner, J. Atomic Energy (USSR) 1, 3, 11 (1956).*

[3] K.W. Geiger and D.C. Rose, Canad. J. Phys. 32, 498 (1954).

[4] V.I. Kalashnikova, V.I. Lebedev and P.E. Spivak, J. Atomic Energy (USSR) 2, 18 (1957).*

[5] R.L. Henkel and J.E. Brolley, Phys. Rev. 103, 1292 (1956).

[6] J.E. Brolley, W.C. Dickinson and R.L. Henkel, Phys. Rev. 99, 159 (1955).

[7] J.S. Fraser, Phys. Rev. 88, 536 (1952).

Received July 8, 1957

*Original Russian pagination. See C.B. translation.

MEAN NUMBER OF PROMPT NEUTRONS IN THE FISSION OF U^{233}, U^{235}, Pu^{239} BY 4 AND 15 MEV NEUTRONS*

G.N. Smirenkin, I.I. Bondarenko, L.S. Kutsaeva, Kh.D. Mishchenko, L.I. Prokhorova and B.P. Shemetenko

A knowledge of the dependence of ν on the energy E of neutrons inducing fission is of interest from the point of view of studies of the fission process and also has practical importance for the design of fast neutron reactors.

In recent times, a number of works [1-6] on this question have been published. The dependence $\nu(E)$ was calculated in 1953 by Usachev and Trubitsyn [3] and also by Fowler [1] on the assumption that the kinetic energy of fission fragments was independent of the energy of the neutrons inducing fission.

The results of these calculations agree with one another and indicate that with increase of neutron energy E, ν must grow according to a linear law

$$\nu(E) = \nu_T + aE,$$

where ν_T is the mean number of neutrons emitted in fission by thermal neutrons. The coefficient a, which determines the increment of ν for an increase of neutron energy by 1 Mev, for U^{235} is 0.125 Mev^{-1} (T = 1.4 Mev), according to the results of calculations in [1], and 0.145 Mev^{-1} (T = 1 Mev), according to the results of [3]. The difference is due mainly to the difference in the temperature T taken by the authors for the excited fragments.

The dependence $\nu(E)$ has also been studied experimentally. In [1, 4] ν for spontaneous fission of Pu^{240} was compared with ν for Pu^{239} fission by thermal neutrons. In experiments with neutrons of energies E = 0.7 and 1 Mev for U^{235} [1, 2], and with neutrons of the fission spectrum for U^{233}, U^{235}, Pu^{239} [5, 6], the value $\nu(E)/\nu_T$ was measured. The results of these experiments confirm the expected growth of ν with increase of neutron energy.

In the present work the ratio ν/ν_T was measured in the fission of U^{233}, U^{235} and Pu^{239} by 4 and 15 Mev neutrons. We used the reaction $D(d, n)He^3$ for obtaining neutrons with energy 4.0±0.3 Mev, and the reaction $T(d, n)He^4$ for neutrons with energy 15.0±0.5 Mev. For obtaining thermal neutrons a paraffin block was placed close to the target.

The measurements were carried out with a double ionization fission chamber placed directly in the neutron flux. The primary neutrons induced fissions in both halves of the chamber. A secondary neutron arising from fission in one half of the chamber could induce fission in the other half. Such events were registered by a coincidence circuit. The number of coincidences is proportional to ν. By measuring the number of coincidences per single fission in the chamber due to fast and thermal neutrons the ratio ν/ν_T was determined.

To increase the efficiency of registration of secondary neutrons the distance between the layers of fissionable material was reduced by depositing them on both sides of fine platinum foil ~30μ thick. The maximum proximity of the layers of fissionable material and their great thickness (~2 mg/cm^2) enabled us with such a simple experimental arrangement as the double fission chamber to attain an efficiency of registration for secondary neutrons of $\sim 5 \cdot 10^{-5}$ and made it possible to employ a coincidence circuit with resolving time $\sim 2 \cdot 10^{-7}$ sec.

*This work was carried out in 1955-1956.

For creating the required fission intensity in the chamber (~300 sec^{-1}) we had to deposit on each side of the foil considerable amounts of fissionable material (50 mg U^{235}, 35 mg U^{233}, 20 mg Pu^{239}). By reducing the pulse duration with the addition of 5-10% CO_2 to the argon, by decreasing the pressure of the working gas in the chamber (50-200 mm Hg) and by choosing the most suitable geometry for the electrodes we succeeded, despite the great thickness of the layers and their high α-activity, in obtaining satisfactory counting characteristics for all the substances investigated.

With the resolving time of the coincidence circuit equal to $2 \cdot 10^{-7}$ sec, and the fission rate in the chamber equal to 300 sec^{-1}, the coincidence count was 3-5 min^{-1}. The background of chance coincidences did not exceed 30-40% of the number of coincidences registered. Chance coincidences were excluded by using a delay line. In the measurements for each substance investigated 5-8 thousand coincidences were registered for both fast and thermal neutrons.

TABLE

Results of Measurement of $\nu(E)$ and $\Delta\nu/\Delta E$

Isotope undergoing fission	ν_T	E, Mev	$\nu(E)/\nu_T$	$\nu(E)$	$\Delta\nu/\Delta E$
U^{233}	2.55±0,06	4 15	1.20±0.04 1.73±0.06	3.06±0.12 4.42±0.17	0.127±0.025 0.124±0.011
U^{235}	2.47±0,05	4 15	1.22±0.04 1.82±0.07	3.01±0.12 4.51±0.19	0.136±0.025 0.135±0.012
Pu^{239}	2.91±0,06	4 15	1.18±0.03 1.62±0.06	3.43±0.11 4.71±0.20	0.131±0.022 0.121±0.013

The following corrections were introduced in the values ν/ν_T obtained in the experiment:

1) for the difference in the efficiency of registering secondary neutrons in measurements with fast and thermal neutrons, which arises from the asymmetry in the angular distribution of the fragments – the fast incident neutron [7, 8] and the dependence of the fission neutron spectrum [9, 10] on the excitation energy of the nucleus undergoing fission;

2) for the presence in the fast neutron flux of neutrons inelastically scattered by the walls of the ionization chamber, the existence of a background of ultra-cadmium neutrons in the room, and also for the presence in the thermal neutron flux of fast neutrons which had passed through the paraffin block;

3) for U^{238} impurity in the uranium layers used.

The table gives the final results of determining $\nu(E)/\nu_T$ with these corrections taken into account, the data on ν_T [11] and the values calculated from it for $\nu(E)$ and $\frac{\Delta\nu}{\Delta E} = \frac{\nu(E) - \nu_T}{E}$.

The values for $\Delta\nu/\Delta E$ show that the linear dependence of $\nu(E)$, predicted in [1, 3], is realized within the limits of experimental error up to E = 15 Mev, despite the fact that at this energy the reaction (n, n'f) takes place with the boiling-off of a neutron from the excited compound nucleus before its fission. This is explained by the fact that the increase of ν due to the emission of an inelastically scattered neutron is compensated by the reduced excitation of the residual nucleus, and also by the fact that ν for neighboring isotopes differs insignificantly [12].

The value $a = \Delta\nu/\Delta E$ for U^{235} is somewhat higher than for U^{233} and Pu^{239}. This is due, apparently, to the fact that in the fission of U^{235} the mean binding energy of the neutron in the fragments is less, and the spectrum of the fission neutrons is softer [9].

The authors express their deep gratitude to Active Member of the Academy of Sciences Ukrainian SSR, A.I. Leipunskii and O.D. Kazachkovskii for their attention and constant interest in the work, to A.N. Serbinov, V.A. Romanov and the whole staff of the neutron generator for their help in carrying out the measurements and their efficient operation of the plant.

LITERATURE CITED

[1] R.B. Leachman, Proc. Intern. Conf. Peaceful Uses Atomic Energy, Geneva, 1955 Vol. 2 (U.N., New York, 1956) p. 193.

[2] R.B. Leachman, Phys. Rev. 101, 1005 (1956).

[3] L.N. Usachev and V.P. Trubitsyn, in the book: Report of Acad. Sci. USSR* (1953).

[4] V.I. Kalashnikova, V.P. Zakharova, A.V. Krasnushkin, V.P. Lebedev and M.I. Pevzner, in the book: Session of Acad. Sci. USSR on the Peaceful Uses of Atomic Energy (Meeting of the Section of Phys.-Math. Sciences)* (Izd. AN SSSR, Moscow, 1955).

[5] V.I. Kalashnikova, V.P. Lebedev and P.E. Spivak, J. Atomic Energy (USSR) 2, 18 (1957).**

[6] J.M. Auclair, H.H. Landon and M. Jacob, Physica 22, 1187 (1956).

[7] J.E. Brolley, W.C. Dickinson and R.L. Henkel, Phys. Rev. 99, 159 (1957).

[8] R.L. Henkel and J.E. Brolley, Bull. Am. Phys. Soc., ser. II 2, 308 (1957).

[9] V.P. Kovalev, V.N. Andreev, M.I. Nikolaev and A.G. Guseinov, J. Exptl.-Theoret. Phys. (USSR) 33, 1069 (1957).***

[10] J.A. Grundl and J.R. Neuer, Bull. Amer. Phys. Soc., ser. II 1, 95 (1956).

[11] J.A. Harvey and J.E. Sanders, Progress in Nuclear Energy, ser. I 1, 1 (London, Pergamon Press, 1956).

[12] B.D. Kuz'minov and G.N. Smirenkin, J. Exptl.-Theoret. Phys. (USSR) 34, 503 (1958).***

Received July 8, 1957

*In Russian.

**Original Russian pagination. See C.B. translation.

***See English translation.

FISSION CROSS SECTIONS OF Th^{232} AND Np^{237} FOR 14.6 MEV NEUTRONS

A.N. Protopopov, Iu.A. Selitskii and S.M. Solov'ev

The only source from which it is possible to extract information on the fission cross sections of Th^{232} and Np^{237} for 14 Mev neutrons is the atlas of neutron cross sections [1]. The cross sections given in the atlas, however, are taken from unpublished works and contain no indications of the errors in measurement. The aim of the present work is to make these data more accurate.

For obtaining fast neutrons we used the reaction $T(d, n)He^4$ where the deuterons, accelerated to an energy of 175 kev, bombarded a thick zirconium-tritium target mounted at an angle of 45° to the direction of the deuteron beam. The effective energy of the deuterons, allowing for the slowing-down in the target and the dependence of the reaction cross section on the deuteron energy, was equal to 118 kev [2]. The neutron flux was evaluated by registering on a proportional counter α-particles travelling at an angle of 90° to the direction of the deuterons.

The fissile material was deposited by electrolysis on a platinum disc. The 20 mm diameter target made from it was placed in an ionization chamber at a distance of 6.2 cm from the neutron source. The neutrons inducing fission had an energy of 14.6 Mev.

To simplify the calculations and to attain greater accuracy the deuteron beam was passed through a diaphragm so that its diameter on the tritium target was less than 5 mm, and the neutron source could be considered as a point source. In this case, allowing for the anisotropy in the distribution of α-particles and neutrons in the laboratory system of coordinates [2], the fission cross section σ is determined by the following formula [3]:

$$\sigma = \frac{4\pi r_0^2 k \omega_\alpha N_f}{\ln\left(1+\frac{r_0^2}{R_0^2}\right) N N_\alpha}, \qquad (1)$$

where r_0 is the radius of fissile layer; R_0 is the distance from neutron source to target; ω_α is the solid angle within which α-particles are registered; $\underline{k}$ is a coefficient which allows for the angular distribution of α-particles and neutrons; N is the number of atoms of fissile isotope ; N_f is the number of fissions in active layer; N_α is the number of α-particles registered by counter.

The weight of the fissile isotope and its degree of purity were determined with particular care. In determining the weight of the thorium target a negligible weight of Th^{230}, which has a half-life $\tau = 8.0 \cdot 10^4$ years, was mixed with the Th^{232} in order to increase the specific activity.

After verifying the chemical purity by spectral analysis the preparation was heated to a temperature of 1400°C which ensured the complete transformation of thorium to thorium oxide ThO_2, and was then weighed to an accuracy of 0.5%. After that, the oxide was dissolved and the solution diluted with distilled water. The weight of the solution was also determined with great accuracy. For determining the specific activity of the mixture of thorium isotopes, i.e., the number of α-particles counted per unit weight of thorium, samples from the solution were deposited on platinum discs and weighed on an automatic balance. The discs with the dried samples were fired and their activity was measured in an ionization chamber. By taking the average of six samples of different weight the specific activity of the thorium was found to be 36.7 ± 0.3 counts/min · μg in a solid angle 2π. The amount of thorium in the target was found by comparing its specific activity with that of thorium electrolytically deposited from an alcoholic solution of thorium nitrate. This quantity was equal to 248 ± 3 μg.

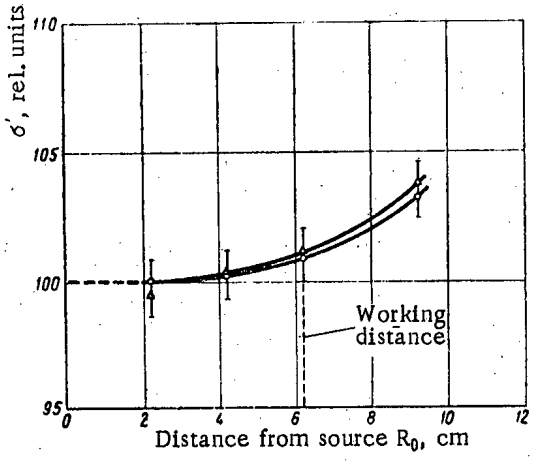

Fig. 1. Determination of background due to neutron scattering: O) points for Th^{232}; Δ) for Np^{237}.

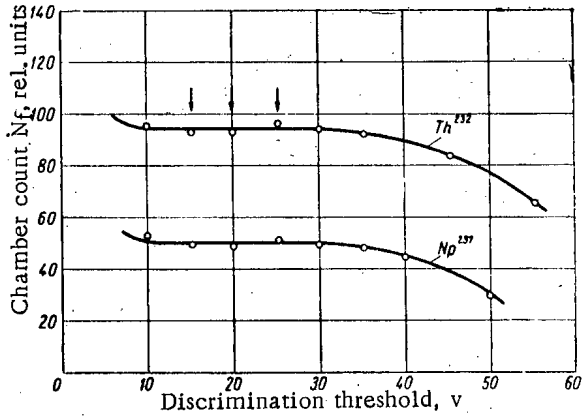

Fig. 2. Characteristics of ionization chamber. The arrows denote thresholds at which the measurements were made.

The weight of the Np^{237} target was determined from the α-activity after verification of the α-spectrum and the half-life $\tau = (2.2 \pm 0.1) \cdot 10^6$ years, given in [4]. The number of neptunium atoms in the target was $(5.57 \pm 0.03) \cdot 10^{16}$.

In determining the fission cross section of any isotope it must be borne in mind that fission is caused by neutrons from the source itself and by neutrons scattered by surrounding objects. The share of background fissions is determined by the distance between the target and the neutron source and by the nature of the dependence of the fission section on the neutron energy. The fission of Th^{232} and Np^{237} is only induced by fast neutrons and therefore we should expect that the effect of scattered neutrons would be slight.

For a quantitative determination of the share of fissions induced by scattered neutrons, we measured the distance dependence of the value

$$\sigma' = \frac{N_f}{\ln\left(1+\frac{r_0^2}{R_0^2}\right) N_\alpha}, \qquad (2)$$

which comes into the Formula (1). The graphs of this dependence are shown on Figure 1. On extrapolation of the curves to zero distance it was assumed that σ' for small distances remains constant, since the share of scattered neutrons becomes negligibly small. A correction was determined from the difference between σ' for a working distance $R_0 = 6.2$ cm and for $R_0 = 0$. It amounted to $(1 \pm 1)\%$ for both Th^{232} and Np^{237}.

Before each experiment for determining the fission cross section we checked the characteristics of the α-particle counter and the ionization chamber. The number of fissions was measured at three different thresholds of the discriminator (Figure 2); the agreement of the results indicated the preservation of the plateau in the measurement process.

Measurements carried out twice with thorium and neptunium targets gave results in good agreement. It was found that for Th^{232}

$$\sigma = 0.35 \pm 0.02 \text{ barn}$$

and for Np^{237}

$$\sigma = 2.4 \pm 0.2 \text{ barn.}$$

These results agree well with those given in [1].

By a more accurate determination of the half-life of Np^{237}, on the basis of which the target weight was determined, the value of the fission cross section of Np^{237} can be calculated with less error.

The authors express their gratitude to A.G. Samartseva for the chemical purification and preparation of the neptunium target, and also to T.A. Il'inskaia, who was of great help in conducting the spectral analysis of the thorium sample.

LITERATURE CITED

[1] D.J. Hughes and J.A. Harvey, Neutron Cross Sections (McGraw-Hill Co., New York, 1955).

[2] K.E. Larsson, Arkiv. fys. 9, 293 (1955).

[3] A.N. Protopopov, Iu.A. Selitskii and S.M. Solov'ev, Trudy Radievogo Instituta AN SSSR (in print).

[4] L.B. Magnusson and T.J. Lachapelle, J. Amer. Chem. Soc. 70, 3534 (1948).

Received August 31, 1957

CROSS SECTION FOR INELASTIC INTERACTION OF 14 MEV NEUTRONS WITH SOME LIGHT ELEMENTS

V.M. Gorbachev and L.B. Poretskii

Among the published results of studies of the transmission of neutrons by various substances there are no data on the values of the effective cross sections for inelastic interaction σ_{in} of 14 Mev neutrons with the lithium isotopes (Li^6 and Li^7). In addition, the values of the cross section σ_{in}, obtained for the next three light nuclei, are either solitary ones (for instance, for Be^9 [1]) or do not agree satisfactorily with one another [1-4].

In the present work we measured the cross sections for inelastic interaction of 14 Mev neutrons with the lithium isotopes Li^6 (90%) and Li^7 (99%), beryllium, boron and carbon.

The source of 14 Mev neutrons was a zirconium target saturated with tritium and bombarded with deuterons accelerated to an energy 150 kev. The monitor was a proportional counter which registered α-particles produced in the reaction $T(d, n)He^4$.

TABLE

Results of Measuring the Inelastic Interaction Cross Section for 14 Mev Neutrons in 10^{-24} cm^2

Element	Data of present work	Data of [2]	Data of [3]	Data of [4]	Data of [1]
Li^6	0.66±0.05	–	–	–	–
Li^7	0.52±0.06	–	–	–	–
Be^9	0.55±0.04	–	–	–	0.64±0.02
B	0.74±0.07	0.69±0.10	–	–	0.64±0.04
C	0.63±0.06	0.76±0.04	0.601±0.006	0.63±0.05	0.73±0.02

The cross section was determined from the diminution of the primary neutron flux in passing through a layer of the substances under investigation.

The thickness of the layer of substance, expressed as the number of nuclei per 1 cm^2 was $(2-3)\cdot 10^{23}$ for the different specimens.

As threshold detectors we employed a scintillation counter with a naphthalene crystal activated by anthracene and a proton telescope composed of three proportional counters connected in a coincidence circuit.

The discriminator voltage of the scintillation counter and the thickness of the aluminum filter of the telescope were chosen so that the threshold for neutron registration was approximately equal to 7 Mev, which ensured the registration only of primary and elastically-scattered neutrons.

The detectors registered neutrons travelling at an angle of 90° to the direction of the deuteron beam.

The results of our measurements and also the data of other authors are given in the table.

The results obtained show that the cross section for inelastic interaction of 14 Mev neutrons with the lightest nuclei is not, apparently, a monotonic function of the mass number.

The authors express their thanks to Iu.S. Zamiatin for his constant interest and discussion of the results.

LITERATURE CITED

[1] N.N. Flerov and V.M. Talyzin, J. Atomic Energy (USSR) 1, 4, 155 (1956).*

[2] D.D. Phillips, B.W. Davis and E.R. Graves, Phys. Rev. 88, 600 (1952).

[3] E.R. Graves and B.W. Davis, Phys. Rev. 97, 1205 (1955).

[4] V.M. Pasechnik, in the book: Physical Investigations (Reports of the Soviet Delegation to the International Conference on the Peaceful Uses of Atomic Energy) [in Russian] (Izd. AN SSSR, 1955), p. 319; V.I. Strizhak, J. Atomic Energy (USSR) 2, 1 (1957).*

Received September 30, 1957

*Original Russian pagination. See C.B. translation.

CALCULATION OF ELASTIC NEUTRON SCATTERING IN CYLINDRICAL LUMPS

T. Kh. Sedel'nikov

The scattering of neutrons in control rods is of great interest. Since the elements which are usually found in control rods have poor moderating properties and the cross-sections for these elements are weak functions of neutron energy, the problem can be considered in the monoenergetic approximation. This problem can be solved directly using an equation such as the Ambartsumian equation [1-4], which relates the emitted radiation to the incident radiation. Since this equation was not derived in the paper in which it is described [4] it is desirable to present a derivation.

It will be assumed that the scattering is isotropic. Let a beam of unit intensity be incident on a cylinder of radius r at angles Θ_0 and φ_0. The emitted radiation can be expressed as follows:

$$\delta(\omega_0)\, e^{-\gamma(r,\ \omega_0)} + I(r,\ \omega,\ \omega_0),$$

where $\gamma(r, \omega_0)$ is the optical thickness at the angles Θ_0 and φ_0 while $I(r, \omega, \omega_0)$ is the scattered radiation. To the cylinder we add an infinitesimally small layer of thickness Δ; as a result the intensity of the scattered radiation is changed [1] by the following factors:

1. Attenuation of the radiation in passing through the supplementary layer:

$$-I(r,\ \omega,\ \omega_0)\frac{\Delta}{l(r)}\left[\frac{1}{\mu\sin\Theta}+\frac{1}{\mu_0\sin\Theta_0}\right]l(r)=\frac{1}{\Sigma_s+\Sigma_c},$$

where $\mu = \cos\varphi$ and $\mu_0 = \cos\varphi_0$.

2. Scattering of the radiation $\lambda^{(r)}/4\pi\cdot\Delta/l(r)\cdot 1/\mu\sin\Theta$, where $\lambda = \Sigma_s/(\Sigma_s + \Sigma_c)$. This expression must be multiplied by $1 + e^{-\gamma(r, \omega_0)}$ to take account of scattering of the incident radiation and the transmitted radiation and by $1 + e^{-\gamma(r, \omega)}$ to take account of scattering in the direction ω and the opposite direction where $\gamma(r, \omega) = 2r\mu/\sin\Theta$.

3. Internal scattering of the radiation followed by subsequent scattering from the main cylinder:

$$\frac{\lambda(r)}{4\pi}\frac{\Delta}{l(r)}\int\frac{I(r,\ \omega,\ \omega')}{\mu\sin\Theta}\,d\omega'(1+e^{-\gamma(r,\ \omega_0)}),$$

(the last factor takes account of the transmitted radiation).

4. Scattering of the radiation in a definite direction where the radiation is partially reflected from an internal boundary:

$$\frac{\lambda(r)}{4\pi}\frac{\Delta}{l(r)}\frac{1}{\mu\sin\Theta}\int I(r,\ \omega',\ \omega_0)\,d\omega'\,(1+e^{-\gamma(r,\ \omega)}),$$

where the last factor takes account of the probability of emission of a neutron scattered in the direction $-\omega$.

5. Back scattering of the radiation with subsequent reflection, where the radiation is partially reflected

from an internal boundary:

$$\frac{\lambda(r)}{4\pi}\frac{\Delta}{l(r)}\int\frac{I(r,\omega,\omega'')}{\mu''\sin\Theta''}d\omega''\int I(r,\omega',\omega_0)\,d\omega'.$$

Combining these effects we obtain the equation for a thick cylinder:

$$I(r+\Delta,\omega+\Delta\omega,\omega_0+\Delta\omega_0)=I(r,\omega,\omega_0)\frac{r+\Delta}{r}\frac{\cos(\varphi_0+\Delta\varphi_0)}{\cos\varphi_0}-$$

$$-I(r,\omega,\omega_0)\frac{\Delta}{l(r)}\left(\frac{1}{\mu\sin\Theta}+\frac{1}{\mu_0\sin\Theta_0}\right)+\frac{\lambda(r)}{4\pi}\frac{\Delta}{l(r)}(1+e^{-\gamma(r,\omega_0)})\frac{1+e^{-\gamma(r,\omega)}}{\mu\sin\Theta}+$$

$$+\frac{\lambda(r)}{4\pi}\frac{\Delta}{l(r)}\left(1+e^{-\gamma(r,\omega_0)}\right)\int\frac{I(r,\omega,\omega')}{\mu'\sin\Theta'}d\omega'+\frac{\lambda(r)}{4\pi}\frac{\Delta}{l(r)}\frac{1+e^{-\gamma(r,\omega)}}{\mu\sin\Theta}\int I(r,\omega',\omega_0)d\omega'+$$

$$+\frac{\lambda(r)}{4\pi}\frac{\Delta}{l(r)}\int\frac{I(r,\omega,\omega'')}{\mu''\sin\Theta''}d\omega''\int I(r,\omega',\omega_0)\,d\omega'.$$

Expanding this equation in powers of Δ and assuming that $\Delta\Theta=\Delta\Theta_0=0$, $\Delta\varphi=-\tan\varphi\cdot\frac{\Delta}{r}$, $\Delta\varphi_0=-\tan\varphi_0\frac{\Delta}{r}$, we have

$$(r)\left[\frac{\partial I}{\partial r}+\frac{1-\mu^2}{r\mu}\frac{\partial I}{\partial\mu}+\frac{1-\mu_0^2}{r}\frac{\partial}{\partial\mu_0}\left(\frac{I}{\mu_0}\right)-\frac{1}{r}I\right]+\left(\frac{1}{\mu\sin\Theta}+\frac{1}{\mu_0\sin\Theta_0}\right)I=\frac{\lambda(r)}{4\pi}\frac{1}{\mu\sin\Theta}\times$$

$$\times\left[1+e^{-\gamma(r,\omega)}+\mu\sin\Theta\int\frac{I(r,\omega,\omega')}{\mu'\sin\Theta'}d\omega'\right]\times\left[1+e^{-\gamma(r,\omega_0)}+\int I(r,\omega',\omega_0)\,d\omega'\right].$$

In Reference [4] no attempt was made to normalize the flux in order to take account of the transmitted radiation; these omissions lead to an error in the results. Inasmuch as the scattered radiation is isotropic at small values of r the second, third, and fourth terms on the left-hand side of the equation are small; at large values of r these terms are again unimportant since they can be neglected in the zero-th approximation. Using $I(r,\omega,\omega_0)=\frac{\mu_0\sin\Theta_0}{\pi}\rho(r,\omega,\omega_0)$, we obtain the equation

$$\mu\mu_0\sin\Theta\sin\Theta_0\frac{\partial\rho}{\partial t}+(\mu\sin\Theta+\mu_0\sin\Theta_0)\rho=\frac{\lambda}{4}\left[1+e^{-\gamma(t,\omega)}+\frac{\mu\sin\Theta}{\pi}\int\rho(t,\omega,\omega')\,d\omega'\right]\times$$

$$\times\left[1+e^{-\gamma(t,\omega_0)}+\frac{\mu_0\sin\Theta_0}{\pi}\int\rho(t,\omega',\omega_0)\,d\omega'\right].$$

This equation has the symmetric solution [1] $\rho(\omega,\omega_0)=\rho(\omega_0,\omega)$ and can be written in the form:

$$\mu\mu_0\sin\Theta\sin\Theta_0\frac{\partial\rho}{\partial t}+(\mu\sin\Theta+\mu_0\sin\Theta_0)\rho=\frac{\lambda}{4}\varphi(t,\omega)\varphi(t,\omega_0);$$

$$\varphi(t,\omega)=1+e^{-\gamma(t,\omega)}+\frac{\mu\sin\Theta}{\pi}\int\rho(t,\omega,\omega')\,d\omega';$$

$$t=\int_0^r\frac{dr'}{l(r')}.$$

Turning now to a system of spherical coordinates with the z-axis perpendicular to the axis of the cylinder we expand $\varphi(r,\eta,\xi)$ in a series in the azimuthal parameter ξ. The total intensity of the scattered radiation, which is of interest to us, can be given as follows for isotropic incident radiation:

$$A=\int_0^1\eta\,d\eta\int_0^1\eta_0\,d\eta_0\,\rho(t,\omega,\omega_0)=\frac{1}{4}\int_0^t\lambda(t')\left[\int_0^1\varphi_0(t',\eta)\,e^{-\frac{t-t'}{\eta}}d\eta\right]^2dt',$$

where $\varphi_0(t,\eta)$ is the zero-th harmonic of the expansion of $\varphi(t,\eta,\xi)$ in azimuth and obeys the equation

$$\varphi_0(t,\eta)=1+\frac{1}{2\pi}\int_0^{2\pi}d\xi\,e^{-\gamma(t,\eta,\xi)}+\frac{1}{2}\int_0^t dt'\,\lambda(t')\,\varphi_0(t',\eta)\times\int_0^1\frac{\varphi_0(t',\eta')}{\eta'}\,d\eta'\,e^{-(t-t')\left(\frac{1}{\eta}+\frac{1}{\eta'}\right)}$$

This equation was solved numerically by replacing the integrals by quadratures (accuracy of 5%) for λ equal to 0.3, 0.5 and 0.8. Using φ_0, the quantity A and the total albedo were found from the increment in the transmitted radiation (cf. table).

TABLE

Total Albedo

λ \ t	0	0.22	0.51	0.92	1.61	∞
1.00	1.00	1.00	1.00	1.00	1.00	1.00
0.8	1.00	1.00	1.00	0.94	0.70	0.34
0.5	1.00	0.86	0.69	0.50	0.33	0.15
0.3	1.00	0.77	0.57	0.40	0.25	0.066
0.0	1.00	0.69	0.47	0.31	0.19	0.00

The present method can also be used to find the albedo for a multi-layer nonmoderating shield.

Using a similar method one can find, in the monoenergetic approximation, an equation for the intensity of neutrons emitted from a multiplying cylindrical lump (in a spherical lump the term sin Θ is dropped):

$$\frac{\partial J(r,\omega)}{\partial r}+\frac{1-\mu^2}{r\mu}\frac{\partial J(r,\omega)}{\partial\mu}+\frac{J(r,\omega)}{l(r)\,\mu\sin\Theta}=\frac{\lambda(r)}{4\pi l(r)\,\mu\sin\Theta}\left(1+e^{-\gamma(r,\omega)}\right)\int J(r,\omega)\,d\omega+$$

$$+\frac{\partial(r)}{4\pi\mu\sin\Theta}\left[1+e^{-\gamma(r,\omega)}+\frac{\mu\sin\Theta}{\pi}\int\frac{I(r,\omega,\omega')}{\mu'\sin\Theta'}\,d\omega'\right]$$

where $\nu(r)$ is the intensity of the sources while $I(r,\omega,\omega')$ is the function introduced above. This equation can be transformed into a one-dimensional inhomogeneous Volterrá equation for the total radiation intensity:

$$J_0(r)=\int d\omega\,J(r,\omega).$$

Using this same method it is possible to solve the problem of transmission through a cylindrical layer by adding to the equation (in the spherical case the term sin Θ is dropped)

$$-\frac{\partial j(r,R,\omega,\omega_0)}{\partial r}-\frac{1-\mu^2}{r\mu}\frac{\partial j}{\partial\mu}-\frac{1-\mu_0^2}{r}\frac{\partial}{\partial\mu_0}\left(\frac{j}{\mu_0}\right)+\frac{1}{r}j+\frac{j}{l(r)\,\mu\sin\Theta}=\frac{\lambda(r)}{4\pi l(r)}\frac{1}{\mu\sin\Theta}\times$$

$$\times\left[e^{-\gamma(r,\omega_0)}+\int j(r,R,\omega',\omega_0)\,d\omega'\right]\times\left[1+e^{-\gamma(r,\omega)}+\frac{\mu\sin\Theta}{\pi}\int\frac{I^*(r,\omega,\omega')}{\mu\sin\Theta'}\,d\omega'\right]$$

where $j(r,R,\omega,\omega_0)$ is the intensity of the diffusion transmission while $I^*(r,\omega,\omega')$ is the strength of the internally scattered radiation for the flux from the inside.

The method described here can be extended to the case in which the scattering is anisotropic and in which slowing down takes place.

All the numerical calculations were carried out by P.A. Bondakov, T.A. Gruev, N.N. Trenin and N.F. Kham'ianov.

The author wishes to express his gratitude to G.I. Marchuk, for his interest in the work and for valuable comments, to D.F. Zaretskii and S.M. Ermakov for a number of important comments and to E.I. Pogudalin and I.P. Tiuterev for advice in carrying out the calculations.

LITERATURE CITED

[1] Ambartsumian, Mustel', Severnyi and Sobol'ev, Theoretical Astrophysics, Chapter 8 [in Russian] (State Tech. Press, Moscow, 1952).

[2] S. Chandrasekhar, Radiative Transfer [Russian translation] (IL, 1953).

[3] B.B. Kadomtsev, Doklady Akad. Nauk SSSR 113, 541 (1957).

[4] R. Bellman and R. Kalaba, Proc. Natl. Acad. Sci. USA vol. 43, 514 (1957).

Received August 28, 1957

THE ANGULAR DISTRIBUTION OF LIGHT AND HEAVY FRAGMENTS IN U^{238} FISSION BY 14 MEV NEUTRONS

A. N. Protopopov and V. P. Eismont

At the present time not a single nuclear model (either liquid drop, shell or collective models) gives any indication of whether the angular distribution of light and heavy fission fragments are the same and whether there exists any difference between the angular anisotropy of these fragment groups. The available experimental data are very scant and the nature of the problem remains unanswered.

Thus, in 1955 Brolley, Dickinson and Henkel [1] investigated the angular anisotropy of fission using an ionization chamber and plotted ionization spectra of Np^{237} fission fragments, ejected at angles of 180° and 90° relative to an incident 14 Mev neutron beam. By comparing the spectra they concluded that the probability of heavy fragment groups flying ahead was somewhat greater than that for light fragments. With the condition that the minimum on the curve describing the ionization spectrum of the fragments divides the heavy and light fragment groups, it was found that at an angle of 0° 10% more heavy fragments are ejected than at an angle of 90°, with an equal total number of fissions at each angle. In the same year Cohen et al. [2] measured the angular distribution of some fragments during U^{238}, U^{235}, U^{233}, Th^{232}, and Th^{230} fission by 22 Mev protons by separating the fission products radiochemically. In this work they found no difference in the angular anisotropy of light and heavy fragments: the angular distribution of light and heavy fission products was found to be symmetrical (with an accuracy up to 1%) relative to a direction perpendicular to the incident proton beam.

An explanation of the role of light and heavy fragments in fission would be of great value for the understanding of the fission mechanism. In this work, devoted to the comparison of the distribution of light and heavy fragments in a direction parallel to that of the incident neutrons, we used a more refined method than that used in paper [1].

The authors of paper [1] themselves note the qualitative character of their method. In fact, a comparison of the ionization spectra of the fragments, taken at various angles, cannot be a method of quantitatively determining the angular anisotropy of fragments of varying mass, as it is well known [3] that the energy distribution of fragments is not completely identical with their mass distribution. In order to determine the distribution of mass of the fragments at a certain angle to the beam of activating particles, it is necessary to measure at the same time the kinetic energy of the additional fragments ejected at this angle. According to the law of the conservation of impulse, the ratio of the fragment energy (in a system with a center of gravity) is equal to the inverse ratio of their mass, while the relative number of these ratios determines the distribution of fission fragment masses in the given direction. The latter method was used in this work.

The simultaneous determination of the energy of the additional fragments was carried out using a double ionization chamber with shielding screens. Openings were drilled in the central part of the common cathode, thus forming a collimator. The target, which was a layer of natural uranium 50 $\mu g/cm^2$ thick deposited on a collodion film that was transparent to fission fragments, was placed on the collimator. The ionization impulses, caused by fission fragments, were registered by an impulse analyzer, using a two-beam oscillograph tube.

The kinetic energy of the fragments was determined by comparing the ionization from fragments and α-particles (taking into account the ionization defect, energy absorption in the collodion film and in the collimator channels).

The chamber was placed at a source of fast neutrons, produced by the reaction $T(d, n)He^4$ from the bombardment of a zirconium – tritium target with deuterons, accelerated to 180 kev. The geometrical conditions were such that the axis of the neutron beam, falling on the chamber, coincided with the axis of the collimator channels and the maximum angle between the direction of the incident neutrons and fission fragments registered was not greater than 15°.

TABLE 1

Distribution of Light Fragments in the Direction Parallel to the Neutron Beam Axis.

Series	Number of recorded fragment pairs	Number of cases of light fragment emission at an angle of 0°	Number of cases of light fragment emission at an angle of 180°
1	303	140	163
2	553	284	269
Total	856	424 ± 21*	432 ± 21*

* The statistical error is indicated.

856 fragment pairs were recorded and the number of fission cases was calculated at which light fragments were ejected at an angle of 0° (to the front) and at an angle of 180° (back) relative to the incident neutrons. These numbers should have shown: 1) whether there was a main direction for the ejection of light fragments; 2) if so, which way (to the front or back in relation to the incident neutrons); and 3) how great was the excess of light fragments in this direction. The table gives the results of two separate series of measurements and the general result.

The table shows that within the limits of statistical error (5%), both directions of light fragment emission at 0° and at 180°, are equally probable, i.e., the angular distribution of the light (and consequently, of the heavy) fragments is symmetrical relative to the 90° direction.

The experimental data obtained in the work also made it possible to determine qualitatively that the angular anisotropy increased with an increase in the ratio of fragment masses during U^{238} fission by 14 Mev neutrons. The same effect was observed in paper [2] in the fission of U^{238}, U^{235}, U^{233}, Th^{232}, and Th^{230} by 22 Mev protons and in paper [4] in Th^{232} fission by γ-quanta with a maximum energy of 16 Mev.

The work is being continued in order to improve the statistical accuracy of the results. A detailed description of the experimental method will be given later.

LITERATURE CITED

[1] J. E. Brolley, W. C. Dickinson, and R. L. Henkel, Phys. Rev. 99, 159 (1955).

[2] B. L. Cohen, B. L. Ferrell-Bryan, D. J. Coombe, and M. K. Hullings, Phys. Rev. 98, 685 (1955).

[3] D. C. Brunton and G. C. Hanna, Can. J. Res. 28A, 190 (1950).

[4] A. W. Fairhall, J. Halpern, and E. J. Winhold, Phys. Rev. 94, 733 (1954).

Received March 28, 1957.

YIELDS OF RARE EARTH ELEMENTS IN THE SPALLATION OF BISMUTH BY 660 MEV PROTONS

A. V. Kaliamin, A. N. Murin, B. K. Preobrazhenskii, and N. E. Titov

We previously published some results of investigating the products of nuclear reactions in the bombardment of bismuth with 460 and 660 Mev protons [1]. However, we did not then study the rare earth reaction products, which belong to the interesting stage of the transition of spallation processes into fission processes. The data given below fill this gap for 660 Mev protons.

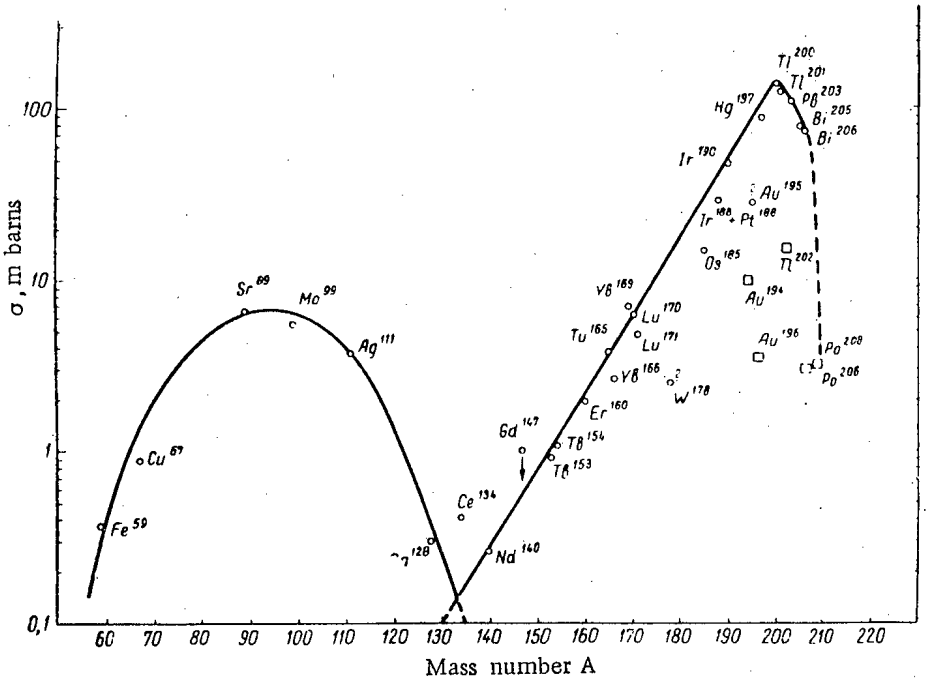

Fig. 1. Formation cross section of reaction products in Bi^{209} spallation with 660 Mev protons. The squares show the yields of "screened" nuclei, not including the yield of the whole mass number.

The chemical separation of the reaction products was carried out chromatographically [2]. The methods of measuring radiation intensity and determining product yields was essentially the same as described earlier [1]. It is not perfect. In calculating spallation reaction product yields (mainly those undergoing electron capture),

we measured the intensity of the Kx x-rays, following K-capture. However, here we could also count the soft rays of nuclear origin (similar to them in energy) as well as the x-ray K-quanta, whose emission is caused by γ-ray conversion. Both these factors may affect the magnitude of the yield. This, apparently, was the reason why the total calculated cross section of inelastic interaction was even somewhat greater than the geometric cross section ($\sim$ 2.5 barn). A more accurate determination of yield was difficult in this case due to the lack of exact decay schemes for the investigated nuclei.

Apparently, the ratio of the fission cross section to the spallation cross section indicated by us [1] is also somewhat low, as the yields of fission products are, as a rule, determined more accurately (by electron radiation).

Figure 1 shows the formation cross section of reaction products investigated by us (the rare earth section is new data, the other points were determined previously).

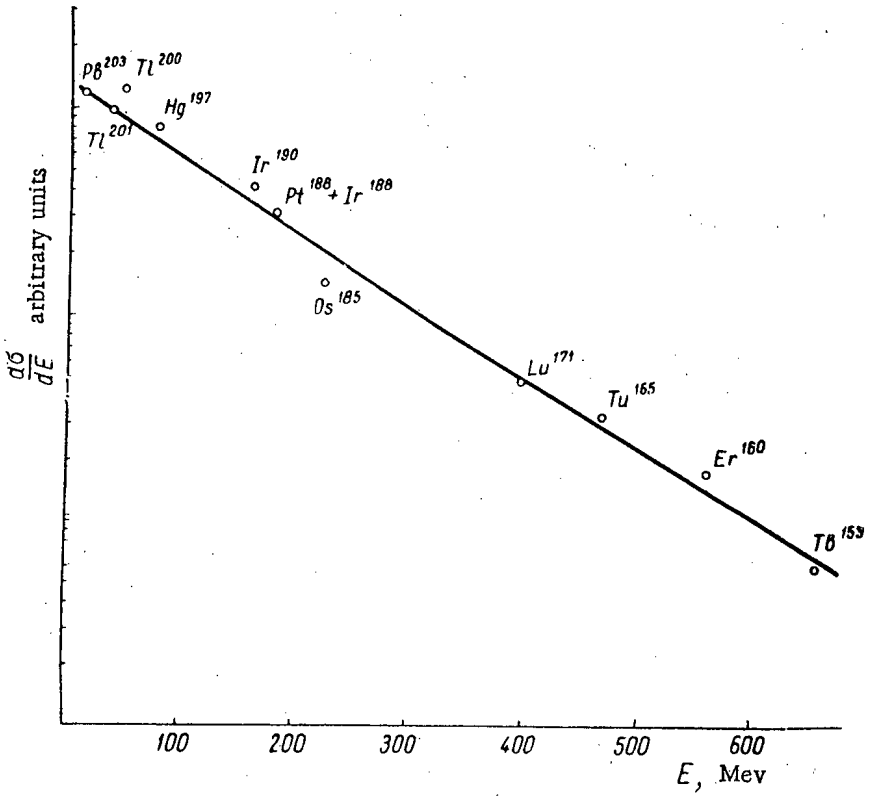

Fig. 2. Partial formation cross section $\frac{d\sigma}{dE}$ of products of bismuth spallation as a function of the activation energy of the intermediate nuclei (E).

The chipping products were clearly traced from Z = 84 (polonium) to Z = 58 (cerium), i.e., the extent of 27 elements with a change in mass number from 209 (the target nucleus) to 134. Here, the product yields decreased by approximately 3 orders. The right branch of the spallation curve crosses the fission curve, and the yields in the intermediate section are added together (the Ce^{134} yield is composed of the yields of this isotope in fission and spallation processes).

It is interesting to note that the general character of the distribution of the product-nuclei of a deep spallation reaction [3] is apparently the same as in the case of the spallation of nuclei lighter than bismuth, for example, copper [4] and silver [5].

Figure 1 shows that the cumulative yield of an isobar with a given mass number A is governed (in the region of masses not close to that of the target nucleus) by an expontential law, i.e.,

$$\log_e \sigma_A = pA + \text{const},$$

where the value of the parameter p is readily calculated from the angular coefficient of the line in Fig. 1 and was found by us to be equal ~ 0.11. This value is close to the value ~ 0.15 measured previously [4] for copper spallation with protons of the same energy. Apparently, it has the tendency to decrease with an increase in the mass number of the target nucleus A due to the increase in activation energy.

Figure 2 shows the change in the probability of activation of nuclei formed from Bi^{209} as a result of a cascade – nuclear process (with $E_p = 660$ Mev). This change also proceeds with an exponential relation to the mass number (the calculation method was described in paper [1]).

We should note, however, that due to the insufficient accuracy of the calculations* or the particular character of the spallation process at high activation energies (ejection of large fragments, which was not accounted for in the calculation) the calculated activation energy of Tb^{153} was close to the energy of the incident particles.

The other general rules of the process corresponded to those given in the preceding reports.

LITERATURE CITED

[1] A. N. Murin, B. K. Preobrazhenskii, and N. E. Titov, Bull. Acad. Sci. USSR, Div. Chem. Sci. 4, 578 (1955); A. N. Murin, B. K. Preobrazhenskii, I. A. Iutlandov, and M. A. Iakimov, Session Acad. Sci. USSR on the Peaceful Uses of Atomic Energy (Meeting Div. Chem. Sci.) (Acad. Sci. USSR Press, 1955), p. 160.

[2] B. K. Preobrazhenskii, O. M. Lilova, et al., J. Inorg. Chem. 1, 2294 (1956); 2, 1164 (1957).

[3] S. G. Rudstam, Phil. Mag. 46, 344 (1955); 44, 1131 (1953).

[4] A. N. Murin and I. A. Iutlandov, Bull. Acad. Sci. USSR, Div. Chem. Sci. 4, 408 (1957).

[5] B. V. Kurchatov, V. N. Mekhedov, M. Ia. Kuznetsova, L. N. Kurchatova, N. I. Borisova, and L. V. Chistiakov, Session Acad. Sci. USSR on the Peaceful Uses of Atomic Energy (Meeting Div. Chem. Sci.) (Acad. Sci. USSR Press, 1955), p. 178.

Received September 30, 1957.

* The basic premises of the calculations most probably do not hold true for the whole range of product-nuclei masses.

HALF-LIFE OF Sr^{90} AND ITS YIELD IN U^{233} FISSION

M. P. Anikina, R. N. Ivanov, G. M. Kukavadze, and B. V. Ershler

Data on the half-life of Sr^{90} given in the literature vary from 19.3 to 28 years [1-3]. The present work attempts to make these data more precise.

Strontium is isolated from fission products obtained by the irradiation of a U^{233} sample with reactor neutrons, which was investigated earlier [4, 5]. The work was carried out 4.25 years after the uranium sample was removed from the reactor, so practically no Sr^{89} remained in the sample. The amount of Sr^{88} and Sr^{90}

TABLE

Results of Determining the Amounts of Sr^{88} and Sr^{90} in the Sample.

Element	Atomic weight	Isotopic composition			Number of strontium atoms in the irradiated sample
		natural strontium	fission fragments	mixture of natural strontium with fragments *	
Strontium	84	0.055±0.001	—	—	—
	86	1 **	—	0.08±0.004	—
	87	0.74±0.01	—	0.061±0.005	—
	88	8.5±0.2	1.01±0.015	1.66±0.02	$(1.625\pm0.062)\cdot10^{18}$
	90	—	1 **	1 **	$(1.61\pm0.06)\cdot10^{18}$

* In calculating the total number of fragments in the sample, equal to 11.9 ± 0.2 mg [4, 5] 185 μg of natural strontium was added to the fission fragments.

** Taken as one.

in the sample was determined by isotopic dilution on a mass-spectrometer of the MS-1 type. A two filament ion source with surface ionization was used as the ion source [6]. The results obtained are given in the table.

A β-counter with a mica end-window of 1.2 mg/cm^2 thickness was used for determining the rate of strontium decay. An average value for the number of disintegrations per minute was obtained from a series of three measurements: $dN/dt = (7.25 \pm 0.14)\cdot10^{10}$ disintegrations per minute (calculated for the total number of Sr^{90} atoms in the irradiated sample N and considering the efficiency of the counter).

The half-life of Sr^{90} was calculated from the data obtained:

$$T_{1/2}=\frac{0.693N}{\frac{dN}{dt}}=29.3\pm1.6 \text{ years.}$$

As the amount of fragments in the given sample was known (11.9 ± 0.2 mg), the yields of Sr^{88} and Sr^{90} in U^{233} fission could be determined. The values obtained were (5.3 ± 0.3)% for Sr^{88} (without taking into account possible neutron absorption by the mother nucleus Kr^{88}) and (5.8 ± 0.4)% for Sr^{90} (with correction for decay).

Remarks. In the article by Anikina and Ershler [7], in determining the Sr^{90} yield in U^{233} fission, the half-life of Sr^{90} was taken as 19.9 years, in agreement with article [1].

However, as the present work showed, the value of $T_{1/2}$ is equal to 29.3 ± 1.6 years for Sr^{90}. Therefore, in calculating the Sr^{90} yield by the data in paper [7] one should consider the new correct value for $T_{1/2}$, found in the present work. Such a calculation gives a value for the Sr^{90} yield of 6.3 ± 0.3, which is in agreement with the data in this work within the limits of experimental error.

LITERATURE CITED

[1] R. I. Pawers and A. F. Voigt, Phys. Rev. 79, 175 (1950).

[2] D. J. Hughes, and J. A. Harvey, Neutron Cross Sections, (McGraw Hill Co., New York, 1955).

[3] E. P. Steinberg and L. E. Glendenin, Proc. Intern. Conf. Peaceful Uses of Atomic Energy, Geneva, 1955, U. N., New York, 1956, Vol. 7, p. 3.

[4] G. M. Kukavadze, M. P. Anikina, L. L. Gol'din, and B. V. Ershler, Session Acad. Sci. USSR on the Peaceful Uses of Atomic Energy (Meeting Div. Chem. Sci.) (Acad. Sci. USSR Press, Moscow, 1955), p. 205.

[5] G. M. Kukavadze, L. L. Gol'din, M. P. Anikina, and B. V. Ershler, Material International Conference on the Peaceful Uses of Atomic Energy, Geneva, 1955, (Acad. Sci. USSR Press, Moscow, 1957), Vol. 4, p. 275.

[6] R. N. Ivanov and G. M. Kukavadze, Pribory i Tekhnika Eksperimenta 1, 106 (1957).

[7] M. P. Anikina and B. V. Ershler, J. Atomic Energy (USSR) 2, 275 (1957).*

Received September 18, 1957.

* Original Russian pagination. See C. B. Translation.

USE OF NUCLEAR PHOTOEMULSIONS FOR THE DETERMINATION AND EVALUATION OF THE RADIOCHEMICAL PURITY OF α-EMITTING ISOTOPES

V. I. Baranov, K. B. Zaborenko, and V. I. Korobkov

Determination of the absolute content of radioactive isotopes by counting α-particles requires a high radiochemical purity of the preparation used, as the presence of foreign α-emitters introduces substantial errors. In any purification operations involving processes of co-precipitation, adsorption, etc., it is always possible that traces of other isotopes, emitting α-particles, would be present in the end-products. The application of the usual methods for evaluating radiochemical purity is extremely difficult for preparations with low activity.

This work describes a method of using nuclear photoemulsions for detecting ionium and evaluating its radiochemical purity.

In 1935, Baranov and Krechmer [1] used photo plates with a thick emulsion layer for studying the distribution of radioactive elements in rock and noted the high sensitivity of this method. The specific activity may be determined by the density of α-particles, using formulas given in [2, 3].

The resolution capacity of present-day nuclear emulsions for α-particles is about 400-500 kev, using the contact method, and 400-300 kev, introducing the radioactive substance into the emulsion [4]. This makes it possible to determine separately and completely reliably many α-active isotopes in the presence of a mixture of isotopes with similar radiation energy values.

We used NIKFI photo plates of the A-2 type with a 50 μ thick emulsion layer. A calibration curve of the relation of α-particle path in the emulsion to radiation energy was first plotted. For this purpose solutions of the isotopes U^{238}–U^{234}, Th^{232}, Po^{210}, and Bi^{212} (ThC)–Po^{212} (ThC') in a radiochemically pure state without carrier, were used.

Characteristics of the Solutions

1. A 1% solution of uranyl nitrate in water was prepared from a uranium salt that had been subjected to thorough radiochemical purification. The purity of the uranium was checked by measuring the specific activity of the α-radiation.

2. A 1% solution of thorium nitrate was prepared from thorium sulfate by a simplified method described in paper [4].

3. Polonium was extracted from an old ampule containing radon [5]. The nitric acid solution was evaporated down in a platinum dish, acidified with a drop of nitric acid and diluted with water so that the specific activity of the solution was 500-1000 dis/min·ml. *

* All the measurements were carried out on equipment of the "Da" type. The efficiency of the ionization chamber was 26%.

4. Bi^{212} (ThC)–Po^{212} (ThC'). Thoron decay products were precipitated on a gold plate in an emanator. The plate was washed with concentrated nitric acid and the acid evaporated. The invisible deposit was treated with water; the specific activity was 1800-3500 dis/min • ml.

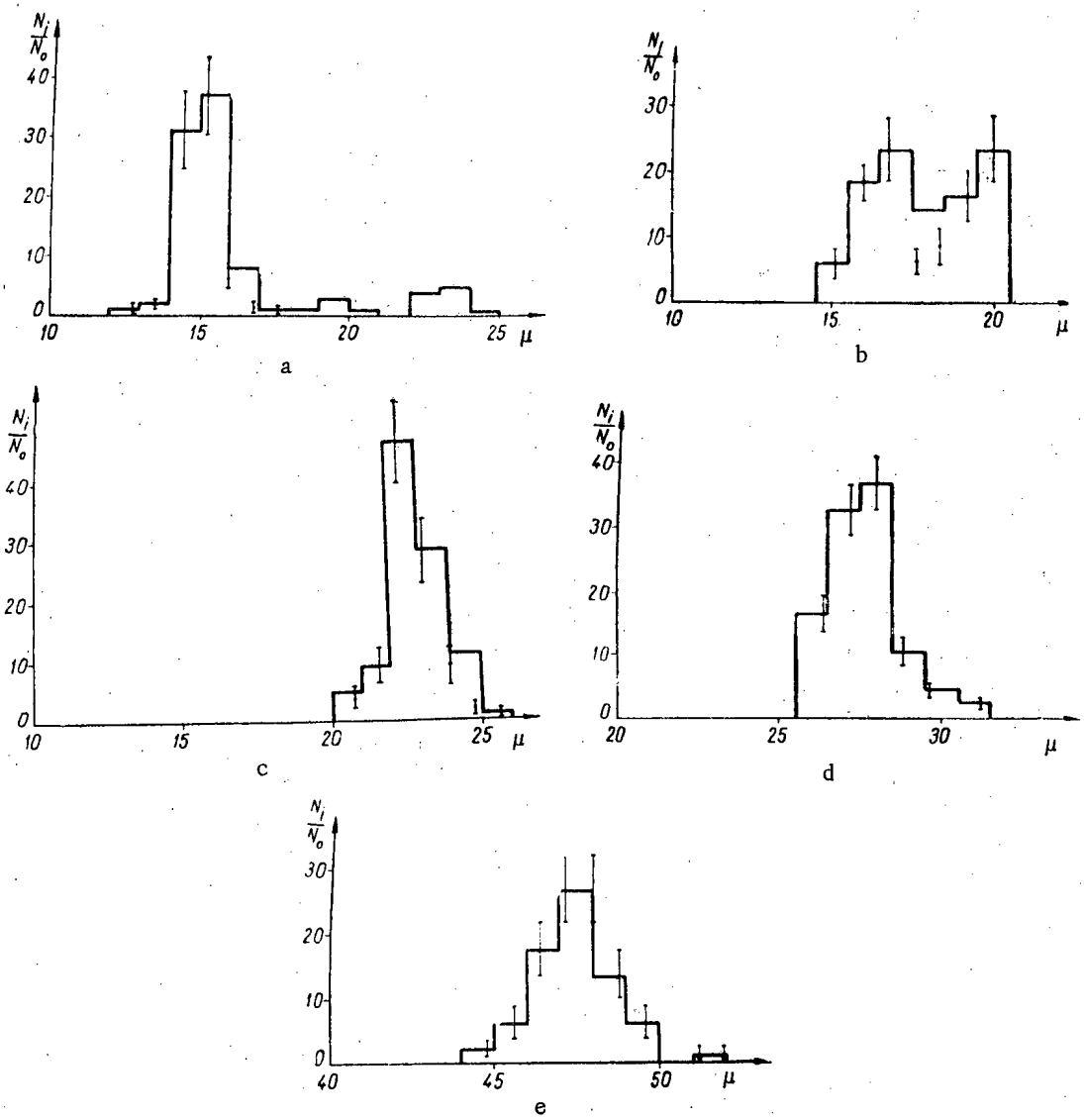

Fig. 1. Distribution of α-particle track lengths of the isotopes Th^{232} (a), U^{238} (b), Po^{210} (c), Bi^{212} (d), and Po^{212} (e).

In developing the procedure, much attention was paid to selection of the method for introducing radioactive isotopes into the emulsion. The best method was found to be one of impregnation and consisted of the following. The photo plate was first submerged for 30 minutes in distilled water and then in a solution of the radioactive substance being investigated. The solutions had to be weakly acidic or neutral. After impregnation, the plate was submerged for 2 minutes in an alcohol bath and dried under a ventilator. The exposure time was selected so as not to exceed 15-25 hours and so that during this period about 10^4 α-particle tracks would be formed in 1 cm^2 of the emulsion layer. As the exposure time was much greater than the impregnation time, we may consider that almost all the tracks were formed in the dry emulsion.

Before development, the plates were washed with running water for an hour. The plates were developed by the generally accepted method.

The tracks were scanned with a MBI-2 microscope with a magnification of 90 × 15 × 1.5 and measured with an ocular scale. In order to plot a calibration scale, we determined the average values for the paths in the emulsion of the α-particles emitted by the isotopes U^{238}, U^{234}, Th^{232}, Po^{210}, Bi^{212} and Po^{212}. In order to avoid the effect of the contraction coefficient, only those tracks were measured which were in the objective's focus along the whole length in the microscope's field of vision.

TABLE

Average α-Particle Path in the Emulsion

Isotope	Magnitude of the average path, μ	
	our data	data of [11]*
Th^{232}	14.9±1.5	14.7
U^{238}	16.4±2.6	15.5
Po^{210}	22.7±2.27	21.8
Bi^{212}	27.7±3.9	26.5
Po^{212}	47.2±4.7	46.1

*Ilford emulsion C-2, 50μ, was used.

100-120 tracks were measured for each isotope. The distribution of the track lengths for each isotope is shown in Fig. 1: the track lengths are plotted along the abscissa and the relative number of tracks N_i/N_0 along the ordinate, where N_i is the number of tracks corresponding to a definite value of the path and N_0 is the total number of tracks counted.

The average path $\bar{R}$ of an α-particle in the emulsion was calculated by the formula

$$\bar{R}=\frac{\Sigma \mu_i n_i}{\Sigma n_i},$$

where μ_i is the track length in microns and n_i is the number of tracks of μ_i length. The values of average α-particle paths in the emulsion are given in the table.

Using the values obtained, we plotted curves for the relation of average α-particle path in the emulsion $\bar{R}\mu$ to the energy E (Fig. 2) and to the magnitude of the path in air R_{air} (Fig. 3). The data of other authors are given for comparison in Fig. 2.

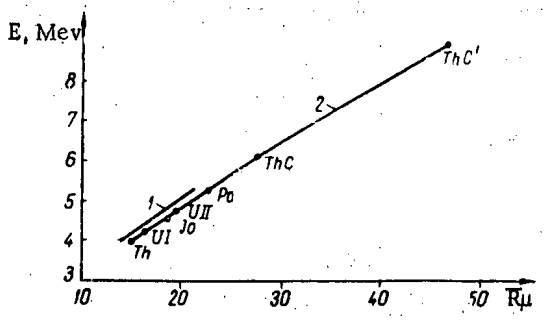

Fig. 2. Relation of the average α-particle path in the emulsion $\bar{R}\mu$ to energy E.
1) According to Farraggi's data [4]; 2) our experimental curve, which agrees with Rotblat's data [6].

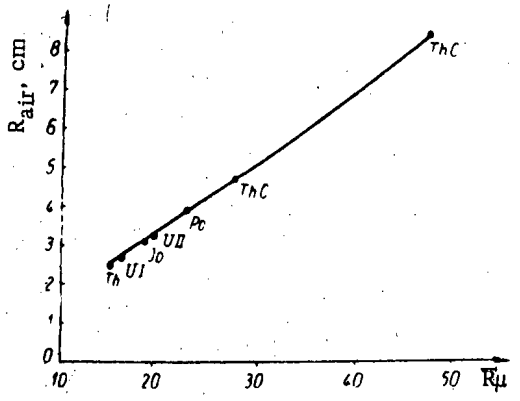

Fig. 3. Relation of the average α-particle path in the emulsion $\bar{R}\mu$ to the magnitude of the path in air R_{air}.

From these curves it appears that in the low energy range (4-6 Mev) there is a direct proportionality between path and energy [2, 4].

The values of the average α-particle paths make it possible to calculate the stopping power (SP) as the ratio of the α-particle path in air to the path in the emulsion. The value of the stopping power, determined for the given isotopes, varied from 1634 ± 11 to 1781 ± 6 for photo plates of the A-2 type.

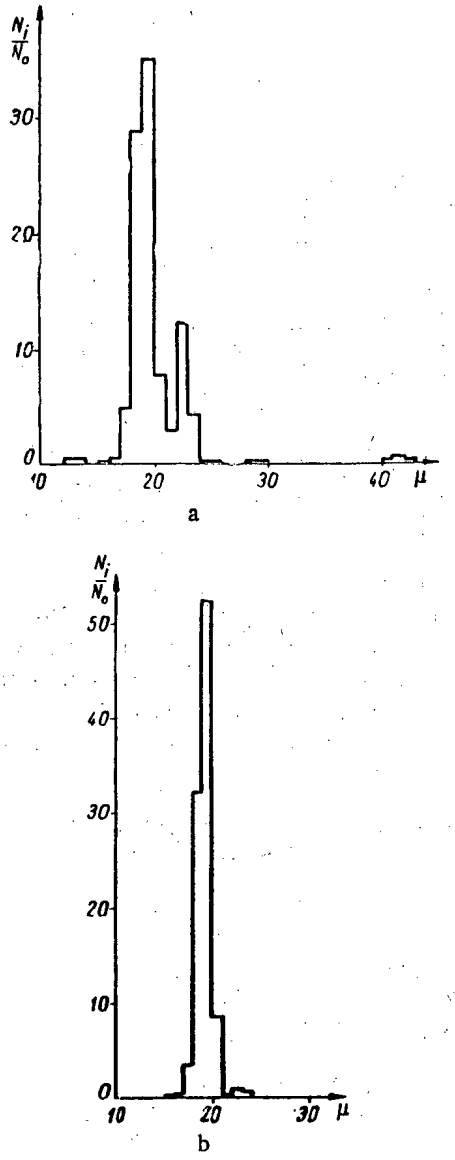

Fig. 4. Distribution of track lengths of the isotope Th^{230} (Io).
a) Before electrolysis; b) after electrolysis.

The calibration curve obtained was used for identifying the isotope Th^{230} (Io). Th^{230} was isolated from the natural raw material, which contained practically no thorium. The radiochemical purification procedure was quite similar to that used earlier [7-10] and included the following main operations:

1) the starting solution was freed from silicic acid and after the addition of a barium salt, radium – barium sulfates were precipitated;

2) the adsorbed thorium isotopes were thoroughly washed out of the sulfate precipitate with 5% HCl;

3) the thorium isotopes were precipitated with ferric hydroxide in a carbonate solution; the operation was repeated until the uranium isotopes were completely separated;

4) the thorium isotopes were twice precipitated with cerium oxalate from a 0.3 N HCl solution.

A Th^{230} (Io) preparation, made a year earlier, was used for the radiographic investigation. No Th^{227} (RdAc), should be present in the preparation and the amount of Th^{232} and Th^{228} (RdTh) should be negligible as the Th^{232} content of the starting material was small. The weakly acidic solution prepared for the investigation had a specific activity of 1000 dis/min • ml.

The measurement results are given in Fig. 4, a, which show that the ionium was not radiochemically pure. Doubtlessly, there was protactinium among the impurities and, apparently, decay products of the thorium series, which emitted α-particles with long tracks. The total amount of impurities was ~ 24%. Therefore, only those tracks whose length was in the range 17.6-20.0 μ were considered for calculating the average path. With this method of calculation, the effect of impurities was avoided. The value found for the average α-particle path in the emulsion was 18.8 (7) ± 0.03 μ.

Electrolysis was used for additional purification of the Th^{230} isotope solution. The same number of tracks (400) was measured on radiographs obtained for the isotopes subjected to electrolysis. Under these conditions, the distribution of the track lengths changed (Fig. 4, b). As a result of electrolysis, the amount of foreign materials decreased considerably and was about 5%. At the same time the magnitude of the average path, equal to $\overline{R}$ = 18.9 (4) ± 0.03 μ, did not differ practically from the magnitude found earlier and agreed well with the literature data.

The average α-particle path in air, R_{air} and α-particle energy E may be readily determined from the curves shown in Figs. 2 and 3. For the isotope Th^{230} (Io) R_{air} = 3.18 cm, E = 4.66 Mev.

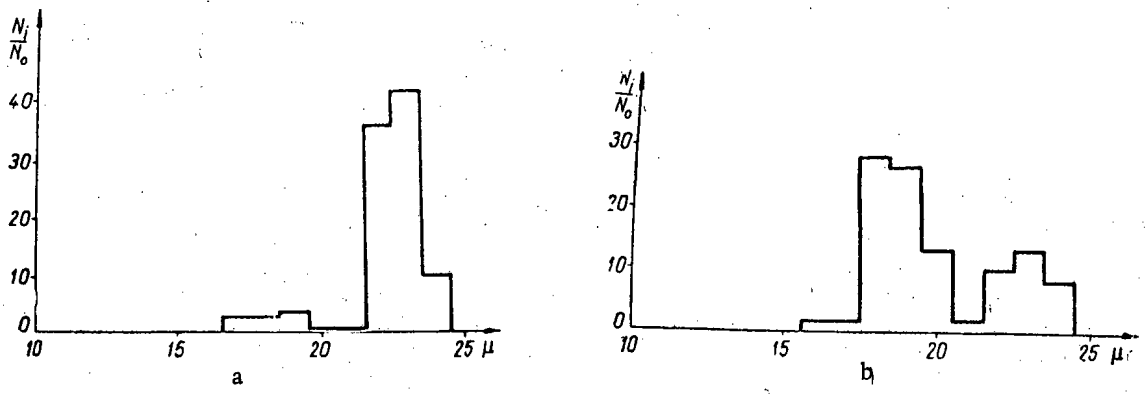

Fig. 5. Determination of the resolution capacity of the method. a) The polonium activity was 10 times greater than that of ionium; b) the polonium activity was 10 times less than that of ionium.

In order to find the resolution capacity of the emulsion, we investigated mixtures of two α-emitting isotopes, polonium and ionium, in quantitative ratios of 10 : 1 and 1 : 10. The measurement data are given in Fig. 5, which clearly shows the characteristic peaks for polonium and for ionium. This makes it possible to determine separately the amount of each isotope in the mixture. The difference in energy of this pair of isotopes was 0.7 Mev. Apparently, isotopes with an energy difference down to 0.3 Mev may be differentiated by the method described.

The authors express their deep gratitude to V. M. Uvarova and A. V. Podgurskaia for help in this work.

LITERATURE CITED

[1] V. I. Baranov and S. I. Krechmer, Doklady Akad. Nauk SSSR 1, 7-8, 543 (1935).

[2] I. Curie, J. Phys. Radium, cep. VIII, 7, 11, 313 (1946).

[3] R. D. Evans, Phys. Rev. 45, 1, 29 (1934).

[4] H. Farraggi, Collection, Photographic Registration of Ionizing Radiations * (Foreign Lit. Press, 1953), p. 280.

[5] A. P. Ratner, Radioactive Indicators and Their Use,** (United Sci. Tech. Press, 1936).

[6] J. Rotblat, Nature 167, 550 (1951).

[7] B. B. Boltwood, Am. J. Sci. 25, 365 (1908).

[8] I. E. Starik, A. S. Starik, G. S. Lozhkina, and L. V. Talitskaya, Bulletin on the Determination of the Absolute Growth of Geological Formations (Acad. Sci. USSR Press, 1955), p. 47.

[9] I. E. Starik, Use of Atoms in Analytical Chemistry ** (Acad. Sci. USSR Press, 1956), p. 192.

[10] A. N. Pylkov, J. Russ. Phys. Chem. Soc. 60, 835 (1928).

[11] L. Vigneron and G. Philbert, Compt. rend. 237, 1675 (1953).

Received January 4, 1957.

* Russian Translation.

** In Russian.

ELECTRIC ABSORPTION OF A GAS BY A METAL WITH A VAPORIZING SURFACE

S. A. Kuchai and A. M. Rodin

Statement of the Problem

It is well known that when certain metals are bombarded with gas ions with energies of the order of tens of electron volts and higher, a gradual accumulation of these gases in the metal is observed – the so-called "electric absorption" [1]. This phenomenon is used in particular for the separation of the isotopes of inert gases [2-4]. If the gas does not react chemically with the metal there is reason to suppose [5] that the concentration of the gas is determined by isotropic diffusion from the place of its deposition, which is at a depth given by the range of the ions.

From what has been said it would appear to follow that after long bombardment one should find the absorbed gas in all layers of the metal plate in comparable concentrations, and that the total amount of the gas so accumulated would be determined only by the thickness of the plate. On the other hand, it has been observed [2, 3, 5] that the total amount of gas accumulated per unit area of the bombarded surface cannot exceed a certain limit, even in thick plates. Moreover, almost all of the gas is found at depths of the order of the range of the ions [5]. For energies of tens of thousands of kilovolts this range does not exceed a fraction of a micron [6].

These contradictions are removed if one assumes that the electric absorption is necessarily accompanied by cathode sputtering of the metal from the surface. In the calculations it is assumed for simplicity that: a) the depth of penetration into the metal is the same for all the ions; b) the thickness of the plate is large; c) the diffusion coefficient is independent of the coordinates and the concentration.

Solution of the Diffusion Equation

The concentration of the gas in the plate vaporized at its surface is given in the simplest case by the one-dimensional diffusion equation

$$\frac{\partial c}{\partial t} = D \frac{\partial^2 c}{\partial x^2}$$

for $x - vt \geq 0$, with the boundary and initial conditions

$$c|_{x=vt} = 0,$$
$$c|_{t=0} = 0$$

and the condition

$$-D\left[\left(\frac{\partial c}{\partial x}\right)_{x=vt+l+0} - \left(\frac{\partial c}{\partial x}\right)_{x=vt+l-0}\right] = Q_0,$$

Here c is the concentration of the gas in units $1/cm^3$; D is the diffusion coefficient in cm^2/sec; v is the speed of displacement of the boundary of the plate because of the cathode sputtering, in cm/sec; Q_0 is the intensity of bombardment in units $1/cm^2 \cdot sec$; and l is the range of the ions in centimeters.

We introduce a system of coordinates with its origin moving with the boundary of the plate:

$$\xi = x - vt.$$

When transformed to this system, the diffusion equation has the form [7]

$$\frac{\partial c}{\partial t} - v\frac{\partial c}{\partial \xi} = D\frac{\partial^2 c}{\partial \xi^2} \tag{1}$$

with the conditions

$$c|_{\xi=0} = 0,$$
$$c|_{t=0} = 0,$$
$$-D\left[\left(\frac{\partial c}{\partial \xi}\right)_{\xi=l+0} - \left(\frac{\partial c}{\partial \xi}\right)_{\xi=l-0}\right] = Q_0.$$

By using the Laplace-Carson transformation

$$C(\xi, p) = p\int_0^\infty c(\xi, t)\, e^{-pt}\, dt$$

one gets from Equation (1) an ordinary differential equation for $C(\xi, p)$; its solution is*

$$C(\xi, p) = \begin{cases} c_0 \dfrac{e^{x(l-\xi)}}{qxl}(\operatorname{ch} qxl - \operatorname{sh} qxl)\operatorname{sh} qx\xi, & \xi \leqslant l, \\ c_0 \dfrac{e^{x(l-\xi)}}{qxl}\operatorname{sh} qxl\,(\operatorname{ch} qx\xi - \operatorname{sh} qx\xi), & \xi \geqslant l, \end{cases}$$

where

$$c_0 = \frac{Q_0 l}{D};\quad q = \sqrt{1 + \frac{p}{Dx^2}};\quad x = \frac{v}{2D}.$$

The transform C corresponds to the primitive [8]:

$$c(\zeta, t) = \begin{cases} c_0 \dfrac{e^{\nu(1-\zeta)}}{\sqrt{\pi}}\displaystyle\int_0^{\sqrt{\tau}} d\sigma e^{-\nu^2\sigma^2} \times \\ \times\left[e^{-\frac{(1-\zeta)}{4\sigma^2}} - e^{-\frac{(1+\zeta)^2}{4\sigma^2}}\right], \zeta \leqslant 1, \\ c_0 \dfrac{e^{\nu(1-\zeta)}}{\sqrt{\pi}}\displaystyle\int_0^{\sqrt{\tau}} d\sigma e^{-\nu^2\sigma^2} \times \\ \times\left[e^{-\frac{(\zeta-1)^2}{4\sigma^2}} - e^{-\frac{(\zeta+1)^2}{4\sigma^2}}\right], \zeta \geqslant 1, \end{cases} \tag{2}$$

* 'ch' ≡ 'cosh', 'sh' ≡ 'sinh' — Publisher.

where

$$\zeta=\frac{\xi}{l}\ ;\quad \tau=\frac{t}{t_0}\ ;\quad t_0=\frac{l^2}{D}\ ;\quad \nu=xl=\frac{vl}{2D}\ .$$

Equation (2) shows that the effect of the displacement of the boundary depends on the number ν, which can be regarded as a ratio of times $\frac{t_0}{t_1}$, where t_0 is the characteristic time for diffusion over a length l and t_1 is twice the time of travel through the distance l at the velocity v of the motion of the boundary.

Special Cases

The Stationary Distribution. If one waits a sufficiently long time, the following distribution of concentration must be set up in the plate (in the system of coordinates moving along with the surface of the plate):

$$c_\infty=c_0e^{\nu(1-\zeta)}\frac{1}{\sqrt{\pi}}\int_0^\infty d\sigma e^{-\nu^2\sigma^2}\left[e^{-\frac{(1-\zeta)^2}{4\sigma^2}}-e^{-\frac{(1+\zeta)^2}{4\sigma^2}}\right],$$

or after carrying out the calculations

$$c_\infty(\zeta)=\begin{cases} c_0\dfrac{e^{-\nu\zeta}}{\nu}\operatorname{sh}\nu\zeta, & \zeta\leqslant 1,\\ c_0\dfrac{e^{-\nu(\zeta-1)}}{\nu}e^{-\nu\zeta}\operatorname{sh}\nu, & \zeta\geqslant 1.\end{cases} \tag{3}$$

In the case of a motionless boundary we get from Equation (3) after taking the limit $\nu\to 0$

$$c_\infty(\zeta)=\begin{cases} c_0\zeta; & \zeta\leqslant 1,\\ c_0; & \zeta\geqslant 1.\end{cases}$$

Figure 1 shows the stationary distributions for the cases $\nu = 0$ and $\nu = 1$.

The Transition Process in the Plane of the Source. According to Equation (2) the increase of the concentration of the gas at $\zeta = 1$ is given by the law

$$c_S(\tau)=\frac{c_0}{\sqrt{\pi}}\int_0^{\sqrt{\tau}} d\sigma e^{-\nu^2\sigma^2}\left(1-e^{-\frac{1}{\sigma^2}}\right).$$

Figure 2 shows curves of $\frac{c_S}{c_0}$ for the cases $\nu = 0$ and $\nu = 1$. The integrals were evaluated graphically with a planimeter. In addition, for $\nu = 0$ the integral can be expressed in terms of tabulated functions:

$$\frac{1}{\sqrt{\pi}}\int_0^{\sqrt{\tau}} d\sigma\left(1-e^{-\frac{1}{\sigma^2}}\right)=$$

$$=\frac{2}{\sqrt{\pi}}\int_{1/\sqrt{\tau}}^\infty e^{-\alpha^2}d\alpha+\frac{\sqrt{\tau}}{\sqrt{\pi}}\left(1-e^{-\frac{1}{\tau}}\right).$$

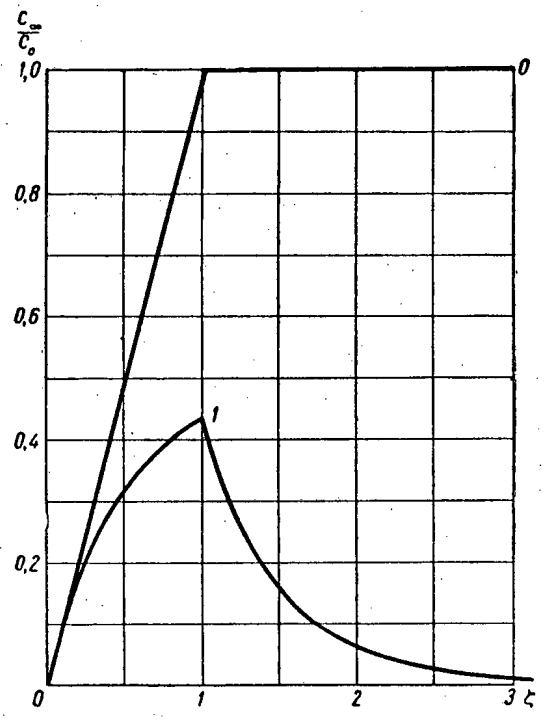

Fig. 1. Stationary distribution of the gas in the metal. ζ=depth in units l; ordinates are concentrations in units $c_0 = \frac{Q_0 l}{D}$; 0 is the absorption without vaporization of the metal; 1 is the absorption with vaporization of metal.

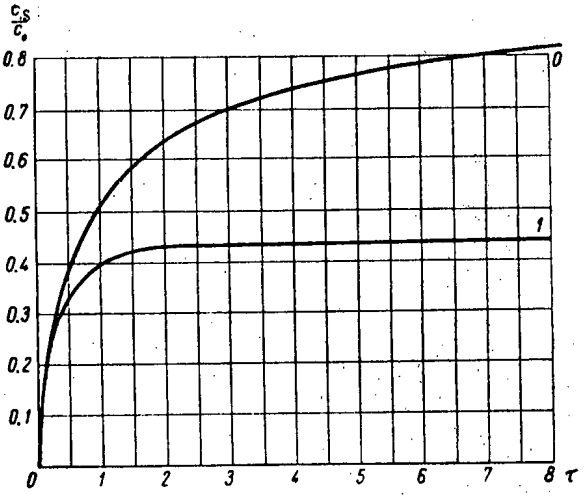

Fig. 2. Increase of the concentration of the gas at a depth equal to the range of the ions, ζ = 1. τ = time in units $t_0 = \frac{l^2}{D}$; ordinates are concentrations in units c_0; 0 is absorption without vaporization of the metal; 1 is absorption with vaporization of metal.

Comparison of the results provides an estimate of the error of the planimeter, which did not exceed 1% in these calculations.

Accumulation of the Gas. The total quantity of the gas per square centimeter of the bombarded surface amounts at the time t to

$$P(t) = \int_0^\infty c(\xi, t)\, d\xi.$$

By the indicated substitutions we get

$$P(\tau) = Q_0 t_0 \frac{2}{\sqrt{\pi}} e^{\nu} \int_0^{\sqrt{\tau}} \sigma\, d\sigma \times$$

$$\times \left(e^{-\nu} \int_{\nu\sigma - \frac{1}{2\sigma}}^{\infty} e^{-\alpha^2} d\alpha - e^{\nu} \int_{\nu\sigma + \frac{1}{2\sigma}}^{\infty} e^{-\alpha^2} d\alpha \right),$$

or, after integrating by parts

$$P(\tau) = Q_0 t_0 \frac{e^{\nu}}{\sqrt{\pi}} \times$$

$$\times \left[\tau f(\tau) + \int_0^{\sqrt{\tau}} e^{-\left(\nu^2\sigma^2 + \frac{1}{4\sigma^2}\right)} d\sigma \right], \qquad (4)$$

where

$$f(\tau) = e^{-\nu} \int_{\nu\sqrt{\tau} - \frac{1}{2\sqrt{\tau}}}^{\infty} e^{-\alpha^2} d\alpha - e^{\nu} \int_{\nu\sqrt{\tau} + \frac{1}{2\sqrt{\tau}}}^{\infty} e^{-\alpha^2} d\alpha.$$

In the case of a motionless boundary ($\nu = 0$)

$$P(\tau) = Q_0 t_0 \frac{1}{\sqrt{\pi}} \times$$

$$\times \left(2\tau \int_0^{1/2\sqrt{\tau}} e^{-\alpha^2} d\alpha + \sqrt{\tau} e^{-\frac{1}{4}} - \int_{1/2\sqrt{\tau}}^{\infty} e^{-\alpha^2} d\alpha \right).$$

As τ increases the first two terms in the parentheses increase without bound, proportional to $\sqrt{\tau}$. If, however, the rate of vaporization (cathode sputtering) is finite, we find from Equation (4) that

$$P(\tau) \to Q_0 t_0 \frac{1}{\sqrt{\pi}} \times$$

$$\times \left(\frac{1}{2} \sqrt{\tau} \frac{e^{-\left(\nu\sqrt{\tau} - \frac{1}{2\sqrt{\tau}}\right)^2}}{\nu^2\tau - \frac{1}{4\tau}} + e^{\nu} \int_0^{\sqrt{\tau}} e^{-\left(\nu^2\sigma^2 + \frac{1}{4\sigma^2}\right)} d\sigma \right);$$

$$\lim_{\tau\to\infty} P(\tau) = \frac{Q_0 t_0}{2\nu} = \frac{Q_0 l}{v}.$$

This same result is obtained by calculation of the integral

$$J = \int_0^{\infty} c_{\infty}(\zeta)\, d\zeta,$$

where c_{∞} is the stationary distribution described by Equation (3).

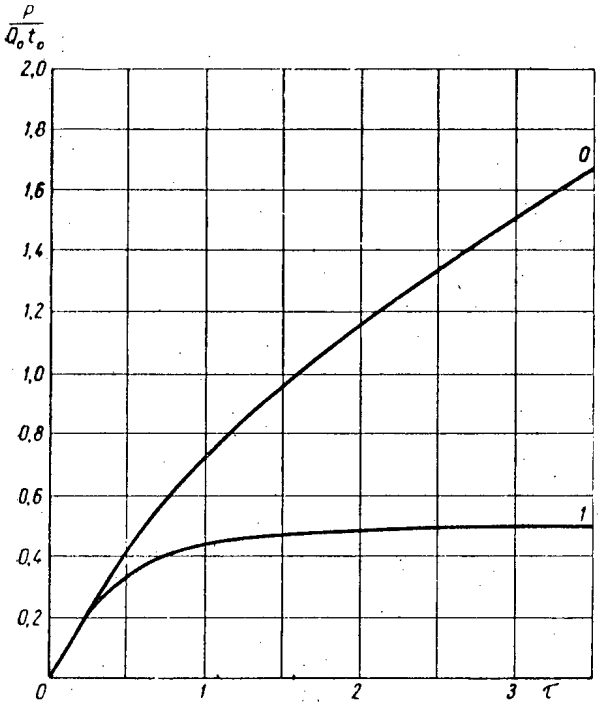

Fig. 3. Accumulation of gas per square centimeter of bombarded surface. Ordinates are amounts of gas in units $Q_0 t_0$; 0 is absorption without vaporization of the metal; 1 is absorption with vaporization of metal.

Thus, when there is cathode sputtering the amount of gas accumulated in a very thick plate has a limit which is independent of the rate of diffusion.

Figure 3 shows curves of $P(\tau)$ for the values $\nu = 0$ and $\nu = 1$.

LITERATURE CITED

[1] S. Dushman, Scientific Foundations of Vacuum Technique [Russian Translation] (IL, 1950) Chapter 10.

[2] J. Koch, Nature 161, 566 (1948).

[3] S. Thulin, Arkiv. Fyz. 9, 107 (1954).

[4] J. Koch et al., Phys. Rev. 76, 279 (1949).

[5] A. D. Le Clair, and A. H. Row, Rev. Metall. 52, 94 (1955).

[6] S. D. Warshaw, Phys. Rev. 76, 1759 (1940).

[7] M. Jacob, Heat Transfer, (Wiley, 1949). Vol. 1.

[8] V. Ditkin and P. Kuznetsov, Handbook of Operator Calculus [In Russian], (Gostekhizdat, 1951).

Received August 30, 1957.

BACK-SCATTERING OF γ-RADIATION IN ALUMINUM

V.A. Vasil'ev and V.A. Shishkina

The results of an investigation of back-scattering of γ-radiation in various materials under conditions of good geometry have been given in References [1, 2]. Thus, in Reference [1], a source in contact with the scatterer was placed at a distance of 2 cm from the crystal in the detection system while in Reference [2] the distance between the counter and the γ-radiation source, which was also in contact with the scatterer, was 25 cm. In Reference [2] results were also given for experiments in which the scatterer was moved out to a distance of 70 cm from the source. However, in a number of situations it is necessary to have a quantitative picture of the back-scattering of γ-photons in the case of a wide beam when the distance from the source to the scattering material varies over several meters.

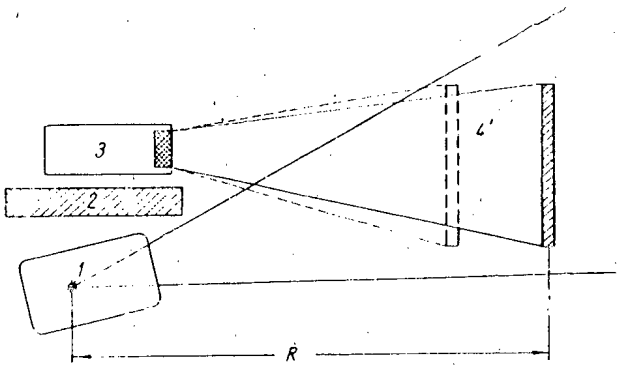

Fig. 1. Experimental geometry. 1) source of γ-radiation, 2) lead shield, 3) scintillation counter, 4 and 4') different positions of the scatterer.

In Fig. 1 is shown a diagram of the experimental geometry used in obtaining the results reported in the present paper. The sources of γ-radiation were the radioactive isotopes Cs^{137} (activity 4.7 curies, E_γ = 661 kev) and Co^{16} (activity 2.57 curies, E_γ = 1.17 and 1.32 Mev). The scatterers were sheets of the same thickness, 1.5 m^2 in area. The gamma-radiation was detected with a scintillation counter using a NaI(Tl) crystal (diameter 29 mm, thickness 17 mm) mounted on a FEU-19 photomultiplier.

The direct flux of γ-radiation was uniform over the entire area of the scatterer. The flux of back-scattered γ-photons was taken as the difference between two measurements: one with the scatterer present and the other without the scatterer.

In Fig. 2 is shown the flux of back-scattered γ-photons I_p as a function of R, the distance between the γ-radiation source and the scatterer, which was varied from 2 to 10 meters. The thickness of the scatterer was held constant and was 11 mm. From the results the following ratio was found:

$$\frac{I_p(Cs^{137})}{(Co^{60})} = \frac{N(Cs^{137})}{N(Co^{60})} \frac{A(Co^{60})\, n(Co^{60})}{A(Cs^{137})\, n(Cs^{137})},$$

where N is the result of the measurement, A is the activity of the source in curies, n is the number of γ-photons in decay. This ratio shows by how many times the flux of back-scattered γ-radiation from Cs^{137} is larger than that from Co^{60} if it is assumed that the number of γ-photons is the same for the both sources. At two distances, 3 and 5 meters between the γ-radiation source and the scatterer, this ratio is 8.3. No correction was made for detection efficiency because the energy of the back-scattered γ-photons is essentially the same for Cs^{137} and Co^{60} (184, 210 and 214 kev, respectively).

In Fig. 3 is shown the dependence of the back-scattered flux I_p on scatterer thickness x. The distance between the source and the scatterer was held at 3.5 meters. The thickness of the aluminum sheets was varied

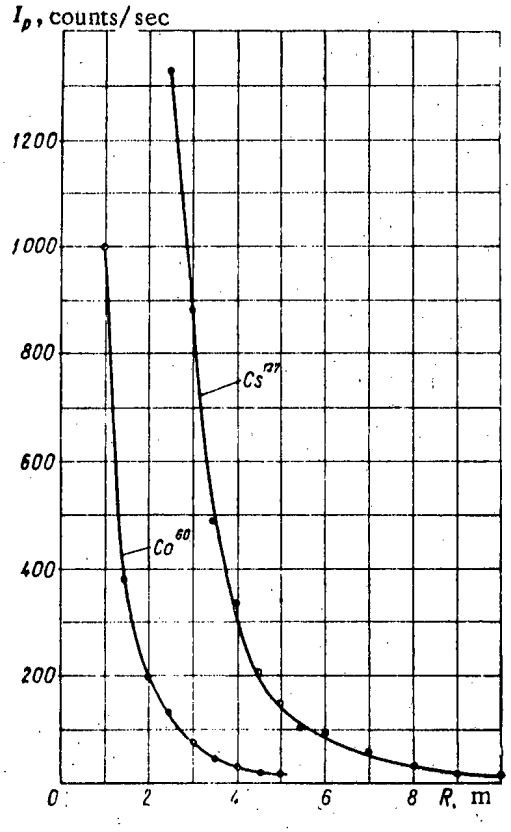

Fig. 2. The flux of backscattered γ-radiation I_p as a function of R the distance between the source and scatterer.

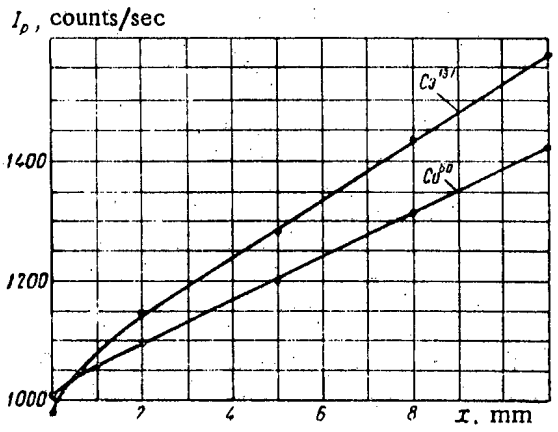

Fig. 3. The flux of backscattered γ-radiation I_p as a function of the scatterer thickness x.

from 2 to 11 mm. As is apparent from the graph this relation is essentially linear in the limits indicated above.

LITERATURE CITED

[1] U. A. Ulmanis and N. A. Dubinskaia, J. Atomic Energy (USSR) 3, 59 (1957).*

[2] G. J. Hine and R. C. McCall, Nucleonics 12, No. 4, 27 (1954).

Received September 9, 1957.

* Original Russian pagination. See C. B. Translation.

INVESTIGATION OF IRON ORE DENSITY USING γ-RAY ABSORPTION

M. L. Gol'din

Measurements of ore density by penetrating radiation have the marked advantage, as compared with other methods, that no contact with the ore is required.

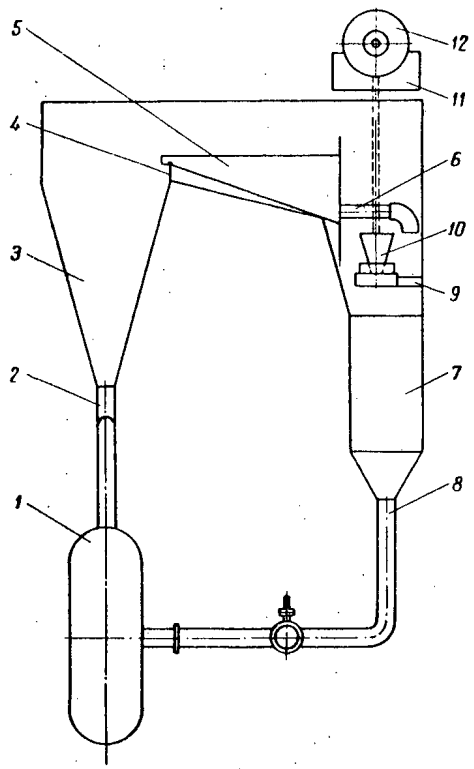

Fig. 1. Diagram of the apparatus for measuring pulp density.

In Fig. 1 is shown a schematic diagram of an experimental arrangement similar to an industrial spiral separation system used for enriching iron ores. The pump 1 forces the pulp of the ore being enriched into pipe line 2 from which it is directed into the hopper 3. An ore mixture from the mine has the following average chemical makeup: SiO_2 – 29.64%; Al_2O_3 – 1%; Fe_2O_3 – 64.35%; CaO – 0.63%; MgO – 2.88%; the remainder of the impurities total 1.5%. The pulp which passes through the port 4 enters the overflow chamber 5 and then passes into the pulp line 6 with the same diameter as 2; it then enters the hopper denoted by 7, whence it moves to the intake line 8. Because of the overflow chamber 5 the cross section of the pulp line 6 is always completely filled since the pulp in the chamber is at the level of the top of 4. A collimator 10, is rigidly fastened to the bracket 9; this collimator forms a narrow beam of γ-rays parallel to the pulp line. The γ-rays pass through the pulp line and the collimating aperture 11 in the lead cover 12 which is 21.5 mm in diameter and 50 mm long; finally the beam enters the counting tube (MS-4). The distance from the axis of the counting tube to the radioactive source (19.5 mcuries of Cs^{134}) is 370 mm. The radiation is recorded with a B-2 radiometer.

At the beginning of the experiment water was poured into the system, the sand pump was started, and the measurement level was checked for constancy. In all measurements the water counting rates were within 2% of each other. After this check, the hopper 3 was filled with ore of the 1 mm grade with the chemical composition given above; then a determination of the density of the pulp was made by weighing samples in a container of known volume. For each pulp density 8-10 selection tests were made by weighing and 5-6 measurements by counting rate. The absolute value of the deviation in each measurement was less than 1.5%.

The counter background, when covered by the lead collimator, was 45 pulses/min; the initial counting rate, using corrections for dead-time and background, was 16,015 pulses/min. The maximum pulp density was 2.3 kg/liter. Higher densities could not be used without choking the pulp line 2.

In computing the mean counting rate corrections were introduced for the background and for the counter dead-time. Then a determination was made of the mean-square error and the probable error for the individual measurements [1]. In Table 1 are shown the results of four series of experiments. In Table2 are shown the counting rates determined from a curve showing the intensity of the γ-radiation which penetrates the pulp I_p as a function of pulp density ρ_p, plotted with the data shown in Table 1. The γ-ray absorption in the pulp is given by the following empirical formula:

$$I_p = 10483e^{-0,2609\rho_p} \quad (1)$$

The linear absorption coefficient for the ore μ_T was determined by three methods, using the B-2 system to record the counting rate.

TABLE 1

ρ_p, kg/liter	1.010	1.189	1.461	1.699	1.885	2.080	2.137
I_p, counts/min	8044±24	7683±27	7219±28	6758±21	6545±4	6105±21	5970±26
ρ_p, kg/liter	1.025	1.223	1.580	2.059	2.173	2.299	—
I_p, counts/min	7915±9	7552±11	6943±10	6152±13	5911±13	5622±13	—
ρ_p, kg/liter	1.015	1.353	1.691	2.035	2.197	2.308	—
I_p, counts/min	7955±18	7250±23	6840±18	6286±8	5922±7	5679±7	—
ρ_p, kg/liter	1.035	1.460	1.700	2.026	2.314	—	—
I_p, counts/min	7902±14	7271±3	6753±4	6218±8	5640±2	—	—

In the first method the intensity of the radiation from the Cs^{134} was measured after absorption I_T in a plane parallel slab of ore as a function of thickness l. The functional relation $I_T = f(e)$ is of the form

$$I_T = I_0 e^{-\mu_T l}, \quad (2)$$

where I_0 is the intensity of the radiation when the absorber is not present. A diagram of the experiment is shown in Fig. 2. Using collimator 2, 7 mm in diameter, a narrow parallel beam of γ-rays from Cs^{134} was defined and detected by the counter 5 (MS-4). To eliminate effects due to scattered radiation the diameter of the aperture in the lead cover 4, which was 100 mm long, was made the same as that of the collimator. The plane parallel sample of the ore 3 was placed on a special support and irradiated. In making these tests ores were used which were taken from different places in an operating mine. The chemical composition of the ores was close to the composition given above. Using the experimentally determined relation $I_T = f(e)$ the linear absorption coefficient for the ore was determined and found to be 0.234 cm.

In the second method the linear absorption coefficient of the ore was determined using the apparatus itself (see Fig. 1) by employing the bulk coefficient for the ore $\rho_T = 3.4$ g/cm^3. A cylindrical aluminum container was fastened to collimator 10; the position of this cover was fixed. Ores of the 1 mm grade were irradiated and the intensity of the γ-ray flux was determined as a function of the amount of ore deposited in the cylinder.

TABLE 2

ρ_p, kg/liter	1.0	1.2	1.4	1.6	1.8	2.0	2.3
I_p, counts/min	8035	7635	7245	6890	6548	6222	5755

The dependence $I_T = f(G)$ is given by the equation

$$I_T = I_0 e^{-\frac{\mu_T}{\rho_T} \cdot \frac{G}{F}}, \quad (3)$$

where G is the weight of the sample in grams and F is the area of the bottom of the cylinder in square centimeters.

TABLE 3

ρ_p, kg/liter	1.0	1.2	1.4	1.6	1.8	2.0	2.3
μ_p, cm^{-1}	0.1025	0.114	0.125	0.135	0.145	0.155	0.171
μ_T, cm	—	0.250	0.240	0.234	0.232	0.229	0.230

The linear absorption coefficient was determined from this relation. In this series of experiments the coefficient was found to be $\mu_T = 0.231$ cm, using the same ore analyzed above.

The third method was a theoretical method, based on the experimental relation for $I_p = f(\rho_p)$. Using the formula

$$I_p = K I_0 e^{-\mu p d} \quad (4)$$

(where K is a fixed factor which determines the attenuation of the γ-rays between the source and the detector when a pulp line of inner diameter d is filled with air) the linear absorption coefficient of the pulp μ_p was computed as a function of density.

The factor K was determined from experiments on measurement of the pulp density using the ratio $K = \frac{I}{I_0}$, where I is the intensity of the radiation after absorption by walls in the pulp line. Introducing corrections for the counter dead-time and background, K = 0.847. Using the formula for linear absorption coefficient [2], we obtain

$$\mu_T = \frac{\mu_p(\rho_T - \rho_w) - \mu_w(\rho_T - \rho_p)}{\rho_p - \rho_w}, \quad (5)$$

where ρ_w is the density of the liquid (water) in g/cm^3; μ_w is the linear absorption coefficient for a liquid in cm^{-1}. For each value of ρ_p and μ_p obtained from the data in Table 2, a calculation was made of the corresponding value of μ_T (Table 3).

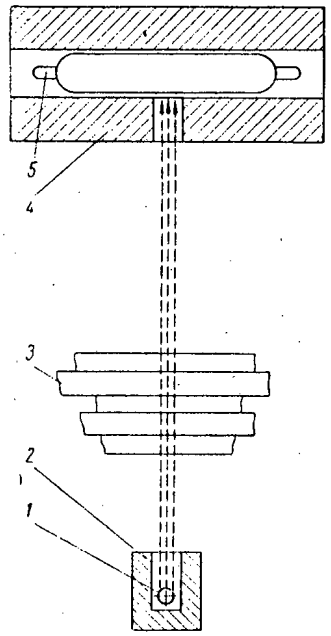

Fig. 2. Diagram of the experiment used to determine the linear absorption coefficient of ore.

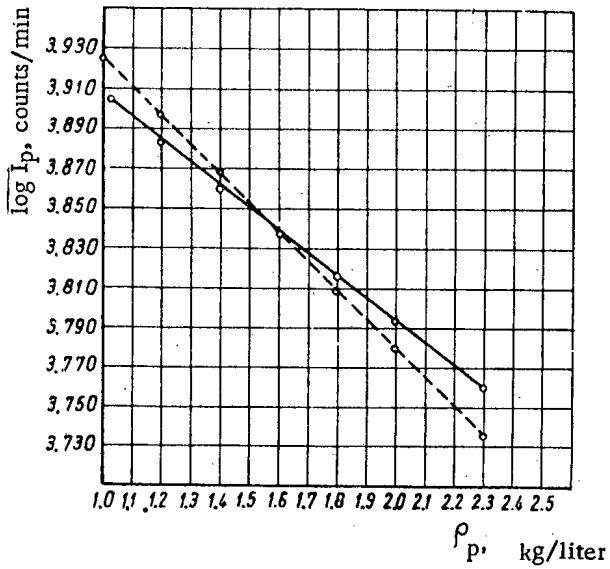

Fig. 3. Experimental and theoretical intensity of a narrow beam of γ-radiation from Cs^{134} as a function of density of iron ore pulp ρ_p. ——) Experimental curve; – – – – –) calculated curve.

The arithmetic average of these values is 0.236 cm^{-1}; this value differs by less than 1% from the ore absorption coefficients determined by the first method. The theoretical value of this coefficient is μ_T = = 0.244 cm^{-1} and differs from the experimental value by 3.2 + 5.2 %

In Fig. 3 is shown the dependence of the experimental and calculated radiation intensity of a narrow beam of γ-rays from Cs^{134} as a function of iron-ore pulp density. The maximum discrepancy in the results is less than 5 %.

In conclusion the author wishes to express his gratitude to Professor A. K. Val'ter, Academician of the Academy of Sciences, Ukranian SSR, and Candidate in Physical Mathematical Sciences, N. G. Afanas'ev for their continued interest and valuable advice in carrying out this work.

LITERATURE CITED

[1] K. P. Iakovlev, Mathematical Analysis of the Results of Measurements* (State Tech. Press, 1953), p. 339.

* In Russian.

[2] A. K. Valter and M. L. Gol'din, Calculation and Investigation of the Density of Iron Ore Pulp by γ-Ray Absorption. Report to the All-Union Technical Scientific Conference on the Application of Radioactive Isotopes and Radiation in Science and the National Economy, (Acad. of Sci. Press, USSR, Moscow, 1958) (In Press).

Received February 26, 1957.

GAMMA-GAMMA ROCK SAMPLING

P.K. Verbovenko and I.G. Fakidov

Gamma-gamma sampling is used mainly to determine the density of rocks on the basis of the intensity of the scattered radiation from a point source as a function of ρ, the density of the material which scatters the γ-radiation.

In the present note we consider the form of the function relation $J = J(\rho)$.

The dependence of the scattered γ-radiation on the density of the scattering material has been investigated by Grazhdankina and Fakidov, who reported their results in 1951 at the All-Union Conference on γ-Defectoscopy of Metals [1].

In [2] the following formula is given for $J = J(\rho)$ in the point-source case:

$$J = \frac{Q}{780\pi} \rho^2 \frac{e^{-\rho \frac{R}{14}}}{R}, \tag{1}$$

where Q is the source intensity, R is the distance from the source to the scattered γ-radiation detector (probe), and ρ is the density of the material which scatters the γ-radiation.

Equation (1) is obtained from a diffusion analysis of γ-photons in an absorbing medium; the diffusion analysis can be used, however, only in the case in which the location of the probes is such that the condition $R > L$ is satisfied, where L is the diffusion length, approximately equal to the γ-photon mean free path. Hence, probes shorter than 15-20 cm are not treated.

In [3] another expression was given for the relation between the intensity of the scattered γ-radiation and the density of the scattering rock:

$$J \sim \rho / l e^{-0.06 \rho l}. \tag{2}$$

In the present paper we consider the validity of these two formulas.

To shed some light on this problem, in the figure we show curves computed from Equations (1) and (2) and an experimental curve 4, taken from [1].

The curve marked 2 is computed from Equation (2) and the curve marked 1 is computed from Equation (1). As is to be expected, curve 2 is in satisfactory agreement with curve 1 only in the region of high densities.

It has been indicated above that the diffusion analysis applies only for probes $R > L$. However, since $L \approx \approx 14/\rho$, the condition $R > L$ depends on density and probes shorter than 15-20 cm, which were excluded from consideration in [2], are amenable to a diffusion analysis at high densities. In spite of the fact that curve 1 has been obtained for probes shorter than 15-20 cm, Equation (1) satisfactorily describes curve 4 at high density. As is apparent from the figure, the diffusion approximation does not apply at small densities and for small probes.

Equation (2) gives a somewhat better approximation to the experimental curve 4, but again, only in the region of comparatively high densities.

We propose that the formula

$$J = k\rho^{1/2}e^{-\lambda\rho}, \tag{3}$$

where k and λ are constant for a given probe and a fixed source strength, yields satisfactory agreement with curve 4, especially at low densities, i.e., in the case in which the diffusion condition is not satisfied.

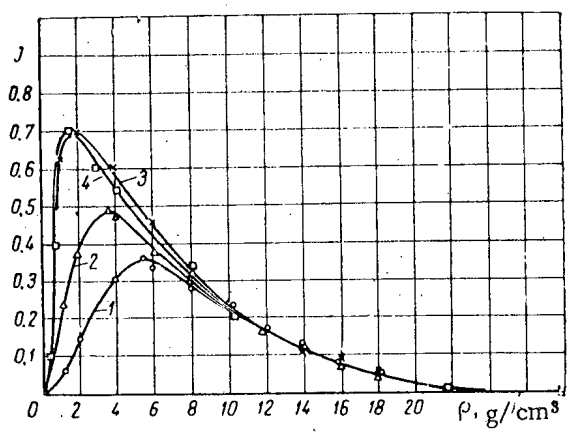

Dependence of γ-ray intensity on rock density.

Curve 3, which has been computed from Equation (3), verifies the above considerations completely. In our opinion Equation (3) is more convenient for work with short probes; short probes are desirable since they allow the use of weaker γ-radiation sources. On the other hand, in work with short probes at low densities there is an uncertainty in the relation between the measured intensity and the density because of the peak in curve 4. Two methods can be used to remove this uncertainty (as is apparent from the expression obtained in Equation (3), the uncertainty arises at $\rho_m = 1/2\lambda$, corresponding to a maximum in the intensity of the scattered radiation):

1) Increasing the probe length $R = C\lambda$, where C is fixed. This results in a reduction of ρ_m and allows operation on the part of curve 4 which slopes downward;

2) Reduction of the probe length $R = C\lambda$. This increases ρ_m and makes it possible to work on the rising part of curve 1.

The choice of which of these methods is used is determined by actual conditions (the source strength, the density of the rock being investigated, and the feasibility of making long probes, etc.).

SUMMARY

1. Equations (1) and (2) used for computing the intensity of scattered γ-radiation in gamma-gamma sampling can be used only when long probes are used; Equation (2) is less accurate as far as the diffusion limitation R > L is concerned.

2. Equation (3), proposed by the present authors for computing the intensity of scattered γ-radiation, is not restricted by the limitation R > L and gives satisfactory agreement with the experimental curve for both short and long probes.

LITERATURE CITED

[1] N.P. Grazhdankina and I.G. Fakidov, Collection: Gamma Defectoscopy of Metals [in Russian] (Acad. Sci. Press USSR, 1955), p. 61.

[2] I.G. Diad'kin, Izv. Akad. Nauk SSSR, Ser. Geofiz. 4, 323 (1955).

[3] Iu.P. Bulashevich and G.M. Voskoboinikov, Izv. Akad. Nauk SSSR, Ser. Geofiz. 1, 109 (1957).

Received August 10, 1957

SCIENTIFIC AND TECHNICAL NEWS

TEMPERATURE DEPENDENCE OF RESONANCE NEUTRON ABSORPTION IN URANIUM

Recent data have been acquired on resonance absorption of neutrons in cylinders of uranium and thorium [1, 2]. The measurements were carried out at the Hanford Experimental Reactor HER using the danger-coefficient method.

In [1] measurements were made of the neutron resonance absorption integral $\int \sigma_a \text{eff}\ dE/E$ as a function of the ratio of surface S to mass M of uranium cylinders. In this work the uranium cylinders, of various diameters, were enclosed in cadmium containers and inserted into the reactor. They were then replaced by empty cadmium containers. In both cases the reactivity of the reactor was measured from the position of the control rod which was calibrated in inverse hours. The change in reactivity was then an indication of the resonance absorption for the cylinders.

A standard lump from the HER reactor was used as a reference. The contribution of epicadmium neutrons from U^{235} fission was taken into account by using the results obtained in experiments with uranium of different isotopic composition.

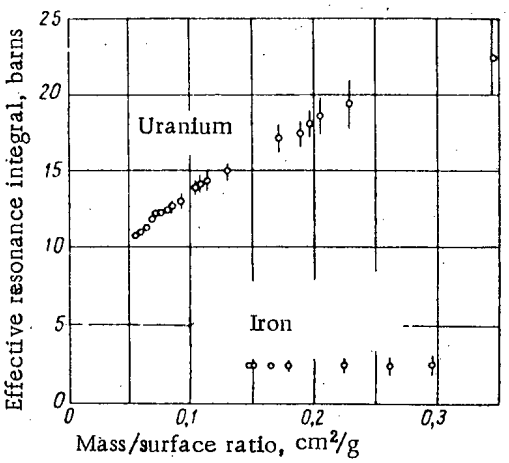

Results of measurements of the effective resonance integrals.

The results of the measurements are shown in the figure. This figure contains data for iron along with the U^{238} data. Iron does not exhibit any strong resonances and the fact that the iron resonance integral shows no dependence on the ratio S/M indicates that the mean neutron flux in the reactor is constant when the samples are introduced.

The points in the figure lie on the curve

$$\int \sigma_a \text{eff}\ \frac{dE}{E} = $$

$$= 6.0 \left\{ 1 + 15.6 \frac{S}{M} \left[1 - 2.18 \frac{S}{M} + 2.19 \left(\frac{S}{M} \right)^2 \right] \right\}.$$

This formula gives a somewhat different relation between the effective resonance integral and S/M than that reported in [3]. However, the numerical values of the resonance integrals for the values of S/M which were investigated are in agreement with those obtained in [3] (within the experimental errors).

In [2], using this same method a determination was made of the effective resonance integrals and the values of φ – the resonance escape probability – for cylinders of radius 1.73 cm made from uranium, uranium oxide, thorium, and thorium oxide.

The results are shown in the table.

In [1] the temperature coefficient of φ was also measured and found to be

$$\frac{1}{\varphi} \frac{d\varphi}{dT} = -(2.14 \pm 0.16) \cdot 10^{-5}/^\circ \text{C}.$$

TABLE

Sample	Density in g/cm³	φ	$\int \sigma_{a\,eff}\, dE/E$	$\left(\int \sigma_{a\,eff}\, dE/E\right)^*$
U	18.9	0.872**	12.2	10.9
UO_2	7.96	0.92±0.04	15.3±0.9	14.0±0.9
Th	11.5	0.92±0.02	12.5±0.3	9.2±0.3
ThO_2	9.64	0.93±0.03	15.4±0.8	12.1±0.8

*The contribution due to nonresonance absorption is computed on the basis of a 1/v law.

**The value indicated, obtained in another work, is taken as a reference.

In [4], using the oscillating-reactor method at the ZEEP reactor, the reactivity temperature dependence was measured by heating and cooling a uranium sample 3.25 cm in diameter. The following values were obtained

$$\frac{dk}{dT} = -(1.25 \pm 0.09)\cdot 10^{-5}/^\circ C \quad \text{for} \quad 30^\circ C < T < 230^\circ C$$

and

$$\frac{dk}{dT} = -(1{,}58 \pm 0{,}18)\cdot 10^{-5}/^\circ C \text{ for } -140^\circ C < T < +10^\circ C.$$

All three values of the temperature coefficients are smaller than the corresponding values obtained in [5].

P.K.

LITERATURE CITED

[1] M.V. Davis, J. Appl. Phys. 28, 250 (1957).

[2] M.V. Davis, Nucl. Sci. and Eng. 2, 488 (1957).

[3] R.L. Macklin and H.S. Pomerance, Progress in Nuclear Energy, ser I, vol. 1 (Pergamon Press, London, 1956), p. 179.

[4] R.M. Pearce and D.H. Walker, Nucl. Sci. and Eng. 2, 24 (1957).

[5] Egiazarov, Dikarev and Madeev, Conference of the Academy of Sciences USSR on the Peaceful Use of Atomic Energy (Division of Physico-Mathematical Sci.) [in Russian] (Academy of Sciences Press, USSR, Moscow, 1955), p. 67.

USE OF RADIOMETRIC ANALYSIS IN CHEMICAL INVESTIGATIONS

In the Institute of Physical Chemistry of the Academy of Sciences, USSR, V. I. Spitsyn and the author developed a method of radiometric analysis using two radioactive indicators.

This method consists essentially of the following. The compound being investigated was prepared from substances containing radioactive isotopes of two elements with different half-lives. Then the specific radioactivity of the starting substances and the radioactivity of the compound being investigated were determined. After the decay of the greater part of the short-lived isotope, the radioactivity of the same preparations was again measured.

The starting radioactivity of both isotopes in the compound may be calculated from the data, obtained by this method, by solving the following system of equations:

$$I_1 + I_2 = I_{1+2},$$

$$k_1 I_1 + k_2 I_2 = i_{1+2},$$

where I_1 and I_2 are the unknown radioactivities of elements 1 and 2 in the compound being analyzed, at the first measurement; I_{1+2} and i_{1+2} are the radioactivities of the preparation being investigated at the moment of the first and the second measurements; k_1 and k_2 are the coefficients showing how many times the radioactivity of elements 1 and 2 decreased during the time between the first and second measurements. Knowing I_1 and I_2 and the specific radioactivities of elements 1 and 2, we can calculate the weight or atomic ratio of the elements in the compound. In this way, this method of radiometric analysis makes it possible to determine the ratio of two elements in a compound without separating them chemically.

Using P^{32} and W^{187}, we determined the ratio P: W in sodium phosphotungstate. In this case the accuracy of the radiometric analysis ($\pm$ 2.5 %) was greater than the accuracy of chemical analysis.

The proposed method of radiometric analysis was used for determining the ratio K : P in potassium phosphotungstate, precipitated from solutions of varying acidity. As a result of the investigations, we established the formation of solid solutions of phosphotungstic acid and its potassium salt and therefore phosphotungstic acid should be considered an oxonium compound with the composition $(H_3O)_3\ PW_{12}O_{40} \cdot 26\,H_2O$.

N. B. Mikheev

THE USE OF LEACHABLE URANIUM IN PROSPECTING FOR URANIUM ORES

Uranium occurs in rocks in different forms, part of it generally leachable in weak acids. This leachable uranium in rocks has attracted the attention of investigators as a solution to the problems of genesis of ore and of prospecting for it [1].

Experiments have been made on the Colorado Plateau in the U.S.A. on the use of leachable uranium in prospecting for ore. The experiments were made in the area of the Homestake ore body in Big Indian Wash, Utah.

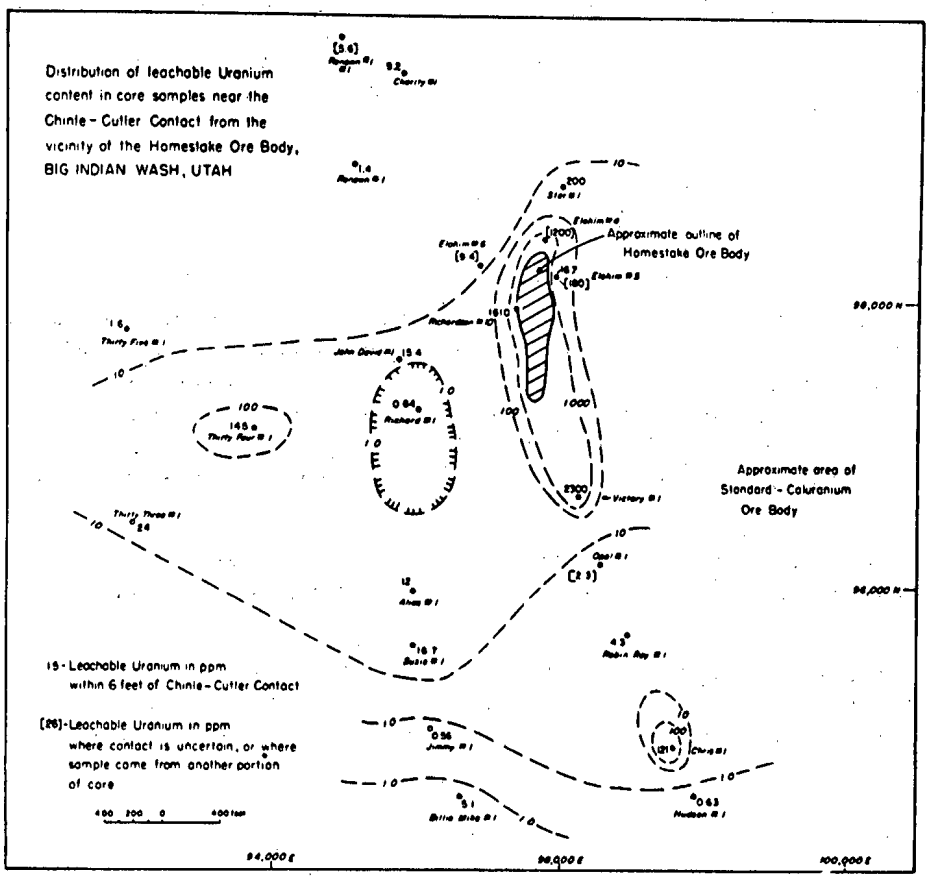

Map showing distribution of leachable uranium content in core samples near the Chinle-Cutler contact from the vicinity of the Homestake ore body, Big Indian Wash, Utah.
The figures indicate uranium content (in parts per million) in samples taken six feet from the contact; those in brackets give the content either of core samples whose position in relation to the contact was not determined, or of samples from other parts of the hole. [This figure has been reproduced in its original form by courtesy of the editors of Economic Geology.]

The ore body occurs in the lower part of the Triassic Chinle formation, which dips to the southwest at about 13° and unconformably overlies the Permian Cutler formation. The ore-bearing horizon of the Chinle formation consists of medium- and coarse-grained sandstones. Mudstones, siltstones, and similar rocks lie above it.

The area, embracing the ore body, was drilled in a number of places and the cores were sampled each 1.5 m (5 feet). The samples were placed in steel or aluminum containers and later studied in detail.

Two grams of crushed rock from each sample was treated with a solution of nitric acid, after which the leachable and residual parts of the uranium were measured. The data was plotted on a map of the deposit (see figure). Isopleths of the leachable uranium content clearly outline the Homestake ore body.

A comparison of these data with radiometric measurements have shown that knowledge of the distribution of leachable uranium gives a clearer picture than knowledge of radiometric anomalies [2].

These experiments furnish a foundation for conducting further investigations in the use of leachable uranium in prospecting for uranium deposits.

M. K.

LITERATURE CITED

[1] V. I. Gerasimovskii, J. Atomic Energy (USSR) 3, 12, 525 (1957).

[2] Econ. geol. 5, 5, 547 (1957).

NEW RAW-MATERIAL SOURCES OF THORIUM IN FOREIGN COUNTRIES

The production of thorium in capitalistic countries amounts in all to about 500 tons per year [1]. This small quantity attests to a low opinion of thorium as a source of nuclear energy. Davidson, showing some preference for obtaining nuclear fuel from thorium, explains this low opinion by the huge investments already made in the production of U^{235} and plutonium [2].

In the face of this, there is the fact that large deposits of thorium have been discovered in recent years in the capitalistic countries (in association with other metals), a fact that makes the using of it a problem all the more timely.

During the study of the uraniferous conglomerates of Blind River, Canada, it was shown that thorium occurred in economic quantities, the ratio of thorium to uranium being 1:2. It follows from this that the thorium reserves in this deposit amount to about 100,000 tons, that is, they approach in scale the largest deposits in India [1]. At present, thorium is not extracted from the Blind River ore during its treatment; but goes into the dump. The size of the projected concentration plant at Blind River, under construction or already built, will be such that, if the plant were organized to extract thorium, up to 5,000 tons of thorium might be obtained per year.

The Department of Atomic Energy of India has reported the discovery, in the northeastern part of the country, of a complex deposit of radioactive ores (apparently monazite), the reserves of which are estimated at 3,300,000 tons of ore, containing 330,000 tons of thorium and about 10,000 tons of uranium. In addition, the deposit contains 80,000,000 tons of ilmenite. The reserves of the largest earlier known deposit of thorium, occurring along the coast of Travancore (India), is evaluated at 150,000 tons of thorium. The new deposit is apparently twice as large as this one [3].

A third large thorium deposit, which has been discovered and studied in recent years, occurs in Brazil, in the Paranaiba River basin near Tapiro de Sacramento, Minas Gerais. It is a rarely found, unusual type of complex deposit, in which the valuable elements are associated with pyrochlore. The pyrochlore of this deposit contains 54% niobium pentoxide, 6% rare-earth elements of the cerium group, 9% thorium, 0.22% uranium oxide, and other elements. The mass of pyrochlore-bearing rock is large. It was discovered in 1954 by aerial methods. Exploratory drilling has uncovered reserves to a depth of 45 m of 4,000,000 tons of niobium pentoxide, 130,000 tons of thorium oxide, 60,000 tons of uranium, and 90,000 tons of rare-earth elements [4].

The discovery of such large raw-material sources of thorium, in the majority of cases in complex ores from which thorium may be extracted along with other metals, substantially increases the possibility of obtaining thorium in large quantities.

M. K.

LITERATURE CITED

[1] Atomwirtschaft, July-August (1957).

[2] C. F. Davidson, Min. Mag. 94, 4, 197 (1956).

[3] Min. J. 248, 6356, 749 (1957).

[4] S. Afr. Min. and Eng. J. 3346, 583 (1957).

THE URANIUM-OXYGEN SYSTEM

The phase diagram of the uranium-oxygen system, which contains a considerable number of compounds and wide ranges of solid solutions, is complex and so far has not been fully investigated. Figure 1 shows the most complete diagram, constructed in [1] on the basis of [2-6], in which individual regions were investigated.

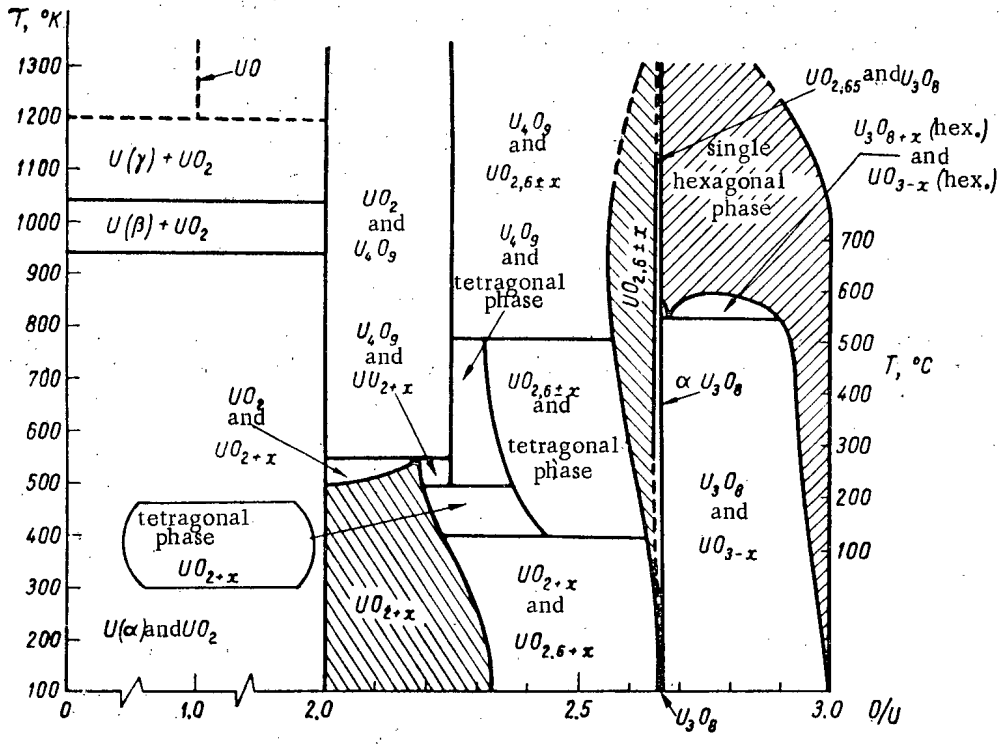

Fig. 1. Phase diagram of uranium-oxygen system.

The table gives the characteristics of some properties of uranium oxides, in regard to which the following comments are necessary. The monoxide UO, discovered by x-ray analysis, has only recently been obtained in small quantities [6]. The difficulty in obtaining it is supposed to be due to the fact that it is stable only at high temperatures. It is distinguished from the compounds UC and UN, which are isomorphous with it, by the fact that it does not change color when heated in air (the purple UN becomes darker), or when reacted with equal volumes of HNO_3, CH_3OOH and H_2O (UC darkens), slowly dissolving in the last case.

Uranium dioxide oxidizes readily in air, absorbing oxygen without change in lattice structure, the lattice constant varying as shown in Fig. 2. Recent investigations have shown that at 28° K, UO_2 is converted into an

antiferromagnetic state, and in the phases UO_{2+x} and $UO_{2.6+x}$, the excess oxygen occupies the lattice interstices. Ion vacancies are not formed in uranium. The oxide U_4O_9 has a special cubic structure, which has not been completely established [5].

TABLE 1

Structure and Some Properties of Uranium Oxides

Formula or phase	Color	Structure	Lattice constants, kX	Theoretical density, g/cm³	Region of stability or m. p., °C
UO	Gray	Cubic, NaCl type	$a_0 = 4.943$		Above 1200
UO_2	Dark brown	Cubic, CaF_2 type	$a_0 = 5.4581$	10.95	M. p. 2850
U_4O_9	Black	Cubic	$a_0 = 5.427$		
Tetragonal phase	Black	Tetragonal	$a_0 = 5.37$		
			$c_0 = 5.54$		
$UO_{2.6 \pm x}$	Black	Rhombic, 32 atoms of uranium in the elementary cell	$a_0 = 6.738$		
			$b_0 = 31.70$	8.38	
			$c_0 = 8.269$		
U_3O_8	Dark green or black	Rhombic, 2 molecules in the cell	$a_0 = 6.704$	8.39	
			$b_0 = 10.95$		
			$c_0 = 4.142$		
U_3O_8	Ditto	Hexagonal, type P3 [8]	$a_0 = 6.798$		Above 450
			$c_0 = 4.120$	8.41	
UO_3 [1]	Orange	Hexagonal	$a_0 = 3.963$		
			$c_0 = 9.160$	8.34	

The tetragonal phase exists in the limits $UO_{2.29}$-$UO_{2.42}$. As the temperature is increased, the constants a and c become equal at about 500° C, and this phase is transformed into the cubic phase, with the constant a = 5.40 kX [4].

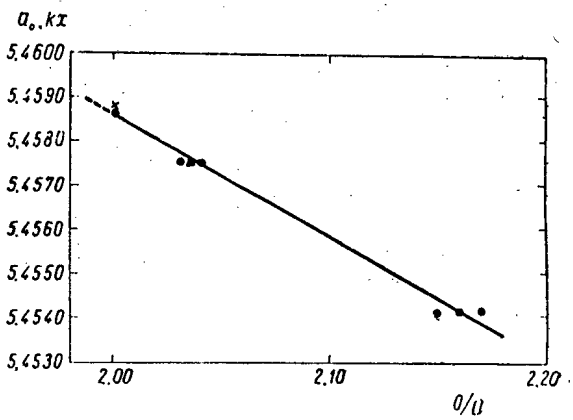

Fig. 2. Dependence of lattice constant of the UO_{2+x} phase on oxygen content.

The $UO_{2.6 \pm x}$ phase (according to Rundle [7] the compound U_2O_5) exists in the limits $UO_{2.55}$ - $UO_{2.65}$.

Uranous-uranic oxide U_3O_8 has two modifications. The low-temperature rhombic modification is transformed at about 450° C into the hexagonal modification, in structure closely resembling the phase $UO_{2.6+x}$ and UO_3 [1].

Uranium trioxide UO_3 exists in four or five modifications, produced by oxidation at high oxygen pressures. The structures of three modifications have been investigated but only one, the hexagonal, has been established. So far, no data are available regarding their mutual equilibrium conditions.

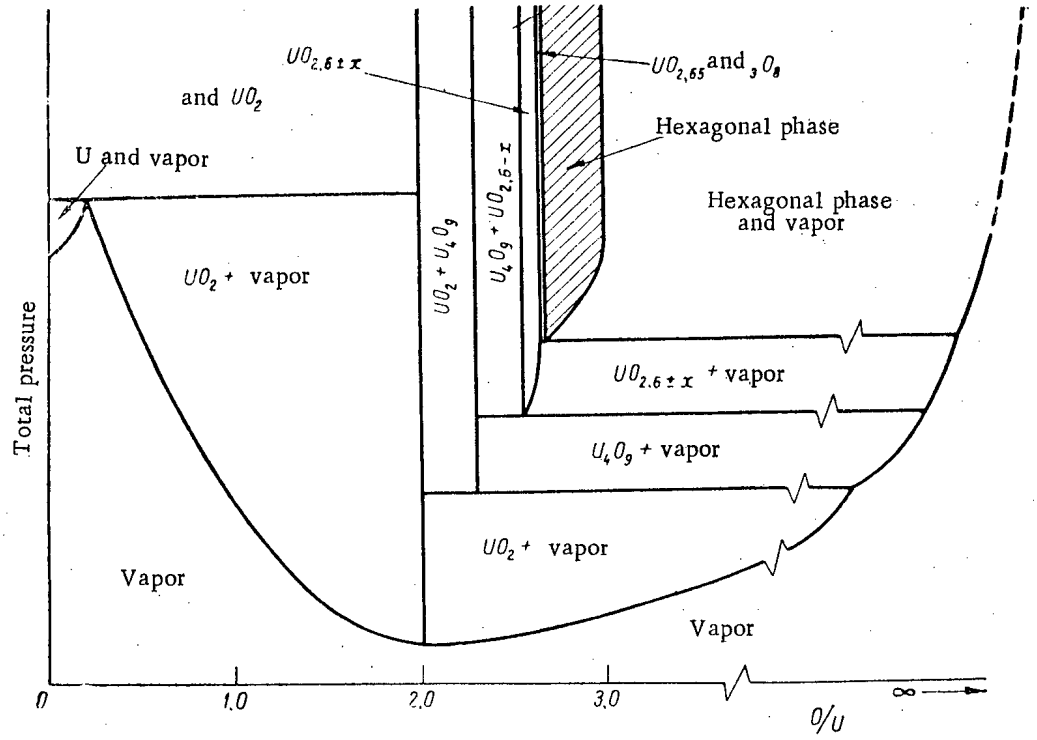

Fig. 3. Schematic diagram of the oxygen-uranium system in pressure-composition coordinates for 900° K.

Figure 3 shows the schematic uranium-oxygen diagram [1] in pressure-composition coordinates for the temperature 900° K.

Ia. S.

LITERATURE CITED

[1] R. I. Ackermann, ANL-5482, Sept. 14, (1955).

[2] W. Biltz and H. Mueller, Z. anorg. allgem. Chem. 163, 257 (1927).

[3] K. B. Alberman and L. S. Anderson, J. Chem. Soc. 303, Suppl. No. 2, 1949.

[4] H. Hering and P. Perio, Bull. Soc. Chim. France, 351 (1952).

[5] H. Hoekstra, S. Siegel, et al., J. Phys. Chem. 59, 136 (1955).

[6] J. Williams and K. Westmacott, Rev. Met. 53, 189 (1956).

[7] R. Rundle, R. Beamziger, et al., J. Am. Chem. Soc. 70, 99 (1948).

[8] S. Siegel, Acta Cryst. 8, 617 (1955).

[9] J. E. Goldman, Phys. Rev. 108, 948 (1957).

POCKET β- AND γ-RADIOMETERS

A pocket radiometer designed for monitoring β and γ radiation levels in plants, laboratories and in the field, has been developed at the Academy of Medical Sciences, USSR.

The radiometer allows measurements of dose strength for γ intensity and also makes it possible to determine the β-activity of surfaces contaiminated by active materials. The γ-radiation measurements can be carried out over four ranges: 0-1; 0-10; 0-100; and 0-1000 μr/sec at γ-photon energies ranging from 0.25 up to 2 Mev. The instrument ranges for β-radiation are 0-50 and 0-500 part/cm^2 • sec.

Pocket radiometer (external view).

The β-particle energy range is from 0.5 up to 2 Mev. The rear wall of the radiometer has a window which can be covered by a shield when γ-radiation measurements are made; thus, it is possible to distinguish between β and γ radiation.

The errors in the instrument readings are less than ± 15% for all operating ranges.

Transistors are used throughout. The total supply for the radiometer consists of a single 1 KSUZ cell which provides 200 hours of continuous operation of the radiometer. The instrument is designed for operation in dusty and moist locations at temperatures ranging from −10° C to +50° C. The weight of the instrument is 600 grams. The dimensions are 160 × 72 × 45 mm.

The operating principle of the radiometer is as follows: pulses from halogen counters are applied to the base of a P6G germanium transitor through intermediate RC-circuits; the transitor is connected as an emission detector. The average current from the emitter is measured with an M-592 microammeter having a sensitivity of 50 μ amps.

The P6G transitor has a high enough value for α (order of 0.97) to furnish a current gain of the order of 30. The counters are supplied from an oscillator-generator which also uses P6G transitors. The high voltage is stabilized by means of a SG-7S corona stabilizer.

At maximum deflection of the meter the current in the counter circuit is 2-3 μamps so that the drain on the generator is small. Under these conditions the current required from the cell is less than 10-15 ma.

V. V. Markelov, A. M. Lushchikhin, and V. I. Nikiforov

UNIVERSAL SCINTILLATION DOSIMETER

A portable instrument with interchangeable scintillation pickup units has been developed at the Academy of Medical Sciences, USSR; this instrument will be useful in solving a number of basic problems in practical dosimetry.

The inventory for the instrument includes: a γ-pickup unit, a β-pickup unit, an α-pickup unit, and a unit for measuring neutron fluxes. All units make use of the domestic FEU-25 photomultiplier and have calibrating radioactive preparations.

The gamma unit detects γ-radiation at levels from 0.25 to 50 μ r/sec. The scintillation unit is a polycrystalline screen of stilbene 20 mg/cm^2 in thickness, so that the unit shows very little sensitivity variation with energy. A removable lead collimator makes it possible to localize radioactive materials which emit soft γ-radiation (for example, I^{131}).

Fig. 1. External view of the universal scintillation dosimeter.

The beta unit is intended for monitoring contamination of surfaces by β-active materials. A shield is used to distinguish β-radiation from γ-radiation. The scintillator is a polycrystalline screen of stilbene with a thickness of approximately 40 mg/cm^2 and 75 cm^2 in area. The screen is pressed against the cathode of the photomultiplier by means of a removable conical light pipe.

Using this unit fluxes ranging from $2.5 \cdot 10^3$ to $2.5 \cdot 10^6$ β-part/min at the surface of the screen can be measured. A γ-background up to 50 μr/sec can be compensated for in the apparatus.

The alpha unit is designed for monitoring contamination of surfaces by α-active materials. The scintillator is fabricated from zinc sulfide which is deposited directly on the end of the light pipe; the end of the light pipe is 75 cm^2 in area. Using this dosimeter fluxes ranging from $3 \cdot 10^2$ to $3 \cdot 10^5$ α-part/min can be measured at the screen. Weaker fluxes can be detected using earphones. The unit is insensitive to β-radiation and γ-radiation.

The unit for recording thermal neutron fluxes has a thin plastic screen with a ZnS–Ag, B phosphor and can detect from 15 to $1.5 \cdot 10^4$ neut/cm^2 · sec. The unit is insensitive to γ-radiation and only slightly sensitive to fast neutrons. The unit is furnished with a cadmium collimator to facilitate location of neutron-leakage points.

The control panel for the instrument is fed from an alternating-current source. The unit consists of a stabilized high-voltage rectifier for the photomultiplier and a recording circuit which includes a discriminator, a

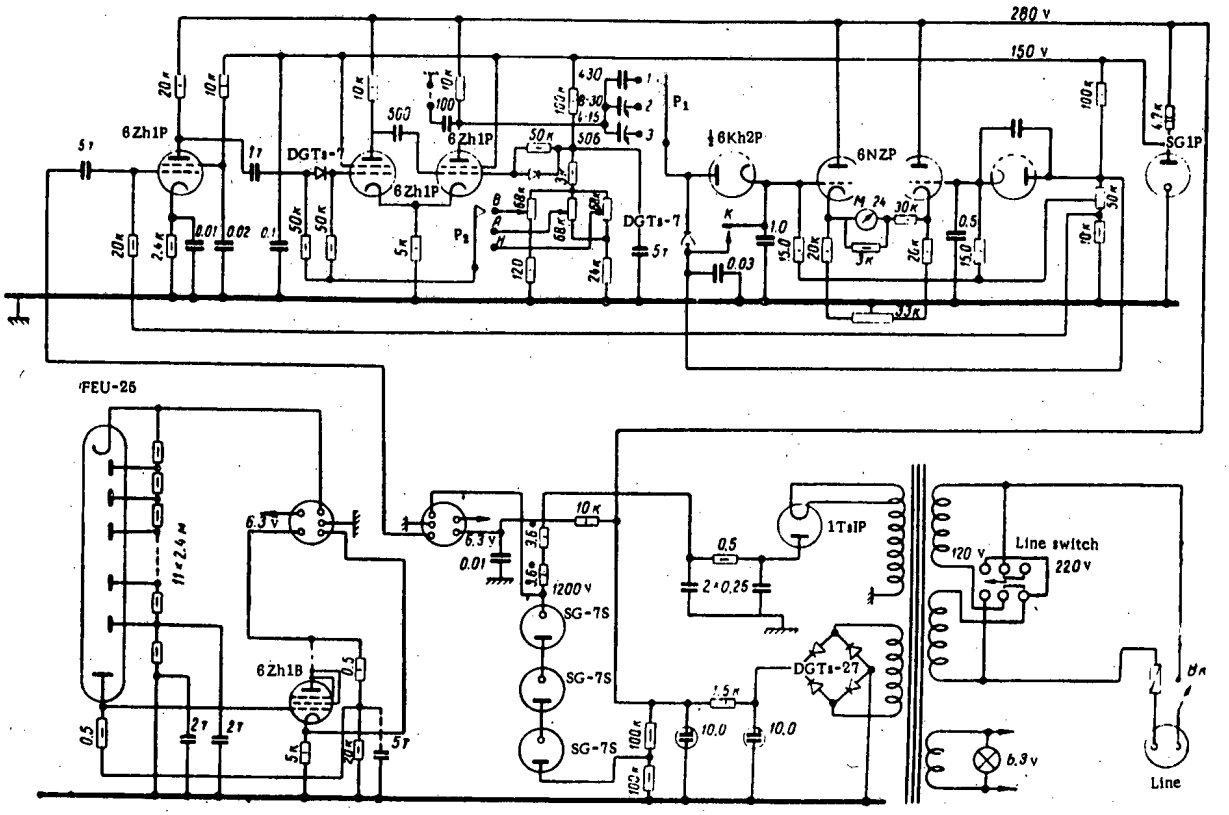

Fig. 2. Schematic diagram of the universal scintillation dosimeter.

shaping unit and a counting-rate unit. The entire instrument consumes 35 watts; the weight is 5 kg.

I.B. Keirim-Markus, V.V. Markelov,
V.I. Nikiforov and L.N. Uspenskii

BRIEF COMMUNICATIONS

USSR. At the Mining and Geology Institute of the Ural Branch of the Academy of Sciences of the USSR, a geophysical method of exploration of coal beds based on the observation of the intensity of scattered gamma-radiation from radioactive cobalt has been developed. The large-scale utilization of this method, brought about by the "Geofizuglegeologiia" trust, made possible a transition to highly productive and economical core drilling of coal formations.

A method for determining the presence of industrial grades of heavy metals (lead, mercury, tungsten, etc.) in the cross section of bore holes, with the aid of soft gamma-radiation, has been developed experimentally at the Institute and has been checked under production conditions. Se^{75} is used as the emitter.

USSR. At the K.A. Timiriazev Agricultural Academy in Moscow, an isotope training laboratory equipped with the latest apparatus has been opened up. Here, studies will be devoted to questions of applying radioactive and stable isotopes in biology and agriculture. Scientists from Czechoslovakia and Yugoslavia are now serving apprenticeship in the isotope laboratory.

England. In November, 1957, construction was begun on the new atomic scientific research center near WinfrithHeath. Twenty million pounds sterling have been earmarked for the erection of this center. Work at the new center will be concentrated entirely on developing new types of nuclear reactors.

The installation of an experimental high-temperature, zero power, gas-cooled reactor on the premises of the center has been proposed. This reactor will operate on fuel made up of a Th and U^{233} mixture. Hollow ceramic heat-exchanger elements will make it possible for the reactor to function at temperatures of the order of 800°C. Producing power with this reactor will be considerably cheaper than with Calder-Hall type reactors. In addition, this reactor requires 100 times less graphite than Calder-Hall reactors.

Among the experimental reactors probably to be built at the atomic center are two prototypes of reactors slated for installation in sea-going surface vessels. It is also possible that a power reactor will be constructed, operating on fuel elements in the form of solutions of uranium salts mixed with water.

England. Installation of a 2 Mev Van de Graaff accelerator is proposed for the Edinburgh General Hospital, for use in the therapy of cancer ailments.

England. The British National Institute for Atomic Research has announced the signing of a contract for the delivery of a magnet yoke for the 7 Bev proton synchrotron under construction in the vicinity of Harwell. 340 steel units (each weighing 20 tons) will be delivered, to a total cost of over 1250 thousand pounds sterling.

England. Work is being conducted in England (and the Netherlands) on designing of a particle accelerator with x-ray heads, which may be used in industry for x-ray testing of welded seams and other purposes. It is expected they will prove especially useful in the welding of heavy steel plates directly at the assembly point, as for instance in the construction of such bulk design items as reactor containment vessels and heat exchangers for atomic electric power stations. Moveable particle accelerators not equipped with x-ray heads may also find use in industry for the irradiation of various materials, as, for example, plastics.

England. According to a statement by Gaunt (British representative in the USA on matters of atomic energy), Calder-Hall type reactors will be under construction in England up to 1965. From 1965 to 1970, reactors of that type will employ heat exchangers with beryllium jackets, and from 1970 to 1975 uranium oxide will be utilized as fuel. By 1980, half of the power reactors in operation in England will be fast reactors.

Construction is approaching completion on the first English experimental fast power reactor in Dounreay.

The reactor is expected to go critical during the summer of 1958. In the beginning, it will be employed for carrying out experiments at zero power, and later for experiments based on the method of oscillator at all power levels, and, finally, after testing at design power, it will be charged with plutonium heat exchanger elements and set into operation. A prototype of the fast reactor for atomic electric power stations will be set up not sooner than 1960.

England. The lower section of the containment vessel of reactor No. 1 has been installed at the building site of the Calder-Hall type power reactor at Berkeley. The vessel is to be made up of plate steel 75 cm in thickness, each unit weighing 3 tons.

England. A patent claim has been issued on a technique for producing a number of zirconium alloys exhibiting high corrosion resistance as a result of the action of high-parameter water and steam. Corrosion dropped off appreciably with addition of 0.5-1% (weight) nickel. From 1 to 5% (weight) tantalum must be included in the make-up of the alloys.

Brazil. The first Brazilian reactor (swimming-pool type, 5 megawatt power) went critical. Construction contractors were the American firm Babcock and Wilcox. The reactor was installed at the São Paulo University.

Brazil. Erection of the second atomic electric power station was announced. The station is to have two reactors, water-cooled and water-moderated type, at 12.5 megawatt power.

Denmark. Danish geologists, prospecting for uranium ores in Greenland in the summer of 1957, came across an ore body in the Marsak area (along the shoreline of the Skav fjord). The ore discovered had a high uranium content. Geological exploration of uranium was begun two years ago in Greenland, even though the first announcements of uranium strikes in that region were made as early as 1948.

Spain. A 3000 kw thermal pool type reactor will be installed in the Madrid area, built and run-in in the USA. Assembly of the reactor in Spain is slated for completion in the beginning of 1958, start of operation scheduled for March, 1958.

Italy. In agreement with the English firm Nuclear Power Plant Company, a 200 megawatt atomic power station will be erected in north Italy, with the aid of the firm mentioned. The reactor at the station will be similar to the reactor operating at the station built at Bradwell (England).

The constuction site has not been decided on yet, although it is suggested that the station be set up on the shore of Lago Maggiore. Utilization of the lake waters will make it feasible to do without cooling towers.

Construction will begin in February-March 1958 and will be completed within three to four years.

Italy. Erection of a 150 megawatt atomic electric power station is slated for a site 64 km from Rome, on the coast of the Tyrrhenian Sea. A pressurized-water reactor will be installed at the power station.

The designing and building of the station, including the reactor itself, will be undertaken by the American firm "Vitro Corporation.

Canada. The next due annual world power conference will be in session in Montreal, from September 7 to 11, 1958. The theme of the conference is "Economic Trends in Production, Transportation and Utilization of Fuel and Electric Power."

Norway. England is delivering 9 tons of uranium heat exchanger elements for the first loading of the water-boiler reactor under construction at Halden. Heavy water to be used as moderator (16 tons) will be obtained from the USA.

Poland. Many scientists from various countries visited Polish atomic research facilities during 1957. Among them were D.I. Blokhintsev (USSR), J. Cockcroft (England), F. Perrin (France), H. Bhabha (India). The guests visited the uranium technology and radiochemistry laboratory (Warsaw), the electronics laboratory (Warsaw), the nuclear physics laboratory and the 12-Mev cyclotron construction site (Krakow). They inspected the nuclear physics and reactor engineering facilities under constuction at Swerk, near Warsaw, as well as the construction of the experimental reactor at that site.

Poland. A Corresponding Member of the Academy of Sciences, Prof. Doctor Pawel Nowackii, has been appointed Director of the Institute of Nuclear Research of the Academy of Sciences of the Polish People's Republic.

The former director of the Institute, Corresponding Member of the Academy of Sciences of the Polish People's Republic Prof. Doctor Andrzej Soltan, was elected as chairman of the Learned Council of the Institute.

USA. The renowned Danish scholar Niels Bohr was awarded an international prize ($75,000) in Washington, on October 24, 1957, for his accomplishments in the field of the peaceful utilization of atomic energy.

USA. Construction was begun on the grounds of Princeton University on a 3 Bev proton energy accelerator. The project will cost $6 million.

USA. At one of the laboratories of the General Dynamics Corporation, installation of a 30 Mev travelling-wave linear electron accelerator is projected. This accelerator will make possible obtaining stronger currents than are achievable with most of the presently available accelerators. Construction should be completed in less than a year. The new linear accelerator will be used for the study of nuclear reactor physics, radiation damage, for research in the field of radiation chemistry, and for radiography.

USA. Operational use of the first industrial 350 kev Cockcroft-Walton* accelerator is scheduled for August 1958 at the University of Arkansas. Total costs of the accelerator, building and electronic equipment will be $150 thousand. Expenses for the construction of the accelerator ($700 thousand) are underwritten by the Atomic Energy Commission. The accelerator will be housed in an underground-level installation measuring 4.5 x 9 x 6 m^3, which is connected to the control room (0.9 m^2 floor space) by an underground tunnel. The roof of the accelerator site will be protected with shielding (0.3 m concrete and 1.5 m earth). The ionic current of the accelerator will attain 400 μamps which will make it a valuable monoenergetic neutron emitter, useful for radiochemical research. It is expected that, as a result of the bombardment of tritium by positively charged ions, the neutron yield will reach 10^{11} per second. Later, when the power is brought up to 500 kev and the current to 3 ma, and new bombardment techniques are introduced, the neutron yield will be increased many times. The new accelerator will be employed to speed up protons, deuterons, He^3 ions, and also heavier ions such as N^{14}, O^{16}, A^{40} and Ne^{20}.

USA. The firm Baldwin-Lima-Hamilton has received an order for the manufacture of 246 magnetic cores for the 25 Bev proton accelerator under construction at the Brookhaven National Laboratory. Delivery of the cores will begin January, 1958.

Installation total costs will amount to $26 million.

USA. In ten months of operation use, the EBWR water-boiler reactor has produced some 2,000 megawatt-days of heat energy, equivalent to 100 work days at full power. The cost of the electric power is 5.2 cents per kw-hour. Replacement of the core by a larger reactor core will up the reactor power 50% and will also bring about a drop in power costs to 3.2 cents per kw-hour.

USA. Congress has commissioned the General Electric Company to begin work on a new design of plutonium reactors for power and plutonium production. (The USA has at present 13 industrial reactors and not even one dual-purpose reactor.) A report on the design, cost evaluation and building time estimate of that line of reactor will be presented to Congress in April, 1958.

USA. The American Coalman Company has developed a tractor for the Convair NB-36 airplane, in which the US Air Force is carrying out tests of atomic power plants. The driver's cab will be shielded from nuclear radiation. Weight of cab will be 4 tons. It is manufactured from sheet steel 6.5 cm in thickness, and window glass of the same thickness contains 75% pure lead. Air fed into the cab is first filtered and then heated or cooled. The driver's cab will have a radio set. Weight of the tractor unit will be 12 tons, top speed 40 km/hr.

USA. The Atomic Energy Commission has decided to look into a suggestion made by American firms relating to the construction in the USA of a modified form of the Calder-Hall reactor. A report on the design, economic aspects and estimated installation time of the reactor will be examined by the Joint Committee on Atomic Energy in April, 1958.

USA. At Mare Island, the atomic submarine "Sargo" was launched. Prior to that, atomic submarine "Skate" (May, 1957) and "Swordfish" (August, 1957) had been launched, the first submarines of that class. Construction of the last submarine of that class, the "Seadragon," is reaching completion at Portsmouth. All of these vessels will have installed water-cooled, water-moderated submarine thermal reactors similar to the reactor installed

*ARCO CW-D4 Cockcroft-Walton Positive Ion Accelerator.

aboard the "Nautilus."

USA. A beryllium-producing plant has been built at Elmore, Ohio. Productive capacity of the plant amounts to 9 tons of beryllium oxide and 4.5 tons of metallic beryllium monthly.

USA. A continuously operating bubble chamber has been built at the Radiation Laboratory of the University of California. The chamber is a vessel filled with a liquid (isoamylacetate, methyl and ethyl alcohol, etc.) at low temperature. Carbon dioxide gas is dissolved in the liquid. The upper portion of the vessel contains a heater, while the bottom is cooled with dry ice (minus 78°C). The middle portion of the vessel has a thin layer sensitive to fast neutrons. The chamber showed no sensitivity to γ-radiation. The chamber may be operative for not more than a few hours at a time, although, if a gas-saturated liquid is continuously added to the bottom of the bubble chamber, and the spent liquid is removed through the top of the chamber, then the unit may retain its sensitivity over an indefinitely long period of time.

USA. The Oak Ridge National Laboratory has developed a cobalt emitter with 15,000 curie activity, equivalent to approximately 15 kg of pure radium. The emitter consists of 300 nickel-coated cobalt discs; total weight is less than a pound.

Radiation intensity of the emitter approaches that of a nuclear reactor.

USA. At the atomic industry exhibit in New York, models of atomic lamps designed for continuous functioning over 10 years were displayed. The lamps are called isolites; they employ a gaseous radioactive isotope Kr^{85}. The light sources are manufactured from specially treated phosphorus crystals housed in a hermetically sealed transparent capsule. The crystals fluoresce when bombarded by Kr^{85} radiation.

West Germany. At the present time in West Germany (also in South Africa), research work is underway directed to finding some cheaper method for producing heavy water. In the production of synthetic gasoline from coals, by-products are formed which are enriched with heavy water, and which lend themselves to use for heavy-water production.

West Germany. The minimum development program for West German atomic power looks forward to the erection of 500-megawatt atomic electric power stations during the next five years.

Sweden. A 76 megawatt research reactor was set into operation near Farst. Its thermal energy will be employed for heating one of the sections of Stockholm. Heavy water will be used as moderator in the reactor, with 26 tons of the water being obtained from the USA for the sum of 6 million marks.

Japan. Construction has started on a zirconium-producing plant, with 30 tons monthly output. The zirconium will be exported to the USA.

Japan. The Atomic Energy Commission plans to convene a conference of representatives of Asian countries in Tokyo during 1958, to set up an organization similar to "Euratom."

BIBLIOGRAPHY

NEW LITERATURE

Books and Symposia

Peaceful Uses of Atomic Energy [Atomnaiia energiia v mirnykh tseliakh]. Symposium of articles, edited by E.G. Komar, L.F. Krylov and V.E. Manoilov (State Power Press, Leningrad, 1957), 222 pp.

The symposium provides a review of the work of Leningrad institutions, organizations and enterprises both on the study of the atomic nucleus and on the application of atomic energy to peaceful uses. The symposium contains the materials of the Anniversary congress of workers in industry, transport and construction, active workers in science and engineering of Leningrad (June, 1957).

The symposium is intended in the main for readers acquainted with the problems of present-day nuclear physics. Some of the articles are interesting even to the uninitiated reader, since they provide an understanding of the manifold pathways and tremendous perspective present in the peaceful utilization of atomic energy.

A Ship Powered by Atomic Energy [Korabl' na atomnoi energii] by V.V. Lakhanin and N.M. Shilov, publ. by "Morskoi transport" [Maritime transport], 1957, 150 pp, 2 rubles, 90 kopeks. The book surveys the possibilities and perspectives of the employment of atomic energy for the propulsion of shipping. The features and advantages of atomic-powered ships, the various types of shipboard power plants and their installation on ships are discussed and evaluated. Various types of nuclear reactors which might be amenable to use as power sources are described. Simple calculations are given to illustrate the determination of the nuclear fuel expenditure, depending on one or another shipboard operating regime. Questions of economic operation of atomic-powered ships using various reactors are discussed.

The bulk of the book is taken up with information touching on the basic topics involved in the utilization of nuclear energy (structure of the atom, radioactivity, methods of unleashing atomic power, radioactive radiations, etc.), and information touching on the fundamentals of reactor engineering (nuclear fuel elements, operating principles of reactors, reactor types, the first Soviet atomic electric power station, reactors in other countries, etc.).

The book will acquaint the reader in general outline with some of the basic problems of atomic shipping.

Questions of Nuclear Power [Voprosy iadernoi energetiki]. Symposium of translations and reviews of foreign periodical literature, No. 5, 1957. Foreign Literature Press, 108 pp., 7 rubles.

In the section on Power Stations and Layout, the following translations are found: "The First Scottish Atomic Power Station" from the Engineer 203, 5272, 216 (1957); 203, 5273, 260 (1957); "Small Liquid-Metal-Fuel Reactor Systems" from Nucl. Sci. and Engineering 1, 2, 135 (1956); "Problems of Liquid-Metal-Fuel Reactors" from Nucl. Engineering 1, 9, 373 (1956), a continuation; for the beginning, cf. "Questions of Nuclear Power" No. 4.

The section Design and Materials has translations of "Electromagnetic a.c. and d.c. Pumps for Liquid Metals" from Engineer 202, 5256, 541 (1956); 202, 5257, 572 (1956).

In the section Transfer Processes, articles translated are: "Procedure for Research on Natural Circulation of Boiling Systems" from Nucl. Sci. and Engineering 1, 6, 461 (1956); "Some Features of Reactor Gas-Coolant Systems" from Nucl. Power 2, 13, 188 (1957).

In the section Reactor Physics: "Physics of Modern Reactors" from Brit. J. of Appl. Phys. No. 5, 9 (1956).

In the section Nuclear Power News: "A 60,000 kw Nuclear Power Plant" from Power Engineering 86, April 1957; "A 20,000 h.p. Nuclear Engine for Merchant Ships" from Motor Ship XXXVII, 442 (1957); "Corrosion of Metallic Materials in Water at High Temperature" from Atompraxis 5, 117 (1957); "Reactor Containers" from

Engineering 183, 47, 250 (1957); "Development of Atomic Power Engineering in England" from Engineering 183, 4748, 282 (1957); 183, 4749, 345 (1957).

Articles from Journals

Akimov, Iu.K., Quick-acting Differential Coincidence Circuit (Pulse Circuit) PTE* No. 4 (1957).

Aleksandrov, Iu.A., et al. Deuteron Photodisintegration at Energies Ranging from 50 to 150 Mev, ZhETF Vol. 33, No. 9 (1957).

Ansel'm, A.A., Scattering of Slow Neutrons by Two-Atom Molecules, ZhETF** Vol. 33, No. 9 (1957).

Bardyshev, G., Application of Gamma Rays in the Flour Milling Industry (from the foreign literature) Mulomol'no-elevat. Promyshlennost' [Flour Milling Industry] No. 9 (1957).

Braginskii, S.I., On Modes of Vibration of Plasma in a Magnetic Field, Doklady Akad. Nauk SSSR 115, No. 3 (1957).

Vaisenberg, A.O. and Smirnitskii, V.A., Energy Dependence of Angular Correlation in $\pi^+ - \eta^+ - e^+$-Decay, ZhETF Vol. 33, No. 9 (1957).**

Vitkin, A.I., Use of Radioactive Isotopes in Studies of Basic Mechanism of Hot Tin-Plating Processes, Doklady Akad. Nauk SSSR 115, 4 (1957).

Gerasimova, N.M., Solution of Kinetic Equations for High-Energy Nuclear Cascade Process, ZhETF Vol. 33, No. 9 (1957). **

Gorbunova, K.M. and Nikiforova, A.A., Studies of Mechanism of Phosphorus Incorporation into Nickel Platings Using Radioisotope P^{32}, ZhFKh [Zhurnal Fizicheskoi Khimii] Vol. 31, No. 8 (1957).

Grishin, V.G. and Saitov, I.S., On Diffraction Scattering of High-Energy Protons by Protons (letter to the editor), ZhETF Vol. 33, No. 10 (1957).**

Dubinskaia, N. and Ulmanis, U., Investigation of Back-Scattered Gamma Radiation, Izvest. Akad. Nauk Latvyshskoi SSR (Latvia) No. 7 (1957).

Elovich, S.Iu. and Prusakov, V.N., Tracer Studies of Chromatographic Behavior of Multivalent Ions (Communication 2), ZhFKh [Zhurnal Fizicheskoi Khimii] Vol. 31, No. 8 (1957).

Zdril'ko, A.F. and Poliakov, I.M., Cross Pollination Studies Using S^{35}- and P^{32}-Tagged Pollen, Biul. Ukr. n.-i. in-ta rastenievodstva, selektsii i genetiki [Bulletin of Ukrainian Research Institute for Plant Husbandry, Selective Breeding and Genetics] No. 1 (1957).

Zel'dovich, Ia.B., Variant of the Theory of Hyperons (letter to the editor), ZhETF Vol. 33, No. 9 (1957)**

Zel'dovich, Ia.B., On Nuclear Reactions in Superdense Cold Hydrogen, ZhETF Vol. 33, No. 10 (1957)**

IMA-1 Intensity Meter for Labeled Atoms, PTE No. 4 (1957).*

Kaduk, B.G., Universal Radiometer (IMA model Intensity Meter for Labeled Atoms), Nauka i peredov. opyt v s. kh. [Science and Progressive Experiment in Agriculture] No. 10 (1957).

Kovalev, V.P., et al. Comparison of Spectra of Neutron Fission in U^{235}, Pu^{239} (letter to the editor), ZhETF Vol. 33, No. 10 (1957).

Kopaleishvili, T.I., On the Nuclear Reaction $Li^6(nt)He^4$ (letter to the editor), ZhETF, Vol. 33, No. 9 (1957). **

Korogodin, V.I., Some Regularities in the Retardation of the Initial Budding of Yeast Cells in Response to Gamma Emission by Radiocobalt, Biofizika Vol. II, No. 5 (1957).

*Pribory i Tekhnika Eksperimenta [Experimental Equipment and Techniques].

**Journal of Experimental and Theoretical Physics [See English Translation].

Kriuk, I.F. and Markevich, S.V., Effect of γ-Radiation from Radioactive Cobalt (Co^{60}) on Some (Technological) Properties of Peas, Uch. zap. Belorussk. in-ta nar. kh-va [Notes of White Russian National Economy Institute] No. 3 (1957).

Kuzin, A.M. and Frank, G.M., Development of Biophysics in the 40 Years Following the Great October Socialist Revolution, Biofizika Vol. II, No. 5 (1957).

Kulikova, V.G. and Timofeeva-Resovskaia, E.A., Distribution of Mixture of Fragments of Uranium, Cerium-144 and Cesium-137 in the Grass-Dwelling Frog, Doklady Akad. Nauk SSSR 115, 4 (1957).

Kumekin, Iu.P., Polarization in Quasielectric p-p-Scattering of 635 Mev Protons on Deuterons (letter to the editor), ZhETF Vol. 33, No. 10 (1957).*

Maleev, S.V., Scattering of Slow Neutrons in Ferromagnetics, ZhETF, Vol. 33, No. 10 (1957).

Meshkovskii, A.G., et al. Formation of Negative π-Mesons by 660 Mev Protons on Nuclei of Various Elements, ZhETF Vol. 33, No. 9 (1957).*

Nikolaev, V.B., et al. Welding of Technological Reactor Chemicals in the First Atomic Electric Power Station, Svarochnoe proiz-vo [Welding Industry] No. 11 (1957).

Panchenkov, G.M., et al. Chemical Separation Technique for Boron Isotopes, ZhFKh Vol. 31, No. 8 (1957).

Pasynskii, A.G., Contribution to the Theory of the Biological Effect of Radiations, Biofizika vol. II, No. 5 (1957).

Pikin, K.I., Peculiarities of the Course and Treatment of Compound Injuries (On Injuries Suffered from an Atomic Bomb Explosion and Their Treatment), Tr. Khar'kovsk. nauch. med. o-va [Transactions of Kharkov Scientific Medical Society] No. 7 (1957).

Poliakov, I.M. and Zdril'ko, A.F., Pathways of Uptake of S^{35}- and P^{32}-Labeled Pollen by the Ovary, Biul. Ukr. n.-i. in-ta. Rastenievodstva, selektsii i genetiki No. 1 (1957).

Sverdlov, Z.M., Investigation of Fluorescence of Uranium-Activated Sodium Fluoride, Optika i spektroskopiia Vol. 3, No. 4 (1957).

Sokolov, A.A., Contribution to the Theory of the Neutrino With Oriented Spin (letter to the editor), ZhETF Vol. 33, No. 9 (1957). *

Tolkacheva, E.N., Quantitative Response of Reparatory Processes Proceeding in the Organism After Total-Body Irradiation, Biofizika vol. II, No. 5 (1957).

Uklonskii, A.S., First Variant of Para-Elements of Uranium, Doklady Akad. Nauk Uzbekskoi SSR No. 8 (1957).

Tselishchev, S.P. and Furman, A.O., Absorption of Beta Radiations in Thin Layers of Matter and the Role of Absorption in Absolute Measurements of Beta Activity, Izv. Timiriazevsk. s.-kh. akad. [Bulletin of Timiriazev Agricultural Academy] No. 3 (1957).

Tselishchev, S.P. and Furman, A.O., Absorption of Radiation in Volumes of Matter Containing Radioactive Isotopes, Izv. Timiriazevsk. s.-kh. akad. No. 3 (1957).

Eidus, L.Kh., et al. Migration Mechanism of Defense Against Radiation Effect, Biofizika vol. II, No. 5 (1957).

* Journal of Experimental and Theoretical Physics [See English Translation].

SOVIET JOURNAL OF ATOMIC ENERGY VOLUME 4, NUMBER 2, 1958

CONTENTS

(continued)

CONTENTS (Continued)

SIGNIFICANCE OF ABBREVIATIONS MOST FREQUENTLY ENCOUNTERED IN SOVIET PHYSICS PERIODICALS

AN SSSR	*Academy of Sciences, USSR*
FIAN	*Physics Institute, Academy of Sciences USSR*
GITI	*State Scientific and Technical Press*
GITTL	*State Press for Technical and Theoretical Literature*
GOI	*State Optical Institute*
GONTI	*State United Scientific and Technical Press*
Gosenergoizdat	*State Power Press*
Gosfizkhimizdat	*State Physical Chemistry Press*
Gozkhimizdat	*State Chemistry Press*
GOST	*All-Union State Standard*
Goztekhizdat	*State Technical Press*
GTTI	*State Technical and Theoretical Press*
GUPIAE	*State Office for Utilization of Atomic Energy*
IF KhI	*Institute of Physical Chemistry Research*
IFP	*Institute of Physical Problems*
IL	*Foreign Literature Press*
IPF	*Institute of Applied Physics*
IPM	*Institute of Applied Mathematics*
IREA	*Institute of Chemical Reagents*
ISN (Izd. Sov. Nauk)	*Soviet Science Press*
I YaP	*Institute of Nuclear Studies*
Izd	*Press (publishing house)*
KISO	*Solar Research Commission*
LETI	*Leningrad Electrotechnical Institute*
LFTI	*Leningrad Institute of Physics and Technology*
LIM	*Leningrad Institute of Metals*
LITMiO	*Leningrad Institute of Precision Instruments and Optics*
Mashgiz	*State Scientific-Technical Press for Machine Construction Literature*
MATI	*Moscow Aviation Technology Institute*
MGU	*Moscow State University*
Metallurgizdat	*Metallurgy Press*
MOPI	*Moscow Regional Institute of Physics*
NIAFIZ	*Scientific Research Association for Physics*
NIFI	*Scientific Research Institute of Physics*
NIIMM	*Scientific Research Institute of Mathematics and Mechanics*
NII ZVUKSZAPIOI	*Scientific Research Institute of Sound Recording*
NIKFI	*Scientific Institute of Motion Picture Photography*
OIYaI	*Joint Institute of Nuclear Studies*
ONTI	*United Scientific and Technical Press*
OTI	*Division of Technical Information*
OTN	*Division of Technical Science*
RIAN	*Radium Institute, Academy of Sciences of the USSR*
SPB	*All-Union Special Planning Office*
Stroiizdat	*Construction Press*
URALFTI	*Ural Institute of Physics and Technology*

NOTE: Abbreviations not on this list and not explained in the translation have been transliterated, no further information about their significance being available to us.—*Publisher.*